Studies on the coordination chemistry of functionalised thiourea ligands

A thesis

submitted in fulfilment

of the requirements for the degree

of

Doctor of Philosophy in Chemistry

at

The University of Waikato

by

Matthew C Risi

THE UNIVERSITY OF
WAIKATO
Te Whare Wānanga o Waikato

2025

Abstract

This thesis explores the coordination chemistry of functionalized thiourea ligands with electron-withdrawing sulfonyl, phosphoryl and diacyl substituents. These ligands, despite their structural similarity to acylthioureas, exhibit unique coordination behaviours that have been largely understudied within the literature, particularly with platinum group and related late transition metals. By utilizing a series of characterization techniques, including single-crystal X-ray diffraction, electrospray ionization mass spectrometry, NMR spectroscopy, and computational methods, this work aimed to establish foundational knowledge to inform future application-driven research within this research domain.

Firstly, dianionic sulfonylthiourea ligands were investigated towards platinum(II), revealing a distinct preference for *distal* isomer (coordinated *via* S,N-sulfonyl) which was found to be a result of a stabilizing chalcogen bond between thiourea sulfur and sulfonyl oxygen atoms. This non-covalent interaction, confirmed computationally and crystallographically, highlights the potential for modulating isomer selectivity of thiourea ligands through ligand design. Following this study, Chapter 3 extends the investigation of dianionic and monoanionic sulfonylthiourea ligands to organometallic ruthenium(II), iridium(III), and rhodium(III) in the piano stool arrangement. The resulting complexes demonstrated how steric factors influence isomerization and resulting coordination modes. While the *proximal* isomer persisted among the prepared complexes, using sufficient steric bulk around the metal centre, the *distal* isomer was formed, exhibiting *proximal* to *distal* isomerization in the liquid state. Anticancer assessments against various human cancer cell lines were performed externally which show moderate activity. Trends indicating enhanced efficacy through increased ligand lipophilicity were observed among the ruthenium(II) complexes. In Chapter 4, platinum(II) complexes with dianionic phosphorylthiourea ligands are characterized, revealing a consistent *distal* isomer preference modulated by bulky substituents. The inclusion of phosphorus atoms

onto the ligand enhances characterization capabilities over similar ligands *via* $^{31}P\{^{1}H\}$ NMR spectroscopy, providing a robust tool for elucidating coordination modes. Chapter 5 introduces symmetric diacylated thioureas as versatile ligands for platinum(II), palladium(II), and gold(III). Their coordination mode, forming four-membered S,N coordinated metallocycles, contrasts with the related monoacylated acylthiourea analogues. Moreover, the inclusion of a second acyl group onto the thiourea core allows for additional chalcogen and hydrogen bonding interactions which dominate the structure of the complex. Finally, Chapter 6 presents a ruthenium cymene complex featuring a neutral monodentate diacylthiourea ligand. Non-covalent interaction analysis identifies chalcogen and hydrogen bonding as determining the structural arrangement, reinforcing the importance of these features in future applications.

Collectively, this thesis provides a comprehensive foundation for understanding the coordination chemistry of functionalized thiourea ligands bearing electronegative substituents, opening avenues for their tailored use in fields ranging from catalysis to medicinal chemistry.

Acknowledgments

First and foremost, I must acknowledge my supervisors Graham Saunders, Bill Henderson and Jo Lane, without whom this PhD would not be possible. Through your guidance, advice and patience I have grown in many respects and am ever grateful. I must give special thanks to Graham who took on the responsibility of chief supervisor following Bill's retirement. Your willingness to allow me to follow my own research path, however your ever presence for advice and guidance is greatly appreciated and has helped me shape my research independence. Secondly, I must give many special thanks to Bill who started my research journey many years ago and despite his retirement continued to provide his greatly appreciated advice when needed.

I would also like to extend my heartfelt acknowledgments to the entire C3.04 research group, past and present. Not only have you provided me with wonderful knowledge and experiences which have made me a better researcher, you have also provided many years of great friendship. I am thankful to have had the privilege to research with you all. I would be remised if I did not also thank the wonderful technical staff Jenny, Annie and Karla who provided their support and expertise throughout my degree. Also, the many wonderful academic staff whom I have had the privilege to work with in my many diverse roles within the university.

My heartfelt thanks to my wonderful parents who provided their unending support throughout not only my PhD but also my entire academic journey. Your contributions are not held lightly and will not be forgotten, I will be ever grateful.

Lastly, but not least, I must extend my thanks to my wonderful partner. Doing a PhD can be a very lonely and difficult period and having someone whom provides not only their understanding but their unequivocal love and support is never be forgotten. I am thankful beyond words.

Table of contents

List of Figures

List of Schemes

List of tables

List of abbreviations

NMR - Nuclear Magnetic Resonance

Hz - Hertz

J - Coupling Constant (in Hz)

ppm - parts-per-million

δ - chemical shift (in ppm)

MHz - Megahertz

ESI-MS - Electrospray Ionization Mass Spectrometry

m/z - mass-to-charge ratio (ESI-MS)

XRD - x-ray diffraction

Å - Angstrom

mp - melting point

COD - 1,5-cyclooctadiene

Dppe - 1,2-bis(diphenylphosphino)ethane

Dppp - 1,3-bis(diphenylphosphino)propane

Bipy - 2,2'-bipyridine

tolyl - *p*-tolyl substituent

bp – 2-benzylpyridyl substituent

PPh_3 - triphenylphosphine

TCEP - tris(2-cyanoethyl)phosphine

PTA – 1,3,5-triaza-7-phosphaadamantane

Py - Pyridine

cym – *p*-cymene

Cp* - pentamethylcyclopentadienyl

en - ethylenediamine

DMF - dimethylformamide

$CDCl_3$ - deuterated chloroform

DMSO - dimethyl sulfoxide

phen - 1,10-phenanthroline

anp - 2-anilinopyridyl

Publications included in this thesis

Chapter 1

Risi, M. C. (2024). A review of the synthesis and coordination of some lesser studied thiourea ligands bearing electronegative sulfonyl, phosphoryl and cyano substituents towards platinum group and related metal centers. *Journal of Coordination Chemistry*, *77*(15-16), 1679-1699.

Chapter 2

Risi, M. C., Lane, J. R., Henderson, W., & Saunders, G. C. (2024). Chalcogen bond stabilization of platinum (II) sulfonyl-substituted thiourea complexes with ancillary phosphine ligands. *Inorganica Chimica Acta*, *561*, 121850.

Chapter 3

Risi, M. C., Stjärnhage, J., Henderson, W., Lane, J. R., Hartinger, C. G., & Saunders, G. C. (2025). The coordination chemistry and anticancer activity of organo-ruthenium (II),-iridium (III) and -rhodium (III) complexes with sulfonyl-substituted thiourea ligands. *Dalton Transactions*, *54*(2), 539-549.

Chapter 4

Risi, M. C., Henderson, W., & Saunders, G. C. (2024). Platinum (II) phosphoryl-substituted thiourea complexes with bis-phosphine ligands and some triphenylarsine and triphenylstibine analogues. *Polyhedron*, *255*, 116992.

Chapter 5

Risi, M. C., Atiga, S., Christopher, T. D., Henderson, W., & Saunders, G. C. Diacylthioureas - an overlooked class of ligands; the coordination chemistry of diacylated thiourea with platinum(II) palladium(II) and gold(III). *Dalton Transactions*, *54*(12), 4977-4989.

Chapter 6

Risi, M. C., & Saunders, G. C. (2025). The first organometallic complex bearing a diacylthiourea ligand. *Journal of Organometallic Chemistry*, *1032*, 123636.

Chapter One

Lesser studied thiourea ligands bearing electronegative sulfonyl, phosphoryl and cyano substituents towards platinum group and related metal centres

Thiourea, $H_2NHC(S)NH_2$, and its related derivatives constitute a diverse group of organosulfur ligands which have garnered widespread interest and attention within practically all realms of chemistry (Figure 1.1).[1, 2] This interest is in no small part because of the ease of synthesis and the facile substitution of the two nitrogen atoms on the core moiety. In combination, these reasons result in a large array of substituted and functionalized derivatives, which are often considered to be classes of ligands in their own right.

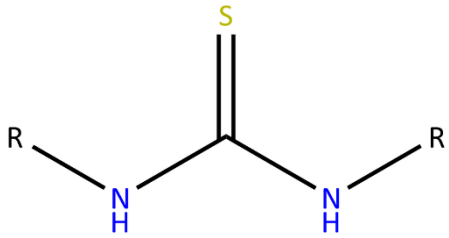

Figure 1.1: General structure of thiourea (R = H) and thiourea derivatives (R = alkyl or aryl).

Thiourea and its derivatives have demonstrated a broad spectrum of applications, serving as antibacterial agents,[3-6] catalysts,[7] antioxidants,[8] and contributors to metal recovery.[9, 10] Of particular relevance to this thesis, is the ability of thioureas to function as versatile ligands towards a large array of transition metal centres. This coordination versatility arises from the combination of the hard nitrogen and soft sulfur donor atoms which allows for a range of coordination possibilities. Typically, simple thioureas act as neutral ligands which bind to metal centres in a monodentate fashion through the thiourea sulfur donor atom.[11] However, they

may also act as mono[12, 13] or dianions.[14, 15] often chelating the metal centre in a four-membered M-S-C-N ring system (Figure 1.2).

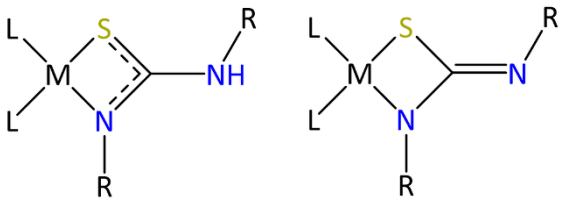

Figure 1.2: Four-membered M-S-C-N coordination mode with mono- and dianionic thiourea ligands. R = H or alkyl, aryl.

The two thiourea nitrogen atoms are easily substituted, leading to mono-, di-, tri-, or more rarely, tetra-substituted derivatives. The coordination chemistry of these functionalized derivatives can differ in some significant ways from the parent ligand, and for this reason, are often differentiated as their own distinct class of ligands. An illustrative and well-studied example is the acylthiourea class of thiourea ligands, where substitution with an acyl group (e.g., benzoyl) leads not only to a new class of thiourea ligand, but also introduces distinct coordination modes by adding a new oxygen donor atom. Acylthioureas have been extensively studied in the literature because of their numerous potential applications,[2, 16] such as their biological[17, 18] and catalytic abilities.[19, 20] As a consequence of the additional oxygen donor atom, acylthioureas have shown a distinct preference for coordination *via* the thiourea sulfur and acyl oxygen atoms to form six-membered M-S-C-N-S-O ring chelates (Figure 1.3). Coordination in this way offers the stability of a six-membered ring motif and is the most common coordination mode for this class of ligands.[16, 21, 22] Although, significantly less common, four-membered *S,N* chelated complexes with acylthioureas are also reported (Figure 1.3), particularly as bidentate ligands for piano-stool complexes of the group 8 and 9 metals.[23]

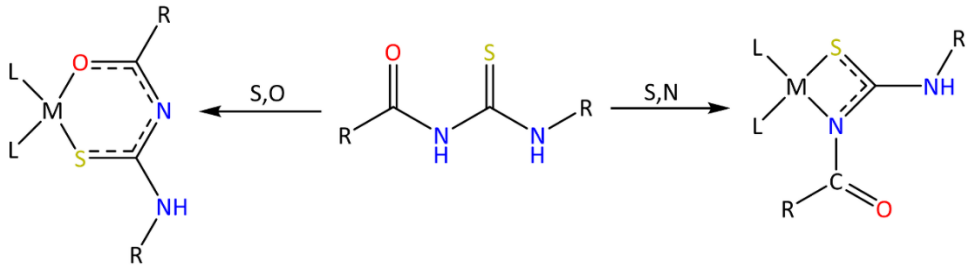

Figure 1.3: Structure and coordination modes of acylthiourea ligands. R = H or alkyl, aryl.

While acylthioureas have received considerable attention, thiourea ligands with other electronegative substituents, such as sulfonyl (RSO_2-), phosphoryl (R_2PO-) and cyano (NC-) thioureas, are much less explored. Moreover, the use of these functionalized thioureas as ligands, especially as mono- or dianionic ligands, remains largely underdeveloped. These similar but distinctly different thioureas represent a potentially overlooked area of coordination chemistry.

1.1 Sulfonylthioureas

Sulfonyl-substituted thioureas, $RSO_2NHC(S)NHR$ (Figure 1.4), most likely prompted by the historical success of sulfonamide pharmaceuticals, have garnered some interest for their potential medical and pharmaceutical applications, including studies exploring their use as anti-thyroid compounds[24] and human carbonic anhydrase inhibitors.[25] Despite this medicinal promise, the exploration of sulfonylthioureas as ligands towards transition metal centres and their applications are seldom explored.

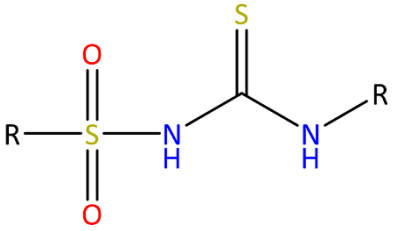

Figure 1.4: General structure of disubstituted sulfonylthiourea R = H or alkyl, aryl

Sulfonylthioureas are able of coordination *via* the core thiourea *S,N* donor atoms, creating a four membered M-S-C-N ring chelate. In principle sulfonylthioureas may also coordinate *via* the core S and sulfonyl O atoms, in a six-membered M-S-C-N-S-O ring chelate, however, no examples of coordination by this mode are reported. Moreover, coordination by the *S,N* donor atoms leads to the formation of two distinct linkage isomers: coordination by the S and N-alkyl atoms herein termed the *distal* linkage isomer (the sulfonyl group being away from the coordination centre) or by the *S,N*-sulfonyl atoms, herein termed the *proximal* isomer (Figure 1.5).

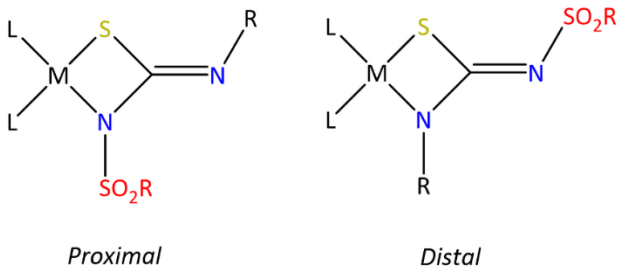

Figure 1.5: General structures of proximal and distal linkage isomers of sulfonylthiourea ligands. R = H or alkyl, aryl

1.1.1 Synthesis of sulfonylthioureas

An early recorded synthetic route for mono-substituted sulfonylthiourea was reported by Arquet and Charpentier in their 1950s patent for the preparation of various aryl sulfonylthioureas.[26] The synthesis involves a simple treatment of hydrogen sulfide with a corresponding aryl sulfonyl cyanamide to yield the corresponding sulfonylthiourea with the general formula $RSO_2HNC(S)NH_2$ (Figure 1.6). While this method provides a straightforward route, the flexibility of the target compound is greatly limited to the variability of the sulfonyl cyanamide. Instead, a more common synthetic route is outlined by Shah *et al,* which involves a simple nucleophilic addition of an alkyl or aryl sulfonamide to an isothiocyanate mediated by alkaline conditions (Figure 1.6),[27] typically achieved using sodium hydroxide, potassium carbonate[28] or more recently potassium and sodium *tert*-butoxides.[25] This route results in a disubstituted sulfonylthiourea of the general formula $RSO_2HNC(S)NHR'$. Synthesis of sulfonylthioureas by this route still remains

the common choice because of its ease, low cost, and the relative abundance of sulfonamide starting materials.

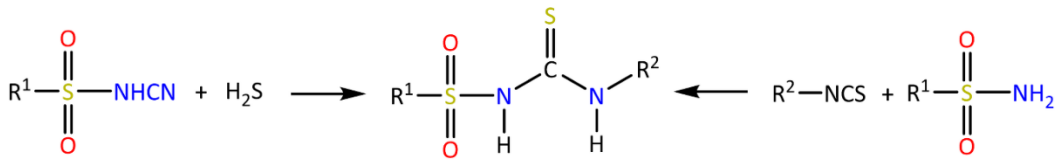

Figure 1.6: Synthetic routes for mono- or disubstituted sulfonylthiourea ligands. R = H or alkyl, aryl

More recently, driven primarily by interest in pharmaceutical applications, alternative methods for the synthesis of sulfonylthioureas using atom-efficient and green chemistry techniques have been explored. One such method is proposed by Ding *et al*, which involves an aqueous phase reaction under mild conditions and short reaction times.[29] The method entails adding a solution of the sulfonamide potassium salt, RSO_2NHK, dropwise to a solution of a dithiocarbonate which results in the corresponding sulfonylthiourea in yields similar to more traditional methods. Another alternative method is presented by Tan *et al*, who were first to demonstrate the use of mechanochemistry in the synthesis of sulfonylthioureas.[30] Base-assisted mechanosynthesis of the sulfonylthiourea with the formula ($TolSO_2NHC(S)NHPh$) was conducted on the gram scale with equal molar amounts of sulfonamide, K_2CO_3 and isothiocyanate. The sulfonylthiourea $TolSO_2NHC(S)NHPh$ (Tol= *p*-tolyl, $CH_3C_6H_4$) was formed in high yield (91%) and high purity.

1.1.2 Coordination of sulfonylthioureas

Three coordination modes are possible for sulfonylthiourea ligands. The first mode is monodentate *via* the core thiourea sulfur donor atom when the ligand acts as a neutral ligand.[31] The second mode is bidentate *via* both the core thiourea S and either one of the two non-equivalent N donor atoms,[32-34] and finally, in principle, bidentate *via* the core thiourea S and one of the O donor atoms of the sulfonyl

group. The latter two are typically exhibited by sulfonylthioureas acting as mono- or dianionic ligands.

1.1.2.1 Sulfonylthiourea acting as monoanionic ligands

Research on metal complexes derived from sulfonylthiourea ligands can be categorized into two distinct periods: the late 1980s to 1990s literature, and more recent advancements. Early work, albeit somewhat esoteric because of limited accessibility and insufficient characterization, indicates a preliminary tendency for sulfonylthiourea ligands to act as monoanionic ligands towards transition metal centres. The earliest of these complexes were reported by Uhlig and Doering in 1988 in the investigation of aryl sulfonated thioureas for metal extraction, resulting in the synthesis of several Cu(II), Ni(II), and Co(II) ML_2 complexes.[32] As a result of IR (Infrared spectroscopy), EPR (Electron paramagnetic resonance) and XPS (X-ray photoelectron spectroscopy) characterization data, the Cu(II) and some Co(II) complexes were assigned the four-membered M-S-C-N bidentate coordination mode while the Ni(II) and some Co(II) complexes were assigned the six-membered M-S-C-N-O coordination mode. Subsequent studies examining sulfonylthiourea ligands towards period 4 transition metals were also observed to observe these trends.[33-38] During this period of research, the first sulfonylthiourea complexes with platinum group metals were reported by Koenig *et al.* in their investigation of the fluorescent metal detection ability of dansyl derived sulfonyl thiourea ligands.[37] The Pt(II) and Pd(II) complexes, as well as the other reported complexes, were all assigned the six-membered M-S-C-N-O coordination mode.

A later study by Schuster and Sandor,[39] also investigating dansyl derived sulfonylthiourea ligands, gave the most comprehensive array of metal centres reported thus far. L_3M complexes were reported with the metal centres Cr(III), Mo(III), W(III), Ru(II) Os(II), Rh(III), Ir(III), Au(III), In(III), Sb(III) and Bi(III) and L_2M complexes with Mn(II), Co(II), Ni(II), Pd(II), Pt(II), Cu(II), Zn(II), Cd(II), Hg(II) and Pb(II). The complexes were assigned the four-membered coordination mode with the exception of Ni(II) which was assigned the six-membered coordination mode.

While these early reports indicate the formation of some M-S-C-N-S-O six-membered chelates, predominantly indicated by IR spectroscopy and similar techniques, no definitive structural characterization was provided. To remedy this, a recent study by Beele, Bill and Mohr reports a crystallographic investigation of some previously reported ML_2 complexes with sulfonylthioureas with metal centres Ni(II), Co(II), Cu(II), Zn(II) in an effort to unequivocally determine the adopted coordination mode.[40] The investigation revealed that despite earlier attempts to characterize these complexes as *S,O* coordinated they were determined by single crystal X-ray diffraction to be *S,N* coordinated instead (Figure 1.7).

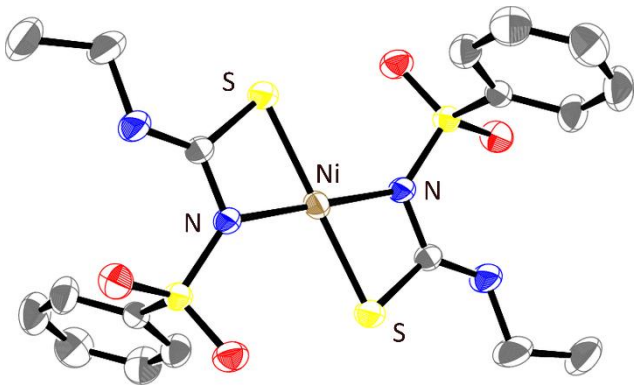

Figure 1.7: Molecular structure of [Ni{PhSO$_2$NC(S)NHEt}$_2$]. Hydrogen atoms removed for clarity and ellipsoids shown at 50% probability levels.[40]

1.1.2.2 Sulfonylthioureas acting as dianionic ligands

All of the historical reports of sulfonylthiourea ligands centre on bis-thiourea complexes in which the ligand acts as a monoanion. Only recently has mixed ligand complexes with dianionic sulfonylthiourea ligands been reported. Recently, we have published our pilot studies on the chemistry of sulfonylthioureas acting as dianionic towards the d^8 centres Ni(II), Pt(II), Pd(II) and cyclometallated Au(III).[41] This work was completed as part of a prior University of Waikato master's degree project and does not form part of the work of this thesis. The sulfonylthiourea complexes featuring triphenylphosphine, 1,2-bis(diphenylphosphino)ethane

(dppe), 1,2-bis(diphenylphosphino)propane (dppp), 2,2'-bipyridine and 2-benzylpyridine (bp) ancillary ligands were characterized by ESI-MS (Electrospray ionization mass-spectrometry), NMR (Nuclear Magnetic Resonance spectroscopy), IR and SC-XRD (Single crystal X-Ray diffraction). Like the bis-sulfonylthiourea complexes reported previously by Mohr and coworkers, the complexes were revealed to be *S,N*-coordinated (Figure 1.8) and were also revealed to be exclusively in the *distal* linkage isomer (*S,N*-alkyl). No evidence of the *S,O* coordination mode was obtained from this study.

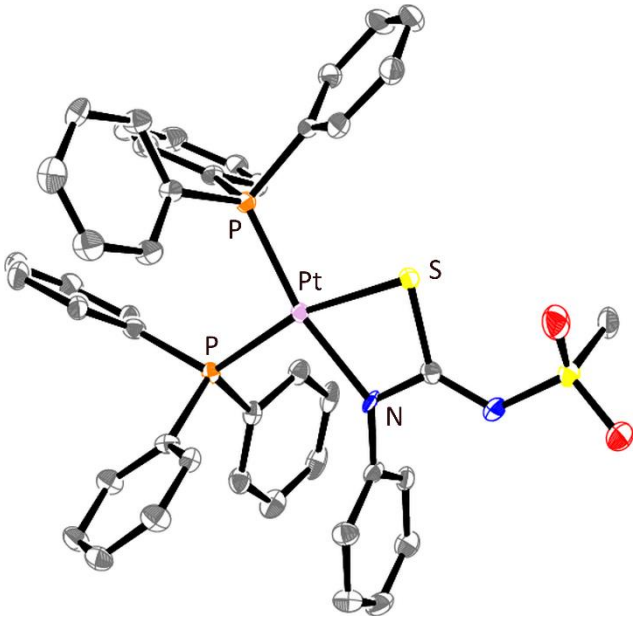

Figure 1.8: Molecular structure of [Pt{MeSO₂NC(S)NPh}(PPh₃)₂]. Hydrogen atoms removed for clarity and ellipsoids shown at 50% probability levels.[34]

1.1.2.3 Sulfonylthioureas as a source of sulfide.

It is known that thioureas may act as a source of sulfide in reactions involving metal ions. Sulfonylthiourea complexes may also undergo desulfurization, theorized to be a result from the hydrolysis of the C-S thiourea bond of the metal complex. This desulfurization is likely promoted by a reduction of electron density around the central thiourea carbon, as a consequence of the sulfonyl substituent, making sulfonylthiourea complexes more susceptible to nucleophilic attack by water and/or hydroxide. This can result in stable metal aggregates, for example,

the trinuclear palladium[42] sulfido aggregate $[Pd_3(\mu\text{-}S)_2(dppe)_3]^{2+}$ which was observed to form in solutions of the sulfonylthiourea complex $[Pd\{TolSO_2NC(S)NPh\}(dppe)]$ over extended periods or elevated temperatures.[41]

1.2 Phosphorylthiourea

Phosphoryl-substituted thioureas, $R_2P(O)NHC(S)NHR$ (Figure 1.9), similar to acylthioureas, have the capacity to coordinate to metal centres in both four-membered *S,N* and six-membered *S,O* coordination modes and are able to function as either neutral, mono-, or dianionic ligands. Interestingly, literature concerning phosphorylthioureas bearing exclusively alkyl substituents on the phosphorus atom (R_2PO-) is relatively few when compared to the significantly more prevalent ester-containing counterparts ($(RO)_2PO$-). This observation is most likely a consequence of the significantly reduced solubility of the alkyl-phosphoryl ligands. Research on alkyl-containing phosphoryl thioureas is primarily concentrated between 1968 and 1987, with relatively limited recent studies. Conversely, ester-containing phosphorylthioureas have attracted considerable attention, most likely a result of the accessibility and low cost of starting materials and straightforward synthetic routes. Recent investigations into ester-containing phosphorylthioureas have explored their potential in various biological applications, including HIV inhibition[43] and antimicrobial activity.[44]

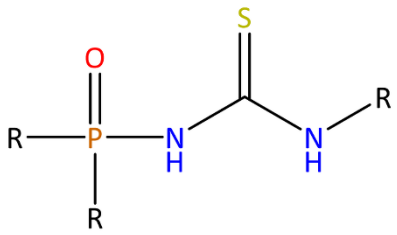

Figure 1.9: General structure of phosphorylthiourea. R = H or alkyl, aryl

1.2.1 Synthesis of Phosphorylthioureas

A common method for the synthesis of thiourea ligands is the reaction between a primary or secondary amide with an isothiocyanate in the presence of a base. In

the case of functionalized thioureas, either the amine or isothiocyanate can bear the functional group, for example, sulfonylthioureas and their corresponding sulfonamides (RSO_2NH_2). Interestingly, only two examples of phosphorylthioureas have been reported to be synthesized in this manner. Both examples were provided by Subramanyam *et al*. in their 2012 study of the synthesis and antimicrobial activity evaluation of phosphorylated urea/thiourea derivatives.[44] In both cases, diethylphosphonic amide reacted with either allyl or aryl isothiocyanate in the presence of triethylamine base to produce the corresponding phosphorylthiourea (Figure 1.10).

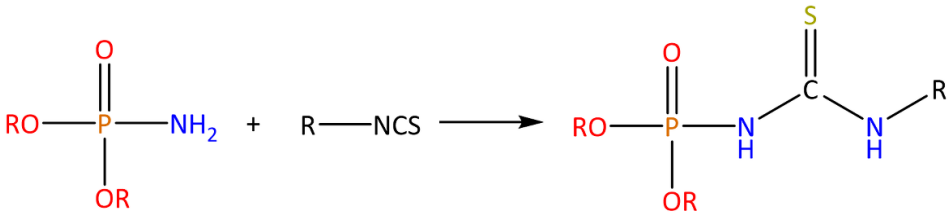

Figure 1.10: Synthesis of phosphorylthiourea from di-phosphoramidate and isothiocyanate. R = H or alkyl, aryl

Phosphorylthioureas are more commonly synthesized by isothiocyanates bearing the P=O functionality reacting with alkyl or aryl amides (Figure 1.11).[45-49] Of note is the distinctive absence of base mediation in reactions involving phosphoryl isothiocyanates because of their increased reactivity towards nucleophilic addition. These phosphoryl-substituted isothiocyanates are typically synthesized from dialkyl or diphenyl phosphites or phosphinyl acids with thiocyanogen *via* a thiocyanate intermediate.[50, 51] This intermediate quickly undergoes isomerization, leading to the final substituted isothiocyanate.[52]

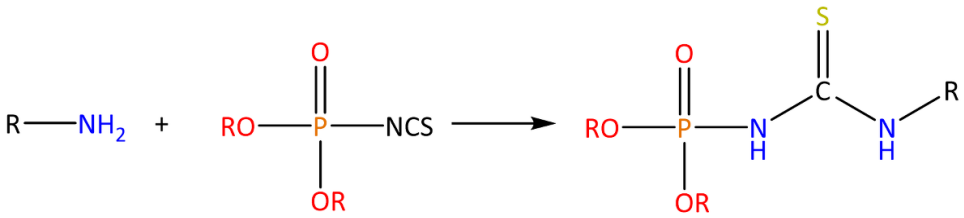

Figure 1.11: Synthesis of phosphorylthiourea from an amide and phosphonic isothiocyanate. R = H or alkyl, aryl

Other examples of alkali pseudohalogenides have also been used in the preparation of functionalized isothiocyanates, such as potassium thiocyanate,[53, 54] which results in the isothiocyanates of the corresponding dialkylphosphoric acid. Potassium thiocyanate is a common reagent in the synthesis of many functionalized isothiocyanates for the preparation of functionalized thioureas. Alternatively, a one-pot procedure involving the reaction of a phosphinyl chloride (diphenyl phosphinyl chloride) with ammonium thiocyanate in the presence of a catalyst (PEG-400), followed by the addition of an amine, has been reported.[55] This method leads to the target phosphinyl thiourea with easy purification and moderate yields.

1.2.2 Coordination of Phosphorylthiourea

While still somewhat obscure compared to the more common acylthioureas, examples of coordination compounds derived from phosphorylated thioureas are notably more common than other lesser-studied functionalized thioureas. Recent examples of phosphorylthioureas coordinating as neutral monodentate ligands and as monoanionic bidentate ligands in both the four-membered[56] M-S-C-N and six-membered[56,57] M-S-C-N-P-O coordination modes are reported (Figure 1.12). The latter is the more commonly observed coordination mode because of the effectiveness of the P=O donor. Of these complexes, only phosphorylthiourea ligands with phosphorus-ester substituents have been reported, presumably due to the reduced solubility of the phosphorus-alkyl analogues. The vast majority of phosphorylthiourea complexes reported to date are mono-ligand of the type L_2M with the exception of selected six-coordinate Ni(II), Zn(II), and Cd(II) mixed ligand complexes bearing the neutral ligands pyrazine, pyridine, and phenanthroline[45] and also with solvent molecules acting as ligands such as dimethylformamide. To date, no examples of phosphorylthiourea ligands acting as dianions towards transition metal centres have been reported.

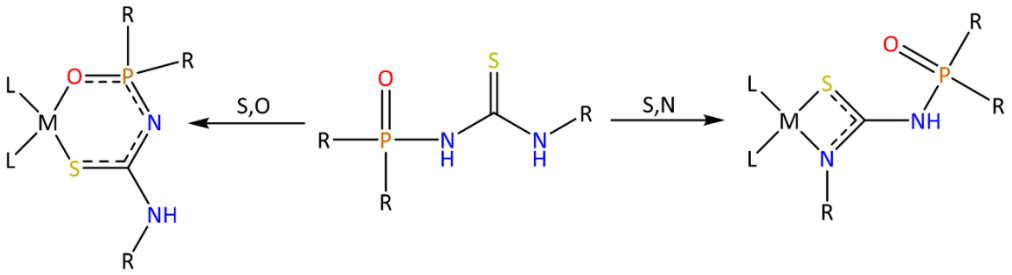

Figure 1.12: S,N and S,O coordination modes of phosphorylthiourea ligands[56,57] R = H or alkyl, aryl

1.2.2.1 Phosphorylthiourea acting as monoanionic ligands

In recent (post-2000) literature, the first example of a metal complex containing a phosphorylthiourea monoanionic ligand was reported in 2005 by Sokolov *et al.* in their study of the Zn(II) and Cd(II) chelate complexes of bis-N-thiocarbamoylamidophosphates.[57] Complexes with Zn(II) were synthesized from the potassium salt of the phosphorylthiourea ligand and were assigned to the six-membered M-S-C-N-P-O coordination mode. Similarly, the six-coordinate mixed ligand solvato complexes of the formula $Cd(DMF)_2L_2$, which contain DMF coordinated as a neutral ligand in each of the axial positions of the structure, were also prepared (Figure 1.13).

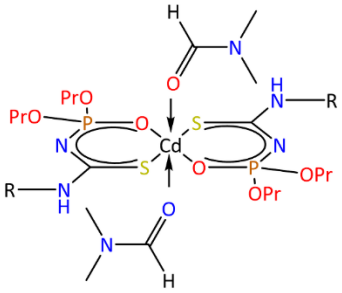

Figure 1.13: General structure of $Cd(DMF)_2L_2$. R = H or alkyl, aryl.[57]

Slightly later, the same team and co-workers studied the coordination diversity of N-phosphoryl-N'-phenylthiourea towards Co(II), Ni(II), and Pd(II) metal centres.[56] This study provides the first reported example of the four-membered (M-S-C-N) coordination mode observed for such ligands. Single crystal XRD analysis of the Ni(II) and Pd(II) complexes (Figure 1.14) shows an expected distorted square

planar MN_2S_2 environment with a *trans* configuration of the ligands, which is analogous to traditional thioureas coordinating in this mode.[56] Conversely, the same ligand chelates Co(II) in the six-membered (M-S-C-N-P-O) coordination mode, resulting in a tetrahedral geometry and CoO_2S_2 environment around the metal centre.

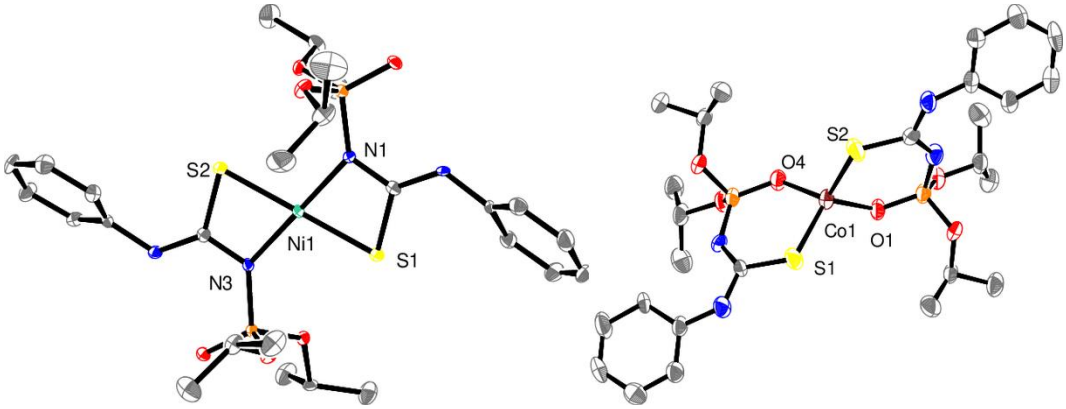

Figure 1.14: Molecular structure of [Ni{PhC(S)NP(O)(OiPr)$_2$}$_2$ and [Co{PhC(S)NP(O)(OiPr)$_2$}$_2$]. Hydrogen atoms removed for clarity and thermal ellipsoids shown at 50% probability.[56]

Following these results, two papers were published by Safin *et al,* exploring phosphorylthioureas containing crown ether and N-thioacylamidophosphates towards Zn and Co.[58,59] Slightly later in 2007, several papers examining the coordination structures and properties of phosphorylthiourea-derived complexes with the metal centres Ni(II), Pd(II), Co(II), Zn(II), and Cd(II) were reported. The bulk of these complexes coordinated in the expected six-membered (M-S-C-N-P-O) coordination mode,[60-62] with a few examples of the four-membered (M-S-C-N) coordination mode being shown for the metal centres Ni(II) and Pd(II).[63, 64] From 2008 to 2013, several papers by Safin and team examined the coordination of monoanionic phosphorylated thiourea ligands towards metal centres Co(II), Ni(II), Zn(II), Pd(II), Cd(II). The coordination modes observed for the complexes were primarily in the common six-membered coordination mode,[63, 65-72] with examples also reported of the less common four-membered coordination mode,[42, 47, 68-71] the latter only being observed for the metal centres Ni(II), Zn(II) and Pd(II). Another paper by the same authors studying the synthesis, characterization, and complexation properties of N-phosphorylated thioureas RNHC(S)NHP(O)(OiPr)$_2$ (R = 2-Py, 3-Py) towards Ni(II) metal centres reported a phosphorylated thiourea

ligand bearing a 2-pyridyl group as a substituent (Figure 1.15).[48] The ligands coordinate to the Ni metal centre through the nitrogen atoms of both the pyridine and the thiourea core as well as the phosphoryl P=O donor atom in a tridentate manner.

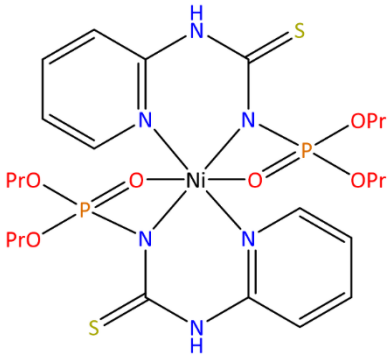

Figure 1.15: Structure of a tridentate 2-PyNHC(S)NHP(O)(OiPr)$_2$ Ni complex.[48]

Following these reports by Safin and team, Babashkina *et al*. reported the synthesis of a neutral 1D coordination polymer from a phosphorylthiourea Ni(II) complex linked together by pyrazine, providing a potential single-source precursor for nickel nanoparticles and metal-organic frameworks (MOFS).[45] Of interest is the observed change in coordination mode upon polymerization of individual complexes. Initial synthesis of the L_2M complex *via* the potassium salt of the phosphorylthiourea ligand led to a square-planar complex in the four-membered coordination mode, frequently observed for such nickel complexes. Further coordination of an additional donor ligand, pyrazine, led to polymerization of the complex. An apparent change in coordination from the four-membered to the six-membered P=O and C=S coordination mode is observed upon reassignment (Figure 1.16). This change in coordination mode is directly observed by comparing the single crystal XRD structures of both the single complex and polymer.

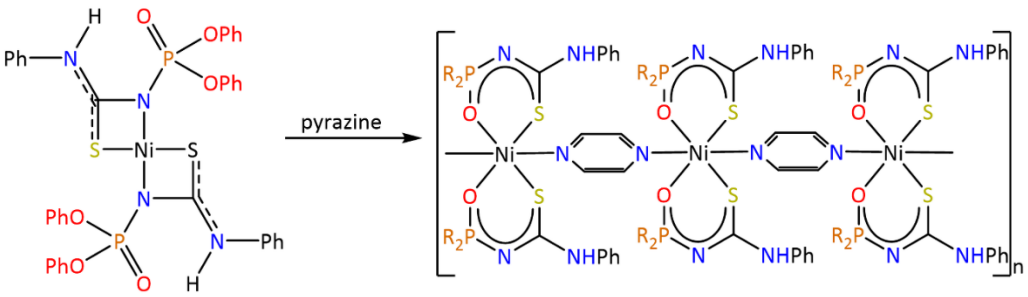

Figure 1.16: Polymerized phosphorylthiourea Ni complex with pyrazine.[45]

1.3 Cyanothioureas

Cyano-substituted thioureas (Figure 1.17), (RNHC(S)NHCN), represent a class of thiourea compounds characterized by the presence of a cyano functional group on one of the core thiourea nitrogen atoms. Several recent potential applications are reported, such as uses as antioxidants,[73] antiviral agents,[74] and anti-tumor agents.[75] Cyanothiourea ligands are comparable to the previously discussed functionalized thioureas: acylthioureas, sulfonylthioureas, and phosphorylthioureas, because of their shared presence of an electronegative substituent on the core thiourea moiety. However, unlike the previous thioureas, the additional functional group cannot chelate because of the geometry of the ligand. Instead, the cyano substituent may act as a bridging ligand. Therefore, the coordination chemistry of cyanothioureas ligands is limited to monodentate (S) or (CN) and bidentate (S and N) binding modes. While many cyanothiourea compounds are known within the literature, their ability to act as versatile ligands towards transition metal centres is seldom explored.

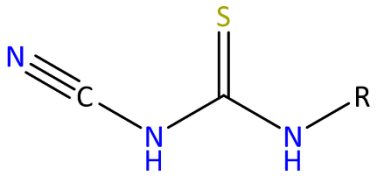

Figure 1.17: General structure of cyanothioureas. R = H or alkyl, aryl

1.3.1 Synthesis of cyanothioureas

The synthesis of cyanothioureas is usually achieved by an equimolar reaction of an isothiocyanate and cyanamide[73, 76, 77] (or the sodium salt thereof)[76] to produce the corresponding thiourea (Figure 1.18). An early reported example is given in 1980 by Jefferson *et al*. in their investigation of 2-aminoethyl thiourea derivatives.[78] This method involves the addition of cyanamide to a sodium ethoxide solution, followed by the addition of an isothiocyanate. After stirring for one hour, the solution is concentrated followed by the addition of ether to precipitate the crude product. This synthetic scheme is similar to other functionalized thioureas, which typically involve a reaction between an isothiocyanate and amide, either of which bears the targeted functionality.[46, 79] In the case of reactions involving neutral cyanamide, a base is used to catalyse the reaction *via* deprotonation of the amine.[73] Alternatively, the sodium salt is used without the need for base assistance.

Figure 1.18: Synthesis of cyanothiourea ligands from an isothiocyanate and cyanamide. R = H or alkyl, aryl

Many alternative synthetic routes have also been reported which utilize an amine[80] or similarly by a reaction between a simple thiourea (such as diimidazole thiourea[77] or dipyridone thiourea[81]), cyanamide and an amine. In some cases, carbamothioic chloride ($R_2NC(S)Cl$) and thiophosgene ($CSCl_2$)[82] have been used as thiourea precursor backbones in reactions involving either a tertiary amine and sodium iodide or a primary amide and cyanamide, respectively. Although these and other minor synthetic routes are generally purpose-fit and are in the minority compared to general procedures involving simple isothiocyanates and cyanamide.

1.3.2 Coordination of cyanothiourea

Two coordination modes are available for cyanothiourea ligands: monodentate through the core thiourea sulfur[14] atom or bidentate through the core thiourea sulfur and one of the two non-equivalent nitrogen atoms (Figure 1.19).[83] The latter coordination mode results in a four-membered metallocycle. The distinctive lack of a third coordination mode, usually observed for functionalized thioureas, is a consequence of the added cyano functionality not containing possible donor atoms that are able to chelate. Instead, cyanothioureas can be thought to resemble traditional thioureas. Because of the non-equivalence of the core thiourea nitrogen atoms, the bidentate four-membered S and N coordination mode of the corresponding metal complexes can be in one of two isomers. In the case of complexes derived from monoanionic cyanothioureas ligands, isomerization has been observed between the two configurations.

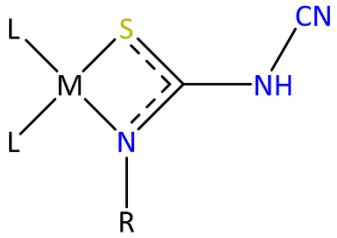

Figure 1.19: general S,N coordination mode of cyanothiourea ligands shown as its monoanion. R = H or alkyl, aryl.[83]

1.3.2.1 Cyanothiourea acting as monoanionic ligands

Metal complexes derived from cyanothiourea monoanions have been reported relatively recently in comparison to other functionalized thioureas. The first reported complex was documented in 2001 by Henderson and his team in their study of platinum complexes derived from thiourea monoanions incorporating chiral, fluorescent, or chromophoric groups.[83] Among the many thiourea complexes reported, a single monoanionic cyanothiourea complex derived from the commercially available sodium salt of methyl cyanothiourea (Na[MeNHC(S)NCN]) ligand is described. The complex was isolated as its cation using sodium tetraphenylborate after the successful ligand substitution of *cis*-

$[PtCl_2(PPh_3)_2]$ in methanol. The resulting complex, contained the cyanothiourea ligand coordinating to the metal centre *via* the core thiourea S and N atoms in the *distal* linkage isomer (a remote cyano group), resulting in a four-membered chelating coordination mode (Figure 1.20). Analysis by NMR revealed a mixture of both possible isomers in a *distal* - *proximal* ratio of 4:1.

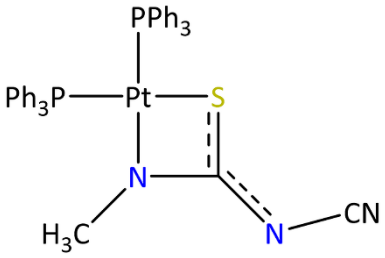

Figure 1.20: Methyl cyanothiourea platinum triphenylphosphine complex in the distal isomer

In 2002, Henderson and team reported monoanionic cyanothiourea Cp* (1,2,3,4,5-pentamethylcyclopentadienyl) rhodium(III) complexes in the monodentate (*via* S) coordination mode.[14] These complexes were synthesized by treatment of previously prepared bidentate dianionic cyanothiourea complexes with aqueous hydrochloric acid (Figure 1.21). The resulting cleavage of the Rh – N bond of the dianionic complex resulted in the corresponding monoanionic complex containing a monodentate S bonded cyanothiourea. Single crystal XRD analysis of one such monodentate complex, $[Cp^*RhCl\{SC(=NCN)NHMe\}(PPh_3)]$, confirmed the monodentate coordination mode and revealed the geometry of the complex to be the archetypal piano stool structure around the rhodium metal centre.

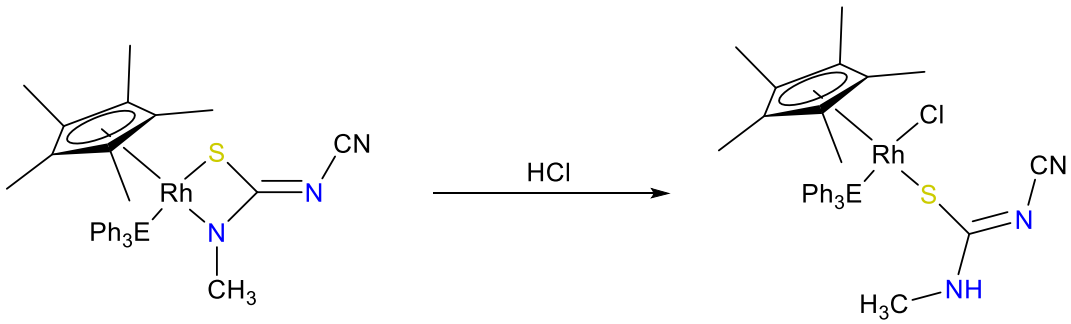

Figure 1.21: Treatment of dianionic cyanothiourea complexes with aqueous hydrochloric acid. R = H, alkyl or aryl. E = P, As or Sb.[14]

The most recent reported example of a monoanionic cyanothiourea complex is given in 2005 by Henderson and team in their study on the synthesis, characterization, supramolecular aggregation, and biological activity of phosphine gold(I) complexes with monoanionic thiourea ligands.[84] A series of phosphine gold(I) complexes containing monoanionic thiourea ligands is reported including examples of multi-ligand cyanothiourea complexes derived from Ph_3PAuCl and $dppe(AuCl)_2$ with the commercially available monoanionic thiourea salt, Na[MeNHC(S)NCN]. Single crystal XRD of these complexes revealed a linearly coordinated gold centre defined by S and P donor atoms, as is typical for thiourea monodentate complexes of this kind. Interestingly, examination of the torsion angles reveals the formally S–C=N1–R thiourea residue is essentially planar, indicating delocalization of π-electron density. However, this does not extend to the remainder of the motif as evident from the significant torsion angle between the C-N2-R containing portion of the thiourea core.

1.3.3 Cyanothiourea acting as dianionic ligands

During the publication history of cyanothiourea monoanionic complexes, a number of papers reporting cyanothioureas acting as dianionic ligands have simultaneously been reported by Henderson and team. The first was reported in 1996 as part of a study on the synthesis and electrospray mass spectrometry of platinum complexes derived from thiourea dianionic ligands, including a series of platinum cyanothiourea complexes. These complexes are analogous to the previously discussed monoanionic platinum complexes. Interestingly, unlike the analogous monoanionic complex, no isomerization was detected in the NMR spectrum. The complex consists of a dianionic cyanothiourea ligand coordinating to the platinum metal centre in the four-membered S and N bidentate coordination mode in the *distal* isomer (remote CN). The geometry around the platinum metal centre is in the expected and typical square planar configuration in a *cis* configuration.

Henderson and team further explored the coordination chemistry of cyanothiourea compounds acting as dianionic ligands in their study of thiourea

mono and dianionic complexes with metal centres rhodium(III) and ruthenium(II).[14] Both di and mono nuclear complexes are reported with the commercially available sodium salt of the methane cyanothiourea ligand, Na[MeNHC(S)NCN]. The former, binuclear complexes were synthezied from $[LMCl(\eta\text{-}Cl)]_2$, [M = Rh, L = η^5-C_5Me_5 (Cp*); M = Ru, L = η^6-*p*-cymene]. The ruthenium complex (Figure 1.22) was characterized by single crystal XRD and revealed the dimeric nature of the complex containing two η^6-*p*-cymene ruthenium groups linked by two cyanothiourea dianion ligands. The coordination of the ligand to the metal centre is in the bidentate four-membered coordination mode with a remote cyano substituent. The sulfur atom of the thiourea moiety bridges the second ruthenium metal centre creating a Ru-S-Ru-S ring system. The mononuclear complexes $[Cp^*Rh\{SCNCN)NMe\}(PPh_3)]$ and $[Cp^*Rh\{SCNPh)NPh\}(PPh_3)]$ contain the ligand bound as a dianion through the S and N centres in the four-membered coordination mode in the *distal* isomer with the archetypal piano stool geometry of the metal centre.

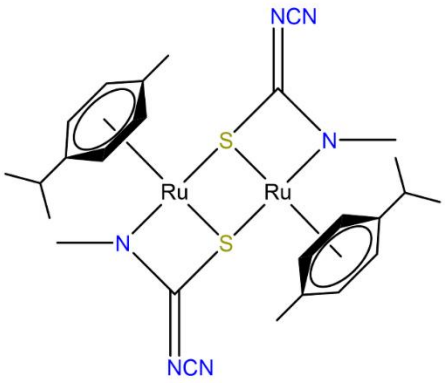

Figure 1.22: Dinuclear ruthenium cyanothiourea complexe containing bridging thiourea dianion ligands.[14]

1.4 Conclusions

The coordination chemistry of functionalized thioureas bearing electronegative substituents centres on bis-monoanionic thiourea ligands, with relatively few examples of complexes being reported with mixed or dianionic ligands. Moreover,

the bulk of the literature relating to these ligands appears before the year 2000, with very little work being done in modern times. The reason for the lack of recent attention for these functionalized thioureas may be a result of the assumption that the coordination chemistry of these ligands is closely related to their more prevalent acylthiourea counterpart. However, the content of this review have highlighted that this may not be the case. Sulfonylthioureas for instance, while in principle the sulfonyl group can participate in coordination, all of the reported complexes are *S,N* chelated like traditional unfunctionalized thioureas. However, unlike traditional thioureas, the presence of the sulfonyl group provides some biological implications and additional non-covalent interactions. It is clear that the chemistry of these sulfonyl, phosphoryl and cyanothiourea ligands is in its infancy and may represent overlooked classes of thiourea ligands.

1.5 Research aims

Research on the coordination chemistry of functionalized thiourea ligands, particularly those with electron-withdrawing substituents, remains surprisingly limited. This is notable given the extensive research and demonstrated success of closely related acylthiourea complexes, which have shown promise in fields such as catalysis, medicinal chemistry, and material sciences. The success of acylthioureas suggests that similar or even superior applications might be achieved by exploring thiourea-based complexes. Although existing studies have primarily focused on first-row transition metals and ML_2-type complexes, relatively little attention has been given to the interactions of these ligands with platinum group metals or in mixed ligand systems. This research gap may result from assumptions that thiourea ligands would behave analogously to acylthioureas, yet this review highlights some significant differences. Moreover, with applications in mind, subtle differences in the ligands can have a large influence on the desired effect which can only be discovered by experiment. It is known that thiourea and its functionalized derivatives provide versatile scaffolds for designing complexes with tailored chemical properties, making them promising for both biological and industrial applications. Electron-withdrawing substituents on these ligands influence their coordination modes and result in

unique properties that distinguish them from the closely related acylthiourea complexes. Therefore, establishing a foundational understanding of their coordination chemistry is a crucial first step in enabling future application-driven research. Thus, this thesis aims to advance knowledge on the coordination chemistry of specific, less-studied functionalized thiourea ligands, offering insights that can provide a foundation for future studies. To this end, single-crystal X-ray diffraction, mass spectrometry, NMR spectroscopy, and density functional theory (DFT) will be employed to thoroughly characterize their coordination behaviour. The broader significance of this work lies in the potential applications of these thiourea-based complexes in areas such as pharmaceuticals, where platinum-based compounds are already widely used. In this regard, Chapter 3 of this thesis contains a small study to evaluate initial potential in the area of cyto-toxic applications.

1.6 References

1. D. C. Schroeder, *Chemical Reviews*, 1955, **55**, 181-228.
2. A. Saeed, U. Flörke and M. F. Erben, *Journal of Sulfur Chemistry*, 2014, **35**, 318-355.
3. S. Karakuş and S. Rollas, *Il Farmaco*, 2002, **57**, 577-581.
4. B. Phetsuksiri, M. Jackson, H. Scherman, M. McNeil, G. S. Besra, A. R. Baulard, R. A. Slayden, A. E. DeBarber, C. E. Barry and M. S. Baird, *Journal of Biological Chemistry*, 2003, **278**, 53123-53130.
5. M. J. Di Grandi, K. J. Curran, G. Feigelson, A. Prashad, A. A. Ross, R. Visalli, J. Fairhurst, B. Feld and J. D. Bloom, *Bioorganic & Medicinal ChemistryLetters*, 2004, **14**, 4157-4160.
6. B. K. Kaymakçıoğlu, S. Rollas, E. Körceğez and F. Arıcıoğlu, *European Journal of Pharmaceutical Sciences*, 2005, **26**, 97-103.
7. Y. Takemoto, *Chemical and Pharmaceutical Bulletin*, 2010, **58**, 593-601.
8. T. Yeşilkaynak, H. Muslu, C. Özpınar, F. M. Emen, R. E. Demirdöğen and N. Külcü, *Journal of Molecular Structure*, 2017, **1142**, 185-193.
9. E. Guibal, T. Vincent and R. N. Mendoza, *Journal of Applied Polymer Science*, 2000, **75**, 119-134.
10. D. Nagai, M. Yoshida, T. Kishi, H. Morinaga, Y. Hara, M. Mori, S. Kawakami and K. Inoue, *Chemical Communications*, 2013, **49**, 6852-6854.
11. S. E. Livingstone, *Quarterly Reviews, Chemical Society*, 1965, **19**, 386-425.
12. T. S. Smith, W. Henderson and B. K. Nicholson, *Inorganica Chimica Acta*, 2013, **408**, 27-32.
13. W. Henderson, B. K. Nicholson and E. R. T. Tiekink, *Inorganica Chimica Acta*, 2006, **359**, 204-214.
14. W. Henderson, B. K. Nicholson, M. B. Dinger and R. L. Bennett, *Inorganica Chimica Acta*, 2002, **338**, 210-218.
15. J. E. Spenceley, W. Henderson, J. R. Lane and G. C. Saunders, *Inorganica Chimica Acta*, 2015, **425**, 83-91.
16. K. R. Koch, *Coordination Chemistry Reviews*, 2001, **216**, 473-488.
17. G. H. Ribeiro, A. R. Costa, A. R. de Souza, F. V. da Silva, F. T. Martins, A. M. Plutin and A. A. Batista, *Coordination Chemistry Reviews*, 2023, **488**, 215161.
18. S. Swaminathan, P. Jerome, R. J. Deepak, R. Karvembu and T. H. Oh, *Coordination Chemistry Reviews*, 2024, **503**, 215620.
19. N. Gunasekaran, N. Bhuvanesh and R. Karvembu, *Polyhedron*, 2017, **122**, 39-45.
20. M. E. Uysal, U. Solmaz and H. Arslan, *Polyhedron*, 2024, **247**, 116707.
21. H. A. Nkabyo, D. Hannekom, J. Mckenzie and K. R. Koch, *Journal of Coordination Chemistry*, 2014, **67**, 4039-4060.
22. H. Nkabyo, G. Bosman, R. Luckay and K. Koch, *Inorganica Chimica Acta*, 2020, **508**, 119644.
23. R. Gandhaveeti, R. Konakanchi, P. Jyothi, N. S. Bhuvanesh and S. Anandaram, *Applied Organometallic Chemistry*, 2019, **33**, e4899.
24. P. Srivastava, J. Upadhyaya and M. Gupta, *Current Science*, 1981, 305-307.
25. D. Idrees, M. Hadianawala, A. D. Mahapatra, B. Datta, S. Roy, S. Ahamad, P. Khan and M. I. Hassan, *International Journal of Biological Macromolecules*, 2018, **115**, 961-969.

26. M. A. a. P. Charpentier, *US Patent 2,498,782.*, 1950.
27. M. Y. M. M. Shah, V. M. Patki and C. V. Deliwala, *Journal of Scientific and Industrial Research*, 1959, **12B**, 202-204.
28. A. G. A. El-Helby, H. Sakr, I. H. Eissa, H. Abulkhair, A. A. Al-Karmalawy and K. El-Adl, *Archiv der Pharmazie*, 2019, **352**, 1900113.
29. C.-W. Ding, H.-F. Yu, R.-M. Li, X.-F. Jiang and B. Luo, *ARKIVOC*, 2012, **9**, 254-261.
30. D. Tan, V. Štrukil, C. Mottillo and T. Friščić, *Chemical Communications*, 2014, **50**, 5248-5250.
31. Y. Huang, Y. Yu, R. Hu, and B. Z. Tang, Journal of the American Chemical Society, 2025, **146(21),** 14685-14696.
32. M. Döring, A. Heppner, E. Uhlig, B. Undeutsch, K. Gloe and P. Mühl, *Zeitschrift für anorganische und allgemeine Chemie*, 1988, **556**, 204-212.
33. M. Döring, E. Uhlig, V. Nefedov and I. Salyn, *Zeitschrift für Anorganische und Allgemeine Chemie*, 1988, **556**, 213-222.
34. P. Thomas, A. Schlebe, A. Seidel and H. Hennig, *Journal für praktische Chemie*, 1991, **333**, 657-660.
35. C. Holzner, K.-H. König and H. Goesmann, *Monatshefte für Chemie/Chemical Monthly*, 1994, **125**, 1339-1352.
36. K. H. König, C. Holzner and J. Boßlet, *Chemische Berichte*, 1988, **121**, 1771-1772.
37. K. H. König, J. Bosslet and C. Holzner, *ChemInform*, 1989, **20**.
38. C. Holzner, *Monatshefte für Chemie/Chemical Monthly*, 1994, **125**, 1353-1364.
39. M. Schuster and M. Šandor, *Fresenius' Journal of Analytical Chemistry*, 1996, **356**, 326-330.
40. B. R. B. Beele, E. Bill and F. Mohr, *Crystal Growth & Design*, 2022, **22**, 3442-3456.
41. M. C. Risi, G. C. Saunders and W. Henderson, *Inorganica Chimica Acta*, 2021, **526**, 120506.
42. A. Shipov, G. Genkina and P. Petrovskii, *Russian Chemical Bulletin*, 2009, **58**, 2512-2516.
43. A. Ivetac, S. E. Swift, P. L. Boyer, A. Diaz, J. Naughton, J. A. Young, S. H. Hughes and J. A. McCammon, *Chemical Biology & Drug Design*, 2014, **83**, 521-531.
44. C. Subramanyam, K. Chandrasekhar, R. Venkata, G. Madhava and R. Naga, *Der Pharmacia Lettre*, 2012, **3**, 869-874.
45. M. G. Babashkina, D. A. Safin, K. Robeyns and Y. Garcia, *European Journal of Inorganic Chemistry*, 2015, **2015**, 1160-1166.
46. M. G. Babashkina, K. Robeyns, Y. Filinchuk and D. A. Safin, *New Journal of Chemistry*, 2016, **40**, 1230-1236.
47. D. A. Safin, M. G. Babashkina, A. Klein, F. D. Sokolov, S. V. Baranov, T. Pape, F. E. Hahn and D. B. Krivolapov, *New Journal of Chemistry*, 2009, **33**, 2443-2448.
48. D. A. Safin, M. G. Babashkina, M. Bolte and A. Klein, *Journal of Chemical Sciences*, 2010, **122**, 409-413.
49. F. D. Sokolov, D. A. Safin, M. G. Babashkina, N. G. Zabirov, V. V. Brusko, N. A. Mironov, D. B. Krivolapov, I. A. Litvinov, R. A. Cherkasov and B. N. Solomonov, *Polyhedron*, 2007, **26**, 1550-1560.

50. A. Łopusiński, L. Łuczak, J. Michalski, M. Kabachnik and M. Moriyama, *Tetrahedron*, 1981, **37**, 2011-2020.
51. R. Salla, *Encyclopedia of Reagents for Organic Synthesis*, 2001.
52. J. Michalski, *Tetrahedron*, 1982, **38**, 679-683.
53. H. R. Barai, K. K. Adhikary and H. W. Lee, *Bulletin of the Korean Chemical Society*, 2013, **34**, 1829-1834.
54. E. Shi and C. Pei, *Synthetic Communications*, 2005, **35**, 669-673.
55. G. M. Dobrikov, V. Valcheva, Y. Nikolova, I. Ugrinova, E. Pasheva and V. Dimitrov, *European Journal of Medicinal Chemistry*, 2013, **63**, 468-473.
56. F. D. Sokolov, N. G. Zabirov, L. N. Yamalieva, V. G. Shtyrlin, R. R. Garipov, V. V. Brusko, A. Y. Verat, S. V. Baranov, P. Mlynarz and T. Glowiak, *Inorganica Chimica Acta*, 2006, **359**, 2087-2096.
57. F. Sokolov, D. Safin, N. Zabirov, P. Zotov and R. Cherkasov, *Russian Journal of General Chemistry*, 2005, **75**, 1919-1926.
58. D. A. Safin, M. G. Babashkina, F. D. Sokolov and N. G. Zabirov, *Inorganic Chemistry Communications*, 2006, **9**, 1133-1135.
59. D. A. Safin, F. D. Sokolov, N. G. Zabirov, V. V. Brusko, D. B. Krivolapov, I. A. Litvinov, R. C. Luckay and R. A. Cherkasov, *Polyhedron*, 2006, **25**, 3330-3336.
60. D. A. Safin, P. Mlynarz, F. D. Sokolov, M. Kubiak, F. E. Hahn, M. G. Babashkina, N. G. Zabirov, J. Galezowska and H. Kozlowski, *Zeitschrift für anorganische und allgemeine Chemie*, 2007, **633**, 2089-2096.
61. M. Kutyreva, N. Ulakhovich, M. Starikova, Y. I. Sal'nikov, V. Brus' ko, F. Sokolov and N. Zabirov, *Russian Journal of Inorganic Chemistry*, 2007, **52**, 1050-1055.
62. F. D. Sokolov, S. V. Baranov, D. A. Safin, F. E. Hahn, M. Kubiak, T. Pape, M. G. Babashkina, N. G. Zabirov, J. Galezowska and H. Kozlowski, *New Journal of Chemistry*, 2007, **31**, 1661-1667.
63. F. D. Sokolov, S. V. Baranov, N. G. Zabirov, D. B. Krivolapov, I. A. Litvinov, B. I. Khairutdinov and R. A. Cherkasov, *Mendeleev Communications*, 2007, **17**, 222-223.
64. D. A. Safin, F. D. Sokolov, Ł. Szyrwiel, S. V. Baranov, M. G. Babashkina, T. R. Gimadiev and H. Kozlowski, *Polyhedron*, 2008, **27**, 1995-1998.
65. D. A. Safin, F. D. Sokolov, H. Nöth, M. G. Babashkina, T. R. Gimadiev, J. Galezowska and H. Kozlowski, *Polyhedron*, 2008, **27**, 2022-2028.
66. D. A. Safin, F. D. Sokolov, Ł. Szyrwiel, M. G. Babashkina, T. R. Gimadiev, F. E. Hahn, H. Kozlowski, D. B. Krivolapov and I. A. Litvinov, *Polyhedron*, 2008, **27**, 2271-2276.
67. D. A. Safin, M. G. Babashkina, M. Bolte and A. Klein, *Phosphorus, Sulfur, and Silicon*, 2010, **185**, 2426-2432.
68. D. A. Safin, M. G. Babashkina, M. Bolte, Ł. Szyrwiel, A. Klein and H. Kozlowski, *Phosphorus, Sulfur, and Silicon*, 2010, **185**, 1739-1745.
69. D. A. Safin, M. G. Babashkina, M. Bolte, D. B. Krivolapov, M. L. Verizhnikov, A. R. Bashirov and A. Klein, *Inorganica Chimica Acta*, 2011, **366**, 19-26.
70. M. G. Babashkina, D. A. Safin, M. Bolte, M. Srebro, M. Mitoraj, A. Uthe, A. Klein and M. Köckerling, *Dalton Transactions*, 2011, **40**, 3142-3153.
71. D. A. Safin, M. G. Babashkina, K. Robeyns, M. P. Mitoraj, P. Kubisiak, M. Brela and Y. Garcia, *CrystEngComm*, 2013, **15**, 7845-7851.
72. S. V. Satheesh, A. V. Radha, K. K. N. Girija, K. N. Rajasekharan and P. R. Maheswari, *Journal of the Serbian Chemical Society*, 2017, **82**, 1087-1095.

73. A. Gomtsian, T. Dekhtyar, K. E. Frank, M. M. Friedman, N. Josephsohn, M.-A. Molla, A. Vasudevan, T. Ng and M. Shafeev, *World Intellectual Property Organization*, 2014, WO2014005129.
74. R. Lin, S. G. Johnson, P. J. Connolly, S. K. Wetter, E. Binnun, T. V. Hughes, W. V. Murray, N. B. Pandey, S. J. Moreno-Mazza and M. Adams, *Bioorganic & medicinal chemistry letters*, 2009, **19**, 2333-2337.
75. S. Gardell, A. B. Pinkerton, E. Sergienko and H. Sessions, *World Intellectual Property Organization*, 2018, WO 2018132372.
76. S. Lin, S. Malkani, M. Lombardo, L. Yang, S. G. Mills, K. Chapman, J. E. Thompson, W. X. Zhang, R. Wang and R. M. Cubbon, *Bioorganic & Medicinal Chemistry Letters*, 2015, **25**, 5402-5408.
77. J. W. Tilley, H. Ramuz, F. Hefti and M. Gerold, *Journal of Medicinal Chemistry*, 1980, **23**, 1438-1439.
78. M. Shah, M. Y. Mhasalkar, V. M. Patki and C. V. Deliwala, *Journal of Scientific & Industrial Research*, 1959, **12B**, 202-204.
79. T. Stellfeld, J. S. Mowart, C. Stresenann, R. H. Kohr, D. Stockigt, J. Weiske, I. Hartung, N. Barak, C. Christ, A. T. Laak, V. Badock, R. H. Crampton and I. Stefanuti, *World Intellectual Property Organization*, 2016, WO 2016166186
80. C. Liu, T. G. M. Dhar, H. H. Gu, E. J. Iwanowicz, K. Leftheris and W. J. Pitts, *World Intellectual Property Organization*, 2000, WO 2000025780.
81. R. J. Altenbach, H. Bai, J. D. Brioni, W. A. Carroll, M. Gopalakrishnan, R. J. Gregg, M. W. Holladay, P. P. HuangJ, o. F. Kincaid, M. E. Kort, P. R. Kym, J. K. Lynch, A. Perez-Medrano and H. Q. Zhang, *World Intellectual Property Organization*, 2001, WO 2001009096.
82. W. Henderson, B. K. Nicholson and E. R. T. Tiekink, *Inorganica Chimica Acta*, 2006, **359**, 204-214.
83 W. Henderson, B. K. Nicholson and C. E. F. Rickard, *Inorganica Chimica Acta*, 2001, **320**, 101-109.
84. W. Henderson and B. K. Nicholson, *Polyhedron*, 1996, **15**, 4015-4024.

Chapter Two

Chalcogen bond stabilization of platinum(II) sulfonyl-substituted thiourea complexes with ancillary phosphine ligands

Recently a preliminary investigation into the coordination chemistry of sulfonyl substituted thiourea ligands towards the d^8 metal centres nickel(II), platinum(II), palladium(II) and gold(III) was reported.[1] X-ray structures of two platinum(II) triphenylphosphine complexes, [Pt{$TolSO_2NC(S)NPh$}$(PPh_3)_2$] and [Pt{$CH_3SO_2NC(S)NPh$}$(PPh_3)_2$], were obtained, both exhibiting expected *N,S*-coordination. Furthermore, both complexes exclusively formed the *distal* isomer with a remote NSO_2R group (Figure 2.1) and no evidence for isomerization to the *proximal* isomer of these complexes in solution was observed.

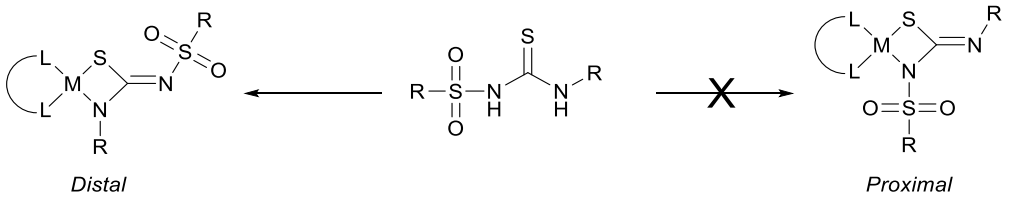

Figure 2.1: Proximal and distal isomers of sulfonylthiourea ligands.

$^{31}P\{^1H\}$ NMR analysis of the remaining complexes ([M{$TolSO_2NC(S)NPh$}(L)] M = Ni(II), Pd(II), Pt(II) or Au(III), L = $Ph_2P(CH_2)_2PPh_2$, 2,2'-bipyridine or 2-benzylpyridine), which could not be characterized using crystallography because no crystals were obtained, was found to also follow a *distal* isomer preference. Initially, this observation was attributed to the bulky nature of the ancillary phosphine ligands (PPh_3 and dppe), which could potentially deter the formation of the *proximal* isomer. However, specific aspects regarding the nature and influencing factors of the coordination of sulfonylthiourea ligands remained largely unexplored. Gaining a comprehensive understanding of these effects could

open new possibilities in ligand design for the use of sulfonylthioureas as viable ligands for application-focused research. In this context, the coordination chemistry of platinum(II) sulfonylthiourea complexes bearing ancillary phosphine ligands was revisited in depth to better comprehend the influencing factors of the chosen isomer. Herein this chapter, Pt(II) complexes with sulfonylthiourea complexes are prepared and characterized in an effort to shed light on this *distal* isomer exclusivity.

2.1 Results and discussion

2.1.1 Synthesis and characterization of sulfonylthiourea ligands

Sulfonylthioureas can be synthesized by a reaction between a sulfonamide (RSO_2NH_2) with an isothiocyanate (RNCS) under alkaline conditions. Previously in our studies[1] on sulfonylthiourea ligands, we have used readily available sulfonamides and isothiocyanates in acetone with aqueous sodium hydroxide, followed by acidification with acetic acid. While synthesis by this route resulted in the target ligand in moderate yields, consecutive crystallizations from hot ethanol were needed to achieve sufficient purity. This was primarily a result of the formation of 1,3-disubstituted thiourea as a by-product from the self-reaction of isothiocyanate in the presence of moisture, i.e., RNHC(S)NHR from RNCS.[2] Moreover, the use of acetone as a solvent posed further challenges because of aldol condensation in the presence of harsh bases such as alkali metal hydroxide. In an effort to minimize these factors, it was instead decided to use minimal volumes of dry dimethylformamide (DMF) and potassium *tert*-butoxide (KO*t*Bu), based on the success of previously reported studies.[3] These changes, combined with a shorter reaction time and higher reaction temperatures, effectively reduced the formation of the by-products and yielded the target sulfonylthiourea with satisfactory purity. Apart from the obvious elimination in aldol condensation products, the change of base from sodium hydroxide to potassium *tert*-butoxide was observed to have made the most promising change. The reason for this is most likely a result of the nature of the non-nucleophilic butoxide base. From the reactions between either *p*-tolyl or ethyl sulfonamide with phenyl or butyl isothiocyanate, the ligands $TolSO_2NHCSNHPh$ (**S-L1**), $EtSO_2NHCSNHPh$ (**S-L2**) and $TolSO_2NHC(S)NHCH(CH_3)_3$) (**S-L3**) were prepared (Figure 2.2).

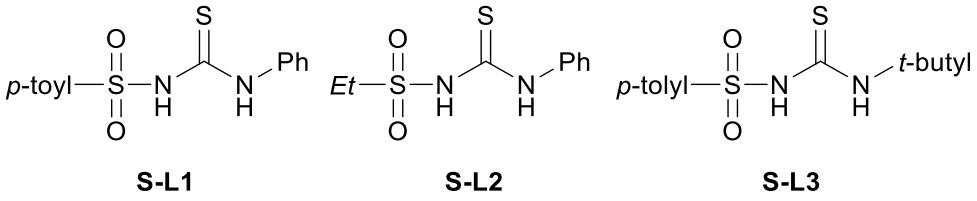

Figure 2.2: Structures of the sulfonylthiourea ligands prepared in this chapter

2.1.2 Attempted synthesis of sulfonylthiourea ligands *via* sulfonyl-isothiocyanates

A common synthetic route to acylated thiourea molecules is by an alkyl or aryl acyl-isothiocyanate precursor. The acyl-isothiocyanate is commonly prepared by reactions of an acyl-chloride with either sodium or potassium thiocyanate (NCS) which can be further reacted *in situ* with a primary or secondary amine to produce the target acylthiourea. In principle, an analogous reaction utilizing sulfonyl chlorides should be feasible. In this regard, reactions between *p*-tosyl chloride and potassium thiocyanate were conducted in refluxing acetone. After approximately 2 hours at refluxing the mixture had turned dark amber and was allowed to cool to room temperature. The solvent was removed under reduced pressure to yield a bright orange reaction mass which was extracted into diethyl either. To the diethyl ether extract, an equal molar amount of morpholine ($O(CH_2CH_2)_2NH$) was added dropwise. The resulting white precipitate was collected and dried in air. The ^1H NMR spectrum of the product showed resonances consistent with the target thiourea product **L4** *i.e.* peaks relating to the tosyl and morpholine groups were present and their were no unexpected features. The ESI-MS(+) mass spectrum of the product, however, revealed a strong ion at an m/z of 242 which was suspected to be the tertiary sulfonamide 4-[(4-methylphenyl)sulfonyl]morpholine (**1**). A generalized scheme of the reaction is included below as Figure 2.3.

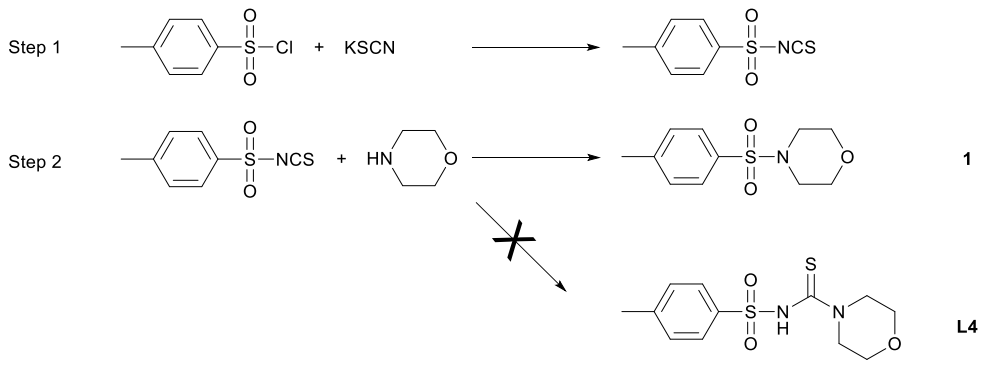

Scheme 2.3: Reactions of p-tosyl-isothiocyanate and morpholine.

The SC-XRD structure of the product, recrystalized from dichloromethane, confirmed the product to be **1** (*vide infra*). The formation of **1** is likely a result of thiocyanate being a good leaving group which is promoted by the presence of the sulfonyl moiety. Additional synthetic attempts were not made, although it is possible that altering reaction conditions, such as lowering the temperature, might result in the target thiourea.

2.1.3 Synthesis and characterization of sulfonylthiourea metal complexes

Reactions between **S-L1**, **S-L2** and **S-L3** and bis(phosphine) platinum(II) complexes bearing triphenylphosphine (PPh_3), tris(2-cyanoethyl)phosphine (TCEP) and 1,3,5-triaza-7-phosphaadamantane (PTA) and *cis* chloride ligands were carried out in hot methanol with triethylamine as base, or in the case of PTA bearing complexes, aqueous sodium hydroxide in open atmosphere. The resulting PPh_3 and TCEP bearing complexes were isolated by precipitation with water. Solutions of the complexes bearing PTA, on account of the extremely high solubility in protic solvents, were initially evaporated to dryness and subsequently redissolved in dichloromethane. The solutions were then filtered through approximately 2 cm of silica to remove traces of insoluble sodium salts before being evaporated to dryness again under reduced pressure to yield the target complex. The mixed-ligand platinum(II) complexes containing triphenylphosphine and pyridine ancillary ligands were synthesized from $[Pt(COD)Cl_2]$ (COD = *cyclo*-octa-1,5-diene) in hot methanol with pyridine and consecutive one molar equivalent additions of PPh_3, and the corresponding sulfonylthiourea ligand. These complexes were

isolated by precipitation with cold water. The structures of the synthesized complexes are shown in Figure 2.4.

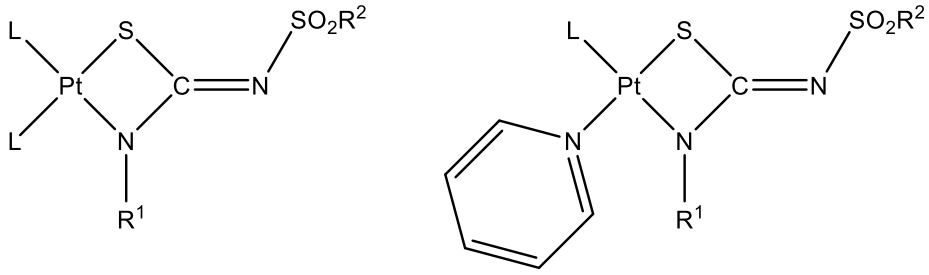

Complex	L_2/L(Py)	R^1	R^2
2a	PTA	Ph	*p*-Tol
2b	TCEP	Ph	*p*-Tol
2c	PPh_3(Py)	Ph	*p*-Tol
2d	PTA	Ph	Et
2e	PPh_3(Py)	Ph	Et
2f	PPh_3	*t*-Butyl	*p*-Tol

Figure 2.4: Sulfonylthiourea complexes prepared in this investigation as the distal isomer.

The ESI-MS(+) mass spectra of the sulfonylthiourea complexes showed no unexpected features in their positive ion spectra. All spectra showed the expected $[M + H]^+$ ions and in some cases the corresponding sodiated ions $[M + Na]^+$. At high capillary exit voltages, ions corresponding to the loss of an ancillary phosphine ligand $[(M - PR_3) + H]^+$ were also observed. No unexpected ions were observed. Isotope patterns of the complexes were also in good agreement with calculated patterns, including the appearance of distinctive platinum isotope patterns. An

example is shown in Figure 2.5, the $[M + H]^+$ ion of complex **2a** including the predicted pattern for the same molecular formula.

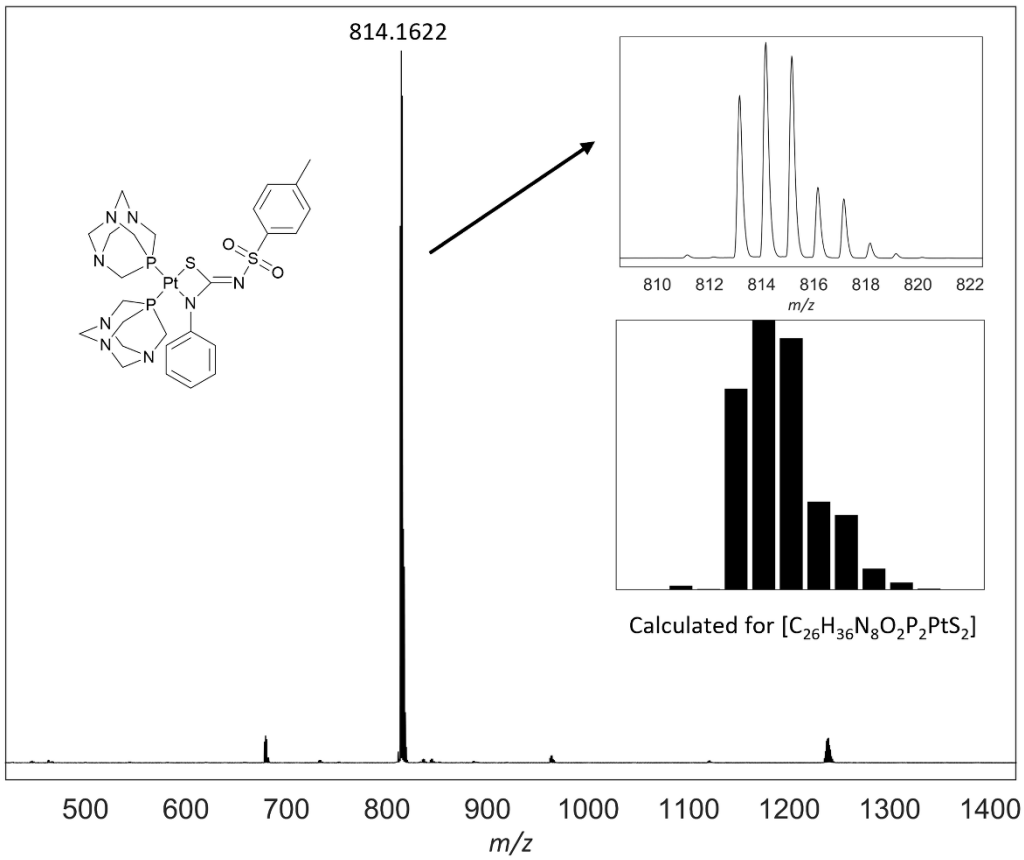

*Figure 2.5:ESI-MS(+) spectrum of complex **2a** showing the isotope pattern of the $[M+H]^+$ ion and the calculated pattern of the same formula.*

2.1.4 NMR spectroscopic analysis

The ^1H and $^{31}P\{^1H\}$ NMR spectra of the bis(phosphine) complexes show the expected features. Archetypal ^1H NMR spectral features of the ancillary phosphine PTA and TCEP can be easily used to characterize the complex. For instance, for complexes **2a** and **2d**, the ^1H spectra show the CH_2 groups of the non-equivalent PTA ligands as two distinctive sets of a doublet of doublets and a singlet peak. Likewise, the ^1H NMR spectrum of **2b** shows four archetypal sets of doublets of triplets that appear as quartets because of overlapping resonances, i.e., J(H-P) ≈ J(H-H) (Figure 2.6).

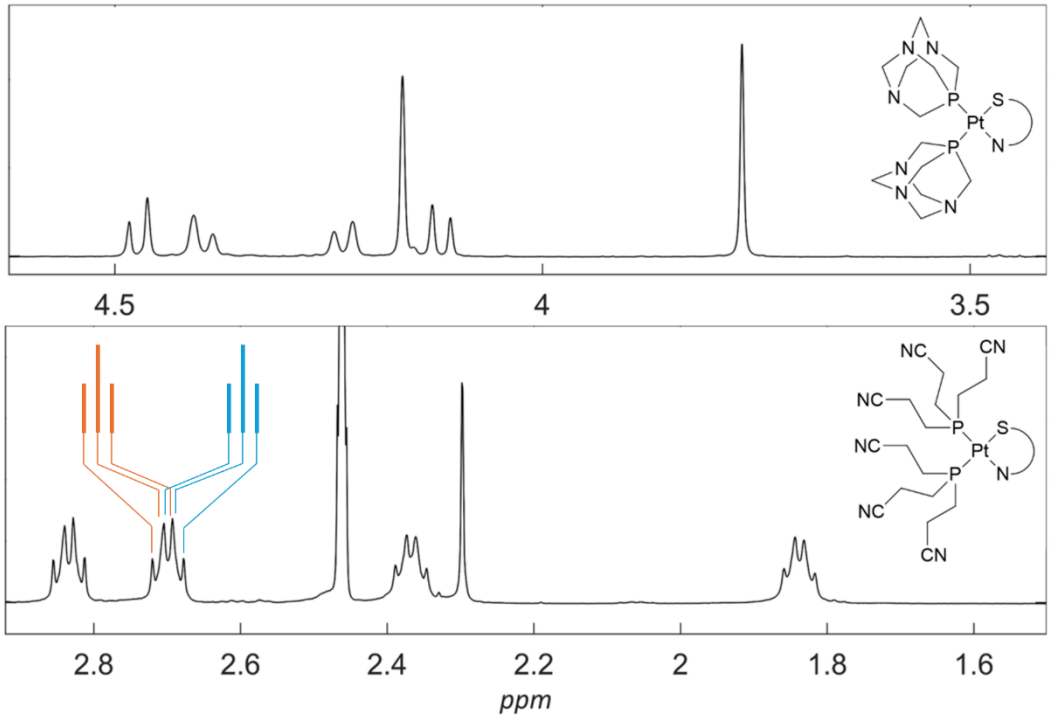

*Figure 2.6: ^{1}H NMR spectra of complexes **2d** (top) and **2b** (bottom) showing characteristic CH_2 resonances of the tertiary phosphine ligands. $CDCl_3$ at 25°C.*

The $^{31}P\{^{1}H\}$ NMR spectra show the expected AB doublet of doublet resulting from the presence of non-equivalent phosphorus atoms (P *trans* to S and P *trans* to N) along with accompanying ^{195}Pt satellite peaks. The $^{1}J(PtP)$ coupling constants for the bis(phosphine) complexes **2a**, **2b**, **2d** and **2f** are within the range of 1407 Hz to 3610 Hz, consistent with the expected S-N bidentate coordination mode.[4, 5] Furthermore, considering the slightly higher *trans* influence exerted by the sulfur atom, the phosphorus nucleus with the smaller coupling constant is assigned to the position *trans* to the sulfur, while the phosphorus nucleus with the higher $^{1}J(PtP)$ coupling constant is assigned to the position *trans* to the nitrogen.[6] In the case of complexes **2a**, **2b** and **2c**, the $^{1}J(PtP)$ coupling constants are 2908 Hz, 1407 Hz and 1881 Hz respectively, tentatively indicating the presence of the *distal* isomer, *i.e*. coordination through the N-alkyl nitrogen atom with a remote NSO_2R group. Conversely, complex **2f** has $^{1}J(PtP)$ phosphorus *trans* to nitrogen coupling of 3610 Hz, which is higher than the typical range of 3300 Hz to 3400 Hz of *distal* isomers of similar bis(PPh_3) complexes, suggesting the formation of the unexpected *proximal* isomer. The latter is most likely as a result of the sterically bulky nature of the *t*-butyl substituent on the thiourea ligand (Figure 2.7).

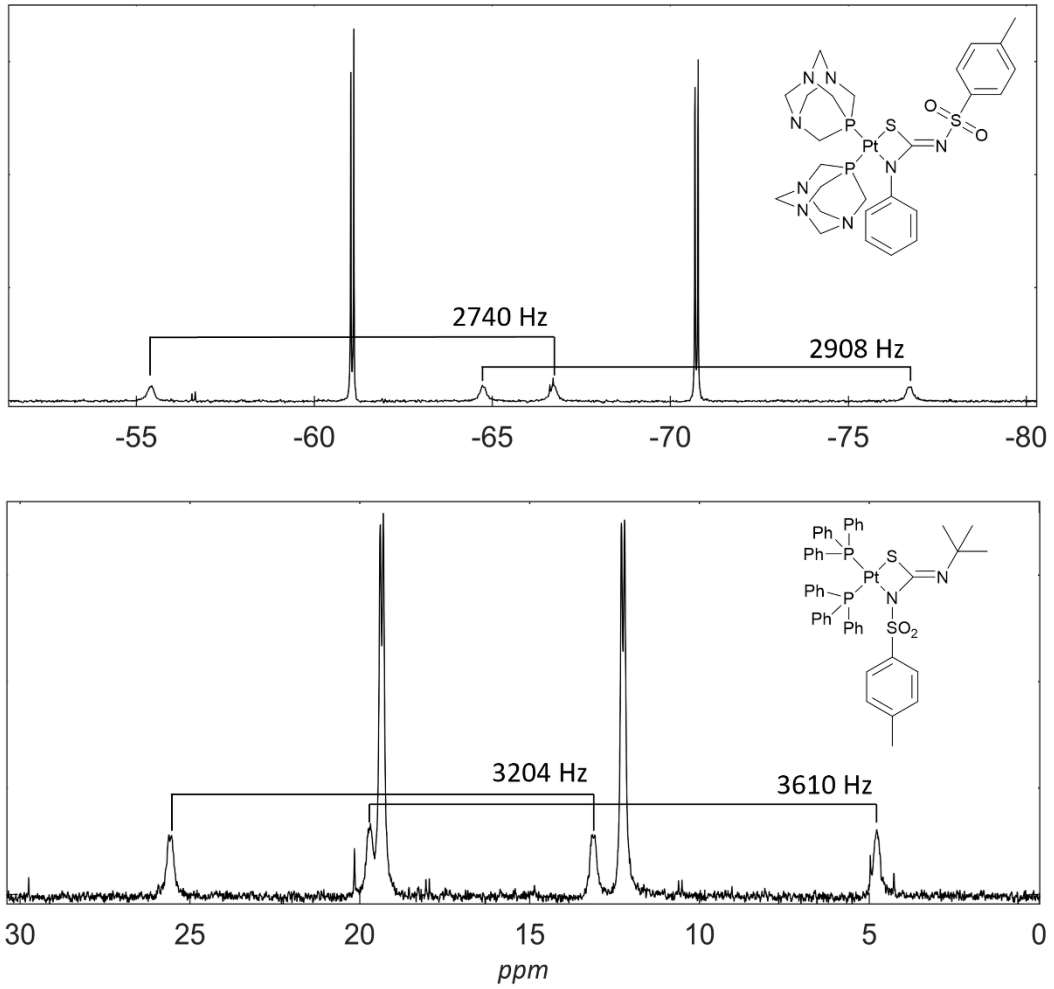

*Figure 2.7: $^{31}P\{^{1}H\}$ spectra comparison of complexes **2a** and **2f** showing $^{1}J(PtP)$ coupling constants. $CDCl_3$ at 25°C.*

The $^{1}J(PtP)$ coupling constants for the bis(PTA) complexes, **2a** and **2d,** were within a relatively narrow range of 2740 to 2908 Hz, which is in accordance with reported values for platinum(II) thiourea complexes with *cis*-PTA ligands.[7] Interestingly, the difference in the magnitude between the coupling constants for complexes **2a** and **2d** are 168 Hz and 127 Hz, respectively, which are larger than typical literature values of around 20 Hz.[7] It is noteworthy that these coupling constants are relatively less pronounced than those observed for similar PPh_3 complexes, where values typically range between 200 to 600 Hz.[1, 4] For the bis(PPh_3) complex **2f**, the $^{1}J(PtP)$ coupling constants are 2610 Hz and 3028 Hz with a difference of 582 Hz, consistent with the aforementioned literature values. In stark contrast, the bis(TCEP) complex **2b** has $^{1}J(PtP)$ coupling constants of 2939 and 1407 Hz with a relatively large difference of 1532 Hz.

Although isomerization of bis(PPh_3) platinum(II) complexes with simple *N,N*-substituted alkyl thioureas has been previously documented,[8] no isomerization has been detected within time scales of up to three months at room temperature for similar sulfonylthiourea complexes. To explore this phenomenon further, variable temperature $^{31}P\{^1H\}$ NMR spectra were recorded at 10°C intervals between 30 and 100°C for complex **2a** and the previously reported complex [Pt{$TolSO_2NC(S)NPh$}(PPh_3)$_2$] in DMSO-d_6. In both instances, no notable changes in the spectra were observed. To investigate possible solvent effects on the observed isomer, spectra of [Pt{$TolSO_2NC(S)NPh$}(PPh_3)$_2$] were recorded in non-deuterated CH_2Cl_2, MeOH and THF. Additionally, [Pt{$TolSO_2NC(S)NPh$}(PPh_3)$_2$] was re-synthesized in CH_2Cl_2, $CHCl_3$ and THF and $^{31}P\{^1H\}$ NMR spectra were collected of the neat reaction mixtures before isolation. Despite these efforts, no change in isomer or any isomerization for complexes **2a** and [Pt{$TolSO_2NC(S)NPh$}(PPh_3)$_2$] was observed. This implies that either the thermodynamically stable and kinetically favourable isomer are the same or there exists a significant energy barrier between the kinetically favourable and the thermodynamically stable isomers.

2.1.5 X-ray structure determinations

Structural analysis of complexes **2a**, **2b** and **2c** was conducted by means of single crystal X-ray diffraction in order to determine the nature of coordination of the complexes. Molecular structures for **2a**, **2b** and **2c** are shown in Figures 2.8, 2.9 and 2.10 with relevant bond lengths and angles are shown in Table 2.1. A table of crystallographic details is included in Appendix 1. The three structures reveal that the sulfonylthiourea ligand chelating the platinum centre is in an S-N bidentate mode, with complex **2a** containing two *cis*-PTA ligands, **2b** containing two *cis*-TCEP ligands and **2c** containing a PPh_3 ligand and a pyridine ligand coordinated in an antisymbiotic manner[9] (N *trans* to S). The resulting square planar geometry around the platinum atom is slightly distorted on account of the small S-Pt-N bite angle of around 69° for **2a, 2b** and **2c** as opposed to the larger P-Pt-P, and P-Pt-N angles of about 100° and 92° respectively. The three complexes **2a, 2b** and **2c** are confirmed

to be the *distal* isomers with N1 coordinated to the platinum and the N2 in the *distal* position, validating the $^{31}P\{^{1}H\}$ NMR spectroscopy observations.

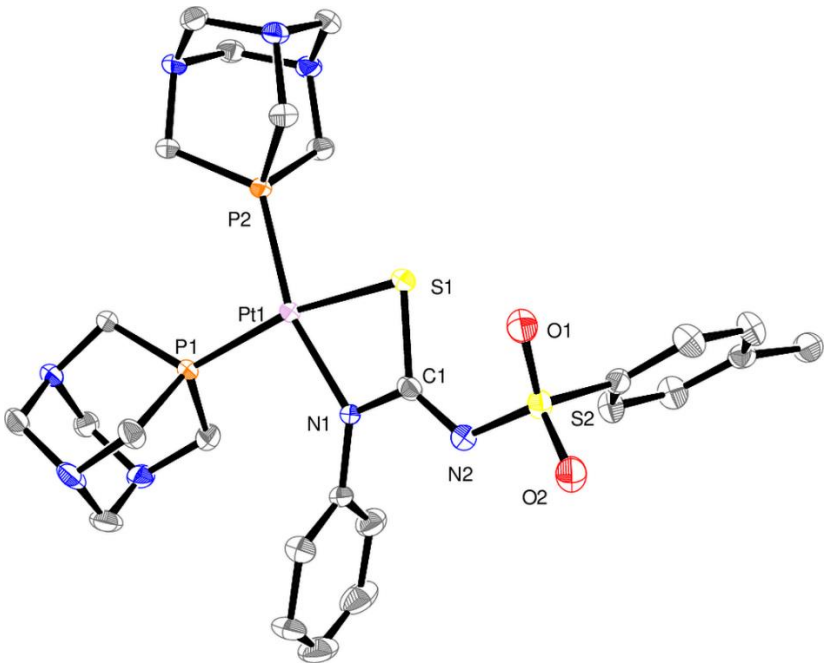

*Figure 2.8: Molecular structure of **2a** showing a partial atom numbering scheme. Hydrogen atoms and solvent of crystallization are omitted for clarity and ellipsoids are shown at the 50% probability level.*

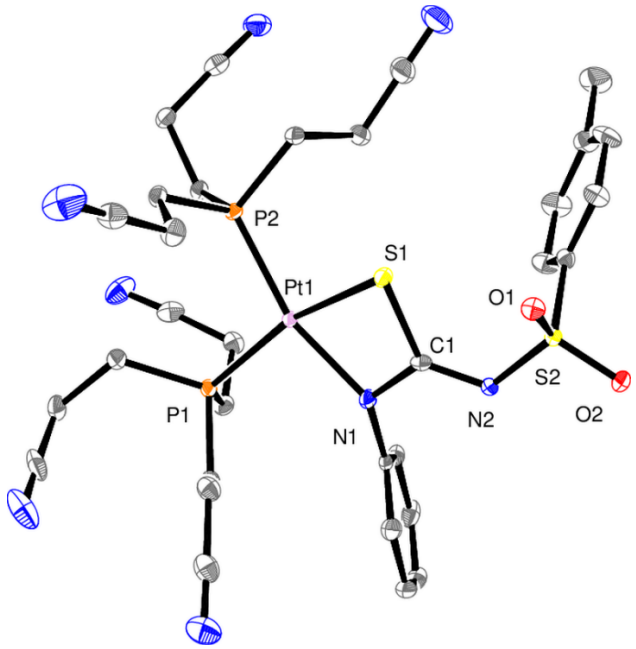

*Figure 2.9: Molecular structure of complex **1b** showing a partial atom numbering scheme. Hydrogen atoms are omitted for clarity and ellipsoids are shown at the 50% probability level.*

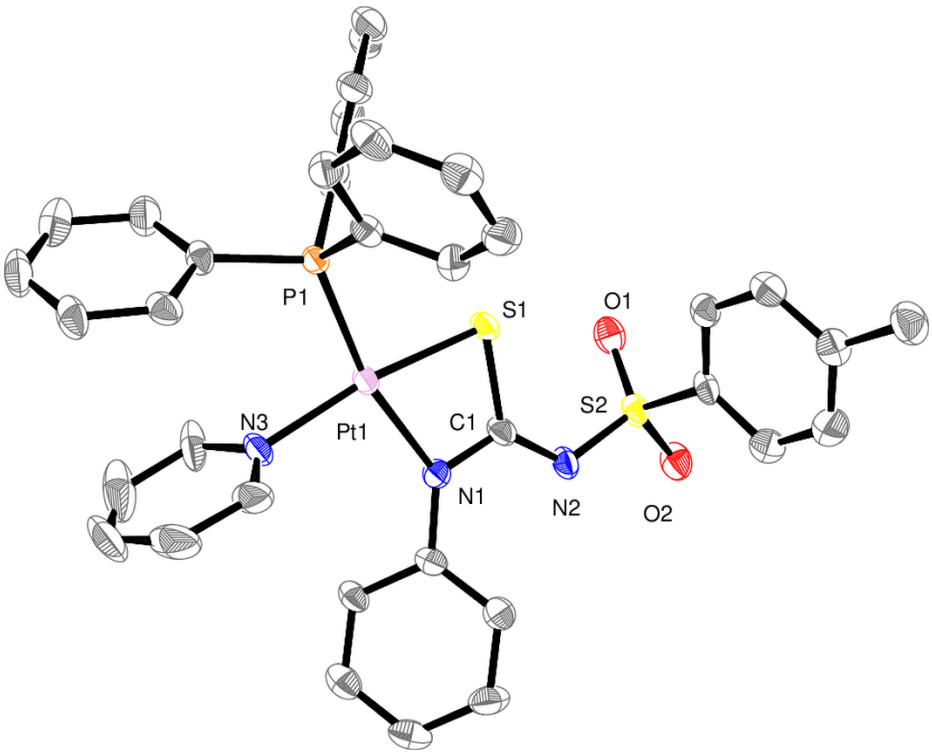

*Figure 2.10: Molecular structure of complex **2c** showing a partial atom numbering scheme. Hydrogen atoms and two water molecules of crystallization are omitted for clarity and ellipsoids are shown at the 50% probability level.*

Metallacyclic bond distances of both complexes are extremely similar averaging [S1-Pt 2.322, N1-Pt 2.085, C1-N1 1.324, C1-S1 1.777 Å], which are in very close agreement with the bis(PPh_3) complex [Pt{$TolSO_2NC(S)NPh$}(PPh_3)$_2$]**,** which has bond distances of [S1-Pt 2.322(2), N1-Pt 2.105(5), C1-N1 1.330(8), C1-S1 1.770(6) Å].[1] Of note is a consistent feature between complexes **2a**, **2b**, **2c** of the orientation of the sulfonyl group and a short S1-O1 distance averaging 3.041 Å, implying the possible presence of a non-covalent interaction (Figure 2.11) between these atoms (*vide infra*).

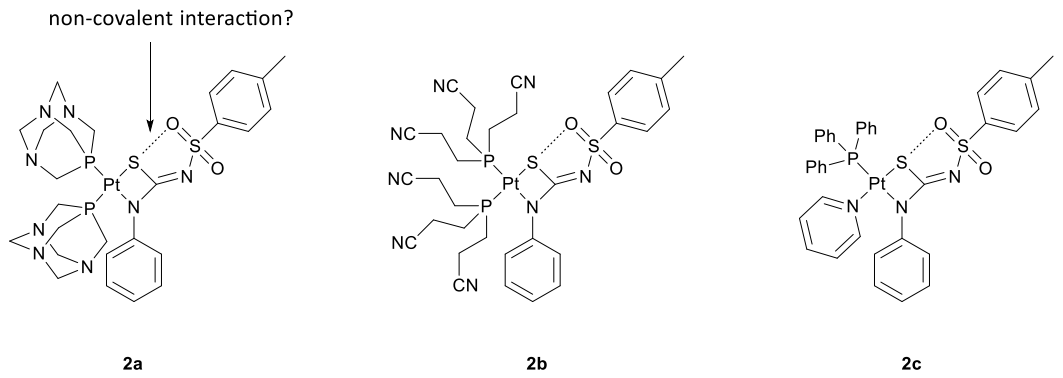

*Figure 2.11: Structures of the distal isomer of complexes **2a**, **2b** and **2c** showing possible non-covalent interactions between the thiourea S and sulfonyl O atoms.*

Previously, it had been assumed that the observation of the ubiquitous *distal* isomer formation of square planar sulfonylthiourea complexes was most likely a direct consequence of the steric bulk of the ancillary phosphine ligands, triphenylphosphine (PPh_3), 1,3-bis(diphenylphosphino)propane (dppp) and 1,2-bis(diphenylphosphino)ethane (dppe) which have cone angles of 150°, 127° and 125° respectively.[10, 11] In an attempt to encourage the formation of the *proximal* isomer by a reduction of the bulk around the coordination sphere, it was selected to instead use PTA because of the ligand's small cone angle[12] (103°), prompting the synthesis of complex **2a**. However, these efforts were unfruitful as evident from the molecular structure and $^{31}P\{^{1}H\}$ NMR spectra.

The second attempt at encouraging the *proximal* isomer was by way of creating a cavity of space around the coordination sphere by the introduction of a slender pyridine ligand, leading to the synthesis of the mixed-ligand complex, **2c**. However, despite the molecular structure showing the pyridine ligand sitting perpendicular to the metallacyclic plane and, creating a large cavity in which the sulfonyl group could sit, the complex also formed the *distal* isomer. Clearly, as the bulk of the ancillary ligands appears to have little consequence on the resulting isomer, attention was turned to the ligand **S-L3** on account of the bulky *t*-butyl moiety. As such, the resulting bis(PPh_3) complex, $[Pt\{TolSO_2NC(S)N(CH_3)_3\}(PPh_3)_2]$ **2f**, was characterized by X-ray diffraction, which confirmed the complex to be in the unexpected *proximal* isomer, with N2 coordinated to the platinum centre. The molecular structure of **2f** is shown in Figure 2.12 and relevant bond lengths and

angles are given in Table 2.1. The coordination sphere of the complex is nearly identical to that of **2a**, **2b** and **2c** with similar metallacyclic bond distances of [S1-Pt 2.325(6), N2-Pt 2.095(2), C1-N2 1.431(4), C1-S1 1.787(3) Å] with a slightly elongated C1-N2 compared to the C1-N1 metallacyclic bond distances of the complexes in the *distal* isomer. As such, it is apparent that while the *distal* isomer is favoured, the incorporation of a bulky substituent on the ligand is able to successfully force the formation of the *proximal* isomer.

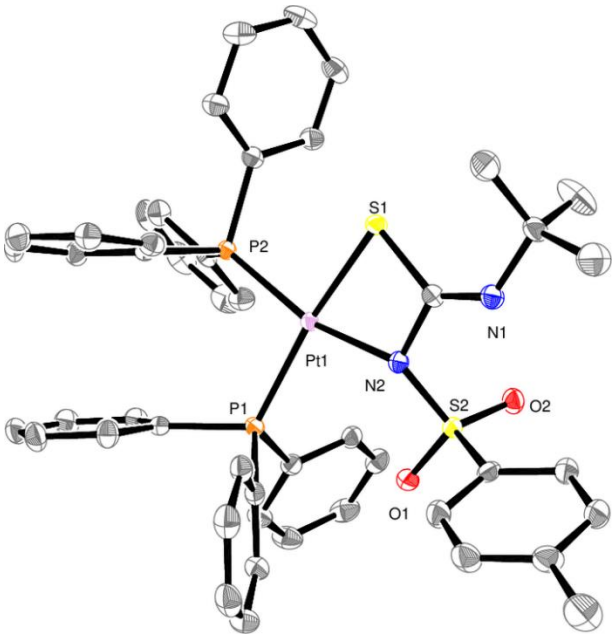

*Figure 2.12: Molecular structure of the complex **2f** showing a partial atom numbering scheme. Hydrogen atoms and a molecule of methanol of crystallization are omitted for clarity and ellipsoids are shown at the 50% probability level.*

*Table 2.1 Selected bond lengths (Å) and angles (°) for the complexes **2a**, **2b**, **2c** and **2f***

	2a	**2b**	**2c**	**2f**
P1 - Pt	2.255(8)	2.280(6)	2.236(9)	2.303(6)
P2 - Pt	2.240(7)	2.257(6)	-	2.244(6)
N3 - Pt	-	-	2.076(4)	-
S1 - Pt	2.348(8)	2.337(6)	2.283(1)	2.325(6)
N1 - Pt	2.092(3)	2.077(2)	2.088(3)	-
N2 - Pt	-	-	-	2.095(2)

C1 - S	1.789(3)	1.771(3)	1.772(4)	1.787(3)
C1 - N1	1.299(4)	1.341(3)	1.332(7)	1.255(3)
C1 - N2	1.325(4)	1.318(3)	1.335(5)	1.431(4)
P1 - Pt - P2	99.97(3)	100.25(2)	-	96.99(2)
P1 - Pt - N3	-	-	92.48(1)	-
S1 - Pt - N1	68.44(8)	69.34(6)	70.01(1)	-
S1 - Pt - N2	-	-	-	70.03(6)

2.1.5.1 X-ray structure determination of 4-[(4-methylphenyl)sulfonyl] morpholine

To determine the structure of the product prepared by the reaction of tosyl isothiocyanate with morpholine (Section 1.1.2), crystals were grown by the slow evaporation of a dichloromethane solution. The molecular structure of the product (4-[(4-methylphenyl)sulfonyl]morpholine) is as in Figure 2.13. The molecule, which crystalized in the $P2_1/c$ space group, contains a not unexpected bent structure as a result of the tetrahedral geometry of S1. Bond lengths, angles and general features are consistent with reported molecular structures of the same compound.[13]

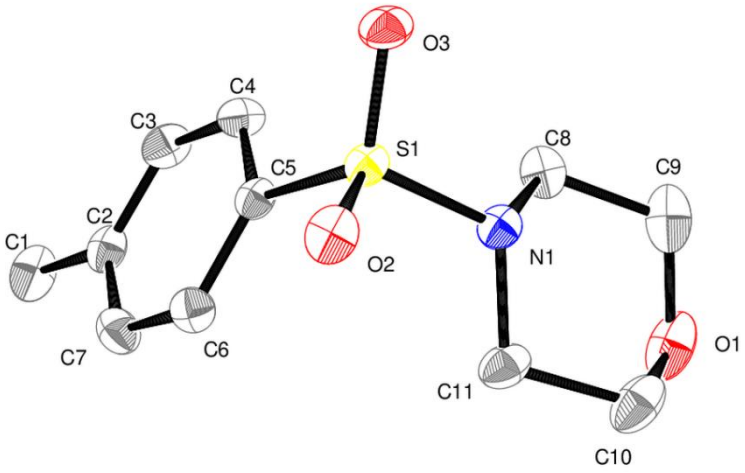

*Figure 2.13: Molecular structure of **1**. Hydrogen atoms and a molecule of methanol of crystallization are omitted for clarity*

2.1.6 Computational investigations and chalcogen bond stabilization

To investigate the thermodynamic aspects of the preferential *distal* isomer formation of the sulfonylthiourea complexes, density functional theory (DFT) calculations were performed on isomeric structural pairs of complexes whose solid-state structures had been previously determined. These complexes included **2a**, **2b**, **2c**, and **2f**, along with the previously reported complexes [Pt{TolSO$_2$NC(S)NPh}(PPh$_3$)$_2$] (**Pt1**) and [Pt{CH$_3$SO$_2$NC(S)NPh}(PPh$_3$)$_2$] (**Pt2**).[1]

To select a basis set and method for the following calculations, initial geometry and single point calculations of the *proximal* and *distal* isomers of complex **Pt1** were conducted using the B3LYP, MO6-2X and ωB97X-D functionals with the LACVP basis set. On account of the observation that the *distal* isomer is exclusively observed (unless otherwise forced) and that no isomerization to the *proximal* isomer could be observed in the NMR trials (Section 1.1.4), it was determined that the *distal* isomer would have the lower ground state energy between the two isomers. With this assumption, the difference in ground state energy values of the isomers ($G_{distal} - G_{proximal}$) termed ΔG would be expected to be a negative value if the *distal* isomer is indeed lower in energy. Therefore, the method/basis set combinations can be accessed by comparing the values of ΔG. The ΔG values for B3LYP/LACVP, M06-2X/LACVP, and ωB97X-D/LACVP were +26, +50, and +9.3 kJ mol^{-1}, respectively. These results indicated that ωB97X-D produced values closer to zero, aligning more closely with expectations and experimental observations; however, no method yielded a negative value of ΔG. These values suggested that ωB97X-D, with its included D3 dispersion correction, may better account for the long-range and short-range intra- and intermolecular interactions that are typically critical in the geometry and behaviour of transition metal complexes. Consequently, dispersion-corrected functionals were determined to be essential for the following calculations.

Current literature supports using VV10 non-local correlation methods to analyze long-range interactions in sulfur-containing compounds,[14] particularly for transition metal complexes,[12] as an alternative to D3 and D4 dispersion corrections. Thus, ωB97X-D and ωB97M-V were compared further, producing ΔG values of +9.9

and +9.3 kJ mol^{-1}, respectively. Given that ωB97M-V demonstrated better performance than ωB97X-D, it was chosen for the following calculations.[14] With this knowledge in hand, optimization of the structures in the gas phase was conducted at the ωB97MV/LACVP level of theory using the LACVP effective core potential for platinum. Complex **Pt1** was also optimized in liquid phase using the universal SMD solvation model in a selection of solvents. The difference in Gibbs free energy between the *proximal* and *distal* isomers (ΔG), was compared and the results are shown in Table 2.2**.**

*Table 2.2 Calculated ground state energies of complexes **2a**, **2c**, **2f**, **Pt1** and **Pt2***

Complex	ΔG (kcal mol^{-1})	ΔG (kJ mol^{-1})	Predicted	Observed
2a	14	58	*Proximal*	*Distal*
2b	17	73	*Proximal*	*Distal*
2c	3	13	*Proximal*	*Distal*
2f	15	65	*Proximal*	*Proximal*
Pt1	10	42	*Proximal*	*Distal*
Pt2	11	45	*Proximal*	*Distal*
Pt1 - Toluene	16	68	*Proximal*	*Distal*
Pt1 - $CHCl_3$	5	20	*Proximal*	*Distal*
Pt1 – CH_2Cl_2	3	14	*Proximal*	*Distal*
Pt1 - THF	3	11	*Proximal*	*Distal*
Pt1 – CH_3CN	1	5	*Proximal*	*Distal*
Pt1 - MeOH	1	5	*Proximal*	*Distal*

As the more thermodynamically stable isomer will have the lower Gibbs free energy, a negative value for ΔG therefore implies that the *distal* isomer is favoured. For complex **2f**, the value of ΔG is +65 kJ mol^{-1}, predicting the *proximal* isomer and confirming the experimental observations. The remaining ΔG values for complexes **2a, 2b**, **2c**, **Pt1** and **Pt2** in the gas phase were in the range of 13 – 73 kJ mol^{-1} and would therefore imply that the *proximal* isomer is favoured, contrary to

experimental observations. Moreover, calculations of **Pt1** in the liquid phase, while closer to zero, are still in disagreement with the experimental results. A possible explanation for the discrepancy between the calculated and observed result could be because of the gas phase nature of the calculations which do not take into account the complex intramolecular interactions that govern solid state structures. An interesting observation of **Pt1** in the liquid phase is the trend of decreasing ΔG with increasing solvent polarity, implying some polar solvent stabilization of the *distal* isomer is taking place. Given that results do not match with the experimental observations, an increase in the level of theory to aug-cc-pV(Q+d)Z/LACVP for P, S, N and O atoms of complex **2a** and **Pt1** in the gas phase was conducted and produced values for ΔG of +28 and +20 kJ mol^{-1} respectively. These results suggest that non-covalent interactions could be playing a stabilizing role and that diffuse basis functions are necessary to accurately model the complexes. The extended basis functions with small exponents offer greater flexibility in the "tail" portions of atomic orbitals, which is essential for accurately analyzing both short- and long-range inter/intramolecular interactions. Consequently, attention was instead turned towards the analysis of non-covalent interactions.

2.1.6.1 Analysis of non-covalent interactions

Motivated by the orientation of the sulfonyl moiety on the complex and the relatively short intramolecular S···O distance of the thiourea sulfur and sulfonyl oxygen observed in the crystal structures (averaging 3.041 Å, Section 1.1.5), exploration of the possibility of a stabilising chalcogen bond (ChB) between these atoms is explored. The presence of such a bond may explain the observation of the preferential *distal* isomer formation. Chalcogen bonds are attractive non-covalent interactions (NCI) characterized by the interaction of an electron deficient region of a polarized chalcogen atom (σ-hole) with an electron donor or Lewis-base that donates to the σ*-orbital of the chalcogen (Ch) atom.[15] (Figure 2.14).

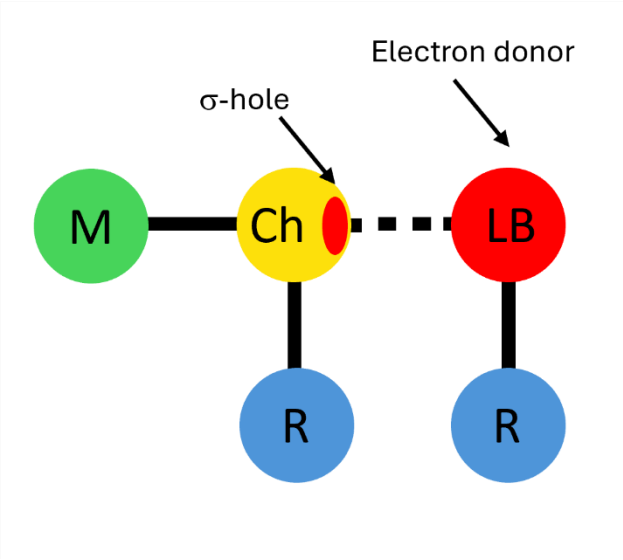

Figure 2.14: Illustration of chalcogen σ-hole interactions as a result of Lewis base electron donation to a σ-hole on the chalcogen atom.

Similar to other NCI, such as the more common hydrogen and halogen bonding, chalcogen bonds have been used to describe interactions in protein folding,[16] crystal engineering[17] and catalysts.[18] It has been well documented that the presence of an electron-withdrawing substituent bonded to, or in the vicinity of, the sulfur atom enhances the Ch bonds strength *via* larger σ-holes, allowing for a greater degree of donation from the donor atom.[19,20] For example, some ML_2 sulfonyl substituted isothiourea complexes with Cu(II) display enhanced Ch bond preference with a strongly electron-withdrawing $-NO_2$ substituent as opposed to a -Cl substituent at the same position[21] (Figure 2.10). Additionally, it has been reported that the coordination of a chalcogen atom to a metal centre enhances the Ch bond by the creation or strengthening of a σ-hole opposite to the Ch–M bond, replacing the necessity for strong electron-withdrawing groups.[22] It is likely that the platinum(II) complexes reported here exemplify this latter effect on account of the coordination of the sulfur atom to the platinum centre with a sulfonyl oxygen located in the opposite direction to the Ch-M bond at the location of a possible σ-hole (Figure 2.15).

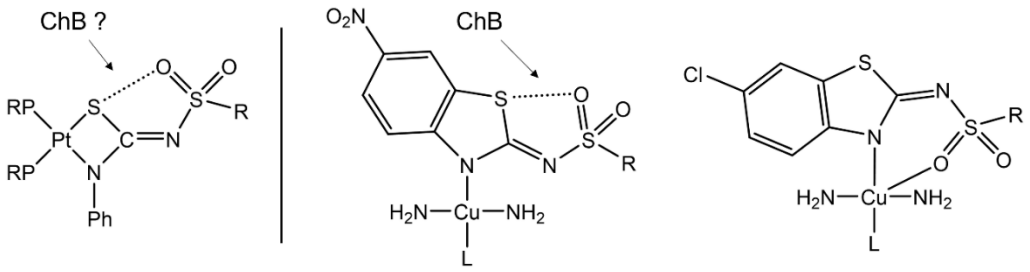

Figure 2.15: Chalcogen bonding positions of the complexes prepared in this investigation compared (left) with isothiourea copper complexes[21] (right).

To investigate the presence of a chalcogen bond of the type M-S··O, the Non-Covalent Interactions index of Johnson and co-workers, which was specifically developed to reveal non-covalent interactions, was utilized.[23, 24] The NCI index centres on the use of the normalized and dimensionless reduced density gradient produced from the electron density and its first diversative (RDG = $1/[2(3\pi^2)^{1/3}]|\nabla\rho|/\rho^{4/3}$) and electron density ρ(r), both conveniently calculated using readily available software (multiwfn).[25] The RDG has long been a useful scaler field used in many aspects of DFT calculations to represent the deviations in homogenous electron density of the system.[26] The corresponding plots of RDG verses ρ(r) oriented by the sign of the second eigenvalue (λ_2) behaves like an exponential curve in the absence of non-covalent interactions, representing the expansional decay of electron density moving away from an atom. The presence of NCI manifest on the plot as troughs or "spikes" in the low-density, low gradient region. These troughs indicate regions of unusually low density (RDG = 0) which are analogues to bond crystal points[27, 28] and are a distinctive and characteristic feature of NCI.

The sign of $\lambda_2\rho$ distinguishes the nature of the interactions: attractive interactions produce a negative sign(λ_2)ρ, while repulsive interactions yield a positive sign(λ_2)ρ.[29, 30] While analysis of the electron density (ρ) itself provides useful indications on the strength of the interaction, the corresponding plots of RDG verses (ρ) produces plots in which both attractive and repulsive interactions of the same magnitude of strength overlap. In this regard, the value of sign(λ_2)ρ has been shown to be more indicative of the type of interaction present.[31] This is usually

described in the literature as being a result of the relationship between the second eigenvalue of the electron-density Hessian matrix (λ_2) and the accumulation or depletion of density in the plane perpendicular to the interaction which is characteristic of the type of NCI present.[24, 32] However, in the original report by Johnson and coworkers, they argue that while some quantitative differences are introduced when considering density relaxation. For noncovalent interactions, the main features of the electron density and its derivatives appear clearly even in the case when the density is constructed from a simple sum of atomic densities.[23] This indicates that while accumulation or depletion of density does play an important role on the positioning of the trough on sign(λ_2)ρ, it is not the only consideration. Therefore, when comparing the value of the trough, similar systems and interactions should be compared. With these considerations in mind, 2D plots of the reduced density gradient verses sign(λ_2)ρ were calculated using optimized structures of complexes **2a**, **2b**, **2c**, **Pt1** and **Pt2** (using single point calculations of ωB97MV/LACVP) with a cubic volume measuring (2.11 Å) which centres on the midpoint between the sulfur and oxygen atoms and encompasses the region of interest. The resulting colourized 2D plot of complex **2a** is shown in Figure 2.16 and 2D plots of the remaining complexes are shown in Figure 2.17.

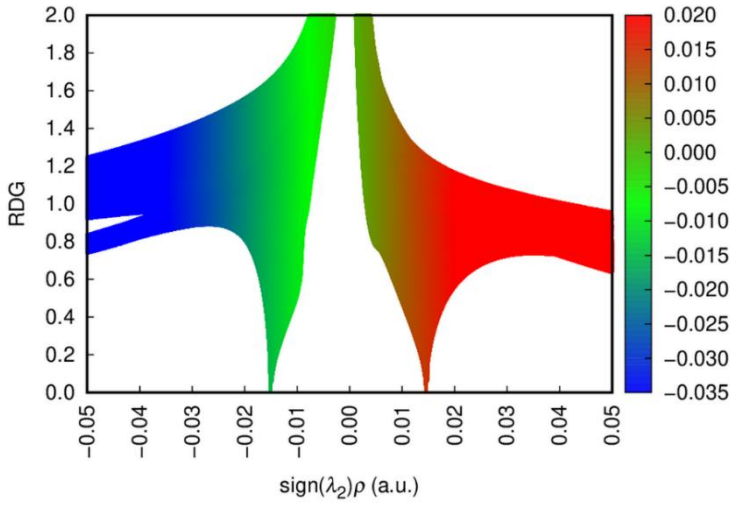

*Figure 2.16: Plot of RDG (s) verses sign(λ_2)ρ for complex **1a** showing troughs related to chalcogen bonding interactions.*

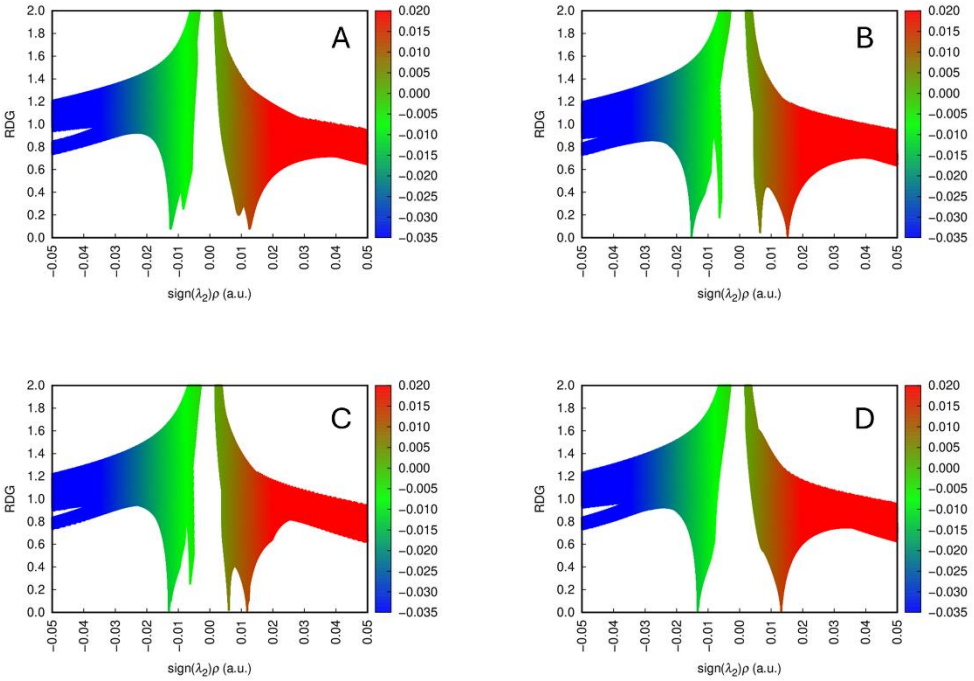

*Figure 2.17: Plots of RDG (s) verses sign(λ_2)ρ for complexes **2b** (A), **2c** (B), **Pt1** (C) and **Pt2** (D) showing troughs related to chalcogen bonding interactions.*

Each plot of RDG verses sign(λ_2)ρ shows a distinctive negative trough with an average sign(λ_2)ρ value of approximately -0.015 which is accompanied by a corresponding positive value ring critical points which relate to steric repulsion interactions from ring-type structural features, *i.e.* those relating to the steric strain of the S-C-N-S-O crescent. Plots 2.17 a, b and c also show much weaker (more positive) troughs relating to common weak Van der Waals interactions from nearby atoms. The primary negative troughs shown in the produced RDG plots (a-d) appear in the region most commonly associated with weak hydrogen boding type interactions. This provides some tentative indication that the strength of the interaction is relatively strong. Moreover, it demonstrates that the interaction is comparatively higher in strength than simple Van der Waals interactions which appear at slightly more positive values. To further illustrate the location and directionality of the NCI present, isosurfaces of the interaction between the thiourea sulfur and sulfonyl oxygen of complex **2a** are presented in 3D space (Figure 2.18) on a representation of the geometry optimized structure. In this case,

the NCI manifests between the thiourea sulfur and sulfonyl oxygen atoms with colouring corresponding to the plot in Figure 2.18.

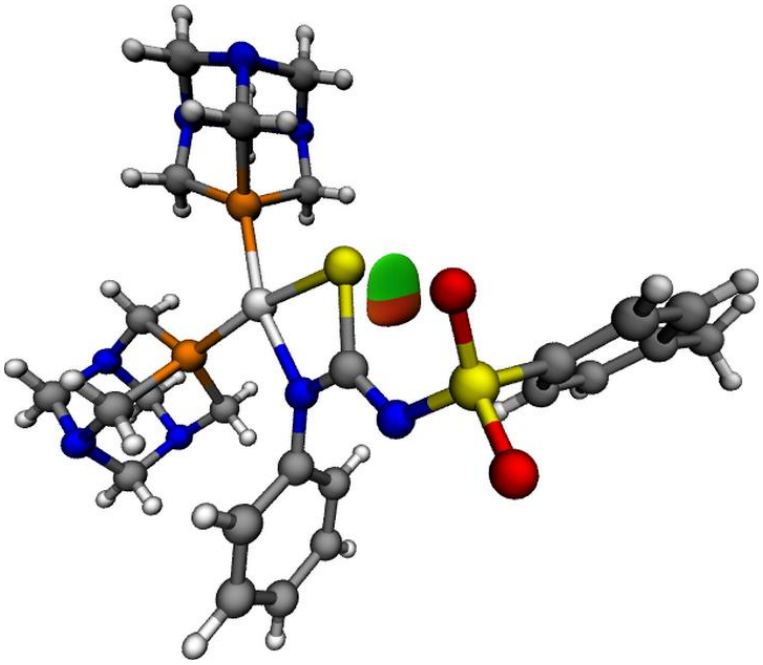

*Figure 2.18: NCI isosurfaces of the chalcogen interaction for complex **1a** using a blue-green-red colour scale from −0.02 < sign(λ_2)ρ(r) < +0.02 au. Isovalue = 0.4 for clarity.*

The presence of this relatively strong NCI between the thiourea sulfur and sulfonyl oxygen atoms validates the initial assumption of a Ch-bond being present based on S-O bond distances in the molecular XRD structures and provides a likely explanation of the observed preferential *distal* isomer formation.

2.2 Conclusions

In this chapter, a series of platinum(II) sulfonylthiourea complexes, which, as shown by NMR and XRD analyses, preferentially form the *distal* isomer unless a sterically bulky ligand forces the adoption of the *proximal* isomer. A crystallographic structural analysis revealed a short S···O distance in the *distal* isomer, indicating the presence of a chalcogen bond. Computational analysis of the non-covalent interactions (NCI) index indicates that indeed such an interaction is possible. While this chalcogen bond appears to contribute significantly to the

overall stability of the *distal* isomer, differences between the calculated lowest-energy structures and the experimentally observed structures suggest that the level of theory applied may not have fully captured all energetic contributions within the system. Despite these theoretical constraints, the presence of the chalcogen bond may account for the observed preference for *distal* isomer formation. These findings establish a good foundation and tools for modulating non-covalent interactions of sulfonylthiourea complexes, opening avenues for future research on ligand design and applications-oriented studies in which isomer selectivity plays an important role.

2.3 Experimental

2.3.1 Materials

The following chemicals were used as supplied from commercial sources: *p*-toluenesulfonamide (BDH), potassium *t*-butoxide, phenyl isothiocyanate, ethyl isothiocyanate, *t*-butyl isothiocyanate and ethanesulfonyl chloride (Sigma Aldrich). The complexes *cis*-$[PtCl_2(PPh_3)_2]$, *cis*-$[PdCl_2(PTA)_2]$ and *cis*-$[PtCl_2(TCEP)_2]$ were prepared by ligand substitution of the cyclo-octa-1,5-diene (COD) ligand of $[PtCl_2(COD)]$[33] with the stoichiometric quantity of phosphine in dichloromethane.

2.3.2 Instrumentation

^{31}P (243 MHz) and ^{1}H (600 MHz) NMR spectra were recorded at 25°C (unless otherwise stated) on a 600 MHz Jeol ECZR NMR spectrometer using $CDCl_3$ or DMSO-d_6 as the solvent. Some ^{31}P spectra, where stated, were recorded from neat reaction mixtures in non-deuterated solvent. Spectra were processed using the Joel Delta software. ESI mass spectra were recorded in methanol using a Bruker Daltonics MicrOTOF electrospray ionization mass spectrometer. Methanolic sodium formate solution was used for calibration. Samples were prepared in Eppendorf tubes by dissolving each sample in 1 drop of dichloromethane and making up to 1.5 mL with methanol. Samples were centrifuged before use to ensure separation of undissolved solids. Spectra were recorded with a *Capillary Exit* voltage of 150 V and a *Skimmer 1* voltage of 50 V unless otherwise stated.

Elemental analysis was performed by the Chemical Analysis Facility, Department of Molecular Sciences, Macquarie University, Sydney, Australia. Single crystal X-Ray diffraction was carried out by the University of Auckland Micro characterization Facility, Auckland, New Zealand. Optimization and single point calculations were conducted using Qchem software[34] on the New Zealand eScience Infrastructure (NeSI) high performance computing facilities. MultiWFN was used for the calculation of non-covalent interactions including the calculation of the reduced density gradient.[25] Gnuplot was used for the representation of 2D RDG plots[35] and VMD[36] was used for the representation of 3D isosurfaces.

2.3.3 Synthesis of *p*-TolSO$_2$NHC(S)NHPh (S-L1)

Thiourea ligands were synthesized by the modified procedure inspired by Idrees et *al.*[3] *p*-Toluenesulfonamide (5.0 g, 0.03 mol) and potassium *tert*-butoxide (3.2 g, 0.03 mol) were added to DMF (20 mL) and warmed to 60°C with stirring to ensure the contents were fully dissolved. To the warmed solution, phenyl isothiocyanate (3.91 g, 0.029) was added portionwise before being stirred for a further 5-10 minutes. The product was precipitated by the single addition of ice cold water (50 mL) which had been acidified with hydrochloric acid (3 mL approx.) before being isolated immediately by vacuum filtration and washed with distilled water (2 x 20 mL). The resulting solid was recrystallized from hot EtOH yielding a white crystalline solid (4.1 g, 46 %). ESI MS: Capillary exit voltage 90 V, *m/z* $[M + H]^+$ 307, $[M+Na]^+$ 330.

2.3.4 Synthesis of EtSO$_2$NHC(S)NHPh (S-L2)

Ethanesulfonyl chloride (5 g, 0.039 mol) was added dropwise to concentrated aqueous ammonia (150 mL, 33%, excess) with rapid stirring, during which time the temperature was allowed to rise to 80 °C before being held at this temperature for 2 h. The solution was then cooled and maintained at room temperature for 48 hours open to the air to allow evaporation of excess ammonia. The product was extracted by three consecutive liquid-liquid separations into acetonitrile (3 x 100 mL) and the combined organic phases were evaporated to a thick oily residue which was used without further purification. The target ligand was synthesized

following the method of **L1** using the freshly prepared ethanesulfonamide (3 g), potassium *tert*-butoxide (3 g) and phenyl isothiocyanate (3.7 g). White crystalline solid (2.6 g, 39 %). ESI MS: Capillary exit voltage 90 V, *m/z* $[M + H]^+$ 245, $[M + Na]^+$ 267.

2.3.5 Synthesis of $TolSO_2NHC(S)NHCH(CH_3)_3$) (S-L3)

The ligand **L3** was synthesized following the method of **L1** using *p*-toluenesulfonamide (5 g, 0.03 mol), potassium *t*-butoxide (3.25 g, 0.03 mol) and *t*-butyl isothiocyanate (3.4 g, 0.029 mol). White crystalline solid (4.1 g, 49 %). ESI MS: Capillary exit voltage 90 V, *m/z* $[M + H]^+$ 287, $[M + Na]^+$ 309.

2.3.6 General synthesis of bis(PPh_3) and bis(TCEP) sulfonylthiourea complexes

Equimolar quantities of the ligand and metal starting material were suspended in MeOH (30 mL) with stirring. The mixture was brought to reflux followed by the addition of triethylamine (0.3 mL, excess). The solution was refluxed for 5 minutes after which time the complex was precipitated by the rapid addition of cold distilled water (40 mL). The mixture was cooled rapidly using an ice bath to facilitate precipitation and coagulation before the solid product was filtered and washed with distilled water (3 x 20 mL) and dried under vacuum. Details pertaining to each compound are given in Table 2.3.

2.3.7 General synthesis of bis(PTA) sulfonylthiourea complexes

Equimolar quantities of the ligand and $[PtCl_2(PTA)_2]$ were suspended in MeOH (30 mL) with stirring. The mixture was brought to reflux and 2 mol L^{-1} aqueous solution of sodium hydroxide (50 µL, excess) was added. The solution was refluxed for a further 10 minutes before removal of the solvent under reduced pressure. The solid product was dissolved in the minimal amount of CH_2Cl_2 (3-5 mL) and passed through 2 cm of silica to remove undissolved solids before the removal of the solvent under reduced presure. Details pertaining to each compound are given in Table 2.3.

2.3.8 General synthesis of mixed ligand sulfonylthiourea complexes

The complex [Pt(COD)Cl_2] in methanol (20 mL) was brought to reflux. Pyridine (3 drops, excess) was added. Equimolar amounts of triphenylphosphine and the thiourea ligand were added consecutively with a duration of 1-2 minutes between each addition. The solution was refluxed for 5 minutes before precipitation with the rapid single addition of cold water (30 mL). The mixture was cooled rapidly using an ice bath to facilitate precipitation and coagulation before the solid product was filtered and washed with distilled water (3 x 20 mL) and dried under vacuum. Details pertaining to each compound are given in Table 2.3.

Table 2.3: Synthesis details for the prepared sulfonylthiourea complexes.

	Starting metal complex			PPh_3/Pyridine	Thiourea		Yield	
Product		mg	mmol	mg	mg	mmol	mg	%
2a	*cis*-[$PtCl_2(PTA)_2$]	100	0.172	-	54	0.176	99	70.5
2b	*cis*-[$PtCl_2(TCEP)_2$]	100	0.167	-	52	0.169	122	82.3
2c	*cis*-[$PtCl_2(COD)$]	40	0.106	28.5/96	33	0.107	64	71.1
2d	*cis*-[$PtCl_2(PTA)_2$]	100	0.172	-	43	0.176	95	73.2
2e	*cis*-[$PtCl_2(COD)$]	40	0.106	28/87	28	0.114	67	80.4
2f	*cis*-[$PtCl_2(PPh_3)_2$]	100	0.126	-	38	0.132	103	81.0

[Pt{TolSO$_2$NC(S)NPh}(PTA)$_2$] ***2a***

Off-white solid. Elemental analysis: Found (%) C 38.4; H 4.5; N 15.7. Calculated (%) C 38.3; H 4.4; N 13.7. ESI MS: *m/z* $[M + H]^+$ 814. NMR (DMSO-d_6 243 MHz): $^{31}P\{^1H\}$, δ -61.06 [d, $^1J_{PtP}$ 2740 Hz, $^2J_{PP}$ 21 Hz] and -77.73 [d, $^1J_{PtP}$ 2908 Hz, $^2J_{PP}$ 21 Hz]; (DMSO-d_6 600 MHz) ^1H, δ 7.52 (d, *p*-tolyl CH, 2 H), 7.35 (t, aromatic CH, 2 H), 7.22 (d, *p*-tolyl CH, 2 H), 7.12 (t, aromatic CH, 1 H), 6.89 (d, aromatic CH, 1 H), 4.41 (dd, N-CH_2-N, 6 H), 4.15 (dd, N-CH_2-N, 6 H), 4.12 (s, N-CH_2-P, 6 H), 3.73 (s, N-CH_2-P, 6 H), 2.30 (s, CH_3 3 H).

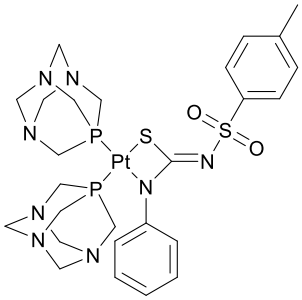

[Pt{TolSO$_2$NC(S)NPh}(TCEP)$_2$] ***2b***

Off-white solid. Elemental analysis: Found (%) C 43.3; H 4.1; N 12.3. Calculated (%) C 43.39; H 4.1; N 12.6. ESI MS: *m/z* $[M + H]^+$ 886. NMR (DMSO-d_6 243 MHz): $^{31}P\{^1H\}$, δ 6.13 [d, $^1J_{PtP}$ 2939 Hz, $^2J_{PP}$ 21 Hz] and -2.86 [d, $^1J_{PtP}$ 1407 Hz, $^2J_{PP}$ 21 Hz]; (DMSO-d_6 600 MHz) ^1H, δ 7.55 (d, *p*-tolyl CH, 2 H), 7.32 (t, aromatic CH, 2 H), 7.20 (d, *p*-tolyl CH, 2 H), 7.17 (t, aromatic CH, 1 H), 6.96 (d, aromatic CH, 2H), 2.83 (dt, CH_2-CN, 2 H), 2.69 (dt, CH_2-CN, 2 H), 2.36 (dt, CH_2-P, 2 H), 2.29 (s, CH_3, 3 H), 1.83 (dt, CH_2-P, 2 H).

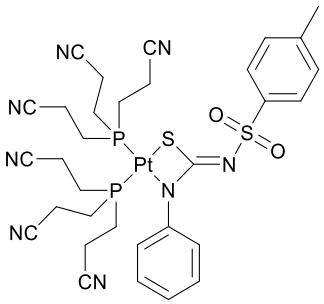

[Pt{TolSO$_2$NC(S)NPh}(Py)(PPh$_3$)] ***2c*** Pale yellow solid. Elemental analysis: Found (%) C 52.4; H 4.0; N 4.9. Calculated (%) C 52.8; H 3.8; N 5.0. ESI MS: *m/z* $[M + H]^+$ 841. NMR ($CDCl_3$ 243 MHz): $^{31}P\{^1H\}$, δ 15.6 [s, $^1J_{PtP}$ 3637 Hz] ($CDCl_3$ 600 MHz) ^1H, δ 8.2-6.6 (m, aromatic, 29 H), 2.15 (s, CH_3, 3 H).

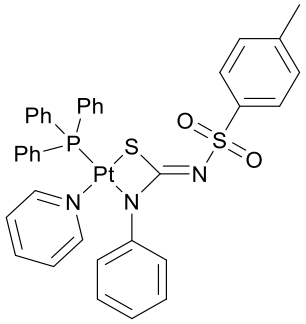

[Pt{EtSO$_2$NC(S)NPh}(PTA)$_2$] ***2d***

Off-white solid. Elemental analysis: Found (%) C 33.7; H 4.8; N 14.7. Calculated (%) C 33.5; H 4.5; N 14.9. ESI MS: *m/z* $[M + H]^+$ 752. NMR (DMSO-d_6 243 MHz): $^{31}P\{^1H\}$, δ -60.9 [d, $^1J_{PtP}$ 2754 Hz, $^2J_{PP}$ 18 Hz] and -70.6 [d, $^1J_{PtP}$ 2881 Hz, $^2J_{PP}$ 18 Hz]; (DMSO-d_6 600 MHz) ^1H, δ 7.35 (t, aromatic CH, 2 H), 7.12 (t, aromatic CH, 1 H), 6.94 (d, aromatic CH, 2 H), 4.43 (dd, N-CH_2-N, 6 H), 4.16 (dd, N-CH_2-N, 6 H), 4.16 (s, N-CH_2-P, 6 H), 3.76 (s, N-CH_2-P, 6 H), 2.83 (q, CH_2, 2 H), 1.05, (t, CH_3, 3 H).

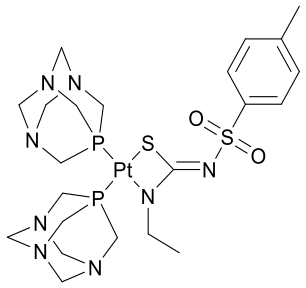

[Pt{EtSO$_2$NC(S)NPh}(Py)(PPh$_3$)] ***2e***

Pale yellow solid. Elemental analysis: Found (%) C 49.5; H 3.7; N 5.4. Calculated (%) C 49.3; H 3.8; N 5.4. ESI MS: *m/z* $[M + H]^+$ 779. NMR ($CDCl_3$ 243 MHz): $^{31}P\{^1H\}$, δ 4.4 [s, $^1J_{PtP}$ 3626 Hz] ($CDCl_3$ 600 MHz) ^1H, δ 7.7-6.7 (m, aromatic, 25 H), 3.67 (q, CH_2, 2 H), 1.50 (t, CH_3, 3 H).

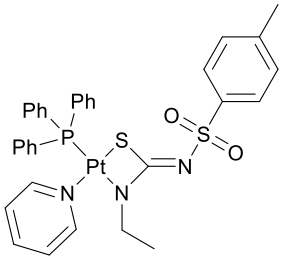

[Pt{TolSO$_2$NC(S)N(t-Butyl)}(PPh$_3$)$_2$] ***2f*** Pale yellow solid. Elemental analysis: Found (%) C 57.1; H 4.6; N 2.9. Calculated (%) C 57.4; H 4.6; N 2.8. ESI MS: *m/z* $[M + H]^+$ 1004. NMR ($CDCl_3$ 243 MHz): $^{31}P\{^1H\}$, δ 19.35 [d, $^1J_{PtP}$ 3204 Hz, $^2J_{PP}$ 22 Hz] and 12.25 [d, $^1J_{PtP}$ 3610 Hz, $^2J_{PP}$ 22 Hz]; ($CDCl_3$ 600 MHz) ^1H, δ 7.6-6.9 (m, aromatic, 34 H), 2.26 (s, CH_3 3 H), 1.07 (s, *t*-butyl, 6 H).

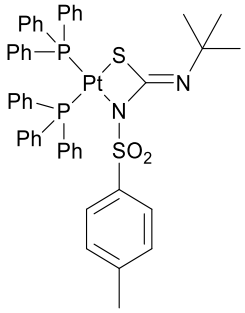

2.3.9 X-ray crystal structure determinations

Crystals of satisfactory quality for single crystal diffraction of complexes **2a** and **2c** were grown by the slow diffusion of diethyl ether into dichloromethane solutions of the complexes. Crystals of **2b** were grown slowly from a DMSO/water mixture and crystals of **2f** were grown by the slow evaporation of a methanol solution containing the complex. Structures were solved using Olex2[37] with the Olex2.solve[38] structure solution programme using Charge Flipping and refined with the Olex2.refine[38] refinement package using Gauss–Newton minimization. Crystal and refinement details are summarized in the supplementary data.

2.4 References

1. M. C. Risi, G. C. Saunders and W. Henderson, *Inorganica Chimica Acta*, 2021, **526**, 120506.
2. S. Perveen, S. M. Abdul Hai, R. A. Khan, K. M. Khan, N. Afza and T. B. Sarfaraz, *Synthetic Communications*, 2005, **35**, 1663-1674.
3. D. Idrees, M. Hadianawala, A. D. Mahapatra, B. Datta, S. Roy, S. Ahamad, P. Khan and M. I. Hassan, *International Journal of Biological Macromolecules*, 2018, **115**, 961-969.
4. W. Henderson, B. K. Nicholson and C. E. F. Rickard, *Inorganica Chimica Acta*, 2001, **320**, 101-109.
5. O. C. Okpareke, W. Henderson, S. Akkoç and B. Coban, *Inorganica Chimica Acta*, 2022, **531**, 120707.
6. T. G. Appleton, *Coordination Chemistry Reviews*, 1997, **166**, 313-359.
7. P. Bippus, M. Skocic, M. A. Jakupec, B. K. Keppler and F. Mohr, *Journal of Inorganic Biochemistry*, 2011, **105**, 462-466.
8. J. E. Spenceley, W. Henderson, J. R. Lane and G. C. Saunders, *Inorganica Chimica Acta*, 2015, **425**, 83-91.
9. R. G. Pearson, *Inorganic Chemistry*, 1973, **12**, 712-713.
10. J. A. Bilbrey, A. H. Kazez, J. Locklin and W. D. Allen, *Journal of Computational Chemistry*, 2013, **34**, 1189-1197.
11. G. Ferguson, P. Roberts, E. Alyea and M. Khan, *Inorganic Chemistry*, 1978, **17**, 2965-2967.
12. A. D. Phillips, L. Gonsalvi, A. Romerosa, F. Vizza and M. Peruzzini, *Coordination Chemistry Reviews*, 2004, **248**, 955-993.
13. P. J. Squattrito and A. Clearfield, *Crystal Structure Communications*, 1989, **45**, 1819-1820.
14. N. Mardirossian and M. Head-Gordon, *The Journal of Chemical Physics*, 2016, **144**.
15. L. Vogel, P. Wonner and S. M. Huber, *Angewandte Chemie International Edition*, 2019, **58**, 1880-1891.
16. R. W. Newberry and R. T. Raines, *ACS Chemical Biology*, 2019, **14**, 1677-1686.
17. N. Biot and D. Bonifazi, *Chemistry–A European Journal*, 2020, **26**, 2904-2913.
18. S. Benz, J. López‐Andarias, J. Mareda, N. Sakai and S. Matile, *Angewandte Chemie International Edition*, 2017, **56**, 812-815.
19. K. T. Mahmudov, A. V. Gurbanov, V. A. Aliyeva, M. F. C. G. da Silva, G. Resnati and A. J. Pombeiro, *Coordination Chemistry Reviews*, 2022, **464**, 214556.
20. U. Adhikari and S. Scheiner, *The Journal of Physical Chemistry A*, 2012, **116**, 3487-3497.
21. M. González-Álvarez, G. Alzuet, J. Borrás, L. del Castillo Agudo, S. García-Granda and J. M. Montejo-Bernardo, *Inorganic Chemistry*, 2005, **44**, 9424-9433.
22. R. M. Gomila, A. Bauzá and A. Frontera, *Dalton Transactions*, 2022, **51**, 5977-5982.

23. E. R. Johnson, S. Keinan, P. Mori-Sánchez, J. Contreras-García, A. J. Cohen and W. Yang, *Journal of the American Chemical Society*, 2010, **132**, 6498-6506.
24. J. Contreras-García, W. Yang and E. R. Johnson, *The Journal of Physical Chemistry A*, 2011, **115**, 12983-12990.
25. T. Lu and F. Chen, *Journal of Computational Chemistry*, 2012, **33**, 580-592.
26. A. J. Cohen, P. Mori-Sánchez and W. Yang, *Science*, 2008, **321**, 792-794.
27. R. F. Bader, *Chemical Reviews*, 1991, **91**, 893-928.
28. C. F. Matta and R. J. Boyd, *The quantum theory of atoms in molecules*, 2007, 1-34.
29. J. R. Lane, J. Contreras-García, J.-P. Piquemal, B. J. Miller and H. G. Kjaergaard, *Journal of Chemical Theory and Computation*, 2013, **9**, 3263-3266.
30. A. Otero-De-La-Roza, E. R. Johnson and J. Contreras-García, *Physical Chemistry Chemical Physics*, 2012, **14**, 12165-12172.
31. C. Lefebvre, G. Rubez, H. Khartabil, J.-C. Boisson, J. Contreras-García and E. Hénon, *Physical Chemistry Chemical Physics*, 2017, **19**, 17928-17936.
32. R. F. Bader, *The Journal of Physical Chemistry A*, 1998, **102**, 7314-7323.
33. J. X. McDermott, J. F. White and G. M. Whitesides, *Journal of the American Chemical Society*, 1976, **98**, 6521-6528.
34. Y. Shao, Z. Gan, E. Epifanovsky, A. T. Gilbert, M. Wormit, J. Kussmann, A. W. Lange, A. Behn, J. Deng and X. Feng, *Molecular Physics*, 2015, **113**, 184-215.
35. T. Williams, C. Kelley, C. Bersch, H.-B. Bröker, J. Campbell, R. Cunningham, D. Denholm, G. Elber, R. Fearick and C. Grammes, *An interactive plotting program. Available online: http://www.gnuplot. info/docs_5*, 2017, **2**.
36. W. Humphrey, A. Dalke and K. Schulten, *Journal of Molecular Graphics*, 1996, **14**, 33-38.
37. O. V. Dolomanov, L. J. Bourhis, R. J. Gildea, J. A. K. Howard and H. Puschmann, *Journal of Applied Crystallography*, 2009, **42**, 339-341.
38. L. J. Bourhis, O. V. Dolomanov, R. J. Gildea, J. A. K. Howard and H. Puschmann, *Acta Crystallographica Section A: Foundations and Advances*, 2015, **71**, 59-75.

Chapter Three

The coordination chemistry and anticancer activity of organo-ruthenium(II), -iridium(III) and -rhodium(III) complexes with sulfonyl-substituted thiourea ligands.

Ruthenium(II) piano-stool complexes and the similar rhodium(III) and iridium(III) analogues have garnered considerable attention as promising alternatives to platinum-based metallodrugs in the treatment of a variety of cancers.[1-6] An important aspect of research in this area is the nature and coordination behaviour of the ligands, which form the robust backbone and foundation of the complex and offer an easily modifiable route for achieving desired characteristics.[7] In this context, an array of organometallic piano-stool complexes with a wide range of ligands have been investigated for both their coordination chemistry and biological activity.[8] Two prominent examples include RAPTA-C [(η^6-*p*-cymeneRu)(PTA)Cl_2] (PTA = 1,3,5-triaza-7-phosphaadamantane) and its many derivatives popularised by Dyson and co-workers[9-11] and RM175 [Ru(η^6-biphenyl)(en)Cl]$^+$ (en = 1,2-diaminoethane) studied by Sadler and colleagues.[12] Acylthiourea compounds have seen extensive interest on account of their facile synthesis, diverse coordination chemistry and promising pharmaceutical properties.[13, 14] Many recent studies on the coordination chemistry and biological activity of ruthenium(II) based acylthiourea complexes have been reported.[15, 16] Promising recent examples include complexes of the type [(cym)Ru(PPh_3)(T)Cl]PF_6 (**A1**) and [(cym)Ru(PPh_3)(T)]PF_6 (**A2**) (Figure 3.1) (cym = η^6-*p*-cymene), which show sub-micromolar IC_{50} values in human lung cells (T = *N*-acyl-*N'*(monosubstituted)thiourea).[17]

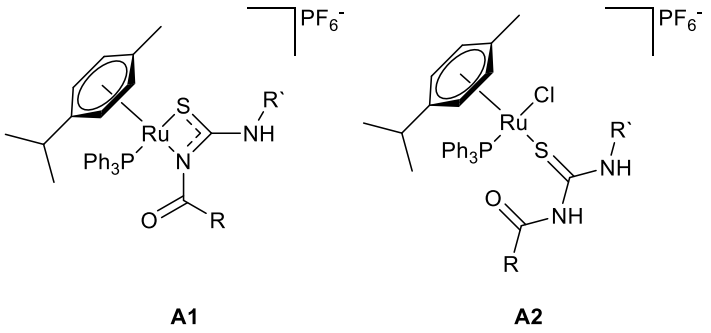

*Figure 3.1: General structures of [(cym)Ru(PPh$_3$)(T)Cl]PF$_6$ (**A1**) and [(cym)Ru(PPh$_3$)(T)]PF$_6$ (**A2**)*[17]

While acylthiourea-based compounds have seen a significant increase in interest,[16, 18] functionalized thiourea derivatives with other electron-withdrawing groups have not. For example, those of sulfonylthiourea ligands, which differ by the replacement of the acyl C=O functional group with a similar sulfonyl group are promising given the significant biological activity often associated with sulfonamide and sulfonylurea-based pharmaceuticals. Unlike acylthiourea ligands which typically favour S,O or S,N chelation, sulfonylthiourea ligands have been shown in this thesis to coordinate to metal centres exclusively *via* the S,N donor atoms.[19-21] Presumably, this is because of the reduced nucleophilicity of the sulfonyl group compared to that of the acyl C=O group (Figure 3.2). Because of this reduced nucleophilicity, sulfonylthiourea ligands are not expected to coordinate *via* the O atoms. In principle, sulfonylthioureas may also coordinate as monodentate neutral or monoanionic ligands through the core thiourea S donor atom, although no prior examples have been reported to date.

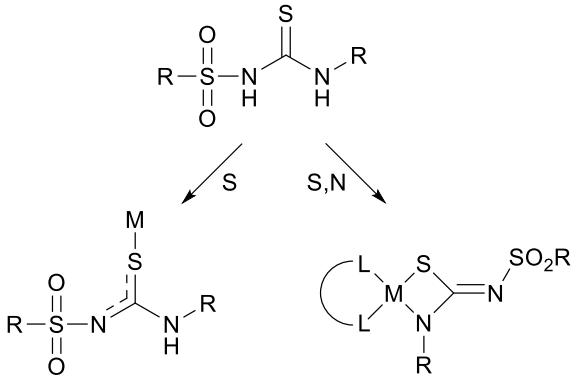

Figure 3.2: Monodentate S and bidentate S,N (distal) coordination modes of sulfonylthiourea ligands.

Given that no organometallic complexes of sulfonylthiourea ligands have been reported, and prompted by the potential antiproliferative and antimicrobial biological activity often exhibited by sulfonyl-containing compounds and related acylated thiourea analogues, this chapter investigates these ligands' piano-stool complexes. In this chapter a preliminary investigation onto the coordination chemistry of sulfonylthiourea ligands with ruthenium(II) arene and iridium(III) and rhodium(III) Cp* piano-stool complexes and studies on the antiproliferative activity are given.

3.1 Results and discussion

3.1.1 Synthesis and characterization of organometallic complexes with mono- and dianionic sulfonylthiourea ligands.

Given the significant differences in coordination chemistry, reactivity and behaviour that often result from the change of metal centres, different avenues of synthesis to those reported in Chapter 2 are explored. As there is currently no literature precedent for the synthesis of organometallic piano-stool complexes with sulfonylthiourea ligands, a series of reactions and conditions are investigated in this section using the sulfonylthiourea ligands *p*-TolSO_2NHCSNHPh (**S-L1**) and $CH_3CH_2SO_2$NHCSNHPh (**S-L2**) (Prepared in Chapter 2, Figure 3.3). The ligand CH_3SO_2NHCSNHPh (**S-L3**) is also shown in Figure 3.3.

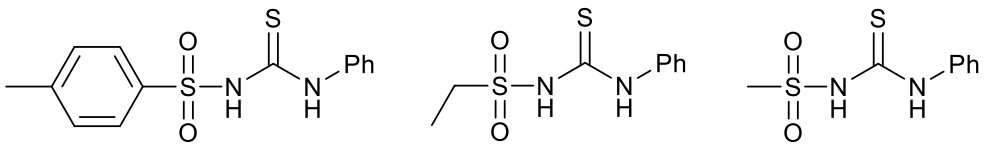

S-L1 **S-L2** **S-L3**

Figure 3.3: Structures of the sulfonylthiourea ligands referred to in this chapter

Because of the large quantity of intermediates and various reaction paths, a different numbering scheme is used in this chapter which will be explained briefly here. Letters a-d indicate type of arene ring and metal on the piano stool complex, a = *p*-cymene and ruthenium(II), b = benzene and ruthenium(II), c = Cp* and iridium(III) and d = Cp* and rhodium(III). The numbers 1-3 indicate the type of phosphine on the central metal atom, 1 = PPh_3, 2 = PTA and 3 = TCEP (TCEP = tris(2-cyanoethyl)phosphine). The suffix L1-L3 indicates the sulfonylthiourea ligand as indicated in Figure 3.3. A complete reaction mechanism for this chapter is included as Appendix 2. Complexes [(η^6-*p*-cymene)Ru{$CH_3SO_2NC(S)NPh$}(PPh_3)] **1aL3**, [(η^6-benzene)Ru{$CH_3SO_2NC(S)NPh$}(PPh_3)] **1bL3** and [(η^6-*p*-cymene)Ru{$CH_3SO_2NC(S)NPh$}(tcep)] **3aL3** were prepared in a previous MSc research project and are included for discussion only.[22]

Initial investigations centred on sulfonylthiourea ligands acting as monoanionic ligands towards the Ru(II) *p*-cymene dimer. In this regard, the synthesis of the chlorido-containing complexes **aL1** and **aL2** was achieved by the reactions of the Ru(II) dimeric precursor $[(cym)RuCl_2]_2$ (**a**) with two mole equivalents of the sulfonylthiourea ligands **S-L1** and **S-L2** in methanol (Scheme 3.1). The complexes were isolated in good yield and purity by removal of the solvent under reduced pressure, followed by washing with petroleum spirits and hexane. By the same method, complex **dL1** was prepared by the reaction between the Rh(III) precursor $[Cp^*RhCl_2]_2$ and **S-L1**. The complexes were confirmed uing ESI-(+) mass spectrometry by the observation of ions relating to the fragmentated loss of the chlorido ligand, $[M - Cl]^+$.

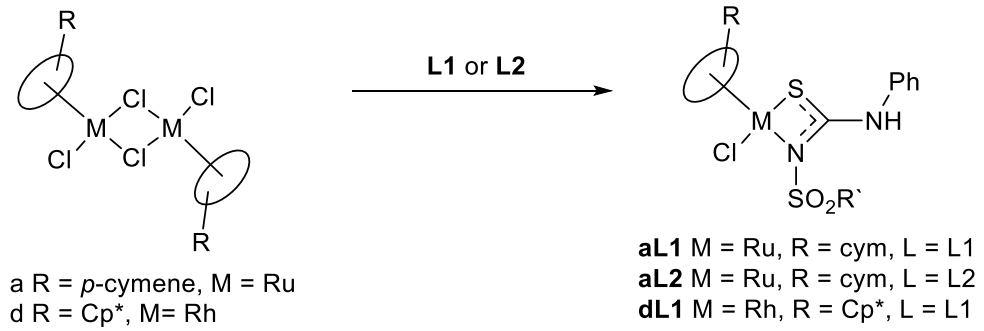

Scheme 3.1: Reactions between the Ru(II) p-cymene or Rh(III) Cp dimers with **S-L1** and **S-L2**.*

The tertiary phosphine-containing complex **2cL1**, which also contains the sulfonylthiourea ligand bound as a monoanion, was prepared from the Ir(III) precursor [Cp*$IrCl_2$(PTA)] (**2c**) in methanol in the presence of NaOH (Scheme 3.2). Using the same method, complexes **2dL1** and **2dL2** were prepared from [Cp*$RhCl_2$(PTA)] **(2d**) with **S-L1** and **S-L2** respectively. The complexes were isolated by removal of solvent under reduced pressure. Removal of residual NaOH was achieved by dissolving the product in dichloromethane before passing the dissolved complex through approximately 1cm of silica.

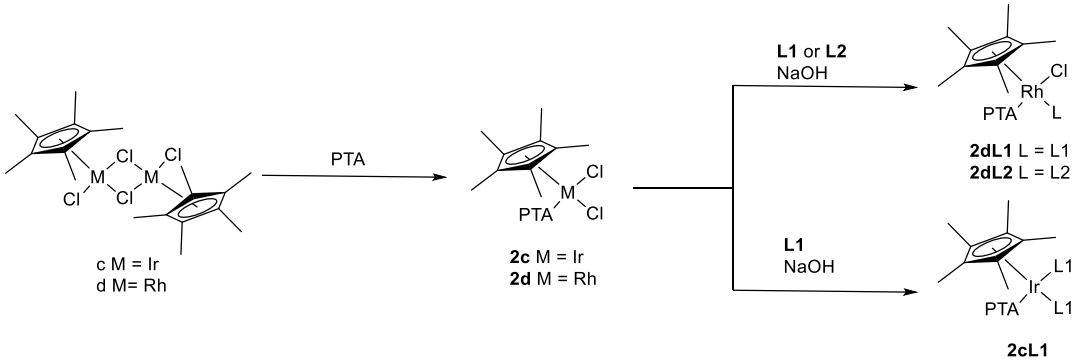

*Scheme 3.2: Reactions between **S-L1** and **S-L2** with Ir(III) and Rh(III) precursors **2c** and **2d**.*

ESI-MS(+) mass spectrum of complex **2cL1**, which contains two monodentate sulfonylthiourea ligands, showed an ion relating to the loss of a single thiourea ligand, $[M - L]^+$, with minor ions being observed corresponding to $[M + Na]^+$ and $[M + K]^+$ adducts. Complexes **2dL1** and **2dL2** were confirmed by the appearance of ions relating to the intact protonated complex, herein termed the pseudo-

molecular $[M + H]^+$ base peak. Minor ions which could be assigned to the fragmented loss of the phosphine ancillary ligand (PR_3) from the protonated complex, $[M – PR_3 + H]^+$, were also observed. ^1H NMR spectra of these complexes display a broad singlet resonance between 9.4 and 9.9 ppm which could be assigned to the thiourea NH, confirming the monoanionic nature of these ligands. The remaining ^1H and $^{31}P\{^1H\}$ spectra show the archetypal features. Interestingly, despite the addition of base to the reaction mixture and therefore the possibility of the sulfonylthiourea ligands to act as a dianion, by the removal of both thiourea hydrogen atoms, the complexes contained the ligand bound as a monoanion instead. It is also noteworthy that with reactions between the sulfonylthiourea ligands and the Ru(II) *p*-cymene dimer, the ligand acts as a monoanionic ligand despite the absence of base. This observation indicates that the sulfonyl-amidic proton must be quite acidic and therefore easily removed.

To investigate the sulfonylthiourea ligands acting as dianionic ligands a series of reactions with L1-L3 with phosphine containing precursor complexes were investigated. Thus, reactions between the sulfonylthiourea ligand **S-L1** and the ruthenium(II), rhodium(III) and iridium(III) precursors **1a**, **1c**, **1d** and **2a** in mixture of methanol and triethylamine stirred at room temperature for approximately 12 hours gave the corresponding complexes **1aL1**, **1cL1**, **1dL1** and **2aL1** respectively (scheme 3.3)

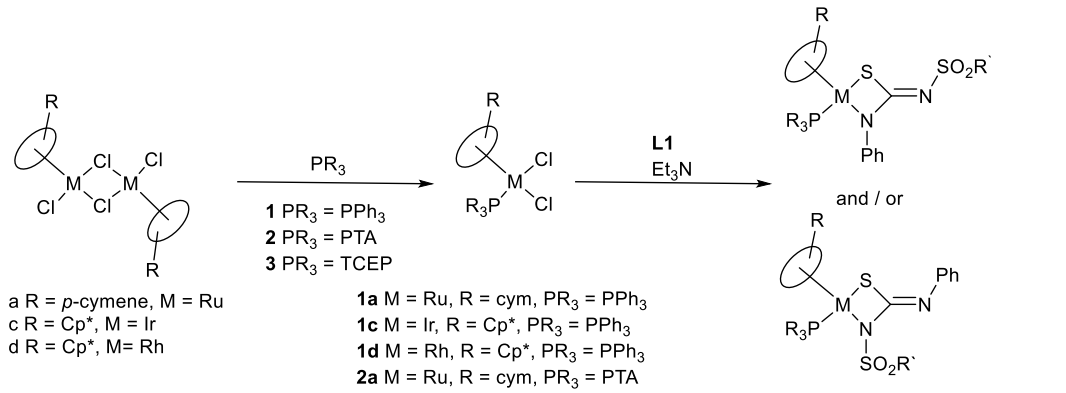

*Scheme 3.3: Reactions of **S-L1** with a series of Ru(II), Ir(III) and Rh(III) phosphine precursor complexes.*

The low solubility of the resulting complexes, with the exception of complex **2aL1**, resulted in the target compound precipitating out of the methanol solution during the reaction, because of this, the isolation and purification of the complexes was conducted by filtration followed by washing with distilled water. On account of the considerably increased solubility in protic solvents afforded by the PTA ligand, the reaction mixture of **2aL1** required near complete removal of solvent before satisfactory precipitation occurred. It is worth noting that the repeated attempted syntheses of the ruthenium complexes by this route with temperatures exceeding 50 °C, which has been documented previously for piano stool complexes with simple thiourea ligands[23] and acylthioureas,[24] resulted in grey/green coloured, presumably oxidized, species and decomposition products. For unknown reasons, this is presumably a result of the inclusion the phosphine ancillary ligand as reactions of the chlorido containing complexes did not suffer from such degradation during synthesis.

An alternative synthesis of complex **1aL1** was achieved using the chlorido complex **aL1**. The complex was dissolved in chloroform, followed by the addition of PPh_3 and powdered Ag_2O (Scheme 3.4). This resulted in the substitution of the labile chlorido ligand with PPh_3 while the Ag_2O acts as a sufficiently strong base to deprotonate the ligand to its dianionic form and as a halide abstracting agent.

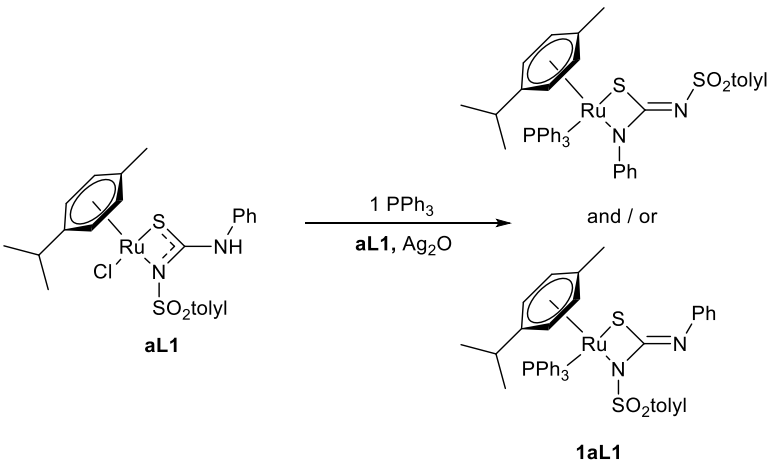

*Scheme 3.4: The conversion of **aL1** into **1aL1** using silver oxide and triphenylphosphine.*

Using a similar method as for complexes **aL1** and **aL2**, the thiourea sulfur-bridged dimeric complex **a_2L1** was prepared from the reaction between **S-L1** and $[(cym)RuCl_2]_2$ in a methanol and triethylamine mixture (Scheme 3.5). In the ESI-MS(+) spectra, the complexes bearing a phosphine ligand were confirmed by the appearance of their pseudo-molecular $[M + H]^+$ base peak and $[M – PR_3 + H]^+$ ions. The dimeric complex **a_2L1** was confirmed by the assigned $[M + H]^+$ base peak and an ion which could be assigned to fragmented splitting of the dimer, $[M/2 + H]^+$. A full synthetic scheme for this chapter is included in Appendix 2.

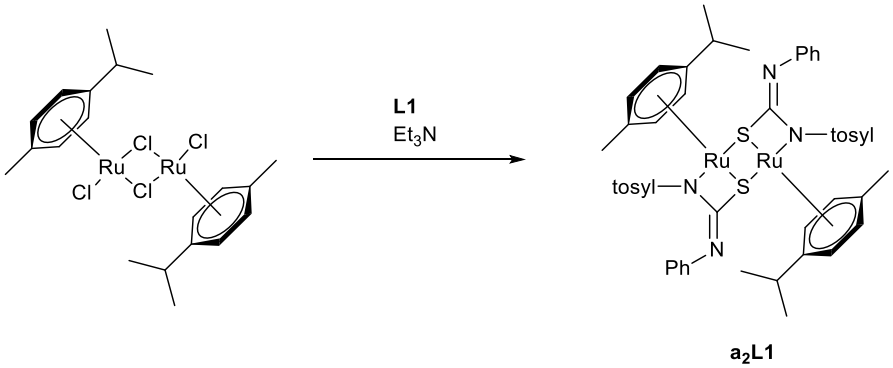

*Scheme 3.5: Preparation of **a_2L1** from the Ru(II) p-cymene dimer and **S-L1** and Et_3N.*

^1H and $^{31}P\{^1H\}$ NMR spectra of the Ru(II), Ir(III) and Rh(III) sulfonylthiourea complexes showed the expected features, *i.e.*, the methyl resonance of the Cp* ligand appeared as a doublet in the phosphine-containing complexes (**1cL1**, **1dL1**, **2dL1**, **2dL2** and **2cL1**) between 1.75 and 1.65 ppm with a J coupling constant of 4 Hz. This resonance for complex **dL1**, which does not contain a phosphine ligand was notably a single peak at 1.75 ppm. This observation indicates that in this case, the phosphorus atom coupling to the methyl hydrogen atoms rather than the rhodium atom is responsible for the doublet peak of the methyl Cp* resonance. This observation was further supported by the $^1H\{^{31}P\}$ NMR spectrum of complex **2dL2** which clearly showed the methyl Cp* resonance as a singlet (Figure 3.3).

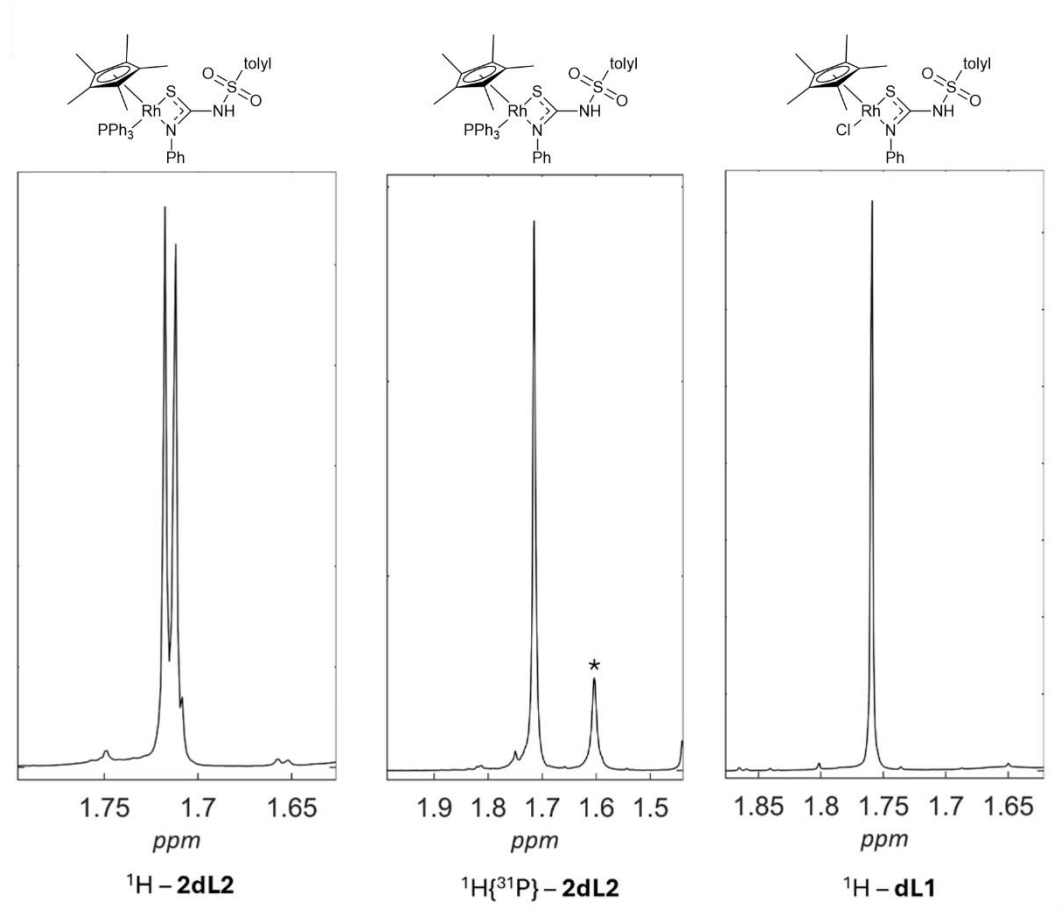

Figure 3.3: Comparison of the ^{1}H Cp resonance of **2dL2**, **2dL1** and the Cp* $^{1}H\{^{31}P\}$ resonance of **2dL2** (Drawn as the distal isomer). * Indicates an unknown impurity. $CDCl_3$ at 25°C.*

The aromatic *p*-cymene resonances of complexes **aL1**, **aL2**, **2aL1** and of the previously reported **1aL3** and **3aL3** in the ^{1}H spectra display as the typical set of four doublets between 4.5 and 6.0 ppm with coupling constants of 6 Hz. On the other hand, these resonances were observed in the spectrum of complex **1aL1** as an unusually well separated set of an AB quartet at d 6.03 ppm and two doublets at δ 5.12 and 3.75 ppm, which were attributed to the *proximal* S,N($_{sulfonated}$) isomer. ^{1}H-^{1}H COSY NMR analysis was consistent with an AB spin system, showing that the AB quartet correlated only with itself, while the two remaining aromatic *p*-cymene doublets correlated with each other (Figure 3.4). Two minor sets of four doublets were also present between 5.0 and 5.5 ppm which were attributed to the *distal* S,N($_{non\text{-}sulfonated}$) isomer and a potential impurity, the latter did not appear in subsequent preparations of the sample. The ratio between the *proximal* and *distal* isomer is approximately 9:1.

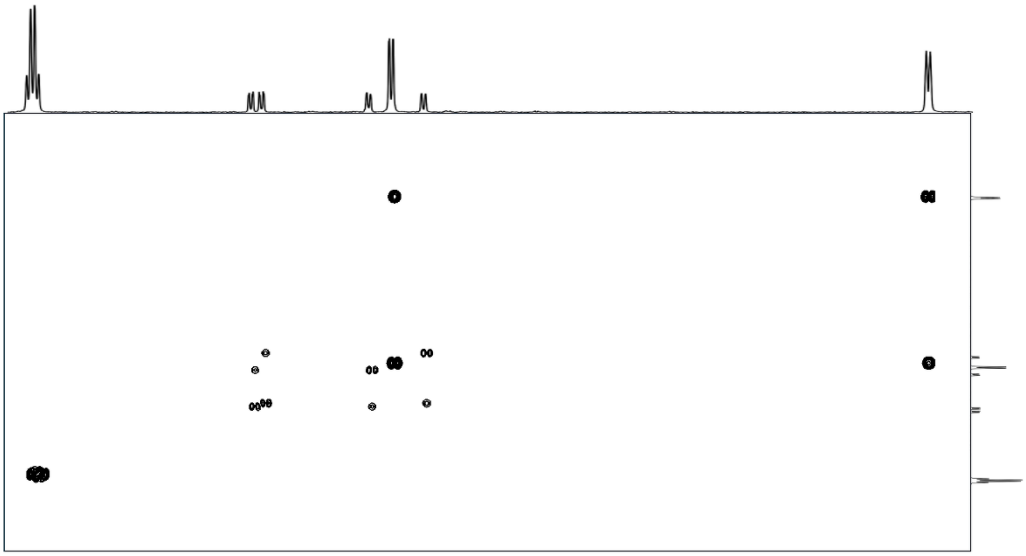

*Figure 3.4: ^{1}H-^{1}H COSY NMR spectrum of a freshly prepared solution of complex **1aL1**.*

Over the course of 7 weeks at room temperature, the sample of **1aL1** underwent isomerization in solution from the *proximal* to *distal* isomer, which resulted in a *proximal* to *distal* ratio of approximately 4:96 (Figure 3.5). Following an additional 5 weeks the ratio between the *proximal* and *distal* isomer did not produce notable change.

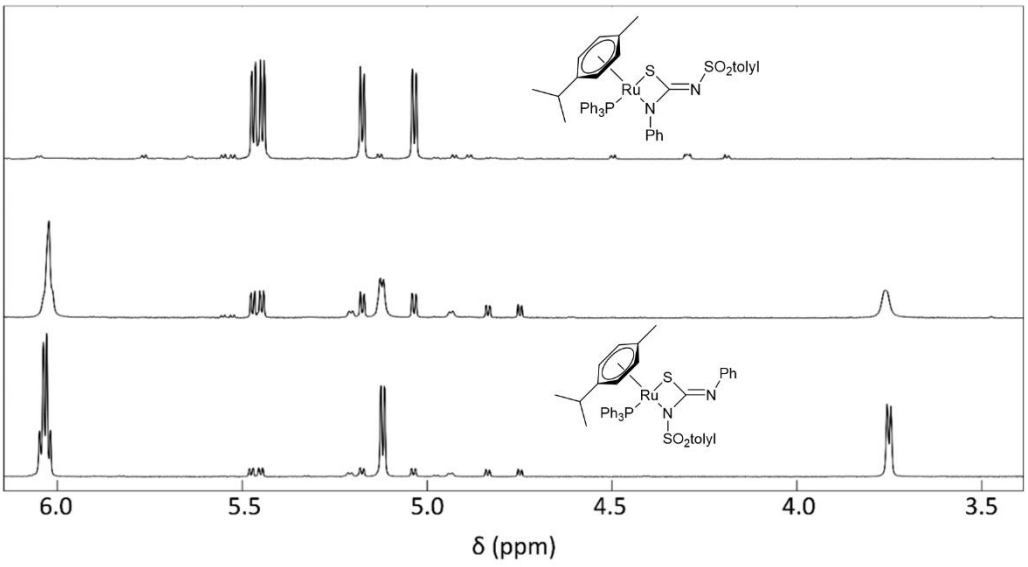

*Figure 3.5: Comparison between the aromatic p-cymene resonances of the proximal isomer of **1aL1** (bottom), the distal isomer (top) and a mixture of isomers (middle) in the ^{1}H NMR spectra recorded in $CDCl_3$.*

The remaining *p*-cymene resonances of complex **1aL1**, specifically the isopropyl CH and two CH_3 resonances (Figure 3.6), are shifted distinctly downfield in the *distal* isomer compared to the *proximal* isomer. For instance, the isopropyl CH resonance of the *proximal* isomer of **1aL1** appears at 2.9 ppm which is similar to both the PTA analogue complex **2aL1** and the chlorido complex **1aL1,** which show this resonances at δ 2.77 and δ 2.90 respectively and are also in the *proximal* linkage isomer. In contrast, the isopropyl CH atom of the newly formed *distal* isomer of complex **1aL1** resonates at δ 2.22. The isopropyl CH_3 of the *proximal* isomer resonances appear as two doublets at δ 1.18 and 1.17, which is similar to both the PTA analogue complex **2aL1** (1.19, 1.14 ppm) and the chlorido complex **1aL1** (1.27, 1.23 ppm). For the *distal* isomer of **1aL1** these resonances are shifted to a lower frequency and appear as two overlapping doublets at δ 0.97 and 0.95 ppm.

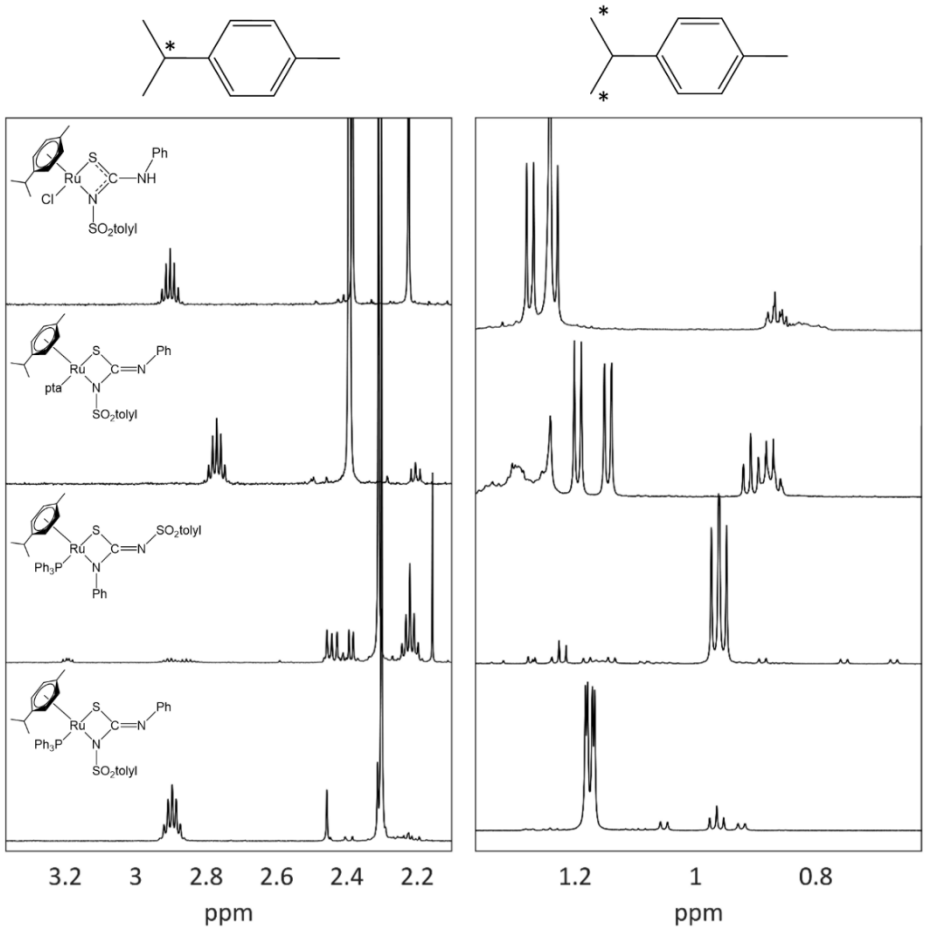

*Figure 3.6: Comparison of the p-cymene isopropyl ^1H resonances in complexes **1aL1** proximal and distal, **2aL1** and **aL1.***

To explore the thermodynamic aspects of the complexes and the isomerization of **1aL1**, geometry-optimized structures were calculated for isomeric structural pairs of ruthenium complexes, where at least one isomer's solid-state structure was experimentally determined (*vide infra*). Specifically, complexes **aL1**, **aL2, 1aL1**, **2aL1** and the previously reported **1bL3** were optimized in the gas phase. The mixed basis sets used included aug-cc-pV(D+d)Z for sulfur and phosphorus, aug-cc-pVDZ for oxygen, nitrogen, and chlorine, cc-pVDZ for carbon and hydrogen, and LANL2DZ with effective core potential for ruthenium. The ωB97M-V functional was applied for all systems. The choice of basis sets was decided based on findings in Chapter 2, Section 2.1.6, which indicated that diffuse functions and additional basis functions were essential for accurately modelling these systems. Using a combination of related basis sets for different atoms provided an optimal balance between computational accuracy and efficiency. LANL2DZ was used as the results generated were found to be more accurate to experimental observations than the LACVP method used in Chapter 2 for the Ru(II) systems in this chapter. The differences in electronic ground state energies between the two isomers (E_{distal} – $E_{proximal}$) termed ΔE are shown in Table 3.1.

*Table 3.1: Energy difference between isomers in their ground state for complexes **aL1**, **aL2**, **1aL1**, **1bL3** and **2aL1**.*

Complex	ΔE (kJ mol^{-1})	Predicted	Observed
aL1	47	*Proximal*	*Proximal*
aL2	66	*Proximal*	*Proximal*
1aL1	-23	*Distal*	*Distal*
1bL3	20	*Proximal*	*Proximal*
2aL1	25	*Proximal*	*Proximal*

Following the methods of Chapter 2, the difference in the ground state energies of each isomer, ΔE, indicates which isomer is more favoured. Hence, a positive value for ΔE implies that the *proximal* isomer is favoured, and *vice versa*. The difference in the ground state energies (Table 3.1) show that complexes **aL1**, **aL2**, **1bL3** and **2aL1** are thermodynamically more stable as the *proximal* isomer. As no isomerization was detected for these complexes, it can also be reasoned that the initially formed, kinetically favourable isomer, is also the *proximal* isomer, as there was no detectable transition between the two. For complex **1aL1**, the difference in ground state energies between the two isomers indicate that in this case, the *distal* isomer is more thermodynamically stable. It can be concluded therefore that the observed isomerization of the *proximal* to *distal* isomers is the result of the initially formed, kinetically favourable product, transitioning to the lower energy, thermodynamically stable, isomer. It can also be extrapolated that as this conversion is relatively slow, the activation energy barrier between the two isomers must be high, although calculation of the exact activation energy is outside of the scope of this study.

3.1.2 X-ray molecular structure determinations

In order to definitively characterize the complexes prepared in this study, the molecular structures of complexes **aL1**, **aL2**, **1aL1**, **a2L1**, **2aL1**, **2dL1** and **2cL1** were determined by single crystal X-ray diffraction. Crystallographic details are included in Appendix 1. A table of selected bond lengths in included in Table 3.2.

*Table 3.2: Selected bond lengths in the molecular structure of complexes **aL1**, **aL2**, **1aL1**, **2aL1**, **2cL1**, **2dL1** and **a$_2$L1**. Arene = cymene or benzene centroid, Cp* = Cp* centroid.*

Bond	**Bond length (Å)**					
	aL1	**aL2**	**2aL1**	**1aL1**	**a$_2$L1**	
Arene - Ru	1.671(2)	1.666(2)	1.723(2)	1.737(3)	1.687(5)	
Ru - P	-	-	2.300(6)	2.349(5)	-	
Ru - Cl	2.412(5)	2.415(5)	-	-	-	
Ru - S1	2.421(5)	2.429(6)	2.389(5)	2.379(7)	2.413(1)	
Ru - S1a	-	-	-	-	2.404(8)	
Ru - N1	-	-	-	2.099(2)	-	
Ru - N2	2.131(2)	2.144(2)	2.113(2)	-	2.126(4)	
S1- C1	1.715(2)	1.712(2)	1.766(2)	1.767(2)	1.829(4)	
C1 - N1	1.337(2)	1.336(3)	1.278(3)	1.328(3)	1.270(5)	
C1 - N2	1.351(3)	1.348(3)	1.393(3)	1.337(4)	1.371(4)	
	2dL1		**2cL1**			
Cp* - Rh	1.834(3)		**Cp* - Ir**	1.870(8)		
Rh - S	2.398(6)		**Ir - P**	2.276(2)		
Rh - P	2.276(8)		**Ir - S1**	2.362(2)	**Ir - S1a**	2.380(2)
Rh - Cl	2.420(1)		**S1 - C1**	1.735(7)	**S1a - C1a**	1.760(8)
S1 - C1	1.755(3)		**C1 - N1**	1.352(9)	**C1a - N1a**	1.343(9)
C1 - N1	1.360(3)		**C1 - N2**	1.315(9)	**C1a - N2a**	1.322(9)
C1 - N2	1.313(3)					

The metallacyclic bond lengths of the bidentate complexes are very similar, averaging 2.404 (Ru-S1), 1.761 (S1-C1), 2.117 (C1-N) and 2.117 Å (Ru-N). These bond lengths agree with literature values for similar piano-stool complexes of acylthiourea complexes.[21,22] For instance, the chlorido complex **aL1** (Figure 3.7) which contains the ligand coordinated as a monoanion, formed as the *proximal* isomer with metallacyclic bond lengths of 2.421(5) (Ru-S1), 1.715(2) (S1-C1), 1.351(2) (C1-N) and 2.131(2) Å (Ru-N). These values are in agreement with a similar Ru(II) chlorido acylthiourea complex reported by Gandhaveeti *et al.* of 2.391 (Ru-

S1), 1.701 (S1-C1), 1.341 (C1-N) and 2.111 Å (Ru-N).[25] The slight deviations in these values are most likely because of the differences between the electronic properties of the sulfonyl and acyl substituents. Complex **aL2** (Figure 3.8) is also in agreement, and in this example, the ligand substituents between **aL1** and **aL2** did not appear to influence the coordination behaviour or adopted linkage isomer. Complexes **2dL1** (Figure 3.9) and **2cL1** (Figure 3.10), whilst also containing the sulfonylthiourea coordinating as a monoanionic ligand, showed a different coordination mode as both coordinated as monodentate ligands *via* the core thiourea sulfur atom. Complex **2dL1** contained only one sulfonylthiourea and a chlorido ligand, while **2cL1** featured two sulfonylthiourea ligands and no chlorido ligand. The reason for this sudden change of isomer between the metal centres (Rh(III) vs Ir(III)) is not immediately apparent. It may be possible that the difference in synthetic routes, such as excess reagents, or reactivity between the Ru(II), Ir(III) and Rh(III) centres may be the reason.

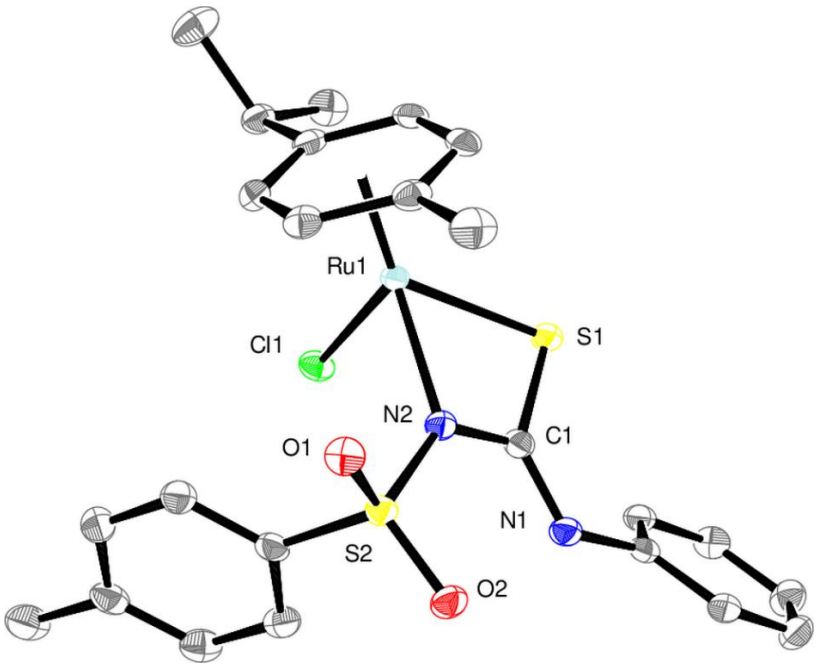

Figure 3.7: Molecular structure of [(η^6-cymene)Ru{TolSO$_2$NC(S)NHPh}Cl] ***aL1*** *showing a partial numbering scheme. Ellipsoids are shown at the 50% probability level. Hydrogen atoms are omitted for clarity.*

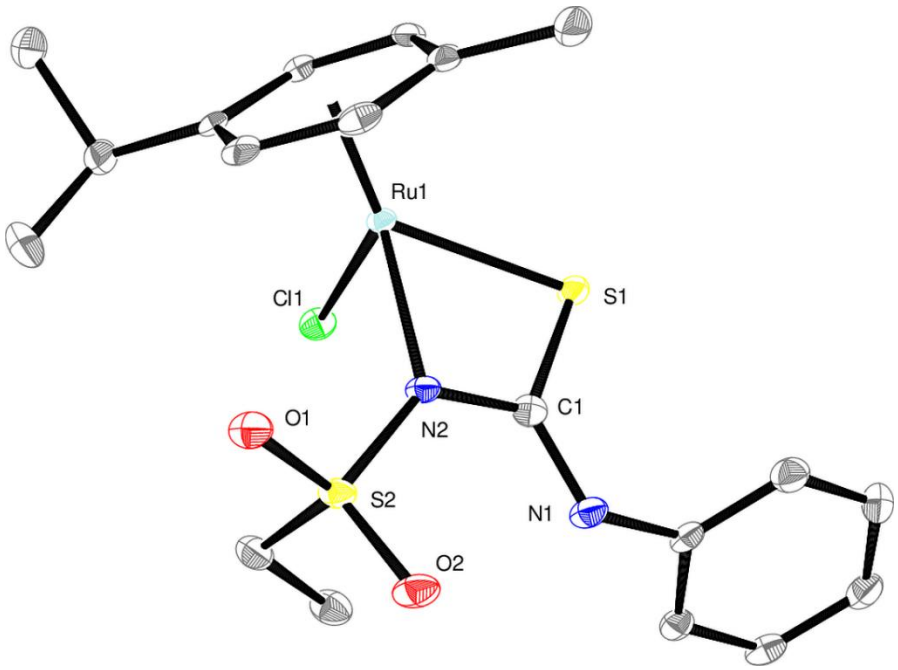

Figure 3.8: Molecular structure of [(η^6-cymene)Ru{$CH_3CH_2SO_2NC(S)NHPh$}Cl] ***aL2*** *showing a partial numbering scheme. Ellipsoids are shown at the 50% probability level. Hydrogen atoms are omitted for clarity.*

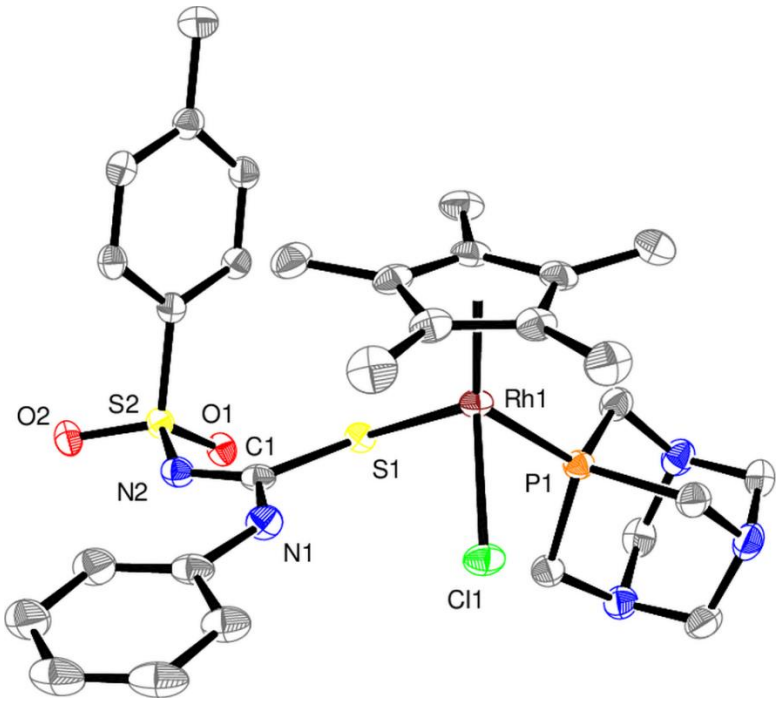

*Figure 3.9: Molecular structure of [Cp*Rh{$TolSO_2NC(S)NHPh$}(PTA)Cl]* ***2dL1*** *showing a partial numbering scheme. Ellipsoids are shown at the 50% probability level. Hydrogen atoms are omitted for clarity.*

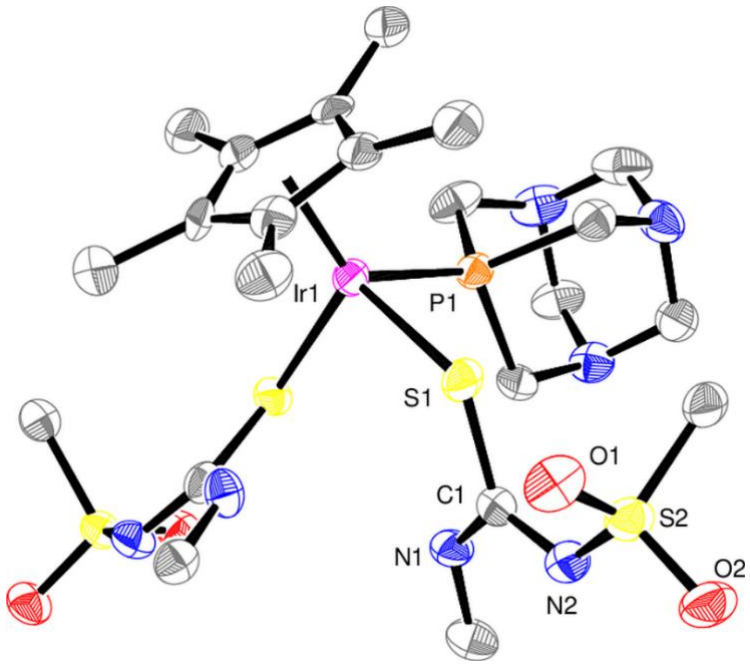

*Figure 3.10: Molecular structure of [Cp*Ir{TolSO$_2$NC(S)NHPh}$_2$(PTA)]* ***2cL1*** *showing a partial numbering scheme. Ellipsoids are shown at the 50% probability level. Hydrogen atoms and ligand substituents are omitted for clarity.*

Complexes **2aL1** (Figure 3.11) and **1aL1** (Figure 3.12) are similar in structure to complex **aL1** and differ only by the replacement of the chlorido ligand on the Ru centre with either PPh_3 or PTA. Complex **2aL1** contains the sulfonylthiourea ligand chelating the Ru(II) centre *via* the *S*,*N*($_{sulfonated}$) donor system as the *proximal* isomer, whilst in contrast, in complex **1aL1** the ligand was found to coordinate *via* the *S*,*N*($_{non\text{-}sulfonated}$) atoms resulting in the *distal* isomer. The *distal* isomer adopted by complex **1aL1** may be a result of the combination between the increased size of the cone angle of the PPh_3 ligand (150°), as opposed to PTA (103°),[26, 27] and the *p*-cymene arene ligand, together providing sufficient steric strain on the *proximal* isomer. This is further indicated by the molecular structure of complex **1bL3** (Figure 3.13),[22] whilst also containing a triphenylphosphine ligand, also contains a slightly smaller benzene arene ligand, and adopts a *proximal* linkage isomer. The thiourea sulfur-bridged ruthenium dimer, complex **a$_2$L1** (Figure 3.14), was also prepared and the structure determined by single crystal X-ray diffraction. The Ru – S – Ru – S core is revealed to be approximately rhomboid with similar S-Ru bond distances of 2.410(6) and 2.418(6) Å. The thiourea core sits on opposite sides of an inversion centre in the *proximal* isomer. The metallacyclic bond distances are

in agreement with a previously reported sulfur-bridged Ru(*p*-cymene) dimeric structure with a cyano-substituted thiourea ligand,[23] *i.e.,* [(η^6-p-cymene)Ru{$NCNCSNCH_3$}]$_2$, (2.398(1) (Ru-S), 1.796(3) (S-C), 1.309(4) (C-N) and 2.084(3) Å (Ru-N), with only minor differences relating to the change of ligand.

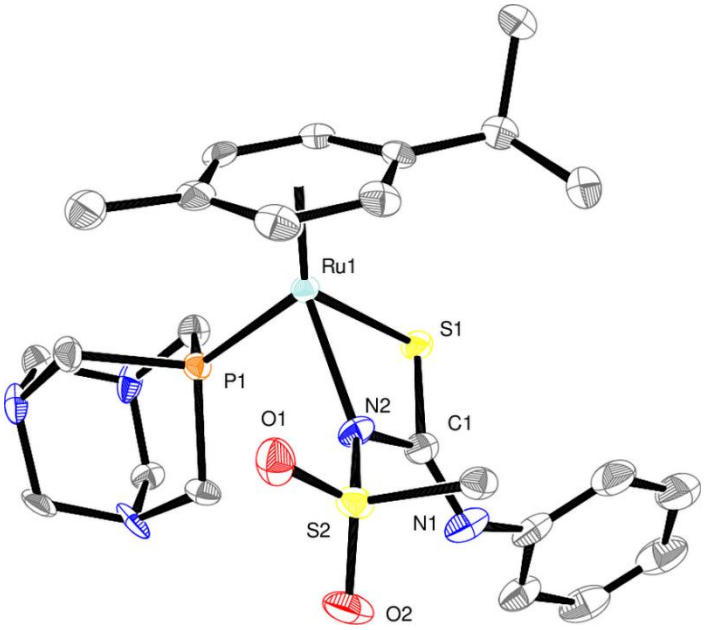

*Figure 3.11: Molecular structure of [(η^6-cymene)Ru{$TolSO_2NC(S)NPh$}(PTA)] **2aL1** showing a partial numbering scheme. Ellipsoids are shown at the 50% probability level. Hydrogen atoms are omitted for clarity.*

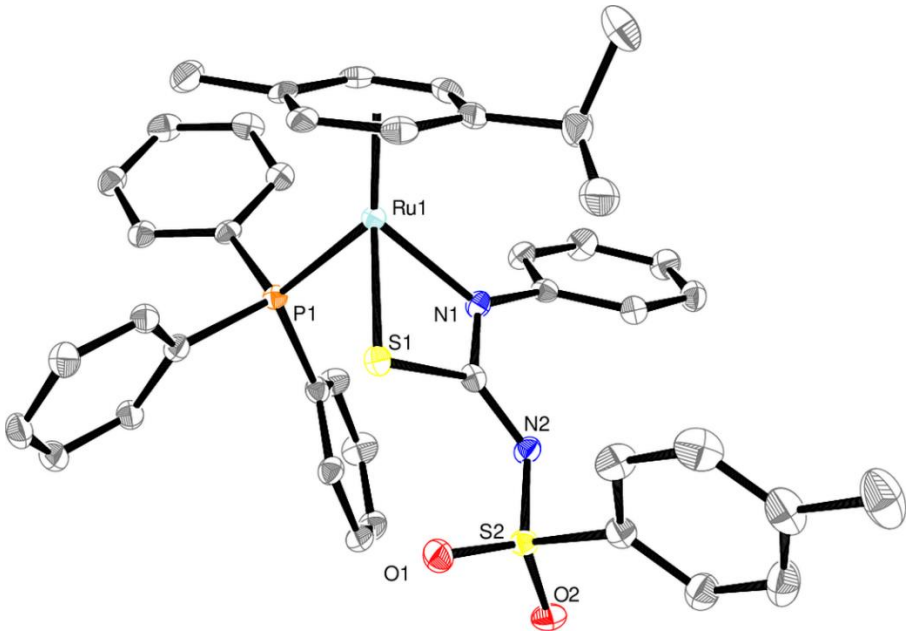

*Figure 3.12: Molecular structure of [(η^6-cymene)Ru{$TolSO_2NC(S)NPh$}(PPh_3)] **1aL1** showing a partial numbering scheme. Ellipsoids are shown at the 50% probability level. Hydrogen atoms are omitted for clarity.*

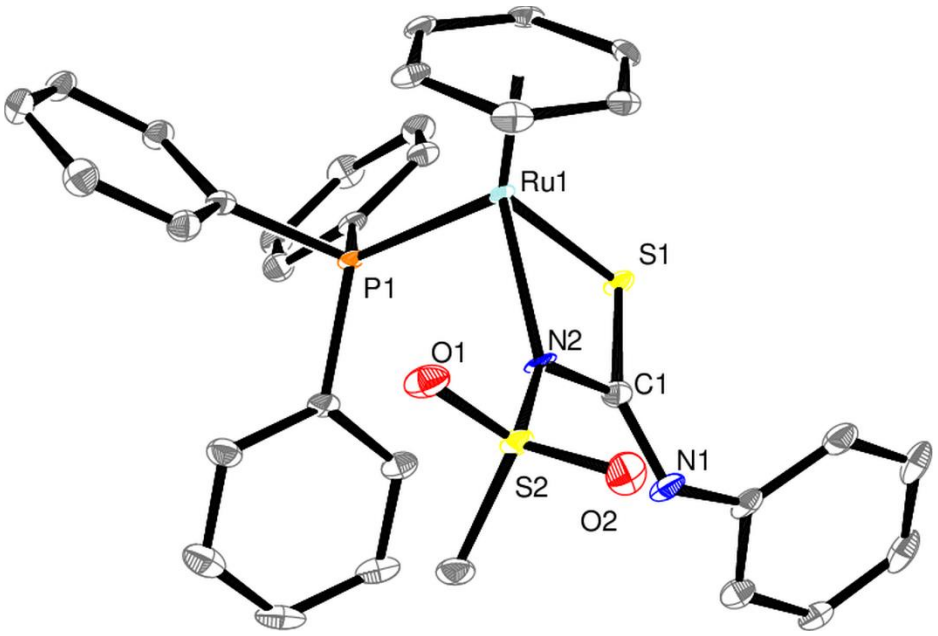

*Figure 3.13: Molecular structures of [(η^6-benzene)Ru{$CH_3SO_2NC(S)NPh$}(PPh_3)] **1bL3** as preparsed in a previous study[22] showing a partial numbering scheme. Ellipsoids are shown at the 50% probability level. Hydrogen atoms are omitted for clarity.*

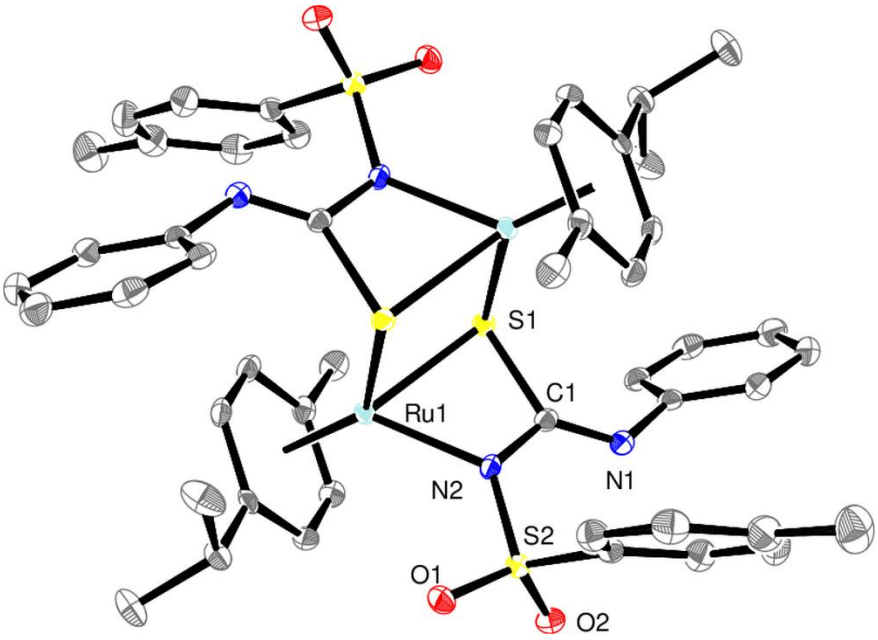

*Figure 3.14: Molecular structure of [(η^6-cymene)Ru{$TolSO_2NC(S)NPh$}]$_2$ **a$_2$L1** showing a partial numbering scheme. Ellipsoids are shown at the 50% probability level. Hydrogen atoms are omitted for clarity.*

The molecular structures imply that the observed isomer for ruthenium(II) piano-stool complexes is related to the size and steric bulk of the ligands around the metal centre. For instance, the *p*-cymene and triphenylphosphine ligands of the complex force the complex into the *distal* isomer because of the large size of these ligands. However, replacement of the *p*-cymene with the smaller benzene (**1bL3**) or replacement of the triphenylphosphine with PTA (**2aL1**) or a chlorido ligand (**aL1**, **aL2**) reduces the steric strain, favouring the formation of the *proximal* isomer. These results correlate with DFT calculations of the ground state energies (*vide supra*) and also with similar acylthiourea ruthenium(II) complexes which also tend to favour the *proximal* arrangement.

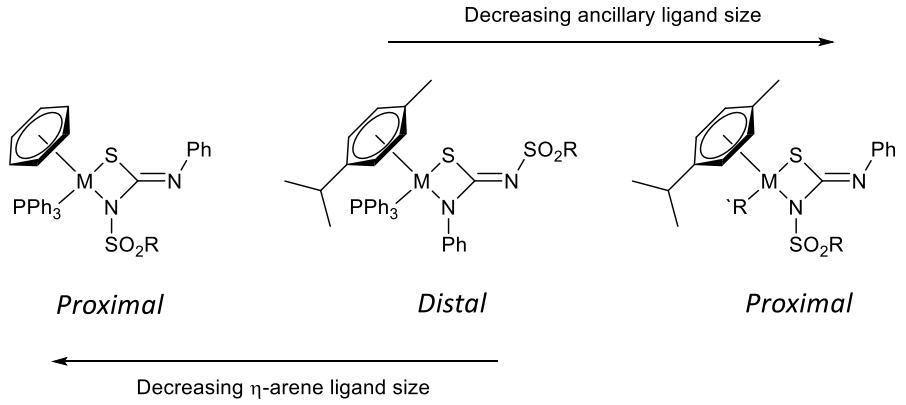

Figure 3.15: Phosphine ligand and arene ligand structure and linkage isomer relationship.

Interestingly, the *proximal* isomer preference observed in this study for the sulfonylthiourea Ru(II), Ir(III) and Rh(III) piano-stool complexes, is in contrast to Pt(II) square-planar complexes with the same ligands prepared in Chapter 2. These Pt(II) complexes have shown to predominantly favour the *distal* isomer as a result of short-ranged chalcogen σ-hole interactions (chalcogen bond) between the thiourea sulfur and sulfonyl oxygen atoms, promoted by the polarisation of the sulfur atom by platinum. To explore the presence of such an interaction for the *distal* isomer of complex **1aL1**, analysis of the non-covalent interactions between the thiourea sulfur and sulfonyl oxygen was conducted using the non-covalent Interactions index of Johnson and co-workers as used in Chapter 2 Section 2.1.6.1. Thus the calculated reduced density gradient (RDG = $1/[2(3\pi^2)^{1/3}]|\nabla\rho|/\rho^{4/3}$) versus the electron density $\rho(r)$, oriented by the sign of the second eigenvalue (λ_2) was

plotted. The plot shows a distinct trough at ~-0.015 sign(λ_2)ρ) which by comparison with previous calculations in Chapter 2, relates to a chalcogen σ-hole interaction, which indicates that this interaction is indeed present in this complex. This chalcogen σ-hole interaction appears to have much less influence on the resulting isomer of the ruthenium(II) complexes as compared to the platinum(II) complexes previously reported.[20] Presumably this is because of the weaker polarization of the sulfur atom by ruthenium(II) compared to platinum(II) or *trans* influence differences.

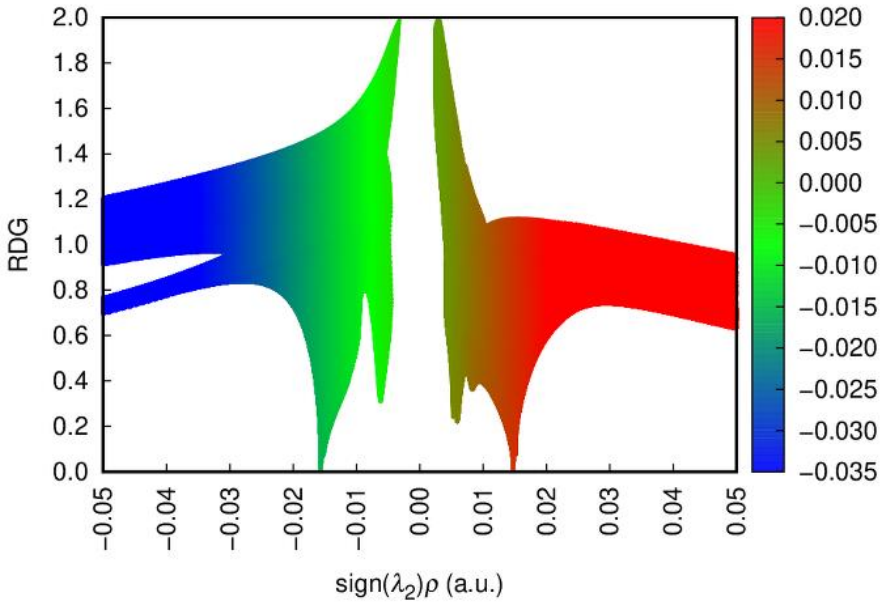

*Figure 3.16: Plot of RDG (s) versus sign(λ_2)ρ for complex **1aL1**.*

3.1.3 Anticancer activity

Complexes **aL1**, **aL2**, **dL1**, **1aL1**, **2aL1**, **2cL1**, **2dL1**, **2dL2**, and **a2L1** were evaluated for antiproliferative activity against human colorectal (HCT116), non-small cell lung (H460), cervical (SiHa), and colon (SW480) carcinoma cell lines *via* an external collaboration with the Hartinger group, University of Auckland. The remaining complexes were excluded due to insufficient aqueous solubility. Overall, most complexes demonstrated modest activity, with complex **2dL2** being the exception, as it was inactive (Table 3.3).

Table 3.3: Anticancer activity of selected Ru(II), Ir(III), Rh(III) complexes against human colorectal (HCT116), non-small cell lung (H460), cervical (SiHa) and colon (SW480) carcinoma cell lines (mean IC_{50} ± standard deviation in mM)

Complex	HCT116	H460	SiHa	SW480
aL1	60 ± 4	81 ± 5	73 ± 9	30 ± 3
aL2	44 ± 3	69 ± 6	84 ± 23	39 ± 6
dL1	58 ± 13	82 ± 23	79 ± 16	36 ± 0.4
1aL1	10 ± 2	14 ± 2	17 ± 4	13 ± 1
2aL1	33 ± 1	53 ± 7	48 ± 4	>100
2cL1	11 ± 2	15 ± 4	16 ± 3	26 ± 5
2dL1	49 ± 8	56 ± 11	99 ± 23	92 ± 19
2dL2	>100	>100	>100	>100
a_2L1	15 ± 2	27 ± 4	17 ± 2	18 ± 1
$[Ru(cym)Cl_2]_2$	433 ± 28[a]	441 ± 46[a]	394 ± 70[a]	346 ± 48[a]
cisplatin	2.5 ± 0.6[b]	0.8 ± 0.1[b]	3.0 ± 1.1[b]	8.1 ± 5.0[b]

[a] is taken from ref. [7]; [b] is taken from ref. [27]

Among the ruthenium complexes, the thiourea-bridged dimer (**a2L1**) and the triphenylphosphine-containing complex (**1aL1**) exhibited the highest activity, followed by the PTA-bearing complex (**2aL1**) and the chlorido complexes (**aL1** and **aL2**). These results suggest a trend of increasing activity with the lipophilicity of the ancillary ligand (Cl < PTA < PPh_3), consistent with observations reported in the literature.[5, 28, 29] Likewise, the dimeric complex **a2L1** showed notable potency relative to its precursor, $[(\eta^6\text{-}p\text{-cymene})RuCl_2]_2$. The iridium(III) complex **2cL1**, containing two thiourea ligands, demonstrated higher activity compared to related rhodium complexes.[37] This difference may be attributed to the increased lipophilicity provided by the second thiourea ligand or to subtle structural and electronic differences between Ir(III) and Rh(III) complexes. It may also be possible that the dissociation of the thiourea ligand is contributing to the activity which may explain why complex **2cL1**, containing two thiourea ligands, has increased activity. Other factors, such as cellular uptake, stability, and biomolecular interactions,[30] likely influence the bioactivity of these complexes, especially in cases like the PTA-bearing complex **2dL2**, which was inactive.

3.2 Conclusions

A series of ruthenium(II), iridium(III) and rhodium(III) complexes with mono- and dianionic sulfonylthiourea ligands were synthesized, characterized and assessed for anticancer activity. Analysis by single crystal XRD revealed that the observed isomer of the ruthenium(II) complexes is a direct result of the steric bulk of the ligands in the coordination sphere, *i.e.* the *distal* isomer is observed only with sterically demanding ligands. XRD analysis also revealed the preference of the monoanionic ligand for monodentate coordination with iridium(III) and rhodium(III) centres. *Proximal* to *distal* isomerization was observed by NMR spectroscopy for complex **1aL1** which was indicated by DFT calculations to be a conversion from the initially formed kinetically favourable to the thermodynamically more stable isomer. Computational analysis also revealed that while the *distal* isomer contains a chalcogen bond between the thiourea sulfur and sulfonyl oxygen atoms, this interaction has much less influence on isomer preference as compared to platinum(II) complexes. The antiproliferative activity of the complexes investigated was found to moderate against human HCT116, H460, SiHa and SW480 cancer cells. However, structural trends indicate a clear improvement in activity with increasing lipophilicity of the ancillary ligands. Overall, the results presented here demonstrate promising avenues for the use of sulfonylthioureas as tailorable ligands for ligand and complex design.

3.3 Experimental

3.3.1 Materials

Triphenylphosphine (Sigma Aldrich), triethylamine (Sigma Aldrich) and Ag_2O (BDH) were used as supplied. The tertiary phosphines tcep[31] and PTA[32] and the complexes $[Cp^*IrCl_2]_2$[33] and were prepared by literature methods and provided by W. Henderson, University of Waikato. The dimers $[Cp^*RhCl_2]_2$,[33] $[(\eta^6\text{-}p\text{-cymene})RuCl_2]_2$[32] were prepared using literature methods or minor variations thereof. Ruthenium and rhodium trichloride hydrates was acquired from Precious Metals Online (Australia). Sulfonylthiourea ligands **S-L1** and **S-L2** were used as prepared in Chapter 2, Section 2.3. Precursor complexes **1a-1d**, **2a**, **2c** and **2d** were prepared by mixing the relevant dimeric precursor complex and 2 mol equivalents of the relevant phosphine in dichloromethane for 3 hours. The target complexes were isolated by precipitation with petroleum spirts, filtered and dried in air. **3a** was prepared following literature methods.[34] Complexes **1aL3**, **1bL3** and **3aL3** were used as prepared in a previous study.[22]

3.3.2 Instrumentation

A 600 MHz Jeol ECZR NMR spectrometer was used to record ^{31}P (243 MHz), $^{31}P\{^1H\}$ (243 MHz), $^1H\{^{31}P\}$ (600 MHz) and ^1H (600 MHz) NMR spectra in $CDCl_3$ or DMSO-d_6 at 25°C. Spectra were processed using the Jeol Delta software. ESI mass spectra were recorded in methanol using a Bruker Daltonics MicrOTOF electrospray ionization mass spectrometer. Sodium formate solution was used for calibration. ESI-MS spectra were recorded with a Capillary Exit voltage of 150 V and a Skimmer 1 voltage of 50 V unless otherwise stated. Elemental analysis was performed by the Chemical Analysis Facility, Department of Molecular Sciences, Macquarie University, Sydney, Australia or the Campbell Microanalytical Laboratory, Department of Chemistry, University of Otago, Dunedin, New Zealand (**1cL1**). Collection of single crystal X-ray diffraction data was carried out by the University of Auckland Microcharacterization Facility, Auckland, New Zealand.

3.3.3 General synthesis of Ru(II), Ir(III) and Rh(III) complexes with monoanionic sulfonylthiourea ligands: aL1, aL2, dL1, 2dL1, 2dL2, 2cL1.

Equimolar amounts of the sulfonylthiourea ligand and metal starting material were suspended in MeOH (30 mL) with gentle stirring. For Ir(III) and Rh(III) complexes, an aqueous solution of sodium hydroxide (2 mol L^{-1}, 50 µL, excess) was added to the reaction mixture. After 6 hours at room temperature the solvent was removed by rotary evaporation to yield the target complex. Complexes **aL1**, **aL2** and **dL1** were washed with petroleum spirits (15 mL) and hexane (15 mL) before drying under vacuum. The residues of complexes **2dL1**, **2dL2** and **2cL1** were dissolved in the minimum volume of CH_2Cl_2 (3-5 mL) and passed through 2 cm of silica to remove undissolved solids before the removal of the solvent to yield the final product. Details pertaining to each compound are given in Table 3.4.

3.3.4 General synthesis of Ru(II), Ir(III) and Rh(III) complexes with dianionic sulfonylthiourea ligands: 1aL1, 1cL1, 1dL1, 2aL1, 3aL1, a_2L1.

Equimolar amounts of the sulfonylthiourea ligand and dimeric metal precursor were suspended in MeOH (30 mL) with gentle stirring. Triethylamine (0.15 mL, excess) was added and the solution was stirred at room temperature for 12 h. Afterwards, the precipitated solids were filtered and washed with water (4 x 10 mL) before being dried under vacuum. For complex **2aL1**, the methanol reaction mixture was reduced in volume (approximately 2-4 mL) under reduced pressure to encourage precipitation before being filtered and washed with ice cold water (1 x 10 mL) and dried under vacuum. Details pertaining to each compound are given in Table 3.4.

Table 3.4: Synthesis details for the prepared sulfonylthiourea piano stool complexes.

Complex	starting material	mg	mmol	Ligand	mg	mmol	Yield (mg)	Yield (%)
aL1	$[(\eta^6\text{-cym})RuCl_2]_2$	60	0.098	**L1**	60	0.196	167	79
aL2	$[(\eta^6\text{-cym})RuCl_2]_2$	60	0.098	**L2**	48	0.196	67	67
dL1	$[Cp^*RhCl_2]_2$	90	0.146	**L1**	89	0.291	112	67
1aL1	$[(\eta^6\text{-cym})RuCl_2(PPh_3)]$	100	0.176	**L1**	54	0.176	96	68
1cL1	$[Cp^*IrCl_2(PPh_3)]$	90	0.136	**L1**	42	0.136	75	62
1dL1	$[Cp^*RhCl_2(PPh_3)]$	90	0.158	**L1**	48	0.158	85	67
2aL1	$[(\eta^6\text{-cym})RuCl_2(PTA)]$	105	0.227	**L1**	69	0.227	98	62
2cL1	$[Cp^*IrCl_2(PTA]$	90	0.162	**L1**	50	0.162	64	36
2dL1	$[Cp^*RhCl_2(PTA)]$	90	0.193	**L1**	59	0.193	96	68
2dL2	$[Cp^*RhCl_2(PTA)]$	90	0.193	**L2**	59	0.242	110	67
a_2L1	$[(\eta^6\text{-cym})RuCl_2]_2$	60	0.098	**L1**	60	0.196	112	65

$[(\eta^6\text{-}p\text{-cymene})Ru\{TolSO_2NC(S)NHPh\}Cl]$ **aL1**

Light red solid. Elemental analysis: Found (%) C 50.1; H 4.5; N 4.4. Calculated for $C_{24}H_{27}ClN_2O_2RuS_2$ (%) C 50.0; H 4.7; N 4.8. ESI MS: *m/z* $[M - Cl]^+$ 541.0290. NMR ($CDCl_3$, 600 MHz): ^1H δ 9.75 (s, NH, 1H), 7.90 (d, ^3J = 8 Hz, tolyl, 2H), 7.39 – 7.12 (m, aromatics), 5.54 (d, ^3J = 5 Hz, cymene-H, 1H), 5.52 (d, ^3J = 6 Hz, cymene-H, 1H), 5.45 (d, ^3J = 6 Hz, cymene-H), 5.12 (d, ^3J = 5 Hz, cymene-H, 1H), 2.90 (sept, ^3J = 7 Hz, isopropyl-CH, 1H), 2.20 (s, CH_3, 3H) 2.14 (s, cymene-*p*-CH_3, 3H), 1.27 (d, ^3J = 7 Hz, isopropyl-CH_3(a), 3H), 1.23 (d, ^3J = 7 Hz, isopropyl-CH_3(b), 3H).

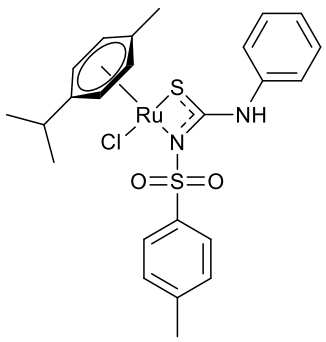

[(η^6-*p*-cymene)Ru{$CH_3CH_2SO_2NC(S)NHPh$}Cl] **aL2**

Light red solid. Elemental analysis: Found (%) C 44.3; H 5.1; N 5.3. Calculated for $C_{19}H_{25}ClN_2O_2RuS_2$ (%) C 44.4; H 4.9; N 5.45. ESI MS: *m/z* $[M - Cl]^+$ 478.9095. NMR ($CDCl_3$, 600 MHz): ^1H δ 9.73 (s, NH, 1H), 7.36 – 7.19 (m, aromatics, 5H), 5.58 (d, ^3J = 6 Hz, cymene-H, 1H), 5.54 (d, ^3J = 6 Hz, cymene-H, 1H), 5.45 (d, ^3J = 6 Hz, cymene-H, 1H), 5.20 (d, ^3J = 6 Hz, cymene-H, 1H), 3.31 (m, CH_2, 2H), 2.95 (sept, ^3J = 7 Hz, isopropyl-CH, 1H), 1.55 (s, cymene-*p*-CH_3, 3H), 1.33 (t, ^3J = 8 Hz, CH_3, 3H), 1.28 (overlapping doublets, isopropyl-CH_3(a,b), 6H).

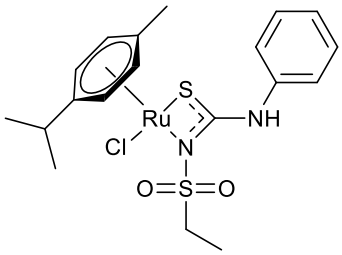

[Cp*Rh{*p*-$TolSO_2NC(S)NHPh$}Cl] **dL1**

Red solid. Elemental analysis: Found (%) C 49.8; H 4.9; N 4.6. Calculated for $C_{24}H_{28}ClN_2O_2RhS_2$ (%) C 49.8; H 4.8; N 4.8. ESI MS: *m/z* $[M - Cl]^+$ 543.1143. NMR ($CDCl_3$, 600 MHz): ^1H δ 9.60 (s, NH, 1H), 7.96 – 6.95 (m, aromatics), 2.35 (s, CH_3, 3H), 1.75 (s, CH_3-Cp*, 15H).

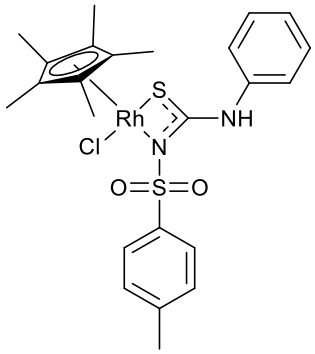

[(η^6-*p*-cymene)Ru{*p*-TolSO$_2$NC(S)NPh}(PPh$_3$)] **1aL1**

Yellow-orange solid. Elemental analysis: Found (%) C 62.3; H 5.1; N 3.3. Calculated for $C_{42}H_{41}N_2O_2PRuS_2$ (%) C 62.9; H 5.15; N 3.5. ESI MS: *m/z* $[M + H]^+$ 803.1394, $[(M – PPh_3) + H]^+$ 541.0503. NMR (*proximal*) ($CDCl_3$, 243 MHz): $^{31}P\{^1H\}$ δ 38.71. ($CDCl_3$, 600 MHz): ^1H δ 7.84 (d, ^3J = 9 Hz, tolyl, 2H), 7.9 – 6.9 (m, aromatics), 6.81 (t, ^3J = 8 Hz, NPh, 1H), 6.37 (d, ^3J = 8 Hz, NPh, 2H), 6.03 (ABq, cymene-H, dd_{AB} = 0.017 Hz, J_{AB} = 6.0 Hz, 2H), 5.11 (d, ^3J = 6 Hz, cymene-H, 1H), 3.74 (d, ^3J = 6 Hz, cymene-H, 1H), 2.89 (sept,^3J = 7 Hz, isopropyl-CH, 1H), 2.30 (s, tolyl-CH_3, 3H), 1.77 (s, cymene-*p*-CH_3, 3H),1.18 (d, ^3J = 3 Hz, isopropyl-CH_3(b), 3H). 1.16 (d, ^3J = 3 Hz, isopropyl-CH_3(b), 3H). NMR (*distal*): $^{31}P\{^1H\}$ δ 39.47. ^1H δ 7.79 (d, ^3J = 8 Hz, tolyl, 2H), 7.7 – 6.9 (m, aromatics), 6.81 (t, ^3J = 11 Hz, NPh, 1H), 5.47 (d, ^3J = 10 Hz, cymene-H, 2H), 5.44 (d, ^3J = 10 Hz, cymene-H, 1H), 5.17 (d, ^3J = 10 Hz, cymene-H, 1H), 5.03 (d, ^3J = 10 Hz, cymene-H, 1H), 2.31 (s, tolyl-CH_3, 3H), 2.22 (sept, ^3J = 11 Hz, isopropyl-CH, 1H), 1.44 (s, cymene-*p*-CH_3, 3H), 0.96 (m, isopropyl-CH_3, 6H).

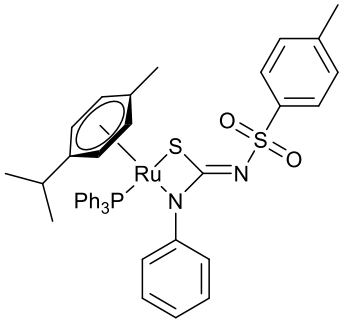

[Cp*Ir{*p*-TolSO$_2$NC(S)NPh}(PPh$_3$)] **1cL1**

Yellow solid. Elemental analysis: Found (%) C 55.3; H 4.6; N 4.4. Calculated for $C_{42}H_{42}IrN_2O_2PS_2{\cdot}CH_4O$ (%) C 55.8; H 5.0; N 3.0. ESI MS: *m/z* $[M + H]^+$ 895.1301, $[(M - PPh_3) + H]^+$ 633.0761. NMR (DMSO-d_6, 243 MHz): $^{31}P\{^1H\}$, δ -6.5. NMR (DMSO-d_6, 600 MHz): ^1H δ 8.1 – 6.8 (m, aromatics), 2.29 (s, tolyl-CH_3, 3H), 1.10 (m, CH_3-Cp*, 15H).

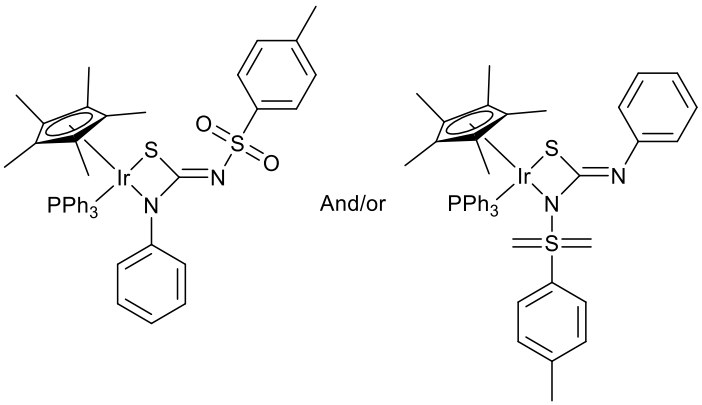

[Cp*Rh{*p*-TolSO$_2$NC(S)NPh}(PPh$_3$)] **1dL1**

Red solid. Elemental analysis: Found (%) C 62.4; H 5.0; N 3.5. Calculated for $C_{42}H_{42}N_2O_2PRhS_2$ (%) C 62.7; H 5.3; N 3.5. ESI MS: *m/z* $[M + H]^+$ 804.9558. NMR ($CDCl_3$, 243 MHz): $^{31}P\{^1H\}$, δ 38.73 [d, $^1J_{RhP}$ 155 Hz]. ($CDCl_3$, 600 MHz): ^1H δ 8.23 – 6.73 (m, aromatic), 2.33 (s, tolyl-CH_3, 3H), 1.66 (d, ^3J = 4 Hz, CH_3-Cp*, 15H).

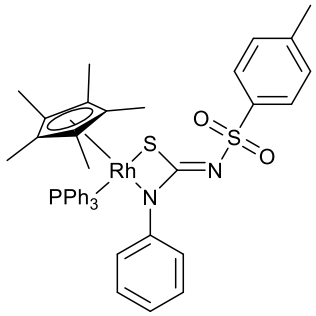

[(η^6-*p*-cymene)Ru{*p*-TolSO$_2$NC(S)NPh}(PTA)] **2aL1**

Yellow-orange solid. Elemental analysis: Found (%) C 51.2; H 5.6; N 9.9. Calculated for $C_{30}H_{38}N_5O_2PRuS_2$ (%) C 51.7; H 5.5; N 10.0. ESI MS: *m/z* $[M + H]^+$ 698.4424. NMR ($CDCl_3$, 243 MHz): $^{31}P\{^1H\}$ δ -33.33. ($CDCl_3$, 600 MHz): ^1H δ 8.02 (d, ^3J = 9 Hz, tolyl 2H), 7.25 (d, tolyl, solvent obstructed), 7.19 (t, ^3J = 8 Hz, NPh, 2H), 6.92 (t, ^3J = 8 Hz, NPh, 1H), 6.84 (d, ^3J = 8 Hz, NPh, 2H) 5.74 (d, ^3J = 6 Hz, cymene-H, 1H), 5.59 (d, ^3J = 6 Hz, cymene-H, 1H), 5.36 (d, ^3J = 5 Hz, cymene-H, 1H), 5.03 (d, ^3J = 5 Hz, cymene-H, 1H), 4.46 (dd, ^3J = 32 Hz, ^4J = 13 Hz, N-CH_2-N, 6H), 4.22 (dd, ^3J = 82 Hz, ^4J = 6 Hz, N-CH_2-P, 6H), 2.77 (sept, ^3J = 7 Hz, isopropyl-CH, 1H), 2.39 (overlapping singlets, cymene-*p*-CH_3 and CH_3, 6H) 1.19 (d, ^3J = 6 Hz, isopropyl-CH_3(a), 3H), 1.24 (d, ^3J = 15 Hz, isopropyl-CH_3(b) 3H).

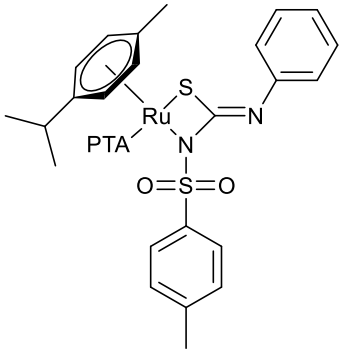

[Cp*Ir{*p*-TolSO$_2$NC(S)NHPh}$_2$(PTA)] **2cL1**

Yellow solid. Elemental analysis: Found (%) C 48.4; H 4.8; N 8.7. Calculated for $C_{44}H_{53}IrN_7O_4PS_4$ (%) C 48.25; H 4.9; N 8.95. ESI MS: *m/z* $[M + H]^+$ 1096.3062, $[M + Na]^+$ 1118.2140, $[M - L]^+$ 790.1937, $[M - (L + PTA)]^+$ 633.1266. NMR (DMSO-d_6, 243 MHz): $^{31}P\{^1H\}$, δ -63.8. NMR (DMSO-d_6, 600 MHz): ^1H δ 9.42 (s, NH, 1H), 8.0 – 7.0 (m, aromatics), 4.61 (dd, ^3J = 41 Hz, ^4J = 13 Hz, N-CH_2-P, 6H), 4.10 (s, N-CH_2-N, 6H), 2.32 (s, tolyl-CH_3, 3H), 1.57 (d, ^3J = 2 Hz, CH_3-Cp*).

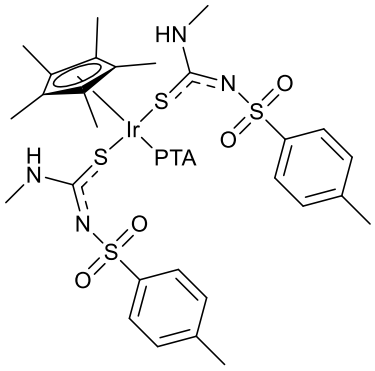

[Cp*Rh{*p*-TolSO$_2$NC(S)NHPh}(PTA)Cl] **2dL1**

Red solid. Elemental analysis: Found (%) C 48.7; H 5.8; N 9.4. Calculated for $C_{30}H_{40}ClN_5O_2PRhS_2$ (%) C 48.95; H 5.5; N 9.5. ESI MS: *m/z* $[M - Cl]^+$ 699.9798, $[M - (Cl + PTA)]^+$ 542.9293. NMR ($CDCl_3$, 243 MHz): $^{31}P\{^1H\}$, δ -32.23 [d, $^1J_{RhP}$ 137]. NMR ($CDCl_3$, 600 MHz): ^1H δ (ppm) 9.56 (s, NH, 1H), 7.94 – 6.91 (m, aromatics), 4.47 (m, N-CH_2-P, 6H), 4.23 (s, N-CH_2-N, 6H), 2.37 (s, CH_3, 3H) 1.66 (d, ^3J = 4 Hz, CH_3-Cp*, 15H).

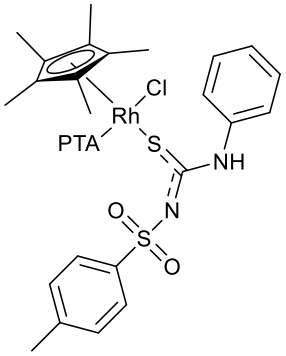

[Cp*Rh{$CH_3CH_2SO_2NC(S)NHPh$}(PTA)Cl] **2dL2**

Red solid. Elemental analysis: Found (%) C 44.1; H 5.7; N 9.9. Calculated for $C_{25}H_{38}ClN_5O_2PRhS_2$ (%) C 44.55; H 5.7; N 10.4. ESI MS: *m/z* $[M - Cl]^+$ 637.9467, $[M - (Cl + PTA)]^+$ 480.9002. NMR ($CDCl_3$, 243 MHz): $^{31}P\{^1H\}$, δ -32.16 [d, $^1J_{RhP}$ 136]. NMR ($CDCl_3$, 600 MHz): ^1H δ 9.56 (s, NH, 1H), 7.6 (d, ^3J = 9 Hz, Ph, 2H), 7.24 (t, solvent obstructed, Ph, 2H), 6.99 (t, ^3J = 8 Hz Ph, 1H), 4.51 (s, N-CH_2-N, 6H), 4.32 (m, N-CH_2-P, 6H), 3.15 (q, ^3J = 7 Hz CH_2, 2H), 1.74 (d, ^3J = 4 Hz, CH_3-Cp*, 15H), 1.42 (t, ^3J = 7 Hz, CH_3, 3H).

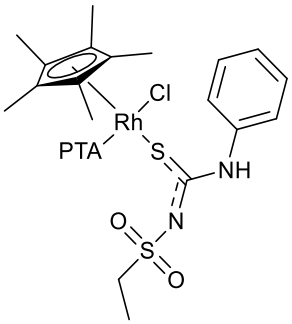

[(η^6-*p*-cymene)Ru{*p*-$TolSO_2NC(S)NPh$}]$_2$ **a_2L1**

Orange solid. Elemental analysis: Found (%) C 53.3; H 4.9; N 5.4. Calculated for $C_{48}H_{52}N_4O_4Ru_2S_4$ (%) C 53.4; H 4.8; N 5.2. ESI MS: *m/z* $[M + H]^+$ 1081.0611, $[M/2 + H]^+$ 541.0240. NMR ($CDCl_3$, 600 MHz): ^1H δ 8.10 (d, ^3J = 9 Hz, tolyl, 2H), 7.34 – 7.01 (m, aromatics), 5.20 (d, ^3J = 5 Hz, cymene-H, 1H), 4.93 (d, ^3J = 6 Hz, cymene-H, 1H), 4.84 (d, ^3J = 6 Hz, cymene-H, 1H), 4.74 (d, ^3J = 5 Hz, cymene-H, 1H), 2.45 (s, cymene-*p*-CH_3, 3H), 2.25 (m, isopropyl-CH, 1H), 1.63 (s, CH_3, 3H) 1.05 (d, ^3J = 7 Hz, isopropyl-CH_3(a), 3H), 0.92 (d, ^3J = 7 Hz, isopropyl-CH_3(b), 3H).

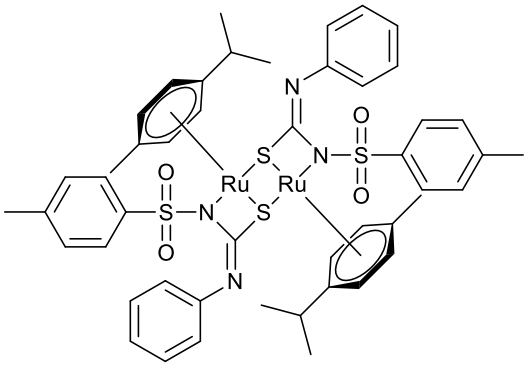

3.3.5 Sulforhodamine B (SRB) assay

In vitro anticancer activity in human colorectal (HCT116), non-small cell lung (NCI-H460), cervical (SiHa) and colon (SW480) carcinoma cell lines was conducted externally by a collaboration with the Hartinger group, University of Auckland, New Zealand. A sulforhodamine B (SRB) assay was used as they have reported previously.[35]

3.3.6 X-ray crystal structure determinations

Crystals of satisfactory quality for single crystal diffraction were grown by slow evaporation of a methanol solution of the complex (Complexes **aL1**, **aL2**, **2cL1**, **2dL1**) or by diffusion of diethyl ether into CH_2Cl_2 (Complexes **1aL1**, **2aL1**). Structures were solved using Olex2[36] with the Olex2.solve[37] structure solution program using Charge Flipping and refined with the Olex2.refine[37] refinement package using Gauss–Newton minimization. Crystal and refinement details are summarized in the supplementary data. The use of a the Olex2 solvent mask was used for the crystal of **2aL1** which was best modelled in the presence of a single molecule of methanol and for **2cL1** which was best modelled in the presence of two methanol and three water molecules. The crystal for **2aL1** contains a disordered PTA ligand on account of rotation about the Ru-P bond which could be modelled as two distinct PTA units of half occupancy. It should also be noted that the crystal of **1aL1** appears to have a minor degree of twinning on account of a small residual peak near S1.

3.3.7 Theoretical investigations

Geometry calculations were conducted using Q-chem software.[38] The mixed basis sets used were aug-cc-pV(D+d)Z for S and P, aug-cc-pVDZ for O, N and Cl, cc-pVDZ for C and H, LANL2DZ for Ru using the effective core potential. The ωB97M-V method was used for all systems. MultiWFN was used for the calculation of non-covalent interactions including the calculation of the reduced density gradient (RDG).[39] Gnuplot was used for the representation of the RDG plot.[40]

3.4 References

1. S. Sadique, A. A. Baqer, A. W. Salman, M. A. Iqbal, M. M. Kadim, F. Jamil, A. Majeed, S. Manahil and A. Altaf, *Reviews in Inorganic Chemistry*, 2023.
2. S. Abdolmaleki, A. Aliabadi and S. Khaksar, *Coordination Chemistry Reviews*, 2024, **501**, 215579.
3. A. Sharma, P. Sudhindra, N. Roy and P. Paira, *Inorganica Chimica Acta*, 2020, **513**, 119925.
4. K. Máliková, L. Masaryk and P. Štarha, *Inorganics*, 2021, **9**, 26.
5. W. D. Tremlett, K. K. Tong, T. R. Steel, S. Movassaghi, M. Hanif, S. M. Jamieson, T. Söhnel and C. G. Hartinger, *Journal of Inorganic Biochemistry*, 2019, **199**, 110768.
6. Z. Liu, C. Hartinger and N. Kulak, Frontiers in Chemistry, 2022, **10**, 979466.
7. A. Ashraf, M. Kubanik, F. Aman, H. Holtkamp, T. Söhnel, S. M. Jamieson, M. Hanif, W. A. Siddiqui and C. G. Hartinger, *European Journal of Inorganic Chemistry*, 2016, **2016**, 1376-1382.
8. T. R. Steel, F. Walsh, A. Wieczorek-Błauż, M. Hanif and C. G. Hartinger, *Coordination Chemistry Reviews*, 2021, **439**, 213890.
9. C. S. Allardyce and P. J. Dyson, *Platinum Metals Review*, 2001, **45**, 62-69.
10. P. J. Dyson, *Chimia*, 2007, **61**, 698-698.
11. B. S. Murray, M. V. Babak, C. G. Hartinger and P. J. Dyson, *Coordination Chemistry Reviews*, 2016, **306**, 86-114.
12. A. L. Noffke, A. Habtemariam, A. M. Pizarro and P. J. Sadler, *Chemical Communications*, 2012, **48**, 5219-5246.
13. İ. Koca, A. Özgür, K. A. Coşkun and Y. Tutar, *Bioorganic & Medicinal Chemistry*, 2013, **21**, 3859-3865.
14. D. H. Al-Amily and M. Hassan Mohammed, *Scientia Pharmaceutica*, 2019, **87**, 28.
15. S. Swaminathan, J. Haribabu, N. Balakrishnan, P. Vasanthakumar and R. Karvembu, *Coordination Chemistry Reviews*, 2022, **459**, 214403.
16. G. H. Ribeiro, A. R. Costa, A. R. de Souza, F. V. da Silva, F. T. Martins, A. M. Plutin and A. A. Batista, *Coordination Chemistry Reviews*, 2023, **488**, 215161.
17. B. N. Cunha, L. Colina-Vegas, A. M. Plutín, R. G. Silveira, J. Honorato, K. M. Oliveira, M. R. Cominetti, A. G. Ferreira, E. E. Castellano and A. A. Batista, *Journal of Inorganic Biochemistry*, 2018, **186**, 147-156.
18. S. Parveen, K. K. Tong, M. Khawar Rauf, M. Kubanik, M. A. Shaheen, T. Söhnel, S. M. Jamieson, M. Hanif and C. G. Hartinger, *Chemistry–An Asian Journal*, 2019, **14**, 1262-1270.
19. B. R. B. Beele, E. Bill and F. Mohr, *Crystal Growth & Design*, 2022, **22**, 3442-3456.
20. M. C. Risi, J. R. Lane, W. Henderson and G. C. Saunders, *Inorganica Chimica Acta*, 2023, **561**, 121850.
21. M. C. Risi, G. C. Saunders and W. Henderson, *Inorganica Chimica Acta*, 2021, **526**, 120506.
22. M. Risi, MSc Thesis, The University of Waikato, 2020.
23. W. Henderson, B. K. Nicholson, M. B. Dinger and R. L. Bennett, *Inorganica Chimica Acta*, 2002, **338**, 210-218.

24. G. F. Grawe, K. M. Oliveira, C. M. Leite, T. D. de Oliveira, J. Honorato, A. G. Ferreira, E. E. Castellano, M. R. Cominetti, R. S. Correa and A. A. Batista, *Dalton Transactions*, 2022, **51**, 1489-1501.
25. R. Gandhaveeti, R. Konakanchi, P. Jyothi, N. S. Bhuvanesh and S. Anandaram, *Applied Organometallic Chemistry*, 2019, **33**, e4899.
26. J. A. Bilbrey, A. H. Kazez, J. Locklin and W. D. Allen, *Journal of Computational Chemistry*, 2013, **34**, 1189-1197.
27. G. Ferguson, P. Roberts, E. Alyea and M. Khan, *Inorganic Chemistry*, 1978, **17**, 2965-2967.
28. S. Parveen, M. Hanif, S. Movassaghi, M. P. Sullivan, M. Kubanik, M. A. Shaheen, T. Söhnel, S. M. Jamieson and C. G. Hartinger, *European Journal of Inorganic Chemistry*, 2017, **2017**, 1721-1727.
29. Z. Riaz, B. Y. Lee, J. Stjärnhage, S. Movassaghi, T. Söhnel, S. M. Jamieson, M. A. Shaheen, M. Hanif and C. G. Hartinger, *Journal of Inorganic Biochemistry*, 2023, **241**, 112115.
30. C. M. Muller, M. V. Babak, M. Kubanik, M. Hanif, S. M. Jamieson, C. G. Hartinger and L. J. Wright, *Inorganica Chimica Acta*, 2016, **450**, 124-130.
31. W. Vullo, *Industrial & Engineering Chemistry Product Research and Development*, 1966, **5**, 346-349.
32. S. B. Jensen, S. J. Rodger and M. D. Spicer, *Journal of Organometallic Chemistry*, 1998, **556**, 151-158.
33. C. White, A. Yates, P. M. Maitlis and D. Heinekey, *Inorganic Syntheses*, 1992, 228-234.
34. W. Henderson, A. G. Nair, N. R. Halcovich and E. R. Tiekink, *Molbank*, 2018, **2018**, M1025.
35. M. Kubanik, H. Holtkamp, T. Sohnel, S. M. Jamieson and C. G. Hartinger, *Organometallics*, 2015, **34**, 5658-5668.
36. O. V. Dolomanov, L. J. Bourhis, R. J. Gildea, J. A. K. Howard and H. Puschmann, *Journal of Applied Crystallography*, 2009, **42**, 339-341.
37. L. J. Bourhis, O. V. Dolomanov, R. J. Gildea, J. A. K. Howard and H. Puschmann, *Acta Crystallographica Section A: Foundations and Advances*, 2015, **71**, 59-75.
38. Y. Shao, Z. Gan, E. Epifanovsky, A. T. Gilbert, M. Wormit, J. Kussmann, A. W. Lange, A. Behn, J. Deng and X. Feng, *Molecular Physics*, 2015, **113**, 184-215.
39. T. Lu and F. Chen, *Journal of Computational chemistry*, 2012, **33**, 580-592.
40. T. Williams, C. Kelley, H.-B. Bröker, J. Campbell, R. Cunningham, D. Denholm, G. Elber, R. Fearick, C. Grammes and L. Hart, *Environment*, 1986, **4**.

Chapter Four

Platinum(II) phosphoryl-substituted thiourea complexes with bis-phosphine ligands and some triphenylarsine and triphenylstibine analogues

Phosphorylthiourea ligands ($R_2P(O)NHC(S)NHR$) share structural similarities with both acylthioureas and sulfonylthioureas by featuring an electron-withdrawing substituent on a thiourea nitrogen. Consequently, like acyl- and sulfonylthioureas, the coordination chemistry of phosphorylthioureas can differ significantly from that of traditional alkyl thioureas. Sulfonylthioureas have been shown to bind metal centres either in a monodentate fashion through the thiourea S donor or in a bidentate manner *via* S,N donor atoms (Chapters 2 and 3). In contrast, phosphorylthioureas in their monoanionic form often more closely resemble acylthioureas. While phosphorylthioureas have also demonstrated S,N coordination,[1-4] they typically favour S,O coordination with the thiourea sulfur and phosphoryl oxygen donor atoms to form a six-membered ring motif.[2, 5-8] Notably, no examples of phosphorylthioureas acting as dianionic ligands have been reported to date, indicating a significant gap in the literature. This is especially apparent with the consideration that the chemistry of thiourea ligands acting as dianions can differ significantly when compared to thiourea ligands acting as monoanions. Given the potential applications of functionalized thiourea ligands, understanding the fundamental chemistry of these lesser-studied phosphorylthioureas is of considerable interest. Of particular interest is how the dianionic nature of the ligand may change the coordination chemistry. Moreover, the presence of the phosphoryl group raises additional questions in relation to the results of chapter two regarding the possible *distal* isomer selectivity through possible Pt–S···O=P chalcogen bonding interactions. Additionally, the NMR-active phosphorus atom in the phosphoryl group could aid in the characterization of the resulting complexes, providing a useful tool in the further study of these ligands and their complexes. In this context, this chapter presents the synthesis and

characterization of several platinum(II) complexes of phosphorylthiourea ligands, analyzed through X-ray crystallography, nuclear magnetic resonance spectroscopy, and computational methods, including non-covalent interaction analysis.

4.1 Results and discussion

4.1.1 Synthesis and characterization of phosphorylthiourea ligands.

Phosphorylthioureas, of the type $(RO)_2P(O)NHCSNHR$, can be synthesized by the reaction between a phosphoramidate with an isothiocyanate under alkaline conditions[9] or more commonly by the treatment of a phosphoroisothiocyanatidic acid (phosphoryl isothiocyanate, $(RO)_2P(O)NCS$) with a primary amine.[5] By an analogous method,[10] phosphinylthioureas of the type $R_2P(O)NHCSNHR$ can also be prepared. The latter alkyl-containing phosphinylthioureas are notably much less soluble, and therefore more difficult to work with than the ester-containing counter parts. For this reason, investigations centred on the ligand $(EtO)_2P(O)NHCSNHPh$ (**P-L1**) which was synthesized by the rection between the commercially available diethyl phosphoramidate and phenyl isothiocyanate in DMF and potassium *t*-butoxide (Scheme 4.1) following the methods used in the synthesis of sulfonylthioureas in Chapter 2 (Section 2.1.1). By the same method, using ethyl and *t*-butyl isothiocyanates, the ligands $(EtO)_2P(O)NHCSNHEt$ (**P-L2**), $(EtO)_2P(O)NHCSNHC(CH_3)_3$ (**P-L3**) were also prepared. Attempted synthesis using allyl isothiocyanate was unfruitful and there was immediate decomposition into a black solution upon addition of the phosphinamide/potassium *t*-butoxide mixture.

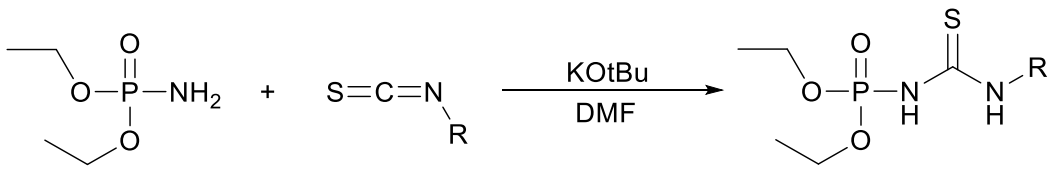

Scheme 4.1: Reaction between diethyl phosphoramidate and alkyl/aryl isothiocyanate in DMF and potassium t-butoxide (KOtBu)

The ligands were characterized by ESI-MS(+) as their pseudomolecular $[M + H]^+$ ion and in some cases their sodium and potassium adducts. Sufficient purity of the ligands for complexation reactions was determined using $^{31}P\{^1H\}$ NMR.

4.2 Synthesis and characterization of phosphorylthiourea metal complexes.

Reactions between the complex *cis*-$[PtCl_2(PPh_3)_2]$ and the ligands **P-L1**, **P-L2** or **P-L3** in a hot methanol/triethylamine mixture gave the corresponding *bis*-triphenylphosphine thiourea complexes which were isolated by precipitation with water and collected by vacuum filtration. By the same method, **P-L1** was reacted with *cis*-$[PtCl_2(SbPh_3)_2]$, $[PtCl_2(AsPh_3)_2]$, $[PtCl_2(P^{**})_2]$, $[PtCl_2(P^{\circ})_2]$ and $[PtCl_2(dppe)_2]$ (P** = $PPh(C_5H_5OMe)_2$, P° = $PPh_2C_6H_4NMe_2$ and dppe = $Ph_2P(CH_2)_2PPh_2$). The structures of the complexes are shown in Figure 4.1. Elemental analysis of complexes **4a** and **4b** show sufficient purity and the purity of the remaining complexes in the series is demonstrated by their NMR spectra. Satisfactory purity of the triphenylstibine and triphenylarsine complexes could not be achieved because of presumed decomposition in solution.

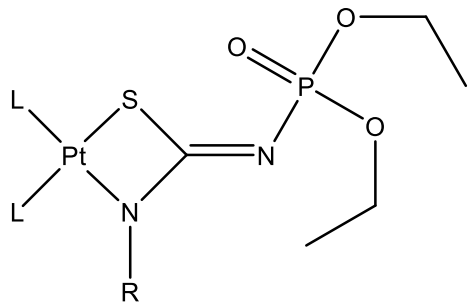

Complex	L	R
4a	PPh_3	Ph
4b	PPh_3	*t*-Butyl
4c	PPh_3	Et
4d	$AsPh_3$	Ph
4e	$SbPh_3$	Ph
4f	P**	Ph
4g	P°	Ph
4h	dppe	Ph

Figure 4.1: Structures of the phosphorylthiourea Pt(II) complexes shown as their distal isomers.

ESI-MS(+) spectra of the phosphorylthiourea complexes showed the typical features. At a capillary exit voltage of 150 V, parent ions of $[M + H]^+$ and in some cases lower intensity sodated ions, $[M + Na]^+$, were observed. Higher capillary exit voltages gave the corresponding $[(M - PR_3) + H]^+$ ions due to a loss of an ancillary monodentate phosphine ligand. An ion of $[M - 60]^+$ was consistently observed in all samples at varying intensities, which was not possible to identify, however, it is presumably a minor decomposition product of hydrolysis that was not detected in the NMR spectra.

4.2.1 NMR analysis

The ^1H and $^{31}P\{^1H\}$ NMR spectra of the bis-phosphine complexes display the archetypal features: in the ^1H NMR spectra, the indicative methyl peaks of the P** and P° ligands are observed as two singlets at 3.80 and 3.78 ppm for complex **4f**

and 2.99 and 2.97 ppm for complex **4g**. For complex **4f**, these peaks overlap with the CH_2 multiplet of the ethyl ester group, while for complex **4g**, the peaks are shifted slightly downfield, allowing for clear interpretation. The CH_2 group of the ancillary dppe ligand in complex **4h** is tentatively assigned to a multiple peak at 2.24 ppm, considering integration and the absence of other discernible resonances.

The incorporation of the phosphorus atom onto the thiourea ligands provides a useful tool for the characterization of the resulting complexes by $^{31}P\{^{1}H\}$ NMR spectroscopy. The *distal* arrangement of the complex places the thiourea phosphorus atom away from the coordination sphere, free from possible J-coupling, and is therefore expected to display as a singlet resonance. In contrast, the *proximal* isomer has the possibility of *cis*-^{3}J(P-P), *trans*-^{3}J(P-P) and Pt-P coupling (Figure 4.2). However, according to the Karplus equation,[11] because the *cis* P-P dihedral angle of the PPh_3 and thiourea phosphorus atoms is close to 90°, ^{3}J coupling of these atoms is not expected to be observed. Previously in Chapter 2, it was demonstrated that the incorporation of a *t*-butyl substituent onto the alkyl portion of the functionalized thiourea forces the formation of the *proximal* isomer by steric means. Using this technique, complex **4b** was prepared to analyse the difference in NMR spectrum between the two possible isomers.

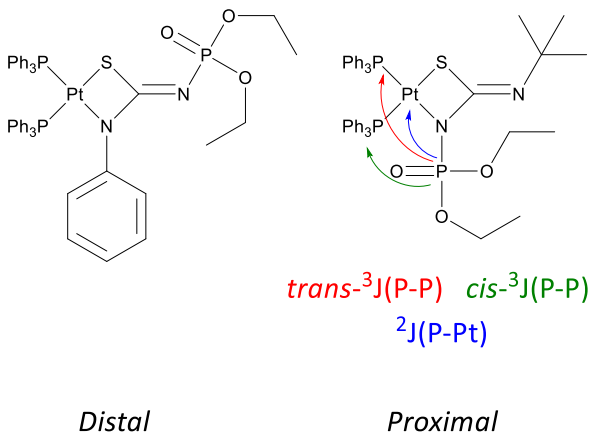

*Figure 4.2: Comparison between the available P-P ^{3}J and P-Pt ^{2}J coupling of the distal and proximal isomers of complexes **4a** (Left) and **4b** (Right).*

The $^{31}P\{^{1}H\}$ NMR spectra of complexes **4a**, **4c**, and **4f**-**4h** show the typical AB doublet of doublets, reflecting the presence of non-equivalent phosphorus atoms (P *trans* to S and P *trans* to N), along with satellite peaks because of coupling to ^{195}Pt which is 33% abundant. The $^{31}P\{^{1}H\}$ NMR spectra of complexe **4a** is shown in Figure 4.3. Singlet resonance peaks related to the phosphorylthiourea ligand's P atom are also evident in the range of 2.4 to 3.1 ppm. The $^{1}J(PtP)$ coupling constants for the complexes fall within the range of 3000 to 3400 Hz, consistent with the expected S-N bidentate coordination mode.[12-14] Moreover, because of the slightly higher *trans* influence exerted by the sulfur atom, the peaks with the smaller of the two $^{1}J(PtP)$ coupling constants are assigned to the P atom positioned *trans* to the S, while the phosphorus with the higher $^{1}J(PtP)$ coupling constant is assigned to the P atoms *trans* to the N for complexes **4a**, **4c**, and **4f**-**4h**.

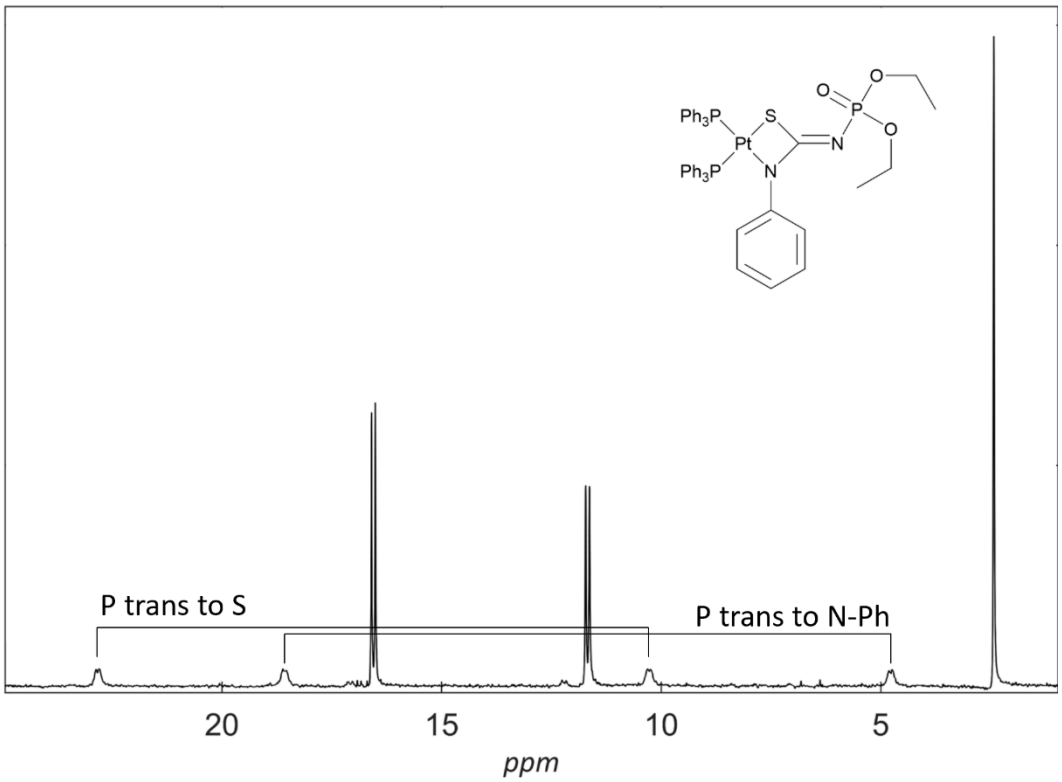

*Figure 4.3: $^{31}P\{^{1}H\}$ NMR spectrum of complex **4a** highlighting the AB doublets and satellite peaks. $CDCl_3$ at 25°C.*

The coupling constants of P *trans* to N for these complexes are in the range of 3126 – 3371 Hz, consistent with the *distal* isomer (P *trans* to N-alkyl). The *t*-butyl-containing complex **4b** shows a slightly larger $^{1}J(PtP)$ coupling constant for P *trans*

to N of 3482 Hz, implying the complex is the *proximal* isomer (P *trans* to N-POR_2). However, the determination of the exact coupling constant value is challenging because of the coincidence of a satellite with the other phosphorus resonance. Further evidence supporting the *proximal* isomer includes the observation of a doublet of doublet resonance for the P *trans* to N and a doublet resonance for the phosphorylthiourea P atom, resulting from new ^3J(P-P) coupling because of the close proximity of the phosphorylthioureas P atom to the coordination sphere. The doublet of doublet resonance of P *trans* to N provides secondary confirmation of the assignment that this resonance relates to the phosphorus atom *trans* to nitrogen, on the assumption that it is indeed the *trans* coupling as opposed to *cis* coupling that is responsible for the splitting. The $^{31}P\{^1H\}$ NMR spectrum of complex **4b** is shown in Figure 4.4. A small ^2J(P-Pt) coupling (around 90-100 Hz) of the phosphorus atom bonded to the platinum(II) centre is also observed as unresolved shoulders on the resonance peak (Figure 4.5) Notably, the resonance for the phosphorylthiourea P atom of complex **4b** appears at 9.14 ppm, a considerable shift from complexes **4a**, **4c**, and **4f**-**4h**, where the ligand's ^{31}P resonances are observed between 2.4 to 2.7 ppm. Moreover, the two phosphoryl ethyl CH_2 groups in the *distal* complexes resonate as a single overlapping multiple, while in the spectrum of complex **4b**, the two CH_2 groups resonate as two distinct multiplets. Both observations align with a significant shift in the environment of the thiourea phosphorus atom.

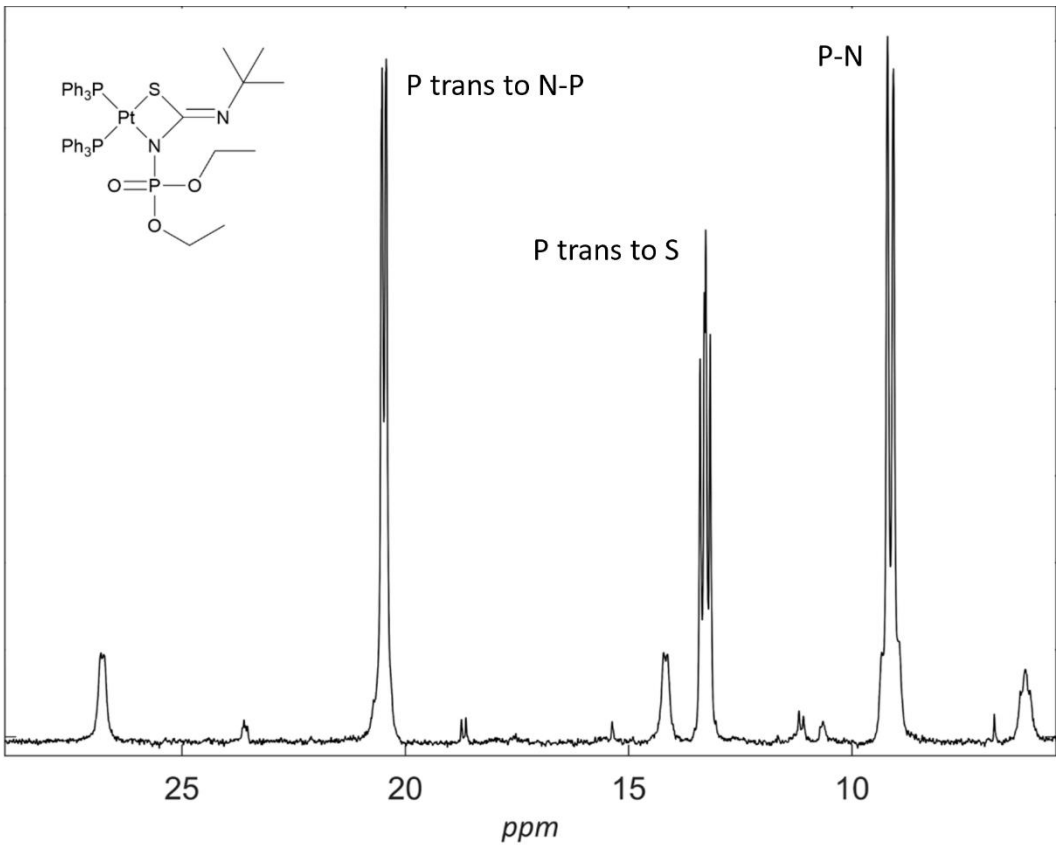

*Figure 4.4: $^{31}P\{^{1}H\}$ NMR spectrum of complex **4b** showing ^{3}J P-P splitting. $CDCl_3$ at 25°C.*

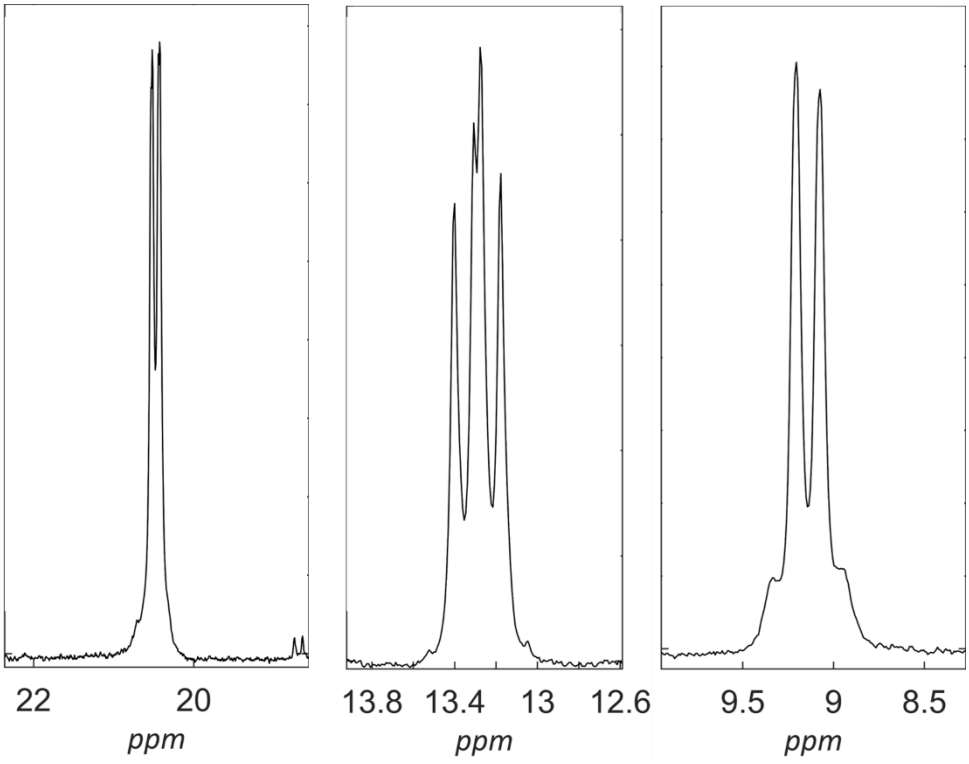

*Figure 4.5: $^{31}P\{^{1}H\}$ NMR spectrum of complex **4b** showing ^{3}J P-P splitting and ^{2}J P-Pt splitting. $CDCl_3$ at 25°C.*

Comparison of the $^{31}P\{^{1}H\}$ spectra of complexes **1a** and **1b** provides a clear distinction between the two isomers. With this knowledge in hand, the remainder of the phosphine containing complexes (**4c**, **4f**-**4h**) can be extrapolated to also be the *distal* linkage isomer by the distinct lack of ligand-phosphine interactions. The *distal* isomer assignment is further supported using $^{1}J(PtP)$ coupling constants which indicate a P *trans* to N-alkyl arraignment (*vide supra*).

4.2.2 X-ray structure determinations

The molecular structures of complexes **4a** (Figure 4.6) and **4b** (Figure 4.7) were elucidated through single-crystal X-ray diffraction, providing unequivocal confirmation of the adopted linkage isomer of each complex. Selected bond lengths and angles are included in Table 4.1. The molecular structure of **4a** reveals the ligand's coordination to the platinum(II) centre *via* the S and N-alkyl atoms as the *distal* isomer, aligning with the ^{31}P NMR observations. Metallacyclic bond distances are 2.326(8) (S1-Pt), 2.088(3) (N1-Pt), 1.345(7) (C1-N1), and 1.796(4) Å (C1-S1), showing close agreement with similar bis(PPh_3) sulfonylthiourea complexes (Chapter 2) and related alkyl thiourea complexes.[13, 14] Further similarities between complex **4a** and analogous bis(PPh_3) sulfonylthiourea complexes are evident in the relatively short PO···S distance of 3.078 Å and the nearly flat plane defined by S1-C1-N2-P-O. Together, these features suggest the likely presence of a short-range chalcogen bond. The molecular structure of complex **4b** reveals the complex to be in the *proximal* linkage isomer, coordinating *via* the S and N-phosphoryl atoms. This adopted coordination mode is likely a result of steric effects of the bulky *t*-butyl substituent, an observation which aligned with the observations in Chapter 2. Despite this difference in the linkage isomer, the average of the metallacyclic bond distances between the two unique molecules of complex **4b** in the asymmetric unit are similar to those of complex **4a** (2.316(2) (S1-Pt), 2.059(6) (N2-Pt), 1.428(1) (C1-N2), and 1.801(7) Å (C1-S1)) with the exception of the slightly elongated C1-N2 bond of 1.434(9) Å compared to the C1-N1 bond of 1.346(7) Å. Both complexes also contain a short C1-N(non-coordinated) bond distance averaging 1.266 Å, suggesting a degree of multi-bond character at this position.

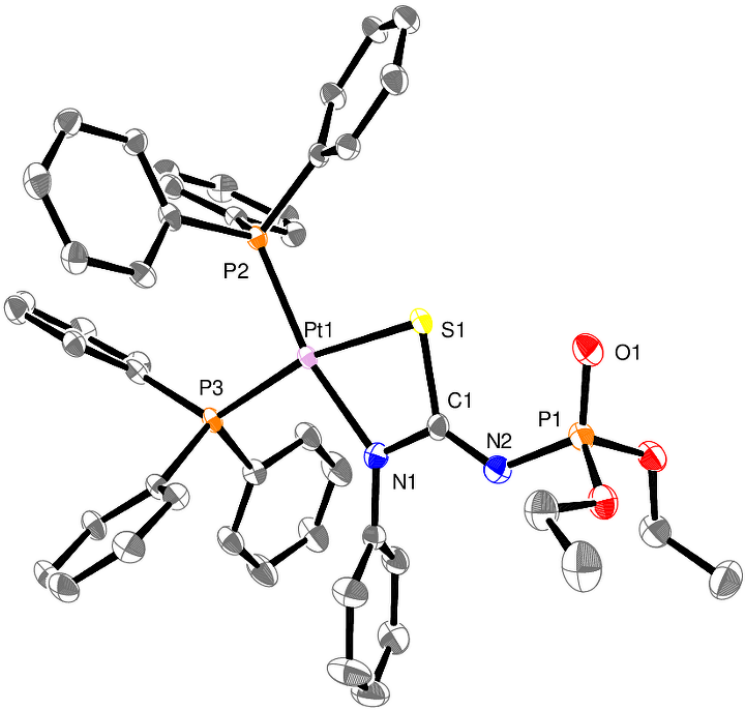

*Figure 4.6: Molecular structure of complex **4a**. Hydrogen atoms are omitted for clarity and thermal ellipsoids are shown at the 50% probability level.*

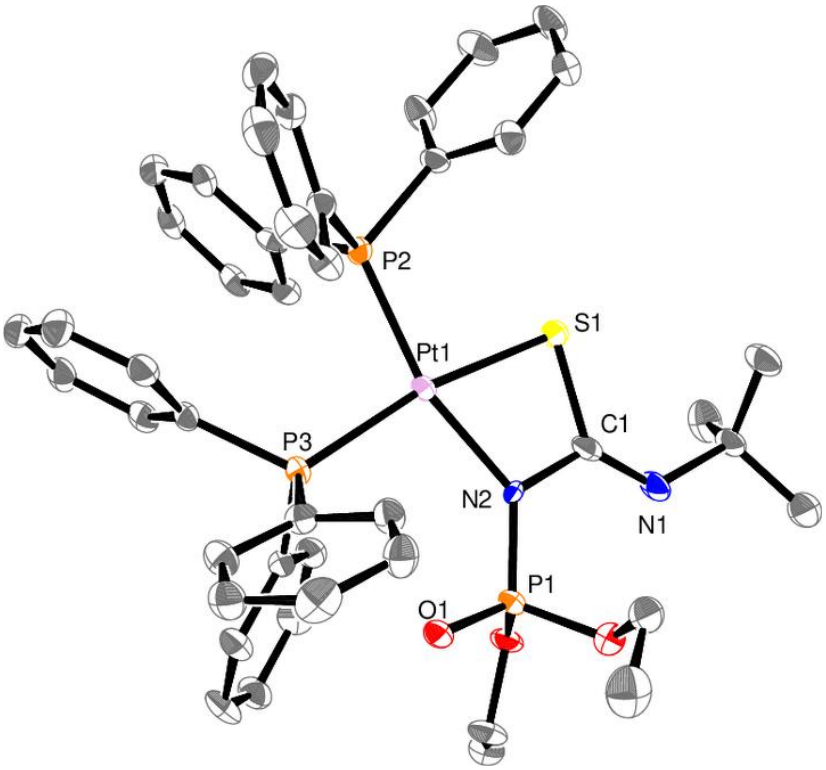

*Figure 4.7: Molecular structure of complex **4b**. Hydrogen atoms and one of the unique molecules of [Pt{(EtO)$_2$PONC(S)N(t-butyl)}(PPh$_3$)$_2$] are omitted for clarity and thermal ellipsoids are shown at the 50% probability level.*

*Table 4.1: Selected bond lengths (Å) and angles (°) for the complexes **4a**, **4b** and the second independent molecule of 4b (4b(a)) in the unit cell.*

	4a	4b	4b(a)
P2 - Pt	2.246(8)	2.248(2)	2.250(2)
P3 - Pt	2.297(1)	2.308(2)	2.301(2)
S1 - Pt	2.326(1)	2.314(2)	2.318(2)
N1 - Pt	2.088(3)	-	-
N2 - Pt	-	2.067(6)	2.051(5)
C1 - S	1.796(4)	1.797(7)	1.806(8)
C1 - N1	1.345(7)	1.250(1)	1.250(1)
C1 - N2	1.287(5)	1.434(9)	1.422(9)
P1 - Pt - P2	97.11(4)	97.10(6)	96.7(6)
S1 - Pt - N1	69.78(1)	-	-
S1 - Pt - N2	-	70.48(2)	69.83(2)

The reason for observed N,S-coordination mode for these platinum complexes instead of the O,S-coordination mode often observed for phosphorylated thiourea ligands is unclear. Potential explanations may include the affinity of platinum(II) towards nitrogen donors following the hard-soft acid-base principle, chalcogen bond stabilization or simple steric effects.

4.2.3 Computational investigations of non-covalent interactions

Previously in Chapter 2, it was determined that the observed *distal* isomer selectivity of the sulfonylthiourea platinum(II) complexes was most likely a result of a stabilising chalcogen bond between the thiourea sulfur and sulfonyl oxygen atoms. Molecular structures and analysis of the non-covalent interactions using the NCI index provided evidence for the presence of such a non-covalent interaction. In Chapter 3, while the complexes demonstrated *proximal* isomer selectivity, the *distal* isomer of the *p*-cymene ruthenium(II) PPh_3 complex was also demonstrated to contain a chalcogen interaction. It can therefore be surmised that the phosphorylthiourea platinum(II) complexes reported in this chapter represent an analogous system. Indeed, the molecular structure of complex **4a** contains a near flat semi-circle arrangement of S-C-N-P-O suggesting a chalcogen

bond is present between the thiourea sulfur and phosphoryl oxygen atoms. Moreover, $^{31}P\{^{1}H\}$ NMR spectroscopic analysis of the remaining complexes indicates they too are in the *distal* isomer, with the exception of complex **4b** (*vide supra*). To provide additional confirmation of the presence of the chalcogen bond in phosphorylthiourea platinum(II) complexes reported in this chapter, the reduced density gradient was calculated between the thiourea sulfur and phosphoryl oxygen atoms, following the methods outlined in Chapter 2. The resulting plot of RDG verses sign(λ_2)ρ is shown in Figure 4.8. The plot clearly shows a distinct low gradient, low density trough which, by comparison to the results in Chapters 2 and 3, relates to a chalcogen interaction and therefore confirming its presence.

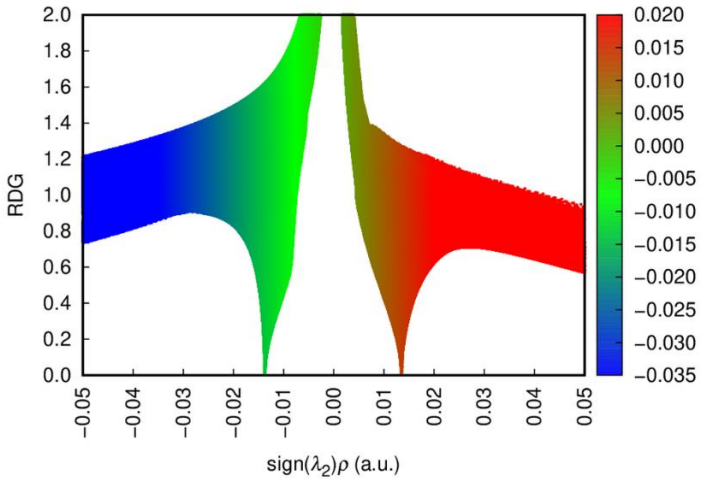

*Figure 4.8: Plot of RDG (s) verses sign(λ_2)ρ for complex **4a** showing a trough (~-0.015) related to chalcogen bonding interactions.*

4.3 Conclusions

In this chapter, a series of new *bis*-phosphine, triphenylarsine and triphenylstibine platinum(II) complexes with dianionic phosphorylthiourea ligands have been prepared. Analysis of the complexes by single crystal X-ray diffraction, ESI-MS, NMR spectroscopy and computational methods, reveal a tendency for the complexes to form the *distal* linkage isomer unless otherwise forced by a bulky *t*-butyl substituent. It has been shown that $^{31}P\{^{1}H\}$ NMR analysis of the complexes

provides a clear indication of the observed coordination mode by indicative $^{1}J(PtP)$ couplings and new $^{3}J(PP)$ couplings which are only present for the *proximal* linkage isomer, providing a powerful tool in the absence of more indicative techniques such as single crystal X-ray diffraction. Further insight into the non-covalent interactions of complex **4a** highlights the potential presence of a short ranged chalcogen bond, supporting the observations from the molecular crystal structure and indicating a potential reason for the observed *distal* isomer preference. In summary, while the coordination chemistry of these ligands acting as dianions towards platinum(II) mimics that of the closely related sulfonylthiourea ligands, the incorporation of a phosphorus atom onto the ligand proves to be an extremely useful tool for characterization by $^{31}P\{^{1}H\}$ NMR spectroscopy.

4.4 Experimental

4.4.1 Materials

Phenyl isothiocyanate, ethyl isothiocyanate, *t*-butyl isothiocyanate, diethyl phosphoramidate and potassium *t*-butoxide were used as supplied by Sigma Aldrich. The complexes *cis*-$[PtCl_2(PPh_3)_2]$, $[PtCl_2(SbPh_3)_2]$, $[PtCl_2(dppe)]$ and $[PtCl_2(P^{**})_2]$ were prepared by ligand substitution of the cyclo-octa-1,5-diene (COD) ligand of $[PtCl_2(COD)$ with the stoichiometric quantity of appropriate phosphine in dichloromethane using a modified procedure[15]. The complexes $[PtCl_2(AsPh_3)_2]$ and $[PtCl_2(P^{\circ})_2]$ were prepared by a similar method using K_2PtCl_4 as the starting material and were used as supplied by W. Henderson, University of Waikato.

4.4.2 Instrumentation

ESI-MS spectra were recorded using a Bruker Daltonics MicrOTOF electrospray ionization mass spectrometer using sodium formate for calibration. Samples were dissolved in a single drop of dichloromethane and made up to 1.5 mL with methanol. Spectra were recorded with a *Capillary Exit* voltage of 150 V and a *Skimmer 1* voltage of 50 V unless otherwise stated. Elemental analysis was performed by the Chemical Analysis Facility, Department of Molecular Sciences,

Macquarie University, Sydney, Australia. Single crystal X-ray diffraction was carried out by the University of Auckland Micro characterization Facility, Auckland, New Zealand. $^{31}P\{^{1}H\}$ (243 MHz) and ^{1}H (600 MHz) NMR spectra were recorded in $CDCl_3$ at 25°C using a 600 MHz Jeol ECZR NMR spectrometer.

4.4.3 Synthesis of $(EtO)_2P(O)NHC(S)NHPh$ (P-L1)

Diethyl phosphoramidate ($(EtO)_2P(O)NH_2$, 3 g, 19.6 mmol), and an equal molar equivalent of potassium *t*-butoxide (2.2 g, 19.6 mmol) were added to DMF (20 mL) with gentle heating and stirring until the contents of the flask were dissolved (approx. 5 minutes). To the warm solution, phenyl isothiocyanate (2.65 g, 19.6 mmol) was added dropwise before being stirred for a further 10 minutes. The product was precipitated by a single rapid addition of ice cold water (50 mL) which had been acidified with concentrated hydrochloric acid (2.5 mL approx.) before being immediately collected by vacuum filtration, washed with distilled water (3 x 20 mL) and dried in vacuum to yield a white powdered solid. (3.75 g, 66 %) ESI MS: Capillary exit voltage 90 V, *m/z* $[M + H]^+$ 289, $[M + Na]^+$ 311, $[2M + Na]^+$ 599. NMR ($CDCl_3$ 243 MHz): $^{31}P\{^{1}H\}$, δ -3.77 (s).

4.4.4 Synthesis of $(EtO)_2P(O)NHC(S)NHCH(CH_3)_3$) (P-L2)

P-L2 was synthesized following the method for the synthesis of **P-L1** using diethyl phosphoramidate (3 g, 19.6 mmol), potassium *t*-butoxide (2.2 g, 19.6 mmol) and *t*-butyl isothiocyanate (2.26 g, 19.6 mmol). Upon addition of cold acidified water, the solution was allowed to sit for three days at room temperature, at which time the white crystalline solid was collected by filtration and washed with distilled water (2 x 10 mL) and dried in vacuum to give the target compound as a crystalline solid. (1.29 g, 25 %) ESI MS: Capillary exit voltage 90 V, *m/z* $[M + H]^+$ 269 $[M + Na]^+$ 291, $[2M + Na]^+$ 559. NMR ($CDCl_3$ 243 MHz): $^{31}P\{^{1}H\}$, δ -3.97 (s).

4.4.5 Synthesis of $(EtO)_2P(O)NHC(S)NHCH_2CH_3$ (P-L3)

P-L3 was synthesized following the method for the synthesis of **P-L1** using diethyl phosphoramidate (5.57 g, 36.4 mmol), potassium t-butoxide (4 g 36.4 mmol) and ethyl isothiocyanate (3.17 g, 36.4 mmol). White powdered solid. (1.57 g, 20 %) ESI MS: Capillary exit voltage 90 V, *m/z* $[M + H]^+$ 241. $[M + Na]^+$ 263, $[M + K]^+$ 279, $[2M + Na]^+$ 503. NMR ($CDCl_3$ 243 MHz): $^{31}P\{^1H\}$, δ -3.60 (s).

4.4.6 General synthesis of the phosphorylthiourea complexes

The ligand, equimolar quantities of the platinum(II) starting material and three drops of triethylamine were suspended in MeOH (20 mL) with stirring. The mixture was brought to reflux until the reactants were completely dissolved and after a further 5 minutes the product was precipitated by the rapid addition of cold water and cooled in an ice bath to aid in precipitation. The target complex was collected by vacuum filtration, washed with distilled water (3 x 10 mL) and dried under vacuum. Details pertaining to each compound are summarized in Table 4.2.

Table 4.2: Synthetic details for the prepared phosphorylthiourea complexes.

Product	starting material	mg	mmol	Ligand	mg	mmol	Yield (mg)	Yield (%)
4a	$[PtCl_2(PPh_3)_2]$	100	0.127	**P-L1**	36	0.127	101	79
4b	$[PtCl_2(PPh_3)_2]$	100	0.127	**P-L2**	34	0.127	97	78
4c	$[PtCl_2(PPh_3)_2]$	110	0.127	**P-L3**	34	0.127	116.5	87
4d	$[PtCl_2(SbPh_3)_2]$	110	0.113	**P-L1**	33	0.113	85	67
4e	$[PtCl_2(AsPh_3)_2]$	117	0.133	**P-L1**	38	0.133	107	57
4f	$[PtCl_2(P^{**})_2]$	100	0.110	**P-L1**	32	0.110	73	59
4g	$[PtCl_2(P^{\circ})_2]$	100	0.114	**P-L1**	33	0.114	106	85
4h	$[PtCl_2(dppe)]$	100	0.151	**P-L1**	43	0.151	110	83

[Pt{(EtO)$_2$PONC(S)NPh}(PPh$_3$)$_2$] ***4a***

Off-white solid. Elemental analysis: Found (%) C 56.07; H 4.757; N 2.97; S 3.125. Calculated (%) C 56.12; H 4.51; N 2.76; S 3.19. ESI MS: *m/z* $[M + H]^+$ 1006, $[M + Na]^+$ 1028. NMR ($CDCl_3$ 243 MHz): $^{31}P\{^1H\}$, δ 16.50 [d, $^1J_{PtP}$ 3051 Hz, $^2J_{PP}$ 22 Hz], 11.67 [d, $^1J_{PtP}$ 3350 Hz, $^2J_{PP}$ 23 Hz], 2.48 (s); NMR ($CDCl_3$ 600 MHz): ^1H 7.53 – 6.93 (m, aromatic), 6.47 – 6.27 (m, 5 H, N-Ph), 3.80 (m, 4 H, OCH_2), 1.06 (t, ^3J = 7, 6 H, CH_3).

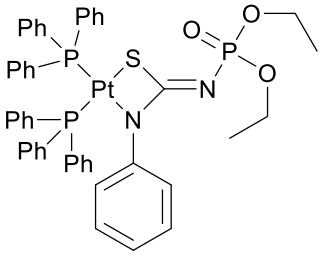

[Pt{(EtO)$_2$PONC(S)N(t-butyl)}(PPh$_3$)$_2$] **4b**

Off-white solid. Elemental analysis: Found (%) C 54.84; H 5.13; N 3.14; S 2.93. Calculated (%) C 54.82; H 5.01; N 2.84; S 3.25. ESI MS: *m/z* $[M + H]^+$ 986, $[M + Na]^+$ 1008. NMR ($CDCl_3$ 243 MHz): $^{31}P\{^1H\}$, δ 20.46 [d, $^1J_{PtP}$ 3059 Hz, $^2J_{PP}$ 22 Hz], 13.27 [dd, $^1J_{PtP}$ 3482 Hz, $^2J_{PP}$ 25 Hz], 9.14 (d, $^3J_{pp}$ 31 Hz); NMR ($CDCl_3$ 600 MHz): ^1H 7.74 – 6.95 (m, aromatic), 3.51 (m, 2 H, OCH_2), 3.30, (m, 2H, OCH_2), 1.26 (s, 9 H, *t*-butyl), 0.85 (t, ^3J = 7 Hz, 6 H, CH_3)

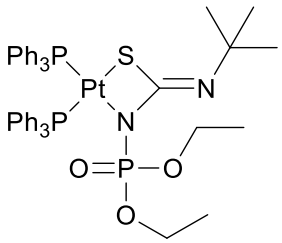

[Pt{(EtO)$_2$PONC(S)NCH$_2$CH$_3$}(PPh$_3$)$_2$] **4c**

Off white solid. ESI MS: *m/z* [M + H]$^+$ 958, [M + Na]$^+$ 980. NMR ($CDCl_3$ 243 MHz): $^{31}P\{^1H\}$, δ 18.79 [d, $^1J_{PtP}$ 3052 Hz, $^2J_{PP}$ 21 Hz], 13.43 [d, $^1J_{PtP}$ 3242 Hz, $^2J_{PP}$ 21 Hz], 3.10 (s); NMR ($CDCl_3$ 600 MHz): ^1H 7.50 – 7.10 (m, aromatic), 3.96 (m, 4 H, O-CH_2), 2.79 (m, 2 H, CH_2) 1.94 (t, ^3J = 7 Hz, 6 H, CH_3), 0.36 (t, ^3J = 7 Hz, 3 H, CH_3)

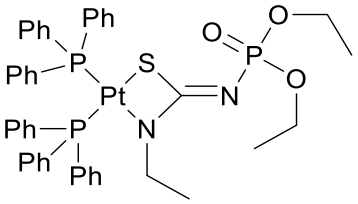

[Pt{(EtO)$_2$PONC(S)NPh}(SbPh$_3$)$_2$] **4d**

Yellow solid. ESI MS: *m/z* [M + H]$^+$ 1094. NMR ($CDCl_3$ 243 MHz): $^{31}P\{^1H\}$, δ 1.38 (s); NMR ($CDCl_3$ 600 MHz): ^1H 7.50 – 6.99 (m, aromatic), 6.60 – 6.45 (m, N-Ph), 3.99 (m, 4 H, OCH_3), 1.21 (t, ^3J = 7 Hz, 6 H CH_3).

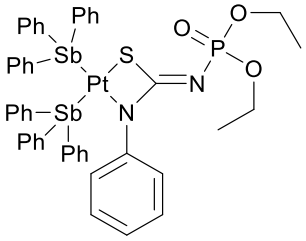

[Pt{(EtO)$_2$PONC(S)NPh}(AsPh$_3$)$_2$] **4e** Pale yellow solid. ESI MS: *m/z* [M + H]$^+$ 1186. NMR ($CDCl_3$ 243 MHz): $^{31}P\{^1H\}$, δ 1.99 (s); NMR ($CDCl_3$ 600 MHz): ^1H 7.52 – 6.28 (m, aromatic), 3.87 (m, OCH_3), 1.11 (t, ^3J = 7 Hz, CH_3).

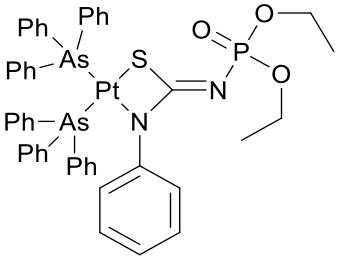

*[Pt{(EtO)$_2$PONC(S)NPh}(P**)$_2$]* **4f**

Off-white solid. ESI MS: *m/z* $[M + H]^+$ 1127, $[M + Na]^+$ 1149. NMR ($CDCl_3$ 243 MHz): $^{31}P\{^1H\}$, δ 14.13 [d, $^1J_{PtP}$ 3072 Hz, $^2J_{PP}$ 21 Hz], 8.76 [d, $^1J_{PtP}$ 3372 Hz, $^2J_{PP}$ 21 Hz], 2.52 (s); NMR ($CDCl_3$ 600 MHz): ^1H 7.46 – 6.93 (m, aromatic), 6.76 – 6.28 (m, 5 H, N-Ph), 3.80 (m, OCH_2), 3.80 (s, PhOMe), 3.78 (s, PhOMe), 1.06 (t, ^3J = 7 Hz, 6 H, CH_3).

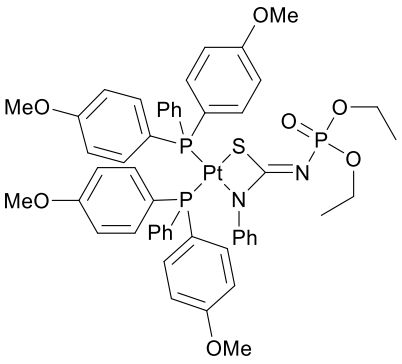

[Pt{(EtO)$_2$PONC(S)NPh}(P°)$_2$] **4g**

Off-white solid. ESI MS: *m/z* $[M + H]^+$ 1093, $[M + Na]^+$ 1115. NMR ($CDCl_3$ 243 MHz): $^{31}P\{^1H\}$, δ 14.56 [d, $^1J_{PtP}$ 3074 Hz, $^2J_{PP}$ 22 Hz], 9.15 [d, $^1J_{PtP}$ 3364 Hz, $^2J_{PP}$ 22 Hz], 2.64 (s); NMR ($CDCl_3$ 600 MHz): ^1H 7.48 – 6.88 (m, aromatic), 6.61 – 6.31 (m, 5 H, N-Ph), 3.80 (m, OCH_2), 2.99 (s, 6 H, NCH_3), 2.97 (s, 6 H, NCH_3), 1.06 (t, ^3J = 7 Hz, 6 H, CH_3).

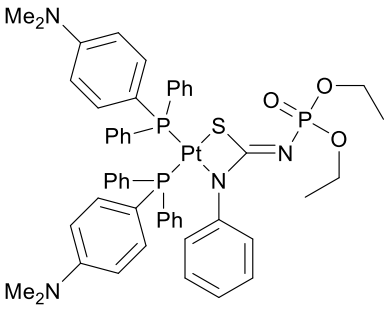

[Pt{(EtO)$_2$PONC(S)NPh}(dppe)$_2$] **4h**

Off-white solid. ESI MS: *m/z* $[M + H]^+$ 880, $[M + Na]^+$ 902. NMR ($CDCl_3$ 243 MHz): $^{31}P\{^1H\}$, NMR ($CDCl_3$ 600 MHz): δ 43.94 [d, $^1J_{PtP}$ 3053 Hz, $^2J_{PP}$ 6 Hz], 37.27 [d, $^1J_{PtP}$ 3142 Hz, $^2J_{PP}$ 6 Hz], 2.69 (s); ^1H 7.83 – 7.13 (m, aromatic), 6.67 – 6.54 (m, 5 H, N-Ph), 3.95 (m, OCH_2), 2.24 (m, 4 H, PCH_2CH_2P), 1.18 (t, ^3J = 7 Hz, 6 H, CH_3).

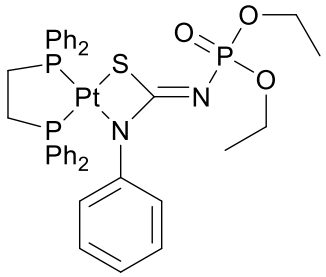

4.4.7 X-ray crystal structure determinations

Crystals of satisfactory quality for single crystal diffraction of complexes **4a** and **4b** were grown by diffusion of diethyl ether into dichloromethane. Structures were solved using Olex2[16] with the Olex2.solve[17] structure solution programme using Charge Flipping and refined with the Olex2.refine[17] refinement package using Gauss–Newton minimization. Crystal and refinement details are summarized in the supplementary data.

4.4.8 Theoretical investigations

Optimization and single point calculations were conducted using Qchem software[18] at the ωB97MV/LANL2DZ level of theory using the LANL2DZ effective core potential for platinum on the New Zealand eScience Infrastructure (NeSI) high performance computing facilities. Global minima were not checked because of the high computational cost. Cartesian coordinates of the optimized systems are provided in the supplementary data. MultiWFN[19] was used for the calculation of non-covalent interactions including the calculation of the reduced density gradient. Gnuplot[20] was used for the representation of 2D RDG plot.

4.5 References

1. F. D. Sokolov, N. G. Zabirov, L. N. Yamalieva, V. G. Shtyrlin, R. R. Garipov, V. V. Brusko, A. Y. Verat, S. V. Baranov, P. Mlynarz and T. Glowiak, *Inorganica Chimica Acta*, 2006, **359**, 2087-2096.
2. F. D. Sokolov, S. V. Baranov, D. A. Safin, F. E. Hahn, M. Kubiak, T. Pape, M. G. Babashkina, N. G. Zabirov, J. Galezowska and H. Kozlowski, *New Journal of Chemistry*, 2007, **31**, 1661-1667.
3. D. A. Safin, M. G. Babashkina, K. Robeyns, M. P. Mitoraj, P. Kubisiak, M. Brela and Y. Garcia, *CrystEngComm*, 2013, **15**, 7845-7851.
4. D. A. Safin, M. G. Babashkina, A. Klein, F. D. Sokolov, S. V. Baranov, T. Pape, F. E. Hahn and D. B. Krivolapov, *New Journal of Chemistry*, 2009, **33**, 2443-2448.
5. M. G. Babashkina, D. A. Safin, K. Robeyns and Y. Garcia, *European Journal of Inorganic Chemistry*, 2015, **2015**, 1160-1166.
6. D. A. Safin, M. G. Babashkina, M. Bolte, Ł. Szyrwiel, A. Klein and H. Kozlowski, *Phosphorus, Sulfur, and Silicon*, 2010, **185**, 1739-1745.
7. D. A. Safin, F. D. Sokolov, H. Nöth, M. G. Babashkina, T. R. Gimadiev, J. Galezowska and H. Kozlowski, *Polyhedron*, 2008, **27**, 2022-2028.
8. D. A. Safin, M. G. Babashkina, M. Bolte, D. B. Krivolapov, M. L. Verizhnikov, A. R. Bashirov and A. Klein, *Inorganica Chimica Acta*, 2011, **366**, 19-26.
9. C. Subramanyam, K. Chandrasekhar, R. Venkata, G. Madhava and R. Naga, *Der Pharmacia Lettre*, 2012, **3**, 869-874.
10. G. M. Dobrikov, V. Valcheva, Y. Nikolova, I. Ugrinova, E. Pasheva and V. Dimitrov, *European Journal of Medicinal Chemistry*, 2013, **63**, 468-473.
11. M. Karplus, *The Journal of Chemical Physics*, 1959, **30**, 11-15.
12. M. C. Risi, G. C. Saunders and W. Henderson, *Inorganica Chimica Acta*, 2021, **526**, 120506.
13. W. Henderson, B. K. Nicholson and C. E. F. Rickard, *Inorganica Chimica Acta*, 2001, **320**, 101-109.
14. O. C. Okpareke, W. Henderson, S. Akkoç and B. Coban, *Inorganica Chimica Acta*, 2022, **531**, 120707.
15. D. Drew, J. Doyle and A. G. Shaver, *Inorganic Syntheses: Reagents for Transition Metal Complex and Organometallic Syntheses*, 1990, **28**, 346-349.
16. O. V. Dolomanov, L. J. Bourhis, R. J. Gildea, J. A. K. Howard and H. Puschmann, *Journal of Applied Crystallography*, 2009, **42**, 339-341.
17. L. J. Bourhis, O. V. Dolomanov, R. J. Gildea, J. A. K. Howard and H. Puschmann, *Acta Crystallographica Section A: Foundations and Advances*, 2015, **71**, 59-75.
18. Y. Shao, Z. Gan, E. Epifanovsky, A. T. Gilbert, M. Wormit, J. Kussmann, A. W. Lange, A. Behn, J. Deng and X. Feng, *Molecular Physics*, 2015, **113**, 184-215.
19. T. Lu and F. Chen, *Journal of Computational Chemistry*, 2012, **33**, 580-592.
20. T. Williams, C. Kelley, H.-B. Bröker, J. Campbell, R. Cunningham, D. Denholm, G. Elber, R. Fearick, C. Grammes and L. Hart, *Environment*, 1986, **4**.

Chapter Five

The coordination chemistry and computational investigation of diacylated thiourea ligands towards platinum(II), palladium(II) and gold(III) metal centres

Throughout this thesis exploring the coordination chemistry of sulfonyl- and phosphorylthiourea ligands towards platinum group and surrounding late transition metals, a reoccurring theme is the comparison of these systems to the related acylthiourea class. Unlike the lesser studied functionalized thiourea ligands investigated here, literature on acylthiourea ligands is numerous,[1-4] with many investigations exploring the complexes for catalytic[5-7] and biological activity.[8-11] The coordination modes available for acylthioureas are also diverse, most commonly, the ligands act as monoanionic ligands, following deprotonation of the amide functionality, to form six-membered ring systems through S,O-chelation involving the thiourea sulfur and the oxygen atoms of the acyl functional group (Figure 5.1).[1, 2] Less commonly, they may also adopt four-membered M-S-C-N ring systems through the core thiourea sulfur and nitrogen donor atoms,[3] or as neutral monodentate ligands through only the thiourea sulfur donor atom.[4]

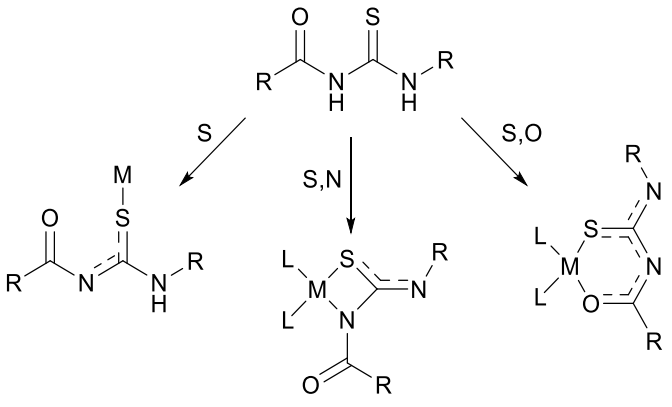

Figure 5.1: Monodentate S and bidentate S,N and S,O coordination modes of acylthiourea ligands.

Because of the considerable interest in acylthioureas, it is surprising that no transition metal complexes of diacylated thiourea ligands, diacylthioureas, have

been reported. Diacylthiourea molecules have been known for at least a century as evidenced by an early 1915 report by E. F. Kohmann detailing the reactions between thiourea and acetic anhydride.[12] Recently, there has been only a small number of reports of the synthesis of both symmetric[13] and asymmetrical[14] diacylthiourea and the corresponding applications. Given that no transition metal complexes have been reported thus far, and the promising avenues of research of the monoacylated counterparts, this chapter explores some preliminary investigations into the coordination chemistry of symmetric diacylthiourea ligands towards Pt(II), Pd(II) and Au(III).

5.1 Results and discussion

5.1.1 Synthesis and characterization of symmetric diacylated thiourea ligands and resulting complexes

The synthesis of diacylthiourea ligands followed an abridged procedure based on that of E. F. Kohmann.[12] Thiourea in excess acetic, propanoic, or benzoic anhydride was heated to approximately 80–100°C for 40 minutes, during which time the thiourea dissolved, and the solution changed from colourless to deep yellow (Figure 5.2). Prolonged heating beyond this point resulted in an orange to amber colouration, which did not significantly impact yield or purity, but was not necessary to achieve satisfactory conversion. Once the solution reached a deep yellow colour, it was removed from heat and allowed to cool to room temperature. In reactions using liquid anhydrides, cooling led to the formation of small to large yellow needle crystals. The product was collected and washed with additional cold anhydride, yielding the target diacylthiourea with excellent purity.

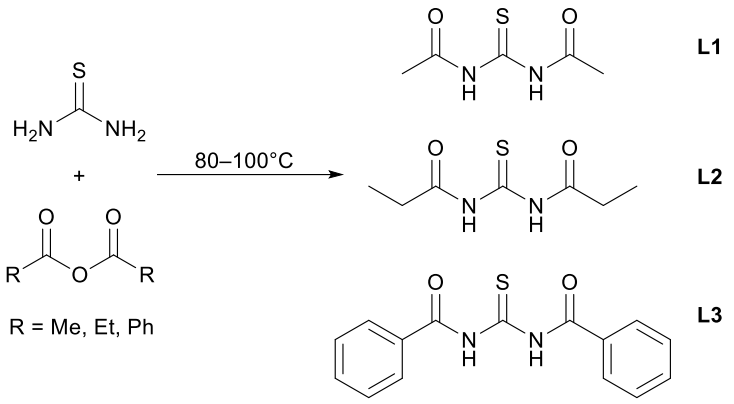

Figure 5.2: Synthesis of the diacylthiourea ligands in this study.

In the case of reactions involving solid benzoic anhydride, on cooling, the target diphenyl-diacylthiourea along with excess benzoic-anhydride and benzoic acid byproduct will solidify. Sufficient purity for further reactions was achieved by consecutive crystallizations of the reaction mass from pure ethanol. Attempts to purify the benzoyl thiourea by dissolving the solid reaction mixture in near-boiling water to remove soluble benzoic acid converts the diacylthiourea to diacylurea *via* substitution of the thiourea sulfur with oxygen (Figure 5.3), as observed by ESI-mass spectrometry. This observation was unexpected, but not surprising given the relatively electron deficient thiourea carbon atom which is primed for hydrolysis by the presence of two adjoining electron-withdrawing acyl groups. Similar thiourea to urea conversions have been reported for mono-acylated thioureas in the presence of permanganate[15] or hydrogen peroxide.[16] The target diacylthiourea ligands are readily identified in the ESI-MS(+) spectra as $[M + Na]^+$ and $[2M + Na]^+$ sodium adduct ions. The ^1H and ^{13}C NMR spectra show the archetypal features, *i.e.* the core thiourea and acyl carbon resonances appear between 183 and 177 ppm for C=S and 174 and 166 ppm for C=O.

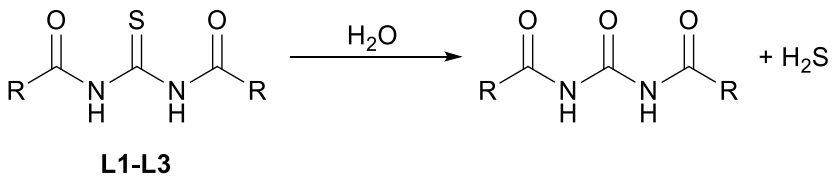

Figure 5.3: Diacylthiourea to diacylurea conversion by hydrolysis

Reactions between the diacylthiourea ligands **DA-L1**, **DA-L2** and **DA-L3** and *cis*-$[PtCl_2(PPh_3)_2]$ in refluxing methanol and sodium hydroxide produced the corresponding triphenylphosphine complexes $[Pt\{(MeCON)_2CS\}(PPh_3)_2]$ (**5a**), $[Pt\{(EtCON)_2CS\}(PPh_3)_2]$ (**5b**) and $[Pt\{(PhCON)_2CS\}(PPh_3)_2]$ (**5c**). The resulting solutions were evaporated to dryness under reduced pressure, dissolved in dichloromethane and passed through approximately 1 cm of silica to remove any insoluble solids. The solutions were again evaporated to dryness to yield the target complexes which were readily identified in the ESI-MS(+) spectra as their pseudomolecular $[M + H]^+$ ions and in some cases also as their $[M + Na]^+$ sodium adducts. At higher capillary voltages (> 180 V), ions relating to the fragmented loss of a single triphenylphosphine were also observed, which is a characteristic feature of bis(phosphine) platinum(II) complexes. In some cases, ions relating to the fragmented loss of an acyl group, $[M – ROOH^- + H]^+$ are also present, which appears to be a characteristic ion for complexes of these ligands.

The ^1H NMR spectra of the complexes showed two sets of resonances relating to the alkyl substituents of the ligand as a result of the breaking of the ligand symmetry by coordination to the platinum(II) centre, providing a good indication that complexation has occurred. In the $^{31}P\{^1H\}$ NMR spectra, the expected set of AB doublet of doublets resulting from the presence of non-equivalent phosphorus atoms (P *trans* to S and P *trans* to N) along with accompanying ^{195}Pt satellite peaks can be seen. The $^1J(PtP)$ coupling constants are between the range of 3116 to 3377 Hz which correlates with an S,N bidentate coordination mode.[17, 18]

Minor decomposition of the platinum(II) complexes was observed after several months in solution or upon refluxing the complex in a methanol-water mixture. ESI-MS(+) analysis of the decomposed samples revealed a strong intensity peak corresponding to the mono-acylated complex $[Pt\{RCONCSNH\}(PPh_3)_2]$ with $[M + H]^+$ m/z values of 835 (R = Me), 849 (R = Et), and 897 (R = Ph). While these peaks are noted as common fragments in the ESI-MS spectra of complexes of this type (*vide supra*), the $^{31}P\{^1H\}$ NMR spectrum of the sample displays a second set of resonances of lower intensity, which were absent in freshly prepared samples. Preparations of complexes **5a**-**5c** from reactions with *cis*-$[PtCl_2(PPh_3)_2]$ and **DA-L1**,

DA-L2 and **DA-L3** in a methanol/sodium hydroxide solution does not initially appear to form the mono-acylated product as evident from ESI-MS, ^{1}H and ^{31}P NMR analysis of the crude reaction mixture. However, attempted isolations of the complexes by precipitation with water gives a mixture of products as indicated by ESI-MS. It can be summarized that the decomposition mechanism of the diacylated complexes involves de-acylation as a result of hydrolysis, producing $[Pt\{RCONCSNH\}(PPh_3)_2]$ and $RCOO^-$ (Figure 5.4). Decomposition *via* this route is consistent with the stability of acetate, propanoate, and benzoate anions as leaving groups, which is further supported by the fragmentation patterns in the ESI-MS spectra of the intact diacylthiourea complex.

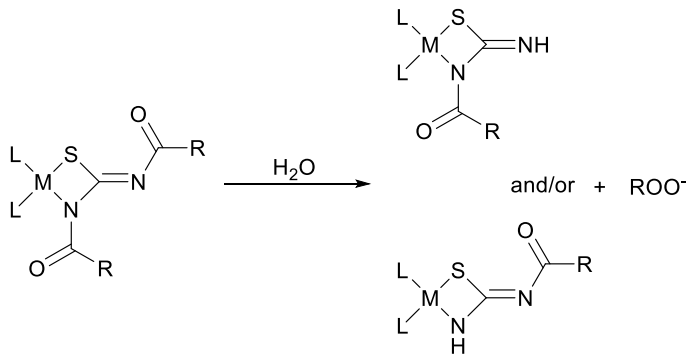

Figure 5.4: Hydrolysis of the complexes prepared in this study to the mono-acylated analogue complex.

Following the methods outlined for complexes **5a**–**5c** (*vide supra*), further reactions of ligand **DA-L2** were conducted with the precursor complexes $[PtCl_2(dppe)]$ (dppe = $Ph_2PCH_2CH_2PPh_2$), $[PdCl_2(phen)]$ (phen = 1,10-phenanthroline), and $[AuCl_2(anp)]$ (anp = cyclometallated 2-anilinopyridyl). The structures of the resulting complexes, **5d**, **5e**, and **5f**, are shown in Figure 5.5. Additionally, chlorido complexes **5g** and **5h** were synthesized from $[PdCl_2(COD)]$ and $[PtCl_2(COD)]$ (COD = 1,5-cyclooctadiene) in methanol with a few drops of pyridine. Complexes **5d**, **5e** and **5f** were readily identified using ESI-MS(+) as their pseudomolecular $[M + H]^+$ ions. Complexes **5e** and **5f** were also identified by $[2M + Na]^+$ sodium adduct ions. The chlorido complexes **5g** and **5h** were identified by their distinctive $[M - Cl + H]^+$ ions, which is characteristic of similar chlorido containing complexes (Chapter 3).

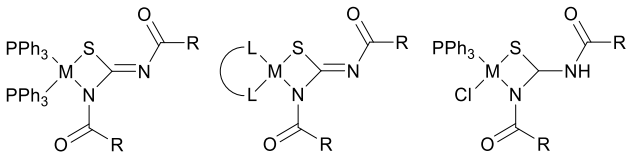

5a-5c **5d-5f** **5g 5h**

Complex	M	L or L-L	R
5a	Pt	PPh_3	Me
5b	Pt	PPh_3	Et
5c	Pt	PPh_3	Ph
5d	Pt	dppe	Et
5e	Pd	phen	Et
5f	Au	anp	Et
5g	Pd	PPh_3/Cl	Et
5h	Pt	PPh_3/Cl	Et

Figure 5.5: Structures of the diacylthiourea complexes of symmetric diacylthioureas ligands prepared in this study.

Previously, in Chapter 2, the reactions between [$PtCl_2$(COD)], triphenylphosphine and sulfonylthiourea ligands in the presence of pyridine produced the mixed ligand complexes of the type [Pt{L}(Py)(PPh_3)] (Py = pyridine, L = dianionic sulfonylthiourea). Interestingly, analogous reactions with diacylthiourea ligands produced only the chlorido complex. Attempts to prepare mixed ligand complexes of the type [Pt{L}(Py)(PPh_3)] with increasing volumes of pyridine (up to 2 mL) were unsuccessful, indicating that in this case, the pyridine is not sufficiently basic to form the dianion of the diacylthiourea ligand. Moreover, it may suggest pyridine as a good base for the selective mono-deprotonation of diacylthiourea.

Because of the absence of phosphorus nuclei in the ancillary ligands in complexes **5e** and **5f**, preventing analysis by ^{31}P NMR spectroscopy, $^{13}C\{^{1}H\}$ NMR spectra were recorded for these complexes. Both complexes displayed resonances in the aromatic range characteristic of their respective ancillary ligands (1,10-phenanthroline and 2-anilinopyridyl). Two pairs of resonances, corresponding to the CH_3 and CH_2 carbon environments of the ethyl group on the diacylthiourea ligand, were observed between 33.7 and 34.5 ppm for CH_2 and between 9.1 and 10.5 ppm for CH_3. These resonances appear slightly downfield compared to the chemical shifts of the free ligand. More pronounced downfield shifts are noted for the thiourea C=S and acyl C=O carbons (Figure 5.6). For instance, the C=S resonance, located at 177.3 ppm in the free ligand, shifts to 185.9 ppm in complex **5e** and 187.2 ppm in complex **5f**. Additionally, the acyl C=O resonance in the free ligand, originally at 173.6 ppm, splits into two distinct peaks upon coordination. The acyl carbon atom attached to the coordinating nitrogen (M–N–C=O) appears at 181.4 ppm for complex **5e** and 174.0 ppm for complex **5f**. This substantial shift relative to the free ligand is likely because of its close proximity to the S,N-acyl coordination sphere. The second acyl resonance for the non-coordinating thiourea nitrogen shows a smaller shift relative to that of the free ligand, at approximately 173 ppm for **5e** and a slight upfield shift to 174 ppm for **5f**. Similar downfield shifts have been previously observed for mono-acylated thiourea complexes, which are attributed to reduced π-electron delocalization characteristic of the S,N metallocycle.[19]

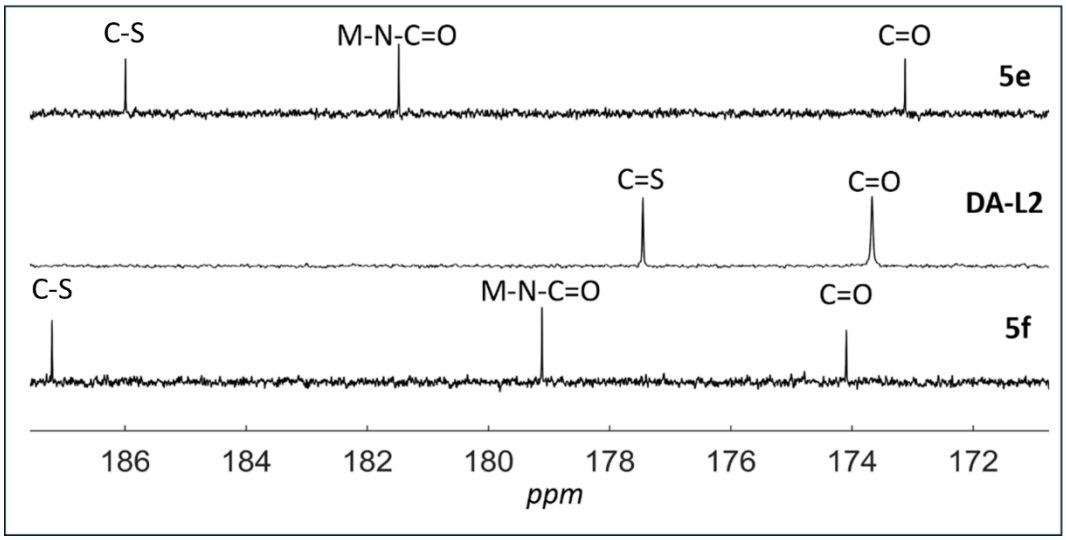

*Figure 5.6: ^{13}C NMR comparison of the thiourea and acyl carbon atoms of complexes **5e**, **5f** and ligand **DA-L2**. Data are scaled for clarity. $CDCl_3$ at 25°C.*

Analogous shifts in resonance are also seen in the ^{1}H NMR spectra, most notably in the ethyl-substituted complexes of ligand **DA-L2**. For example, among the two CH_2-N quadruplet resonances, one resonance is notably downfield relative to the free ligand, presumably because of its proximity to the coordination sphere while the shift of the second CH_2-N quadruplet resonance remains relatively less pronounced.

5.1.2 X-ray molecular structure determination and theoretical investigations

Preparations of the diacylthiourea molecules **DA-L1** and **DA-L2** produced small to medium sized yellow needle crystals upon cooling of the anhydride reaction mixture. While diacylthiourea ligands were first reported in 1915, crystal structures of only the dimethyl[20] and diphenyl[21] diacylated thiourea molecules have been reported thus far. In this regard, the molecular structure of the diethyl diacylated thiourea **DA-L2** was determined (Figure 5.7). Crystallographic details and a table of selected bond lengths are included in Appendix 1. The central thiourea carbon atom adopts the standard trigonal planar geometry with S1-C1, C1-N1 and C1-N2 bond lengths of 1.652(2), 1.382(3) and 1.370(2) Å. The spatial arrangement of the molecule is defined by two intramolecular non-covalent interactions; a hydrogen bond between O1 and the hydrogen of N2, forming a 6-membered ring motif, and a chalcogen bond between S1 and O1, forming a crescent-like arrangement of S1-C1-N1-C2-O1. Both interactions result in a nearly planar geometry of the molecule. Intramolecular hydrogen bonding of this type is commonly observed in acylthiourea molecules.[22, 23] Because the hydrogen bond between the thiourea N−H and the amidic O donor atom of the acyl group is relatively strong, chalcogen σ-hole interactions in acylthiourea lone ligands are typically absent.

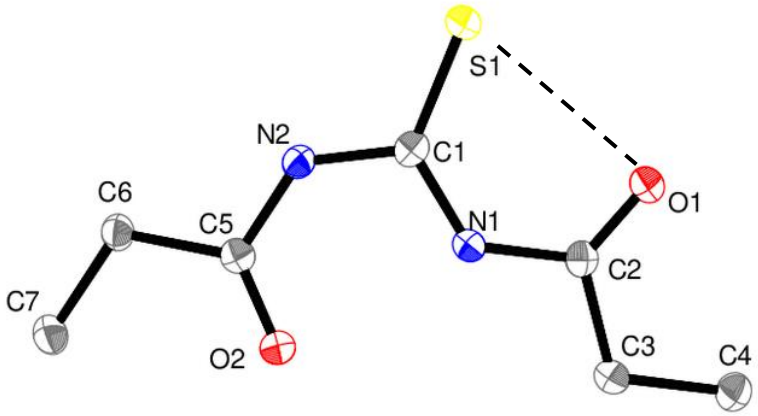

*Figure 5.7: Molecular structure of ligand **DA-L2**. Hydrogen atoms are omitted for clarity. Ellipsoids are shown at the 50% probability level*

To investigate the non-covalent interactions governing the spatial arrangement of the molecular structure of **DA-L2**, the NCI index developed by Johnson and co-workers was employed.[24] This method was used to analyse the chalcogen bond between the thiourea sulfur and acyl oxygen, as well as the hydrogen bond between the thiourea N–H group and the amidic oxygen donor atom of the acyl group, following the method outlined in Chapter 2. The resulting plot of the calculated reduced density gradient versus the electron density $\rho(r)$, oriented by the sign of the second eigenvalue (λ_2) is shown in Figure 5.8 along with 3D isosurfaces of the reduced density gradient colourized by sign(λ_2)ρ which are shown on a geometry optimized structure of the ligand. The RDG plot reveals two distinct troughs in the negative range, with sign(λ_2)ρ values of approximately -0.04 and -0.015 atomic units (a.u.). Additionally, positive ring critical points, indicative of steric repulsion from ring-like structural features are also observed. The magnitude of sign(λ_2)ρ provides useful insight into the type of interaction. In this regard, the trough at ~-0.015 corresponds to a chalcogen bond interaction, as established by comparison with previous calculations in Chapters 2-4, while the more negative trough at ~-0.04 aligns with values commonly attributed to hydrogen bonds.[25, 26] The positioning of these isosurfaces on the structure of **DA-L2** further supports their characterization and highlights the directional nature of these interactions. The presence of the chalcogen interaction is notable, as it

typically occurs when the sulfur atom is polarized by either coordination to a metal centre[27] or by the presence of nearby electron withdrawing groups.[28]

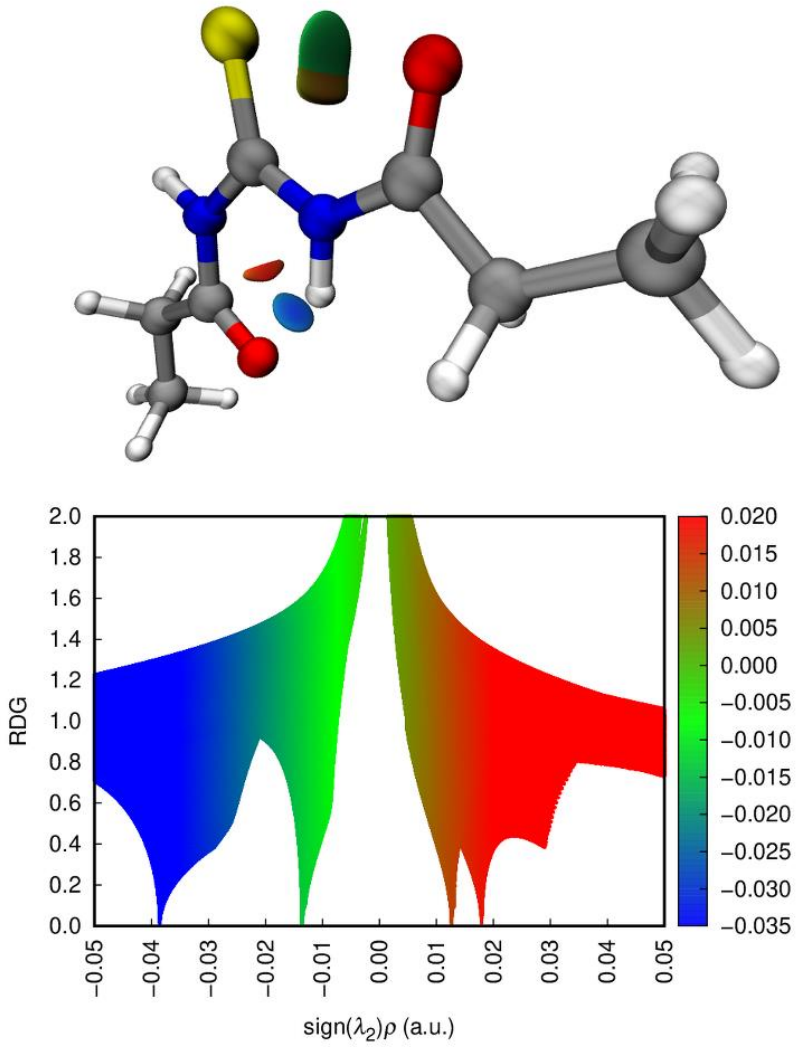

*Figure 5.8: Plot of RDG verses sign(λ_2)ρ for **DA-L2** showing troughs related to chalcogen and hydrogen bonding interactions and NCI isosurfaces using a blue-green-red colour scale. Isovalue = 0.5 for clarity.*

To definitively characterize the structure and coordination mode of the complexes prepared in this study, the molecular structures of complexes **5a**, **5b**, **5f**, **5g**, and **5h** were determined by single crystal X-ray diffraction. All complexes were shown to form a four-membered metallocycle through coordination to the thiourea sulfur and a nitrogen atoms. The metallacyclic bond lengths of the complexes are similar, averaging 2.304 (M-S1), 1.748 (S1-C1), 1.363 (C1-N) and 2.108 Å (M-N). These results are in agreement with literature values for similar square-planar

complexes with S,N bidentate acylthiourea ligands[29, 30] as well as with the S,N chelated molecular structures reported in Chapters 2-4. The molecular structures of complexes **5a** (Figure 5.9) and **5b** (Figure 5.10) are similar, both featuring bis(PPh_3) ancillary ligands. In contrast, complex **5f** (Figure 5.11) incorporates a bidentate, cyclometallated 2-anilinopyridyl ligand, which coordinates *via* the nitrogen atom and a ortho-carbon atom from the adjacent ring. The square-planar geometry of these complexes is slightly distorted, with the relatively small S-M-N bite angle (~69°) contrasting with the larger P-Pt-P and C-Au-N angles, which are approximately 99° and 87°, respectively.

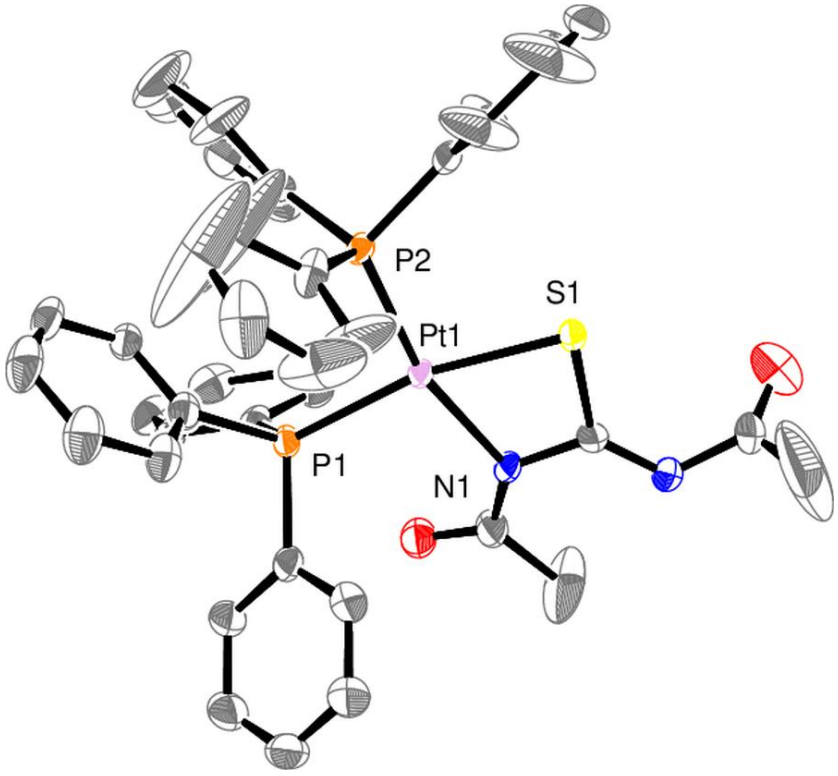

*Figure 5.9: Molecular structure of the complex [Pt{$(CH_3CON)_2CS$}$(PPh_3)_2$] **5a** showing a partial atom numbering scheme. Hydrogen atoms and a molecule of dichloromethane of crystallization are omitted for clarity and ellipsoids are shown at the 50% probability level.*

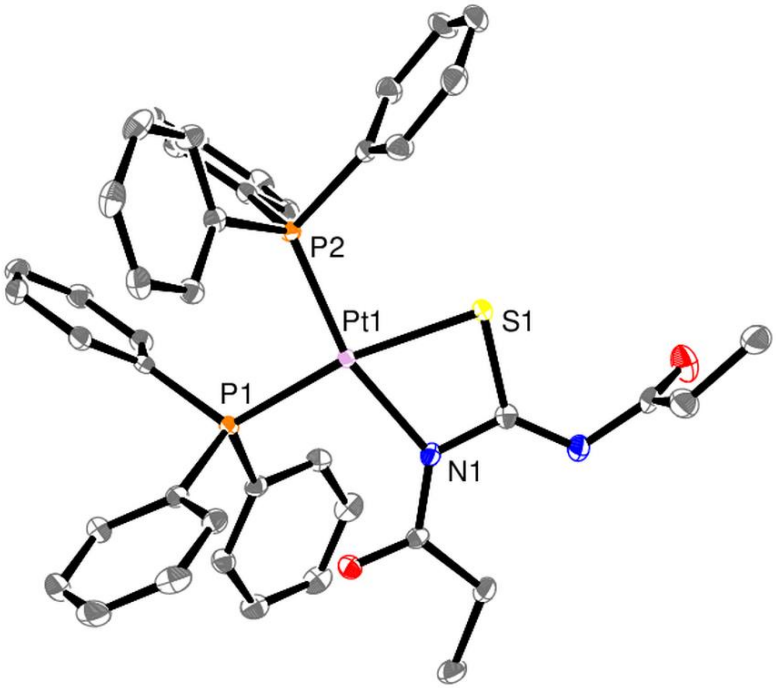

Figure 5.10: Molecular structure of the complex [Pt{(CH₃CH₂CON)₂CS}(PPh₃)₂] ***5b*** *showing a partial atom numbering scheme. Hydrogen atoms and a molecule of dichloromethane of crystallization are omitted for clarity and ellipsoids are shown at the 50% probability level.*

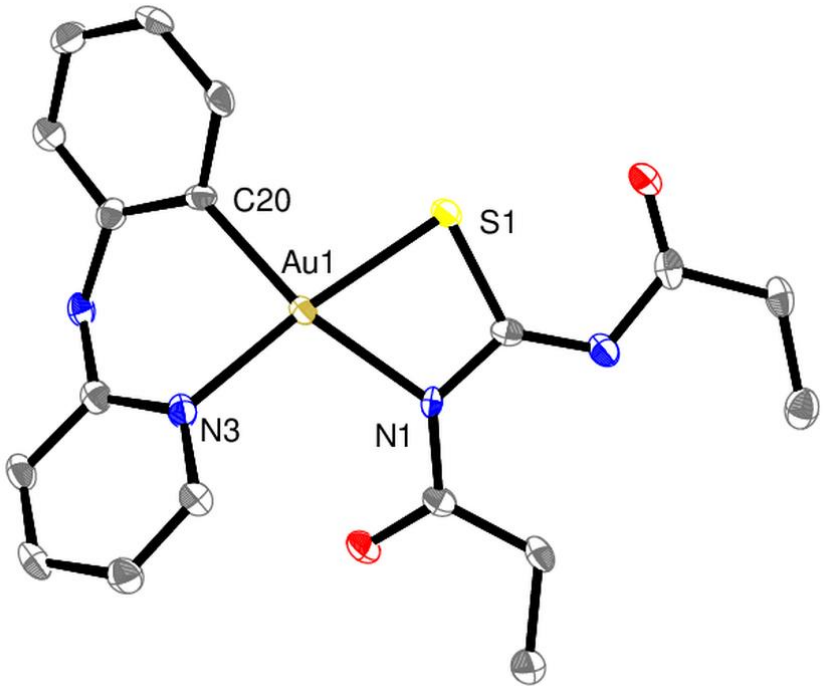

Figure 5.11: Molecular structure of the complex [Au{(CH₃CH₃CONH)₂CS}(anp)] ***5f*** *showing a partial atom numbering scheme. Hydrogen atoms and a molecule of dichloromethane of crystallization are omitted for clarity and ellipsoids are shown at the 50% probability level.*

The arrangement of the diacylthiourea ligand differs notably between the bis(PPh_3) platinum(II) complexes **5a** and **5b** and the gold(III) complex **5f**. In complexes **5a** and **5b**, the non-coordinating N-acyl group is positioned perpendicular to the square-planar coordination plane, whereas in complex **5f**, is coplanar, creating a crescent-like arrangement of S-C-N-C-O, similar to the structure of the free ligand **DA-L2**. This arrangement in **5f** suggests the presence of a potential chalcogen σ-hole interaction between the thiourea sulfur and acyl oxygen atoms. The crystal packing environments provide a likely explanation for these structural differences. In complexes **5a** and **5b**, the bulky triphenylphosphine ancillary ligands of adjacent molecules of the complex impose steric constraints that hinder the planar arrangement observed in complex **5f**. As a result, the formation of intramolecular chalcogen σ-hole interactions, which are often cited as the reason for the planar arrangement in similar S,N-bidentate complexes containing dianionic sulfonylthiourea and phosphorylthiourea ligands, is prevented. NCI interactions in transition metal complexes are of particular interest because of their importance in dictating the spatial arrangement of the structure and by extension processes such as in catalysis[31, 32] and pharmacology.[33, 34] To investigate the presence of the chalcogen bond, RDG plots were made following the method used for the ligand **DA-L2** (*vide supra*). Thus, the RDG was calculated between the thiourea sulfur and acyl oxygen atom and plotted against sign(λ_2)ρ. The corresponding plots and isosurfaces mapped onto a geometry optimized structure of **5f** is shown in Figure 5.12.

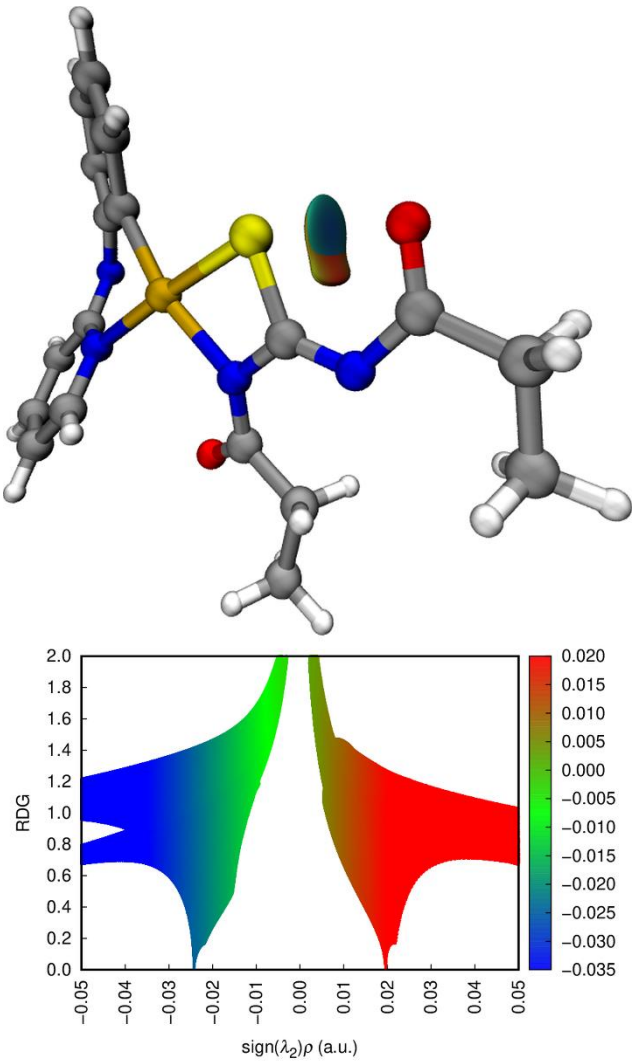

*Figure 5.12: Plot of RDG verses sign(λ_2)ρ for **5f** showing troughs related to chalcogen interactions and NCI isosurfaces using a blue-green-red colour scale. Isovalue = 0.5 for clarity.*

The plot of RDG verses sign(λ_2)ρ reveals a distinctive trough with a sign(λ_2)ρ value of ~-0.025 a.u., confirming the presence of the chalcogen interaction at this position. Notably, the position of the trough on sign(λ_2)ρ is more negative than the ligand **DA-L2** (~-0.015 a.u.). While the value of sign(λ_2)ρ is not directly proportional to the strength of the interaction, stronger interactions typically have more negative values.[24, 35, 36] Therefore, it can be surmised that the chalcogen interaction in complex **5f** is more attractive, *i.e.* stronger, than that of **DA-L2**. This difference is not surprising considering the bonding of the thiourea sulfur atom to a metal centre increases the size of the σ-hole opposite to the S-M bond, therefore increasing the contribution from the Lewis base electron donor and subsequently

increasing the strength of the interaction.[27, 37] It is also noteworthy that, because of the greater polarization of the sulfur atom by gold(III) compared to platinum(II), the position of the trough on sign(λ_2)ρ is distinctly more negative than related chalcogen bond interactions in bis(phosphine) platinum(II) complexes of related sulfonylthiourea complexes which typically have values of around -0.015 (a.u.). This is likely a result of the comparatively high electronegativity of gold.

In addition to the intramolecular chalcogen σ-hole interactions observed in complex **5f**, the crystal packing environment reveals an intermolecular hydrogen bond between the N-H donor of the anp ligand and the C=O acceptor of the acyl group attached to the coordinating nitrogen of a neighbouring molecule. This interaction creates a hydrogen-bond-bridged dimer between two molecules of **5f** (Figure 5.13).

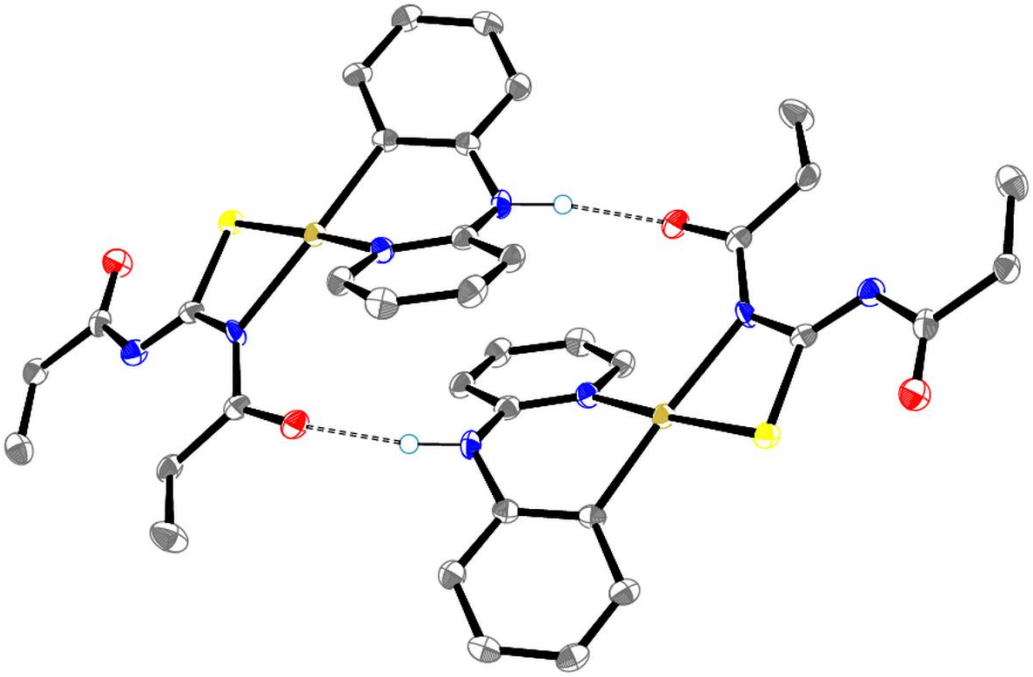

Figure 5.13: Dimeric hydrogen bond bridged dimer of two molecules of [Au{($CH_3CH_3CONH)_2CS$}(anp)] in the molecular structure. Hydrogen atoms, except for the N-H of the anp ligand, are omitted for clarity and ellipsoids are shown at the 50% probability level.

The bonding nature of the gold dimer was investigated using the NCI index and by energy decomposition calculations (ALMO-EDA). The latter has been shown to be a useful tool for unravelling the nature of intermolecular interactions by separating the calculated total interaction energy into separate electrostatic, Pauli repulsion, dispersion, polarization and charge transfer component energies.[38, 39] These separate energy terms describe not only the nature of the interaction in meaningful energy terms, but can also be used to infer the type of interactions occurring. Prior to theoretical analysis of the gold dimer, the hydrogen atoms of the molecular pair were normalized to 1.015 Å to provide the more accurate positioning. The two N-H hydrogens of the 2-anilinopyridyl groups in the dimer were optimized in the gas phase with the remaining atoms fixed in position to provide the most accurate placement of the hydrogen atoms. NCI analysis was then conducted between the two intermolecular N-H···O=C interactions and the RDG isosurfaces colourized by sign(λ_2)ρ were modelled onto the dimer (Figure 5.14). With the presence of the hydrogen bonds reinforced by NCI analysis, the interaction energy of the dimer was calculated using the ALMO-EDA method of Head-Gordon and co-workers.[38, 39] The total energy of the dimer interaction was -149 kJ mol^{-1} which was primarily composed of dispersion interactions (-98 kJ mol^{-1}) followed by non-trivial contributions from polarization (-38 kJ mol^{-1}) and charge transfer terms (-23 kJ mol^{-1}). Interestingly, while the polarization, charge transfer and a portion of the dispersion interactions likely arise and allude to the hydrogen bonds between the individual complexes, the large contribution to the total interaction energy by the dispersion term indicates that a non-insignificant contribution from a series of weaker dispersion interactions between the dimer are present between the molecules of the complex.

The molecular structures of complexes **5a**, **5b**, and **5f** share some notable features, including a distinctively short bond distance between the thiourea carbon and the non-coordinating acyl nitrogen (C1–N2), averaging 1.283 Å. This short bond length suggests double bond character, confirming the dianionic nature of the ligands in these complexes. In contrast, the C1–N2 bond distances in the chlorido complexes **5g** (Figure 5.15) and **5h** (Figure 5.16) are slightly longer, at 1.352(3) and 1.347(3) Å, respectively, indicating that in these structures, the ligand is bound as a monoanion.

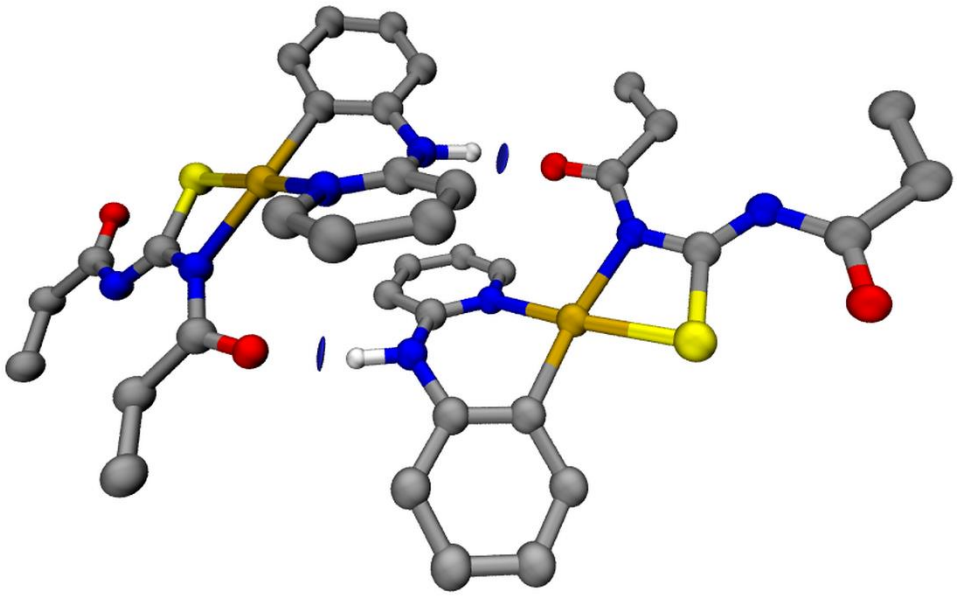

*Figure 5.14: Representation of dimeric hydrogen bond bridged dimer of **5f** with hydrogen atoms, except for the N-H of the anp ligand omitted for clarity. Isosurface = 0.4.*

The molecular structures of complexes **5g** and **5h** are nearly identical, differing only in the metal centre (palladium(II) or platinum(II)), and exhibit similar features to the previously discussed structures. Both complexes adopt a slightly distorted square-planar geometry, with S–M–N and P–Pt–Cl angles of approximately 69° and 89°, respectively. In both cases, the arrangement around the metal centre is Cl *trans* to S and P *trans* to N. The spatial arrangement of the monoanionic diacylthiourea is defined by two intramolecular interactions: a σ-hole interaction between the thiourea sulfur atom and the non-coordinating acyl oxygen atom, as described above, and a hydrogen bond between the carbonyl oxygen atom of the coordinating acyl group and the N–H group of the non-coordinating acyl nitrogen, forming an N–H···O=C interaction. The resulting configuration is reminiscent of the lone ligand **DA-L2**.

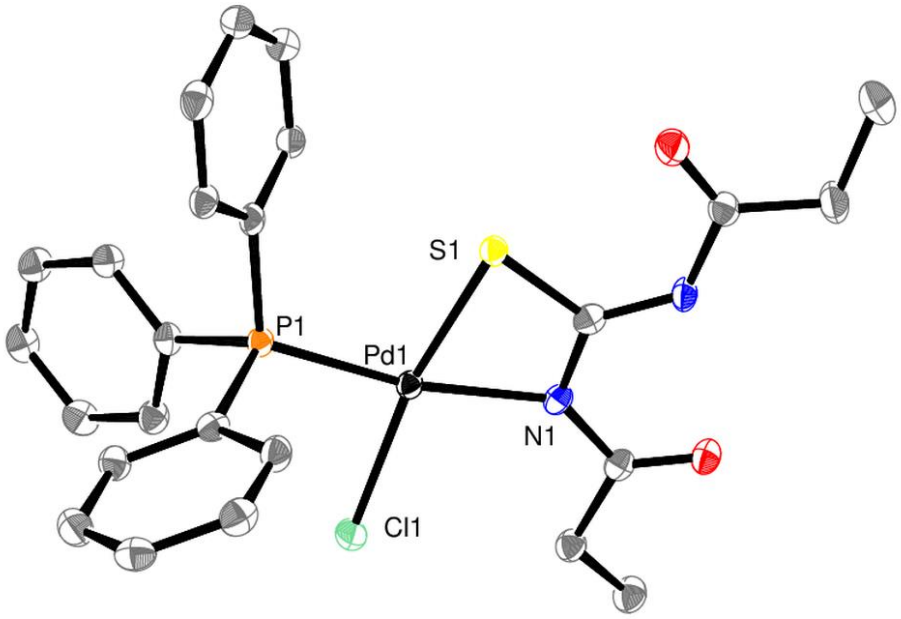

Figure 5.15: Molecular structure of the complex [Pd{(EtC(O)NC(S)NHC(O)Et}(PPh$_3$)Cl] ***5g*** *showing a partial atom numbering scheme. Hydrogen atoms and a molecule of dichloromethane of crystallization are omitted for clarity and ellipsoids are shown at the 50% probability level.*

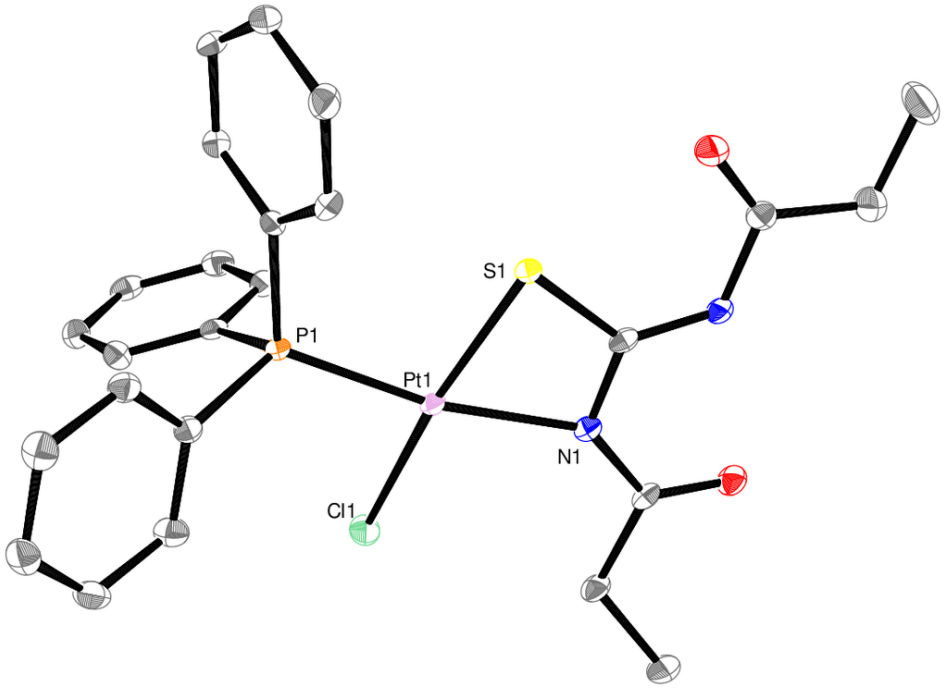

Figure 5.16: Molecular structure of the complex [Pt{(EtC(O)NC(S)NHC(O)Et}(PPh$_3$)Cl] ***5h*** *showing a partial atom numbering scheme. Hydrogen atoms and a molecule of dichloromethane of crystallization are omitted for clarity and ellipsoids are shown at the 50% probability level.*

NCI plots of the two interactions (Figure 5.17) reveal two distinct troughs relating to both the hydrogen bond (~-0.045) and the chalcogen bond (~-0.018). The values of sign(λ_2)ρ for both interactions are more negative than those observed for the free ligand, consistent with the polarization effects induced by coordination to the metal centre. Notably, the chalcogen interaction in complexes **5g** and **5h** is less negative than in the gold(III) complex **5f**, reflecting the weaker polarization of the sulfur atom by palladium(II) or platinum(II) compared to gold(III).

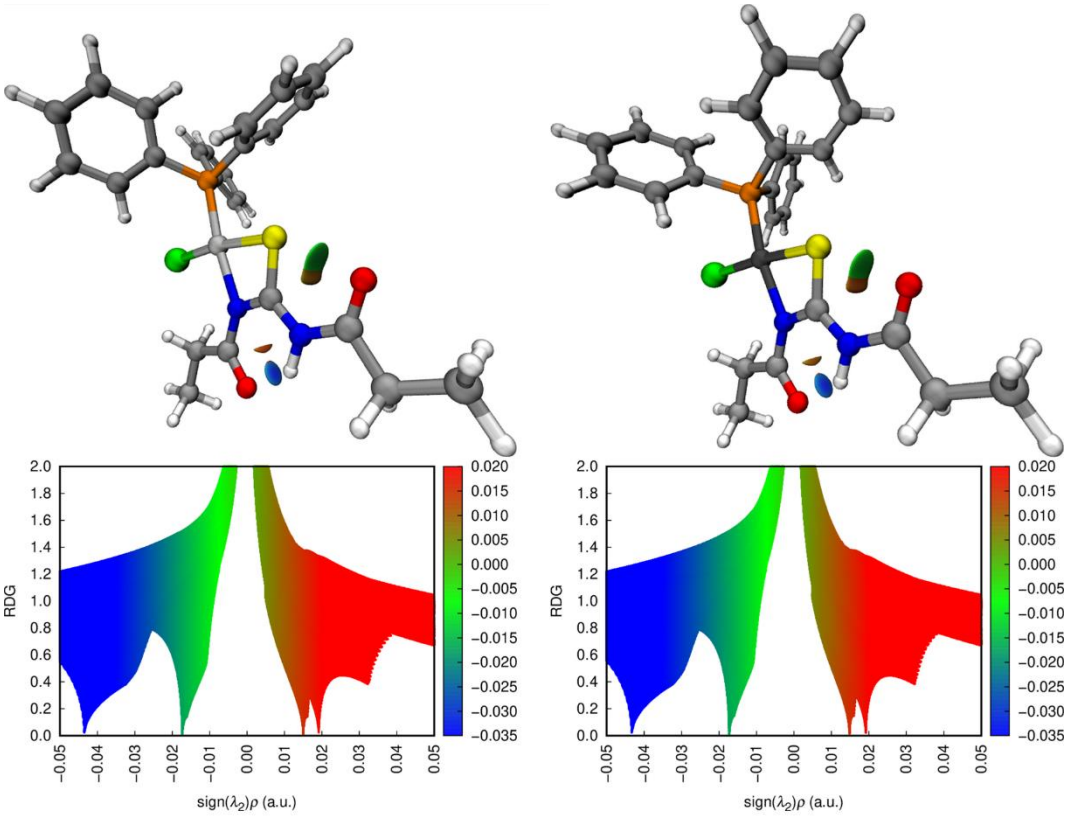

*Figure 5.17: Plot of RDG verses sign(λ_2)ρ for **5g** and **5h** showing troughs related to chalcogen and hydrogen bonding interactions and NCI isosurfaces using a blue-green-red colour scale. Isovalue = 0.5 for clarity.*

5.2 Conclusions

This work has demonstrated the straightforward and facile one-pot synthesis of symmetric diacylated thioureas and their use as both monoanionic and dianionic ligands towards platinum(II), palladium(II) and gold(III). Analysis by a combination of conventional and computational techniques, such as XRD, NMR and NCI revealed the ligands bind to the metal centre through the thiourea sulfur and nitrogen atoms forming four-membered metallocycles. Coordination in this mode is atypical for the closely related acylthiourea class of ligands. The difference in coordination may be a result of the importance of non-covalent interactions which were demonstrated to dictate both the arrangement of the ligand and complexes, as well the formation of intermolecular hydrogen bonded dimers. The results presented here highlight a potentially underexplored class of thiourea ligands and provides the groundwork for further avenues of research in this area.

5.3 Experimental

5.3.1 Materials

The following chemicals were used as supplied from commercial sources: Thiourea, acetic anhydride, benzoic anhydride, deuterated solvents, triphenylphosphine, pyridine, triethylamine (Sigma Aldrich) and propanoic anhydride (BDH). The complexes *cis*-[$PtCl_2(PPh_3)_2$] and *cis*-[$PtCl_2$(dppe)] were prepared by ligand substitution of the cyclo-octa-1,5-diene (COD) ligand of [$PtCl_2$(COD)][40] with the stoichiometric quantity of triphenylphosphine or 1,2-bis(diphenylphosphino)ethane. The complexes [$PdCl_2$(phen)] and [$AuCl_2$(anp)] were prepared by literature procedures or minor variations thereof and used as supplied by W Henderson, University of Waikato.[41, 42]

5.3.2 Instrumentation

^{31}P (243 MHz), ^{1}H (600 MHz) and $^{13}C\{^{1}H\}$ (151 MHz) NMR spectra were recorded in $CDCl_3$ at 25°C using a 600 MHz Jeol ECZR NMR spectrometer. Spectra were processed using the Jeol Delta software. ESI mass spectra were recorded in methanol using a Bruker Daltonics MicrOTOF electrospray ionization mass spectrometer. Sodium formate solution was used for calibration. Spectra were recorded with a Capillary Exit voltage of 90 V and a *Skimmer 1* voltage of 30 V unless otherwise stated. Elemental analysis was performed by the Chemical Analysis Facility, Department of Molecular Sciences, Macquarie University, Sydney, Australia. Complexes **5c** and **5e** contain slightly elevated values for carbon which were corelated to long sample storage times prior to analysis, for unknown reasons. Single crystal X-ray diffraction was carried out by the University of Auckland Microcharacterization Facility, Auckland, New Zealand.

5.3.3 Synthesis of symmetric methyl DA-L1 and ethyl DA-L2 diacylthiourea ligands

Thiourea (4 g) was added to acetic or propanoic anhydride (50-60 mL, large excess) with light stirring. The reaction mixture was under reflux conditions to approximately 80-100°C, during which time the thiourea dissolves completely and the colourless solution took on a yellow hue. The solution was kept at temperature for approximately 40 minutes until which point a deep yellow colour had developed. The solution was removed from heat and let to cool to room temperature until the needle-like crystals appeared which were collected by vacuum filtration and washed with 2 x 20 mL additions of the respective anhydride. The filtrate was evaporated slowly in air to yield additional crystalized product.

$(CH_3CONH)_2C(S)$ **DA-L1** (8.42 g, 77 %) ESI-MS(+): Capillary exit voltage 90 V, *m/z* $[M + Na]^+$ 183.0881, $[2M + Na]^+$ 343.1767. NMR ($CDCl_3$): ^{13}C, δ 177.7 (C=S), 170.3 (C=O), 25.6 (CH_3), ^{1}H, δ 2.29 (s, CH_3).

$(CH_3CH_2CONH)_2C(S)$ **DA-L2** (9.89 g, 80 %) ESI-MS(+): Capillary exit voltage 90 V, *m/z* $[M + H]^+$ 189.1224, $[M + Na]^+$ 211.1122, $[2M + Na]^+$ 399.3881. NMR ($CDCl_3$): ^{13}C, δ 177.4 (C=S), 173.6 (C=O), 31.5 (CH_2) 8.54 (CH_3), ^1H, δ 2.50 (q, ^3J = 7 Hz, CH_2, 2H). 1.20 (t, ^3J = 7 Hz, CH_3, 3H).

5.3.4 Synthesis of symmetric dibenzoyl diacylthiourea ligand

Thiourea (4 g) and benzoic anhydride (30 g, 2.5 molar equivalents) were combined and heated gently until the benzoic anhydride melted completely and the thiourea started to dissolve (approximately 40-50 °C). The temperature of the mixture was raised to approximately 80-100°C for 40 minutes until the solution had a dark yellow hue, at which point, the solution cooled to room temperature to solidify. The reaction mass was recrystalized three consecutive times in 100 % ethanol until a yellow solid remained. $(PhCONH)_2C(S)$ **DA-L3** (4.22 g, 28 %) ESI-MS(+): Capillary exit voltage 90 V, *m/z* $[M + Na]^+$ 307.0754, $[2M + Na]^+$ 591.1651. NMR ($CDCl_3$ 151 MHz) $^{13}C\{^1H\}$, δ 182.4 (C=S), 166.6 (C=O), 133.8 (C-N), 131.6 (CH), 129.2 (CH), 127.7 (CH), ^1H, δ 8.2 – 7.4 (aromatic).

5.3.5 General synthesis of the complexes with diacylthiourea dianionic ligands

Equimolar quantities of the ligand and metal starting material were suspended in MeOH (30 mL) with stirring. The mixture was brought to reflux followed by the addition of 4 drops of a 0.5 molar aqueous solution of NaOH. The solutions were refluxed for a further 5 minutes followed by removal of solvent by reduced pressure. The solid residues, containing the complex, sodium chloride and sodium hydroxide were redissolved in CH_2Cl_2 and filtered through cotton and 1 cm of silica. The filtrate containing the complex was evaporated to dryness by reduced pressure to yield the target complex which was dried further under vacuum. Details pertaining to each compound are given in Table 5.1.

5.3.6 General synthesis of the complexes with diacylthiourea monoanionic ligands

The complex [M(COD)Cl_2] (M = Pt or Pd) in methanol (20 mL) was brought to reflux. Pyridine (5 drops, excess) was added followed by equimolar amounts of triphenylphosphine and the diacylthiourea ligand in subsequent addition. The desired product precipitated immediately upon addition. The mixture was refluxed for a further 2-3 minutes and cooled to room temperature. The solid product was collected by vacuum filtration, washed with 1 x 10 mL increments of water, ice cold methanol and petroleum spirts and dried under vacuum. Details pertaining to each compound are given in Table 5.1.

Table 5.1: Synthesis details for the prepared diacylthiourea complexes.

	Starting metal complex			PPh_3	Thiourea		Yield	
Product		mg	mmol	mg	mg	mmol	mg	%
5a	*cis*-[$PtCl_2(PPh_3)_2$]	160	0.203	-	32	0.203	116	65
5b	*cis*-[$PtCl_2(PPh_3)_2$]	165	0.209	-	39	0.209	146	77
5c	*cis*-[$PtCl_2(PPh_3)_2$]	170	0.215	-	61	0.215	142	66
5d	[$PtCl_2$(dppe)]	152	0.229	-	43	0.229	116	63
5e	[$PdCl_2$(phen)]	181	0.507	-	95	0.507	97	41
5f	[$AuCl_2$(anp)]	340	0.794	-	149	0.794	299	79
5g	[$PdCl_2$(COD)]	203	0.711	186.5	133.7	0.711	334	80
5h	[$PtCl_2$(COD)]	200	0.534	140	100.6	0.534	278	77

[Pt{$(CH_3CON)_2CS$}$(PPh_3)_2$] **5a**

Off-white solid. Elemental analysis: Found (%) C 55.8; H 4.1; N 3.3; S 3.5. Calculated for $C_{41}H_{36}N_2O_2P_2PtS$ (%) C 56.1; H 4.1; N 3.2; S 3.6. ESI-MS(+): Capillary exit voltage 90 V, *m/z* $[M + H]^+$ 878.6225, $[(M - COCH_3) + H]^+$ 835.4705, $[(M - PPh_3) + H]^+$ 616.1955. NMR ($CDCl_3$ 243 MHz): $^{31}P\{^1H\}$, δ 18.0 [d, $^1J_{PtP}$ 3126 Hz, $^2J_{PP}$ 21 Hz], 12.4 [d, $^1J_{PtP}$ 3371 Hz, $^2J_{PP}$ 21 Hz]; ($CDCl_3$ 600 MHz) ^1H 7.50 – 7.10 (m, aromatic), 2.12 (s, CH_3, 3H), 2.05 (s, CH_3, 3H).

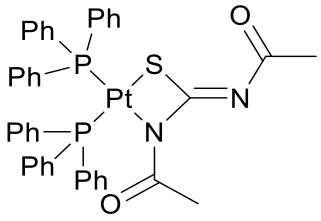

[Pt{$(CH_3CH_2CON)_2CS$}$(PPh_3)_2$] **5b**

Off-white solid. Elemental analysis: Found (%) C 57.0; H 4.5; N 2.3; S 2.82. Calculated for $C_{43}H_{40}N_2O_2P_2PtS$ (%) C 57.0 H 4.4; N 3.1; S 3.5. ESI-MS(+): Capillary exit voltage 90 V, *m/z* $[M + H]^+$ 906.6736. NMR ($CDCl_3$ 243 MHz): $^{31}P\{^1H\}$, δ 18.3 [d, $^1J_{PtP}$ 3127 Hz, $^2J_{PP}$ 21 Hz], 12.6 [d, $^1J_{PtP}$ 3372 Hz, $^2J_{PP}$ 21 Hz]; ($CDCl_3$ 600 MHz) ^1H 7.50 – 7.10 (m, aromatic), 2.55 (q, J = 8 Hz, CH_2, 2H), 2.39 (q, J = 8 Hz, CH_2, 2H), 2.07 (t, J = 8 Hz, CH_3, 3H), 0.53 (t, J = 8 Hz, CH_3, 3H).

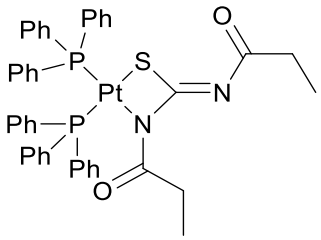

[Pt{$(PhCON)_2$}$(PPh_3)_2$] **5c**

Off-white solid. Elemental analysis: Found (%) C 57.7; H 4.0; N 3.1; S 3.6. Calculated for $C_{51}H_{40}N_2O_2P_2PtS$ (%) C 61.1; H 4.0; N 2.8; S 3.2. ESI-MS(+): Capillary exit voltage 90 V, *m/z* $[M + H]^+$ 1001.0858, $[(M - COCH_3) + H]^+$ 898.0581. NMR ($CDCl_3$ 243 MHz): $^{31}P\{^1H\}$, δ 17.9 [d, $^1J_{PtP}$ 2991 Hz, $^2J_{PP}$ 21 Hz], 12.7 [d, $^1J_{PtP}$ 3475 Hz, $^2J_{PP}$ 21 Hz]; ($CDCl_3$ 600 MHz) ^1H 7.7 – 6.9 (m, aromatic).

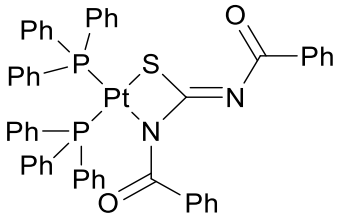

[Pt{$(CH_3CH_2CON)_2CS$}(dppe)] **5d**

White solid. Elemental analysis: Found (%) C 50.9; H 4.4; N 3.5; S 3.6. Calculated for $C_{33}H_{34}N_2O_2P_2PtS$ (%) C 50.8; H 4.4; N 3.6; S 4.1. ESI-MS(+): Capillary exit voltage 90 V, *m/z* $[M + H]^+$ 780.0374, $[(M - COCH_3) + H]^+$ 724.0067, $[M + Na]^+$ 802.0212. NMR ($CDCl_3$ 243 MHz): $^{31}P\{^1H\}$, δ 45.3 [d, $^1J_{PtP}$ 3220 Hz, $^2J_{PP}$ 9 Hz], 40.0 [d, $^1J_{PtP}$ 3171 Hz, $^2J_{PP}$ 9 Hz]; ($CDCl_3$ 243 MHz) ^1H 7.90 – 7.30 (m, aromatic), 2.71 (q, J = 8 Hz, CH_2, 2H), 2.50 (q, J = 8 Hz, CH_2, 2H), 2.20 (m, PCH_2CH_2P, 4H), 1.13 (t, J = 8 Hz, CH_3, 3H), 0.76 (t, J = 8 Hz, CH_3, 3H).

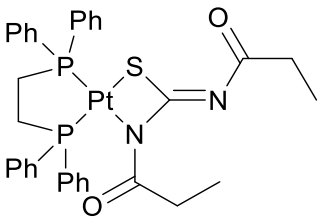

[Pd{($CH_3CH_2CON)_2CS$}(Phen)] **5e**

Yellow solid. Elemental analysis: Found (%) C 47.3; H 3.7; N 11.7; S 6.7. Calculated for $C_{19}H_{18}N_4O_2PdS$ (%) C 48.2; H 3.8; N 11.8; S 6.7. ESI-MS(+): Capillary exit voltage 90 V, *m/z* $[M + H]^+$ 472.8932, $[2M + Na]^+$ 968.7931, $[3M + Na]^+$ 1439.6990. NMR ($CDCl_3$ 151 MHz): ^{13}C 185.9 (C=S), 181.4 (C=O) 173.1 (C=O) 157.0 (aromatic-CH), 150.9 (aromatic-CH), 146.7 (aromatic-CH), 145.6 (aromatic-CH), 138.7 (aromatic-CH), 137.9 (aromatic-CH), 130.3 (aromatic-CH), 130.0 (aromatic-CH), 127.9 (aromatic-CH), 126.6 (aromatic-CH), 126.2 (aromatic-CH), 125.2 (aromatic-CH), 33.9 (CH_2), 33.8 (CH_2), 10.2 (CH_3), 9.5 (CH_3); ($CDCl_3$ 600 MHz) ^1H 10.3 (m, aromatic, 1H), 8.50 – 7.50 (m, aromatic, 7H), 3.00 (q, J = 8 Hz, CH_2, 2H), 2.48 (q, J = 8 Hz, CH_2, 2H), 1.16 (overlapping t, CH_3, 6H).

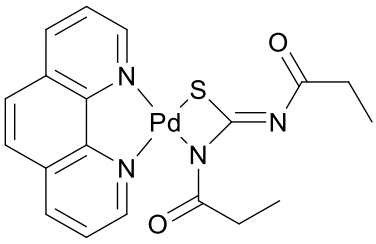

[Au{($CH_3CH_2CON)_2CS$}(anp)] **5f**

Yellow solid. Elemental analysis: Found (%) C 40.4; H 3.5; N 10.1; S 5.8. Calculated for $C_{18}H_{19}AuN_4O_2S$ (%) C 39.1; H 3.4; N 10.1; S 6.9. ESI-MS(+): Capillary exit voltage 90 V, *m/z* $[M + H]^+$ 552.9624, $[2M + Na]^+$ 1126.9245. NMR ($CDCl_3$ 151 MHz): ^{13}C 187.2 (C=S), 179.1 (C=O) 174.0 (C=O), 150.3 (aromatic-CH), 148.2 (aromatic-CH), 141.1 (aromatic-CH), 134.6 (aromatic-CH), 134.3 (aromatic-CH), 129.9 (aromatic-CH), 123.8 (aromatic-CH), 117.3 (aromatic-CH), 116.0 (aromatic-CH), 115.1 (aromatic-CH), 114.1 (aromatic-CH), 34.3 (CH_2), 9.9 (CH_2), 9.3 (CH_3), 8.5 (CH_3); ($CDCl_3$ 600 MHz) ^1H 8.65 (bs, NH, 1H), 8.30 – 6.50 (m, aromatic, 8H), 3.15 (q, J = 8 Hz, CH_2, 2H), 1.32 (q, J = 8 Hz, CH_2, 2H), 1.22 (overlapping t, CH_3, 6H).

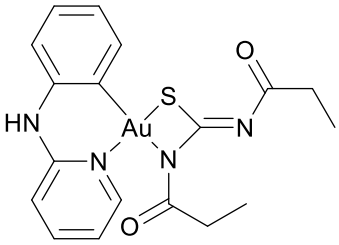

[Pd{(EtC(O)NC(S)NHC(O)Et}(PPh_3)Cl] **5g**

Orange solid. Elemental analysis: Found (%) C 51.2; H 4.6; N 4.6; S 5.2. Calculated for $C_{25}H_{25}ClN_2O_2PPdS$ (%) C 50.8; H 4.2; N 4.7; S 5.4. ESI-MS(+): Capillary exit voltage 150 V, *m/z* $[(M - Cl) + H]^+$ 555.1717. NMR ($CDCl_3$ 243 MHz): $^{31}P\{^1H\}$, δ 31.4 [s]; ($CDCl_3$ 600 MHz) ^1H 7.70 – 7.40 (m, aromatic), 2.81 (q, J = 8 Hz, CH_2, 2H), 2.36 (q, J = 8 Hz, CH_2, 2H), 1.13 (t, J = 8 Hz, CH_3, 3H), 1.06 (t, J = 8 Hz, CH_3, 3H).

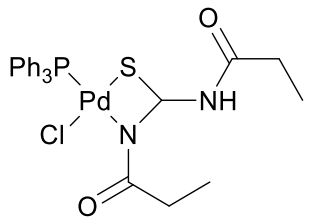

[Pt{(EtC(O)NC(S)NHC(O)Et}(PPh_3)Cl] **5h**

Yellow solid. Elemental analysis: Found (%) C 44.4; H 3.9; N 4.0; S 4.3. Calculated for $C_{25}H_{25}ClN_2O_2PPtS$ (%) C 44.2; H 3.7; N 4.1; S 4.7. ESI-MS(+): Capillary exit voltage 150 V, *m/z* $[(M - Cl) + H]^+$ 644.21651. NMR ($CDCl_3$ 243 MHz): $^{31}P\{^1H\}$, δ 3.39 [s, $^1J_{PtP}$ 3951 Hz]; ($CDCl_3$ 600 MHz) ^1H 7.70 – 7.30 (m, aromatic), 2.85 (q, J = 8 Hz, CH_2, 2H), 2.37 (q, J = 8 Hz, CH_2, 2H), 1.13 (t, J = 8 Hz, CH_3, 3H), 1.07 (t, J = 8 Hz, CH_3, 3H).

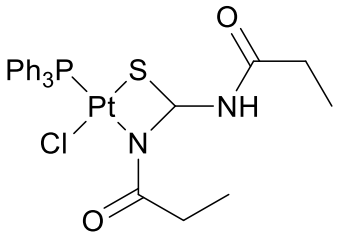

5.3.7 X-ray crystal structure determinations

Crystals of satisfactory quality for single crystal diffraction of **DA-L2** were grown by the slow cooling of the reaction mixture. Crystals of **5a**, **5b**, **5f**, **5g** and **5h** were grown by the diffusion of diethyl ether into a solution of CH_2Cl_2 containing the complex. Structures were solved using Olex2[43] with the Olex2.solve[44] structure solution program using Charge Flipping and refined with the Olex2.refine[44] refinement package using Gauss–Newton minimization. Crystal and refinement details are summarized in Appendix 1.

5.3.8 Theoretical investigations

Geometry optimization, single point, frequency and ALMO-EDA calculations were conducted using Q-chem software.[45] The mixed basis sets used were aug-cc-pV(D+d)Z for S and P, aug-cc-pVDZ for O, N and Cl, cc-pVDZ for C and H, LANL2DZ for Pt, Pd and Au atoms using the effective core potential. The ωB97M-V method was used for all systems. MultiWFN was used for the calculation of non-covalent interactions including the calculation of the reduced density gradient (RDG).[46] Gnuplot was used for the representation of the RDG plot.[47] Frequency calculations were conducted for all geometry optimized systems to ensure a minima, with the exception of complex **5a** because of computational constraints. The N-H hydrogen atoms of the gold(III) dimer were optimized with the remaining atoms fixed in position to remain as true to the solid state molecular structure as possible.

5.4 References

1. A. Rodger, K. K. Patel, K. J. Sanders, M. Datt, C. Sacht and M. J. Hannon, *Journal of the Chemical Society, Dalton Transactions*, 2002, 3656-3663.
2. H. Nkabyo, G. Bosman, R. Luckay and K. Koch, *Inorganica Chimica Acta*, 2020, **508**, 119644.
3. A. M. Plutin, R. Ramos, R. Mocelo, A. Alvarez, E. E. Castellano, M. R. Cominetti, K. M. Oliveira, T. D. de Oliveira, T. E. Silva and R. S. Correa, *Polyhedron*, 2020, **184**, 114543.
4. M. M. Sheeba, M. Muthu Tamizh, L. J. Farrugia, A. Endo and R. Karvembu, *Organometallics*, 2014, **33**, 540-550.
5. S. Swaminathan, P. Jerome, R. J. Deepak, R. Karvembu and T. H. Oh, *Coordination Chemistry Reviews*, 2024, **503**, 215620.
6. M. E. Uysal, U. Solmaz and H. Arslan, *Polyhedron*, 2024, **247**, 116707.
7. U. Solmaz, I. Gumus, M. K. Yilmaz, S. Ince and H. Arslan, *Applied Organometallic Chemistry*, 2021, **35**, e6348.
8. G. H. Ribeiro, A. R. Costa, A. R. de Souza, F. V. da Silva, F. T. Martins, A. M. Plutin and A. A. Batista, *Coordination Chemistry Reviews*, 2023, **488**, 215161.
9. S. Swaminathan, J. Haribabu, M. K. Mohamed Subarkhan, G. Manonmani, K. Senthilkumar, N. Balakrishnan, N. Bhuvanesh, C. Echeverria and R. Karvembu, *Organometallics*, 2022, **41**, 1621-1630.
10. D. Obradović, S. Nikolić, I. Milenković, M. Milenković, P. Jovanović, V. Savić, A. Roller, M. Đ. Crnogorac, T. Stanojković and S. Grgurić-Šipka, *Journal of Inorganic Biochemistry*, 2020, **210**, 111164.
11. T. Peega, R. N. Magwaza, L. Harmse and I. A. Kotzé, *Dalton Transactions*, 2021, **50**, 11742-11762.
12. E. F. Kohmann, *Journal of the American Chemical Society*, 1915, **37**, 2130-2133.
13. A. A. El-Sayed, G. A. Elsayed, S. A. Rizk and M. F. Ismail, *Organic Preparations and Procedures International*, 2024, **56**, 38-51.
14. R. Tailor, V. Akbari, M. Belim, H. Desai, P. Patel, P. Patel and K. Patel, *Journal of the Indian Chemical Society*, 2023, **100**, 101032.
15. A. Saeed, T. Hökelek, M. Bolte and M. F. Erben, *Journal of Molecular Structure*, 2021, **1245**, 131271.
16. R. P. Biasi‐Garbin, M. Fabris, A. E. B. Morguette, G. M. Andriani, W. R. Cabral, P. M. Pereira, T. O. Brito, F. Macedo Jr, C. H. Da Silva Lima and C. A. Lancheros, *ChemistrySelect*, 2022, **7**, e202202117.
17. W. Henderson, B. K. Nicholson and C. E. F. Rickard, *Inorganica Chimica Acta*, 2001, **320**, 101-109.
18. O. C. Okpareke, W. Henderson, S. Akkoç and B. Coban, *Inorganica Chimica Acta*, 2022, **531**, 120707.
19. B. N. Cunha, L. Luna-Dulcey, A. M. Plutin, R. G. Silveira, J. Honorato, R. R. Cairo, T. D. de Oliveira, M. R. Cominetti, E. E. Castellano and A. A. Batista, *Inorganic Chemistry*, 2020, **59**, 5072-5085.
20. L. M. Durosinmi, O. A. Fadare, K. Sanusi, Y. Yilmaz, U. Ceylan and C. A. Obafemi, *Heliyon*, 2020, **6**.

21. R. G. Silveira, A. J. Catão, B. N. Cunha, F. Almeida, R. S. Correa, L. F. Diniz, J. C. Tenório, J. Ellena, A. E. Kuznetsov and A. A. Batista, *Journal of the Brazilian Chemical Society*, 2018, **29**, 2502-2513.
22. W. Zhu, W. Yang, W. Zhou, H. Liu, S. Wei and J. Fan, *Journal of Molecular Structure*, 2011, **1004**, 74-81.
23. S. Swaminathan, J. Haribabu, M. K. M. Subarkhan, D. Gayathri, N. Balakrishnan, N. Bhuvanesh, C. Echeverria and R. Karvembu, *Dalton Transactions*, 2021, **50**, 16311-16325.
24. E. R. Johnson, S. Keinan, P. Mori-Sánchez, J. Contreras-García, A. J. Cohen and W. Yang, *Journal of the American Chemical Society*, 2010, **132**, 6498-6506.
25. M. Hajji, N. Abad, M. A. Habib, S. M. H. Elmgirhi and T. Guerfel, *Journal of the Indian Chemical Society*, 2021, **98**, 100208.
26. J. R. Lane, J. Contreras-García, J.-P. Piquemal, B. J. Miller and H. G. Kjaergaard, *Journal of Chemical Theory and Computation*, 2013, **9**, 3263-3266.
27. K. T. Mahmudov, A. V. Gurbanov, V. A. Aliyeva, M. F. C. G. da Silva, G. Resnati and A. J. Pombeiro, *Coordination Chemistry Reviews*, 2022, **464**, 214556.
28. M. González-Álvarez, G. Alzuet, J. Borrás, L. del Castillo Agudo, S. García-Granda and J. M. Montejo-Bernardo, *Inorganic Vhemistry*, 2005, **44**, 9424-9433.
29. D. P. Dorairaj, J. Haribabu, P. V. Shashankh, Y.-L. Chang, C. Echeverria, S. C. Hsu and R. Karvembu, *Journal of Inorganic Biochemistry*, 2022, **233**, 111843.
30. H. A. Nkabyo, B. Procacci, S. B. Duckett and K. R. Koch, *Dalton Transactions*, 2019, **48**, 17241-17251.
31. R. S. Proctor, A. C. Colgan and R. J. Phipps, *Nature Chemistry*, 2020, **12**, 990-1004.
32. H. J. Davis and R. J. Phipps, *Chemical Science*, 2017, **8**, 864-877.
33. A. S. Novikov, *Crystals*, 2022, **12**, 246.
34. S. U. Rehman, T. Sarwar, M. A. Husain, H. M. Ishqi and M. Tabish, *Archives of Biochemistry and Biophysics*, 2015, **576**, 49-60.
35. J. Contreras-García, W. Yang and E. R. Johnson, *The Journal of Physical Chemistry A*, 2011, **115**, 12983-12990.
36. A. Otero-De-La-Roza, E. R. Johnson and J. Contreras-García, *Physical Chemistry Chemical Physics*, 2012, **14**, 12165-12172.
37. R. M. Gomila, A. Bauzá and A. Frontera, *Dalton Transactions*, 2022, **51**, 5977-5982.
38. Y. Mao, P. R. Horn and M. Head-Gordon, *Physical Chemistry Chemical Physics*, 2017, **19**, 5944-5958.
39. P. R. Horn, Y. Mao and M. Head-Gordon, *Physical Chemistry Chemical Physics*, 2016, **18**, 23067-23079.
40. J. X. McDermott, J. F. White and G. M. Whitesides, *Journal of the American Chemical Society*, 1976, **98**, 6521-6528.
41. F. Wimmer, S. Wimmer, P. Castan and R. J. Puddephatt, *Inorganic Syntheses*, 1992, 185-187.

42. Y. Fuchita, H. Ieda, A. Kayama, J. Kinoshita-Nagaoka, H. Kawano, S. Kameda and M. Mikuriya, *Journal of the Chemical Society, Dalton Transactions*, 1998, 4095-4100.
43. O. V. Dolomanov, L. J. Bourhis, R. J. Gildea, J. A. K. Howard and H. Puschmann, *Journal of Applied Crystallography*, 2009, **42**, 339-341.
44. L. J. Bourhis, O. V. Dolomanov, R. J. Gildea, J. A. K. Howard and H. Puschmann, *Acta Crystallographica Section A: Foundations and Advances*, 2015, **71**, 59-75.
45. Y. Shao, Z. Gan, E. Epifanovsky, A. T. Gilbert, M. Wormit, J. Kussmann, A. W. Lange, A. Behn, J. Deng and X. Feng, *Molecular Physics*, 2015, **113**, 184-215.
46. T. Lu and F. Chen, *Journal of Computational Chemistry*, 2012, **33**, 580-592.
47. T. Williams, C. Kelley, H.-B. Bröker, J. Campbell, R. Cunningham, D. Denholm, G. Elber, R. Fearick, C. Grammes and L. Hart, *Environment*, 1986, **4**.

Chapter Six

Synthesis, structure and non-covalent interactions analysis of [(η^6-*p*-cymene)Ru{($CH_3CH_2CONH)_2CS$}Cl]

The coordination chemistry of acylthiourea ligands as neutral monodentate ligands towards piano stool ruthenium(II),[1, 2] as well as their isostructural rhodium(III)[3] and iridium(III)[4] analogues is well-studied. Interest in these systems is rooted in their demonstrated potential for biological and catalytic activity. In particular, many piano-stool complexes featuring acylthiourea ligands have demonstrated promising sub-micromolar antiproliferative activity[5-7] or high selectivity in catalytic reactions such as transfer hydrogenation.[1, 8] In these systems, the acylthiourea ligand acts as an excellent S-donor backbone, which can be readily modified to fine-tune the chemical properties and reactivity of the overall complex (Figure 6.1). The remaining coordination sites of the piano-stool complex are occupied by an arene ring and typically, though not exclusively, two chlorido ligands, which are often associated with DNA binding[9, 10] or serve as substitutional sites for catalytic processes.[1, 8]

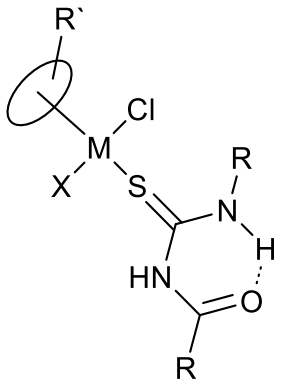

Figure 6.1: Generalized structure of monodentate acylthiourea piano stool complexes.

R = alkyl or aryl, M = Ru(II), Ir(III) or Rh(III), X = Cl or PPh_3. R` = cymene, benzene or cp.*

The structural arrangement of neutral and monoanionic acylthioureas in transition metal complexes is largely defined by an intramolecular hydrogen bond between the acyl oxygen and the amidic hydrogen (Figure 6.1). This interaction persists even in *S,N*-acyl chelates involving monoanionic acylthioureas. Additionally, diacylthioureas exhibit a second non-covalent interaction in the form of a chalcogen bond between the thiourea sulfur and acyl oxygen atoms (Figure 6.2), as demonstrated in Chapter 5. This interaction is observed even when the ligand is in its dianionic form. While the precise mechanisms linking spatial arrangements of ligands to the pharmacological[11, 12] and catalytic properties[13, 14] of the overall complexes is not completely understood, it is well established that the configuration of these ligands plays a crucial role in their activity. Consequently, developing a detailed understanding of these arrangements and the factors influencing them is of importance for future application-focused investigations.

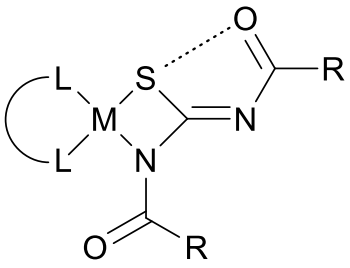

Figure 6.2: General structure of S,N chelated thiourea complexes of chapter 5 highlighting the structurally determining chalcogen interaction.

Notably, despite extensive studies on acylthioureas in piano-stool coordination environments, no analogous complexes featuring diacylthiourea ligands have been reported. In this regard, the ruthenium(II) cymene complex with a neutral monodentate diacylthiourea ligand, [(η^6-*p*-cymene)Ru{($CH_3CH_2CONH)_2CS$}Cl_2] (**6a**), is prepared and its solid-state structure is analysed for non-covalent interactions.

6.1 Results and discussion

6.1.1 Synthesis of [(η^6-*p*-cymene)Ru{($CH_3CH_2CONH)_2CS$}Cl_2] 6a

The reaction between the ruthenium cymene dimer, [(η^6-*p*-cymene)$RuCl_2$]$_2$, and the ligand $(CH_3CH_2CONH)_2CS$ **DA-L2** (prepared in Chapter 5) in dichloromethane at

room temperature produced the complex **6a** after approximately 5 hours (Figure 6.3). Removal of the solvent under reduced pressure followed by several washings with petroleum spirits and diethyl ether gave the product in good yield and purity. ESI-MS(+) of the product displayed a relatively weak ion relating to $[M - H - 2Cl]^+$ which is characteristic of similar ruthenium(II) chlorido complexes with monodentate acylthiourea ligands.[10, 15] More intense ions relating to $[(M - H - 2Cl - CH_3CH_2CO) + H]^+$ and $[M - H - 2Cl + MeOH]^+$ were also observed. The former is a characteristic fragment ion for complexes of diacylthiourea ligands. The ^1H NMR spectrum is consistent with a monodentate coordination mode, showing symmetry around the ruthenium(II) centre, i.e., a single set of aromatic *p*-cymene resonances are observed. The ethyl groups of the diacylthiourea ligand, however, display as two environments; the two CH_3 groups display as two triplet resonances, while the CH_2 groups display as two overlapping quartets. The lack of symmetry for the diacylthiourea ligand is potentially a result of an intramolecular hydrogen bond (*vide infra*). The $^{13}C\{^1H\}$ carbon NMR spectrum displays three significantly low field resonances between 171 and 179 ppm corresponding to the thiourea C=S carbon atom and two non-equivalent acyl C=O carbon atoms. The aromatic *p*-cymene resonances appear in the range of 83-140 ppm while the remaining cymene resonances and diacylthiourea alkyl resonances appear between 0-40 ppm. No atypical features were observed in the spectrum.

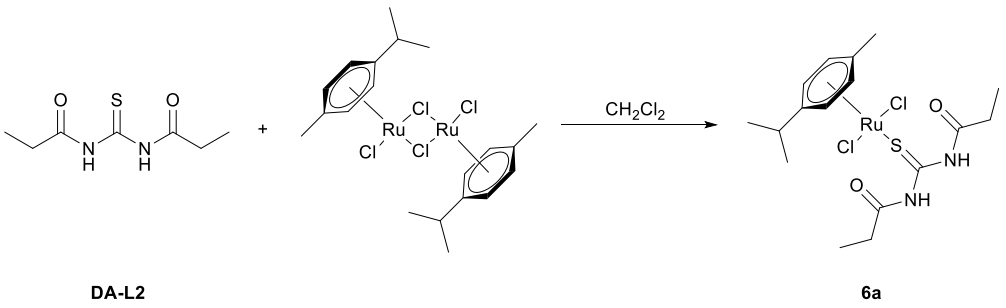

*Figure 6.3: Synthesis of **6a** from **DA-L2** and $[(\eta^6$-p-cymene$)RuCl_2]_2$ in dichloromethane.*

6.1.2 Molecular structure of [(η^6-*p*-cymene)Ru{($CH_3CH_2CONH)_2CS$}Cl_2] 6a

The molecular structure of **6a** was elucidated *via* single-crystal X-ray diffraction using crystals grown by the diffusion of diethyl ether into a dichloromethane solution of the complex (Figure 6.4). The structure was best resolved in the $P4_2/n$ space group, with a single molecule of the complex present in the asymmetric unit. Coordination around the ruthenium centre exhibits the characteristic piano-stool geometry, with two chlorido ligands and one diacylthiourea ligand (**DA-L2**) coordinated in a monodentate fashion through the thiourea sulfur atom. Bonding angles around the ruthenium atom for Cl1-Ru-Cl2, Cl2-Ru-S1 and S1-Ru-Cl1 are 87.7(2), 88.4(2) and 95.0(2) respectively. The bond distances for the two chlorido ligands are 2.441(6) Å (Cl1–Ru) and 2.425(6) Å (Cl2–Ru), slightly longer than the bond distance between the neutral S-donor diacylthiourea ligand and the ruthenium centre, measured at 2.399(5) Å (S1–Ru). The central thiourea carbon in the diacylthiourea ligand adopts a standard trigonal planar geometry, with S1–C1, C1–N1, and C1–N2 bond lengths of 1.685(2), 1.357(3), and 1.360(3) Å, respectively. These bond distances align well with those observed in the molecular structure of the uncoordinated ligand, which were determined as 1.652(2) Å (S1–C1), 1.382(3) Å (C1–N1), and 1.370(2) Å (C1–N2) (Chapter 5).

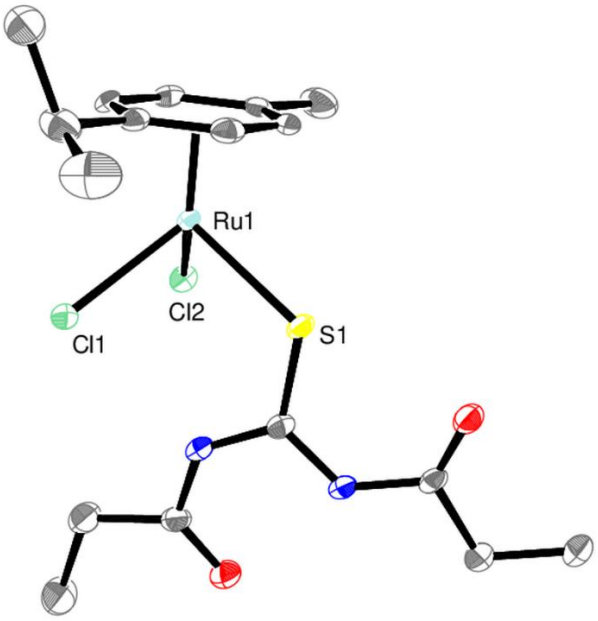

*Figure 6.4 Molecular structure of complex **6a**. Hydrogen atoms are omitted for clarity*

The spatial arrangement of the diacylthiourea ligand in **6a** closely resembles that of the free ligand, characterized by two intramolecular non-covalent interactions. A hydrogen bond between O1 and the hydrogen atom of N2, forming a six-membered ring motif and a chalcogen bond between S1 and O1, resulting in a crescent-like arrangement defined by S1–C1–N1–C2–O1. A third intramolecular interaction, involving the hydrogen atom on N2 and one of the chlorido ligands (Cl2), causes the ligand to tilt slightly, shifting away from the axis defined by Cl1–Ru–Cl2 (Figure 6.5). The packing arrangement of the molecular structure shows no atypical features.

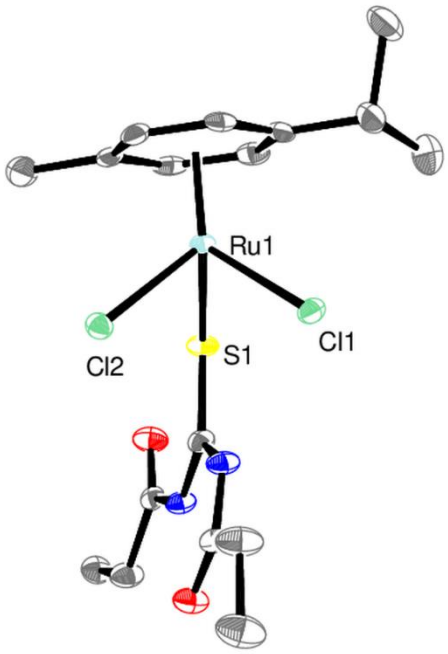

*Figure 6.5 Molecular structure of complex **6a** (side view). Hydrogen atoms are omitted for clarity.*

6.1.3 Non-covalent interactions analysis of [(η^6-*p*-cymene)Ru{$(CH_3CH_2CONH)_2CS$}Cl_2] 6a

The intramolecular interactions determining the spatial arrangement of **6a** were analyzed using the non-covalent interactions (NCI) index, following the methodologies outlined in Chapters 2–5. Specifically, the reduced density gradient (RDG) was calculated for the presumed chalcogen and hydrogen intramolecular interactions at O1–S1, N1–O2, and N2–Cl1. The combined plot of RDG versus

sign(λ_2)ρ (Figure 6.6) reveals three distinct troughs in the low-density, low-gradient region, along with a positive-range trough corresponding to steric repulsion within the S–C–N–C=O ring-like structure. The trough at approximately -0.02 sign(λ_2)ρ, based on comparisons with similar S···O=C interactions (Chapter 5), is attributed to the chalcogen bond between the thiourea sulfur and the acyl oxygen. The second most negative trough, at ~-0.03 sign(λ_2)ρ, corresponds to the Cl–H interaction, while the most negative trough, at -0.04 sign(λ_2)ρ, is associated with the hydrogen bond between the acyl oxygen and the thiourea nitrogen atoms. The 3D isosurfaces of these interactions, color-coded by sign(λ_2)ρ, are shown in a representation of **6a** (Figure 6.7).

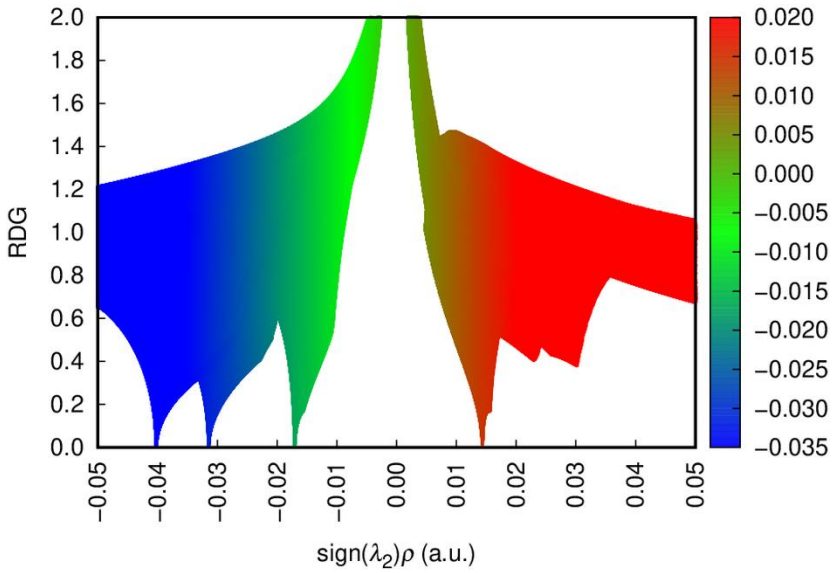

*Figure 6.6: Plot of RDG (s) verses sign(λ_2)ρ for complex **6a** showing troughs related to chalcogen and hydrogen bonding interactions*

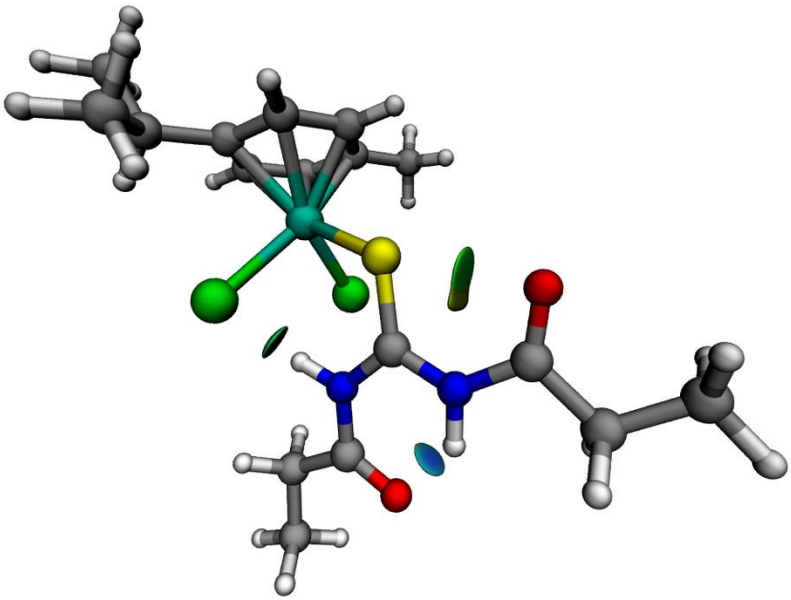

*Figure 6.7: NCI isosurfaces of the chalcogen interaction for complex **6a** using a blue-green-red colour scale from −0.02 < sign(λ_2)ρ(r) < +0.02 au. Isovalue = 0.4 for clarity.*

6.2 Conclusions

In this chapter, complex **6a** was synthesized through the reaction of the diacylthiourea ligand **DA-L2** with the ruthenium cymene dimer. The molecular structure was determined, revealing that the ligand coordinates to the ruthenium centre as a neutral bidentate ligand, accompanied by two chlorido ligands. The ESI-MS and NMR spectroscopic data indicate that the bulk sample is indicative of the single crystal molecular structure. Analysis of the non-covalent interactions using the NCI index identified chalcogen and hydrogen bonding interactions as key factors influencing the spatial arrangement of the complex. Such analyses serve as valuable tools for understanding structural features that play crucial roles in the activity of these complexes in application-oriented research. As such, the results presented here lay the groundwork for future studies in this area.

6.3 Experimental

6.3.1 Materials

The diacylthiourea ligand **DA-L2** was used as prepared in Chapter 5. The ruthenium dimer $[(\eta^6\text{-}p\text{-cymene})RuCl_2]_2$ was used as prepared in Chapter 3.

6.3.2 Instrumentation

A 600 MHz Jeol ECZR NMR spectrometer was used to record ^1H (600 MHz) and ^{13}C (151 MHz) NMR spectra in $CDCl_3$ at 25°C. Spectra were processed using the Jeol Delta software. ESI mass spectra were recorded in methanol using a Bruker Daltonics MicrOTOF electrospray ionization mass spectrometer. A methanol solution of sodium formate was used for calibration. ESI-MS spectra were recorded with a Capillary Exit voltage of 90 V and a Skimmer 1 voltage of 30 V. Elemental analysis was performed by the Chemical Analysis Facility, Department of Molecular Sciences, Macquarie University, Sydney, Australia. Collection of single crystal X-ray diffraction data was carried out by the University of Auckland Microcharacterization Facility, Auckland, New Zealand.

6.3.3 Synthesis of [(*p*-cymene)Ru{$(CH_3CH_2CONH)_2CS$}Cl_2] 6a

$[(\eta^6\text{-}p\text{-cymene})RuCl_2]_2$ (0.150 g) and two molar equivalents of the diacylthiourea ligand **DA-L2** (0.092 g) were dissolved in dichloromethane (20 mL) and kept for approximately 5 hours at room temperature. After this time, the solvent was removed under reduced pressure at 30°C. The dry residue was washed with petroleum spirits (2 x 20 mL) and diethyl ether (2 x 20 mL) and dried under vacuum. Red solid (0.197 g, 81 %). Elemental analysis: Found (%) C 42.3; H 5.5; N 5.5; S 6.0. Calculated for $C_{17}H_{26}Cl_2N_2O_2RuS$ (%) C 41.3; H 5.3; N 5.6; S 6.4. ESI MS: *m/z* $[(M - H - 2Cl - CH_3CH_2CO) + H]^+$ 367.1524, $[M - H - 2Cl]^+$ 423.1790, $[M - H - 2Cl + MeOH]^+$ 455.2201. NMR ($CDCl_3$, 151 MHz): ^{13}C δ 179.8 (C=S), 176.8 (C=O) 171.4 (C=O), 104.7, 100.8, 84.8, 83.9 (aromatic cymene), 31.7(CH_2), 31.5 (CH_2), 30.4, 22.6, 18.4 (aliphatic cymene), 8.5 (CH_3), 7.7 (CH_3); NMR ($CDCl_3$, 600 MHz): ^1H δ 11.10 (s, NH), 5.48 (d, ^3J = 6 Hz, cymene-H, 2H), 5.31 (d, ^3J = 6 Hz, cymene-H, 2H), 3.02 (sept, ^3J = 6 Hz, isopropyl-CH, 1H), 2.44 (m, $COCH_2$, 4H), 2.26 (s, cymene-*p*-CH_3, 3H), 1.30

(d, ^3J = 7 Hz, isopropyl-CH_3, 6H), 1.20 (t, ^3J = 7 Hz, CH_3, 3H), 1.08 (t, ^3J = 7 Hz, CH_3, 3H).

6.3.4 X-ray crystal structure determination

Crystals of satisfactory quality for single crystal diffraction of **6a** were grown by the slow diffusion of diethyl ether into a dichloromethane solution of the complex. The structures was solved using Olex2[16] with the Olex2.solve[17] structure solution program using Charge Flipping and refined with the Olex2.refine[17] refinement package using Gauss–Newton minimization. Crystal and refinement details are summarized in the Appendix 1.

6.3.5 Theoretical investigations

Single point calculations of the molecular structure were conducted using Q-chem software.[18] The mixed basis sets used were aug-cc-pV(D+d)Z for S and P, aug-cc-pVDZ for O, N and Cl, cc-pVDZ for C and H, LANL2DZ for Ru atoms using the effective core potential. The ωB97M-V method was used. MultiWFN was used for the calculation of non-covalent interactions including the calculation of the reduced density gradient (RDG).[19] Gnuplot was used for the representation of the RDG plot.[20]

6.4 References

1. G. Rohini, J. Haribabu, K. Aneesrahman, N. S. Bhuvanesh, K. Ramaiah, R. Karvembu and A. Sreekanth, *Polyhedron*, 2018, **152**, 147-154.
2. G. Rohini, J. Haribabu, M. M. Sheeba, A. KN, N. S. Bhuvanesh, C. Balachandran, R. Karvembu and A. Sreekanth, *ChemistrySelect*, 2018, **3**, 18-28.
3. D. Cauzzi, M. Lanfranchi, G. Marzolini, G. Predieri, A. Tiripicchio, M. Costa and R. Zanoni, *Journal of Organometallic Chemistry*, 1995, **488**, 115-125.
4. A. Lapasam, O. Hussain, R. M. Phillips, W. Kaminsky and M. R. Kollipara, *Journal of Organometallic Chemistry*, 2019, **880**, 272-280.
5. B. N. Cunha, L. Colina-Vegas, A. M. Plutín, R. G. Silveira, J. Honorato, K. M. Oliveira, M. R. Cominetti, A. G. Ferreira, E. E. Castellano and A. A. Batista, *Journal of Inorganic Biochemistry*, 2018, **186**, 147-156.
6. S. Swaminathan, J. Haribabu, N. Balakrishnan, P. Vasanthakumar and R. Karvembu, *Coordination Chemistry Reviews*, 2022, **459**, 214403.
7. G. H. Ribeiro, A. R. Costa, A. R. de Souza, F. V. da Silva, F. T. Martins, A. M. Plutin and A. A. Batista, *Coordination Chemistry Reviews*, 2023, **488**, 215161.
8. M. M. Sheeba, M. M. Tamizh, L. Farrugia and R. Karvembu, *Journal of Organometallic Chemistry*, 2017, **831**, 45-49.
9. L. Colina-Vegas, L. Luna-Dulcey, A. M. Plutín, E. E. Castellano, M. R. Cominetti and A. A. Batista, *Dalton Transactions*, 2017, **46**, 12865-12875.
10. S. Swaminathan, J. Haribabu, N. K. Kalagatur, R. Konakanchi, N. Balakrishnan, N. Bhuvanesh and R. Karvembu, *ACS Omega*, 2019, **4**, 6245-6256.
11. A. S. Novikov, *Crystals*, 2022, **12**, 246.
12. S. U. Rehman, T. Sarwar, M. A. Husain, H. M. Ishqi and M. Tabish, *Archives of Biochemistry and Biophysics*, 2015, **576**, 49-60.
13. R. S. Proctor, A. C. Colgan and R. J. Phipps, *Nature Chemistry*, 2020, **12**, 990-1004.
14. H. J. Davis and R. J. Phipps, *Chemical Science*, 2017, **8**, 864-877.
15. S. Swaminathan, J. Haribabu, M. K. M. Subarkhan, D. Gayathri, N. Balakrishnan, N. Bhuvanesh, C. Echeverria and R. Karvembu, *Dalton Transactions*, 2021, **50**, 16311-16325.
16. O. V. Dolomanov, L. J. Bourhis, R. J. Gildea, J. A. K. Howard and H. Puschmann, *Journal of Applied Crystallography*, 2009, **42**, 339-341.
17. L. J. Bourhis, O. V. Dolomanov, R. J. Gildea, J. A. K. Howard and H. Puschmann, *Acta Crystallographica Section A: Foundations and Advances*, 2015, **71**, 59-75.
18. Y. Shao, Z. Gan, E. Epifanovsky, A. T. Gilbert, M. Wormit, J. Kussmann, A. W. Lange, A. Behn, J. Deng and X. Feng, *Molecular Physics*, 2015, **113**, 184-215.
19. T. Lu and F. Chen, *Journal of Computational Chemistry*, 2012, **33**, 580-592.
20. T. Williams, C. Kelley, H.-B. Bröker, J. Campbell, R. Cunningham, D. Denholm, G. Elber, R. Fearick, C. Grammes and L. Hart, *Environment*, 1986, **4**.

Epilogue

Conclusions and future work

This thesis has explored the coordination chemistry of some lesser studied sulfonylthiourea, phosphorylthiourea, and diacylthiourea ligands with platinum group and related late transition metals. The 34 new compounds synthesized in this work were comprehensively characterized using both traditional techniques (ESI-MS, NMR spectroscopy, elemental analysis, and crystallography) and by computational methods (DFT, NCI, and ALMO-EDA). The key findings of this thesis will be discussed here in brief with recommendations for future work.

Chapter 2

Previous literature on the coordination chemistry of dianionic sulfonylthiourea ligands with platinum group and related metals established that these complexes formed exclusively as the *distal* linkage isomer. To explore potential reasons for this observation, Chapter 2 reports the synthesis and characterization of several bis(phosphine) and mono(phosphine) platinum(II) complexes with various cone angles with dianionic sulfonylthiourea ligands. Initial observations of the molecular structures, which could be elucidated crystallographically indicated that the complexes followed the previously established trend of exclusively forming in the *distal* isomer. $^{31}P\{^{1}H\}$ NMR analysis of the complexes, including those whose solid-state structure could not be determined, confirmed the *distal* isomer and no isomerization was detected. It was extrapolated from these results that the size of the ancillary ligand played no notable role in the coordination mode. Instead, using the molecular structures as a starting point, geometry-optimized structures of some complexes were analysed for possible non-covalent interactions. A potential chalcogen interaction was identified between the thiourea sulfur and sulfonyl oxygen atoms. The presence of this attractive chalcogen interaction provides a likely explanation for the observed *distal* isomer.

Chalcogen bonds have been used previously in research areas where the structural pose of the complexes is important, such as catalytic design and drug development. Following the discovery of the interaction in this thesis, the next step for future work in this area would be to examine applications in which this interaction is important. Examples may include applications as catalysts, where chalcogen bonds have been used to pre-orient substrates, for example in asymmetric acyl transfers on enantiomeric mixtures. Moreover, as the structural pose of the complexes plays vital roles in drug design, impacting both DNA and protein binding, computational analysis such as molecular docking may be of interest.

Chapter 3

Through a series of reactions from ruthenium(II), iridium(III), and rhodium(III) starting materials with monoanionic and dianionic sulfonylthiourea ligands, the first report of a series of piano-stool complexes is presented in Chapter 3. Unlike the square planar complexes prepared in this thesis, the piano-stool complexes demonstrated *proximal* isomer preference. It was demonstrated that the steric bulk around the metal centre imparted by both the arene ring and ancillary ligand played vital roles in the adopted isomer, as sufficient bulk can force the formation of the *distal* isomer. Isomerization from the *proximal* to *distal* isomer was observed in ^{1}H and $^{31}P\{^{1}H\}$ NMR spectra, which demonstrated the thermodynamic change of the complex to the more stable isomer. A series of sufficiently soluble complexes closely related in structure were analysed externally for anticancer activity. As a result of the closely related structures, a structure/activity relationship could be inferred, demonstrating increased activity with increased lipophilicity. The thiourea sulfur-bridged ruthenium dimer (**a_2L1**) also showed non-negligible activity, especially when compared to the ruthenium cymene chloride dimer starting material.

With multiple synthetic routes established and a preliminary bioactivity study conducted, the obvious next steps in the continuation of this work would be to expand the array of complexes prepared and conduct both catalytic and further biological analysis. In particular, as the triphenyl phosphine ruthenium complex (**1aL1**) showed the greatest anticancer activity, a series of related complexes with

various phosphines could be prepared and analysed to further explore structure/activity. Moreover, determining the mechanism of action of the complexes, such as through DNA or protein bonding studies, commonly done using NMR spectroscopy and mass spectrometry analysis. Other applications that were not explored in this thesis may also be undertaken, such as hetrogenius hydrogenation catalysis, which is often demonstrated by the closely related acylthiourea class of ligands.

Chapter 4

In this chapter, phosphorylthiourea ligands were used to prepare a series of platinum(II) phosphine complexes with the goal of comparing their coordination chemistry to the sulfonylthiourea complexes prepared in Chapter 2. While the coordination chemistry and structure of the square planar complexes were consistent with those of the sulfonylthiourea analogues, the presence of the NMR-active phosphorus atom on the ligand aided in characterization. It was demonstrated that through ^{3}J P-P coupling between the phosphorylthiourea ligand and the triphenylphosphine ligand, or the absence thereof, the isomer of the complex can be determined with ease without the need for crystallographic structural elucidation. This technique provides a useful foundational tool for future exploration using this class of ligand.

On account of the similarities between the sulfonylthiourea and phosphorylthiourea ligands in regard to their coordination chemistry, attention was instead turned to diacylthiourea ligands. Because of this, future work in this area would benefit from expanding the array of prepared complexes to the piano stool environment and the analysis of potential catalytic and biological activity. Using the NMR analysis as a useful tool, a wide range of complexes can be examined, particularly in situations where crystallographic determination of the complex is impractical, such as unstable complexes or large series of similar complexes for structural studies.

Chapter 5 and 6

These chapters outline the first investigations into the coordination chemistry of diacylthiourea ligands. Several complexes were prepared from monoanionic and dianionic diacylthiourea ligands with platinum(II), palladium(II), and gold(III) metal centres. The complexes were characterized by traditional methods, which showed that the ligands coordinated to the metal centres through the thiourea sulfur and nitrogen atoms. A comprehensive analysis of the non-covalent interactions governing the structural arrangement of the complexes found that chalcogen and hydrogen interactions dominate the structural pose. Moreover, in the case of the gold(III) anp complex (**5h**), a hydrogen-bonded dimerization of the complex occurs in the solid state. Further investigations of the complex as a neutral ligand in the piano-stool ruthenium environment was conducted, highlighting the difficulty in preparing mono- and diacylated derivatives.

This investigation provides a useful foundation for future investigations into the coordination chemistry of these ligands. Using the same argument for the sulfonylthiourea and phosphorylthiourea complexes, future investigations would benefit from being centred around applications in which the non-covalent interactions play vital roles. Moreover, as the results of this chapter represent the first report, future explorations into piano-stool complexes or other metal centres would be beneficial to expand the knowledge base of these ligands.

Conclusions

Overall, the contents of this thesis examining the coordination chemistry of some lesser studied thiourea ligands bearing electronegative substituents provide a solid foundation for further work in the area. The synthesis and characterization techniques, as well as the fundamental behaviour of these ligands, have been established, paving the way for more specific application-driven research. In this concluding chapter, some potential further directions for this research have been discussed, although the opportunities are vast and the exploration of these ligands is in its infancy.

Appendix 1

Crystallographic data

Identification code	Complex 2**a**	Complex **2b**
Empirical formula	$C_{28}H_{40}Cl_4N_8O_2P_2PtS_2$	$C_{32}H_{36}N_8O_2P_2PtS_2$
Formula weight	983.65	885.85
Temperature/K	120(20)	120.0(4)
Crystal system	triclinic	monoclinic
Space group	P-1	$P2_1$
a/Å	10.33380(10)	9.42184(5)
b/Å	11.43770(10)	19.69407(10)
c/Å	15.55990(10)	9.64562(5)
α/°	99.7440(10)	90
β/°	97.4620(10)	98.6715(5)
γ/°	91.5100(10)	90
Volume/Å^3	1795.02(3)	1769.328(16)
Z	2	2
ρ_{calc}g/cm^3	1.8198	1.6627
μ/mm^{-1}	12.322	9.720
F(000)	974.7	875.8
Crystal size/mm^3	0.22 × 0.1 × 0.1	0.5 × 0.1 × 0.1
Radiation	Cu Kα (λ = 1.54184)	Cu Kα (λ = 1.54184)
2Θ range for data collection/°	5.82 to 148.54	9.28 to 144.48
Index ranges	-12 ≤ h ≤ 12, -14 ≤ k ≤ 14, -19 ≤ l ≤ 19	-11 ≤ h ≤ 11, -23 ≤ k ≤ 23, -11 ≤ l ≤ 11
Reflections collected	54647	49888
Independent reflections	7115 [R_{int} = 0.0871, R_{sigma} = 0.0374]	6761 [R_{int} = 0.0368, R_{sigma} = 0.0200]
Data/restraints/parameters	7115/0/426	6761/1/425
Goodness-of-fit on F^2	1.038	1.039
Final R indexes [I>=2σ (I)]	R_1 = 0.0288, wR_2 = 0.0708	R_1 = 0.0145, wR_2 = 0.0355
Final R indexes [all data]	R_1 = 0.0295, wR_2 = 0.0712	R_1 = 0.0147, wR_2 = 0.0356
Largest diff. peak/hole / e Å^{-3}	1.03/-1.17	0.42/-0.57

Identification code	Complex 2**c**	Complex 2**f**
Empirical formula	$C_{37}H_{36}N_3O_4PPtS_2$	$C_{49}H_{50}N_2O_3P_2PtS_2$
Formula weight	876.90	1036.11
Temperature/K	116(20)	108(6)
Crystal system	triclinic	monoclinic
Space group	P-1	$P2_1/n$
a/Å	9.2445(2)	9.73600(10)
b/Å	13.4886(3)	26.6989(2)
c/Å	15.6935(2)	17.79570(10)
α/°	71.437(2)	90
β/°	82.586(2)	103.4720(10)
γ/°	72.921(2)	90
Volume/Å^3	1771.92(7)	4498.54(7)
Z	2	4
ρ_{calc}g/cm^3	1.6434	1.5297
μ/mm^{-1}	9.290	7.717
F(000)	867.3	2080.4
Crystal size/mm^3	0.14 × 0.1 × 0.1	0.16 × 0.14 × 0.1
Radiation	Cu Kα (λ = 1.54184)	Cu Kα (λ = 1.54184)
2Θ range for data collection/°	5.94 to 148.42	6.08 to 148.4
Index ranges	-11 ≤ h ≤ 11, -16 ≤ k ≤ 16, -18 ≤ l ≤ 19	-11 ≤ h ≤ 12, -32 ≤ k ≤ 33, -22 ≤ l ≤ 20
Reflections collected	52297	71177
Independent reflections	7031 [R_{int} = 0.0704, R_{sigma} = 0.0359]	9059 [R_{int} = 0.0465, R_{sigma} = 0.0237]
Data/restraints/parameters	7031/0/441	9059/0/539
Goodness-of-fit on F^2	1.035	1.045
Final R indexes [I>=2σ (I)]	R_1 = 0.0375, wR_2 = 0.0983	R_1 = 0.0248, wR_2 = 0.0594
Final R indexes [all data]	R_1 = 0.0405, wR_2 = 0.1017	R_1 = 0.0260, wR_2 = 0.0601
Largest diff. peak/hole / e Å^{-3}	1.71/-2.12	1.02/-1.14

Identification code	Complex **aL1**	Complex **aL2**
Empirical formula	$C_{24}H_{27}ClN_2O_2RuS_2$	$C_{19}H_{25}ClN_2O_2RuS_2$
Formula weight	576.14	514.07
Temperature/K	120.0(4)	99.9(6)
Crystal system	monoclinic	triclinic
Space group	$P2_1/c$	P-1
a/Å	11.77638(10)	7.10950(10)
b/Å	18.18345(16)	10.2048(2)
c/Å	11.48870(11)	14.9475(3)
α/°	90	103.603(2)
β/°	100.8584(9)	92.669(2)
γ/°	90	100.473(2)
Volume/Å^3	2416.09(4)	1031.94(4)
Z	4	2
ρ_{calc}g/cm^3	1.5838	1.6543
μ/mm^{-1}	8.082	9.373
F(000)	1183.0	527.3
Crystal size/mm^3	0.35 × 0.04 × 0.04	0.14 × 0.1 × 0.08
Radiation	Cu Kα (λ = 1.54184)	Cu Kα (λ = 1.54184)
2Θ range for data collection/°	7.64 to 144.94	6.12 to 148.12
Index ranges	-14 ≤ h ≤ 14, -22 ≤ k ≤ 22, -14 ≤ l ≤ 13	-8 ≤ h ≤ 8, -12 ≤ k ≤ 12, -17 ≤ l ≤ 18
Reflections collected	73393	29157
Independent reflections	4697 [R_{int} = 0.0659, R_{sigma} = 0.0207]	4084 [R_{int} = 0.0547, R_{sigma} = 0.0309]
Data/restraints/parameters	4697/0/294	4084/0/249
Goodness-of-fit on F^2	1.035	1.027
Final R indexes [I>=2σ (I)]	R_1 = 0.0246, wR_2 = 0.0662	R_1 = 0.0226, wR_2 = 0.0521
Final R indexes [all data]	R_1 = 0.0258, wR_2 = 0.0669	R_1 = 0.0248, wR_2 = 0.0531
Largest diff. peak/hole / e Å^{-3}	0.45/-0.78	0.38/-0.57

Identification code	Complex **2dL1**	Complex **2cL1**
Empirical formula	$C_{30}H_{41}ClN_5O_{2.5}PRhS_2$	$C_{46}H_{67}IrN_7O_9PS_4$
Formula weight	745.156	1213.541
Temperature/K	99.9(5)	99.9(5)
Crystal system	monoclinic	monoclinic
Space group	$P2_1/c$	$P2_1/c$
a/Å	23.0707(3)	11.9061(2)
b/Å	8.9830(1)	16.4040(2)
c/Å	33.0254(3)	26.5797(3)
α/°	90	90
β/°	108.467(1)	91.392(1)
γ/°	90	90
Volume/Å^3	6491.88(13)	5189.69(12)
Z	8	4
ρ_{calc}g/cm^3	1.525	1.553
μ/mm^{-1}	6.988	7.268
F(000)	3100.2	2476.8
Crystal size/mm^3	0.14 × 0.1 × 0.05	0.18 × 0.1 × 0.1
Radiation	Cu Kα (λ = 1.54184)	Cu Kα (λ = 1.54184)
2Θ range for data collection/°	5.64 to 148.7	6.34 to 148.6
Index ranges	-28 ≤ h ≤ 28, -11 ≤ k ≤ 10, -31 ≤ l ≤ 40	-14 ≤ h ≤ 14, -20 ≤ k ≤ 20, -32 ≤ l ≤ 24
Reflections collected	102852	77729
Independent reflections	13075 [R_{int} = 0.0661, R_{sigma} = 0.0383]	10450 [R_{int} = 0.0699, R_{sigma} = 0.0386]
Data/restraints/parameters	13075/3/787	10450/0/558
Goodness-of-fit on F^2	1.015	0.707
Final R indexes [I>=2σ (I)]	R_1 = 0.0295, wR_2 = 0.0641	R_1 = 0.0437, wR_2 = 0.1209
Final R indexes [all data]	R_1 = 0.0375, wR_2 = 0.0674	R_1 = 0.0476, wR_2 = 0.1249
Largest diff. peak/hole / e Å^{-3}	1.28/-0.78	1.61/-1.30

Identification code	Complex **2aL1**	Complex **1aL1**
Empirical formula	$C_{31}H_{44}N_5O_4PRuS_2$	$C_{42}H_{41}N_2O_2PRuS_2$
Formula weight	746.897	801.977
Temperature/K	120.00(10)	100.1(6)
Crystal system	monoclinic	triclinic
Space group	C2/c	P-1
a/Å	38.4923(2)	9.2306(1)
b/Å	9.48930(5)	9.8609(1)
c/Å	18.13669(10)	23.0693(2)
α/°	90	78.126(1)
β/°	97.5287(5)	89.588(1)
γ/°	90	64.356(1)
Volume/Å^3	6567.58(6)	1844.49(4)
Z	8	2
ρ_{calc}g/cm^3	1.511	1.444
μ/mm^{-1}	5.874	5.214
F(000)	3121.3	832.3
Crystal size/mm^3	0.05 × 0.05 × 0.05	0.18 × 0.18 × 0.12
Radiation	Cu Kα (λ = 1.54184)	Cu Kα (λ = 1.54184)
2Θ range for data collection/°	9.28 to 144.92	7.86 to 148.52
Index ranges	-46 ≤ h ≤ 47, -11 ≤ k ≤ 11, -22 ≤ l ≤ 21	-11 ≤ h ≤ 11, -12 ≤ k ≤ 12, -28 ≤ l ≤ 28
Reflections collected	95269	58161
Independent reflections	6377 [R_{int} = 0.0385, R_{sigma} = 0.0138]	7326 [R_{int} = 0.0449, R_{sigma} = 0.0232]
Data/restraints/parameters	6377/0/467	7326/0/456
Goodness-of-fit on F^2	1.065	1.038
Final R indexes [I>=2σ (I)]	R_1 = 0.0234, wR_2 = 0.0627	R_1 = 0.0315, wR_2 = 0.0811
Final R indexes [all data]	R_1 = 0.0244, wR_2 = 0.0631	R_1 = 0.0324, wR_2 = 0.0817
Largest diff. peak/hole / e Å^{-3}	0.67/-0.55	1.72/-0.86

Identification code	Complex **1bL3**	Complex **a_2L1**
Empirical formula	$C_{33}H_{31}Cl_2N_2O_2PRuS_2$	$C_{48}H_{52}N_4O_4Ru_2S_4$
Formula weight	754.702	1079.367
Temperature/K	99.9(5)	120.0(4)
Crystal system	monoclinic	monoclinic
Space group	$P2_1/c$	C2/c
a/Å	8.34223(8)	23.1894(6)
b/Å	20.4172(3)	9.2198(2)
c/Å	18.7826(2)	23.8717(5)
α/°	90	90
β/°	98.1698(11)	112.177(3)
γ/°	90	90
Volume/Å^3	3166.68(6)	4726.2(2)
Z	4	4
ρ_{calc}g/cm^3	1.583	1.517
μ/mm^{-1}	7.547	7.206
F(000)	1547.1	2220.1
Crystal size/mm^3	0.079 × 0.054 × 0.018	0.04 × 0.03 × 0.03
Radiation	Cu Kα (λ = 1.54184)	Cu Kα (λ = 1.54184)
2Θ range for data collection/°	8.66 to 147.76	8 to 144.24
Index ranges	-10 ≤ h ≤ 10, -23 ≤ k ≤ 25, -23 ≤ l ≤ 23	-28 ≤ h ≤ 28, -11 ≤ k ≤ 11, -24 ≤ l ≤ 29
Reflections collected	29462	28202
Independent reflections	6346 [R_{int} = 0.0604, R_{sigma} = 0.0409]	4603 [R_{int} = 0.0796, R_{sigma} = 0.0393]
Data/restraints/parameters	6346/2/395	4603/0/285
Goodness-of-fit on F^2	1.054	1.103
Final R indexes [I>=2σ (I)]	R_1 = 0.0365, wR_2 = 0.0858	R_1 = 0.0494, wR_2 = 0.1290
Final R indexes [all data]	R_1 = 0.0449, wR_2 = 0.0905	R_1 = 0.0551, wR_2 = 0.1338
Largest diff. peak/hole / e Å^{-3}	0.86/-0.98	1.23/-1.35

Identification code	Complex **4a**	Complex **4b**
Empirical formula	$C_{48}H_{47}Cl_2N_2O_3P_3PtS$	$C_{45}H_{49}N_2O_3P_3PtS$
Formula weight	1090.89	985.97
Temperature/K	120.00(10)	120.0(4)
Crystal system	triclinic	triclinic
Space group	P-1	P-1
a/Å	12.45755(13)	12.3489(2)
b/Å	13.38422(14)	15.6910(3)
c/Å	15.53434(15)	21.6968(2)
α/°	111.1972(9)	85.3095(11)
β/°	102.2787(9)	89.9981(12)
γ/°	101.2906(9)	88.2976(15)
Volume/Å^3	2251.45(5)	4188.18(11)
Z	2	4
ρ_{calc}g/cm^3	1.6090	1.5636
μ/mm^{-1}	8.714	8.151
F(000)	1089.6	1976.0
Crystal size/mm^3	0.09 × 0.08 × 0.07	0.08 × 0.05 × 0.05
Radiation	Cu Kα (λ = 1.54184)	Cu Kα (λ = 1.54184)
2Θ range for data collection/°	6.42 to 145.14	6.7 to 145.14
Index ranges	-15 ≤ h ≤ 15, -16 ≤ k ≤ 16, -19 ≤ l ≤ 17	-15 ≤ h ≤ 15, -18 ≤ k ≤ 19, -23 ≤ l ≤ 26
Reflections collected	32501	61330
Independent reflections	8697 [R_{int} = 0.0807, R_{sigma} = 0.0632]	16230 [R_{int} = 0.0555, R_{sigma} = 0.0476]
Data/restraints/parameters	8697/0/543	16230/0/1001
Goodness-of-fit on F^2	0.833	1.064
Final R indexes [I>=2σ (I)]	R_1 = 0.0390, wR_2 = 0.1037	R_1 = 0.0595, wR_2 = 0.1616
Final R indexes [all data]	R_1 = 0.0411, wR_2 = 0.1064	R_1 = 0.0675, wR_2 = 0.1665
Largest diff. peak/hole / e Å^{-3}	2.61/-2.81	8.03/-3.13

Identification code	**DA-L2**	**Complex 5a**
Empirical formula	$C_7H_{12}N_2O_2S$	$C_{41}H_{36}N_2O_2P_2PtS$
Formula weight	188.25	877.85
Temperature/K	100.0(2)	100.0(2)
Crystal system	orthorhombic	monoclinic
Space group	$P2_12_12_1$	$P2_1/c$
a/Å	5.17400(10)	14.7870(2)
b/Å	9.3578(2)	11.88550(10)
c/Å	19.0340(4)	20.6357(2)
α/°	90	90
β/°	90	94.9210(10)
γ/°	90	90
Volume/Å^3	921.57(3)	3613.37(7)
Z	4	4
ρ_{calc}g/cm^3	1.3567	1.6136
μ/mm^{-1}	2.848	8.943
F(000)	402.5	1734.3
Crystal size/mm^3	0.12 × 0.05 × 0.01	0.18 × 0.18 × 0.14
Radiation	Cu Kα (λ = 1.54184)	Cu Kα (λ = 1.54184)
2Θ range for data collection/°	9.3 to 148.16	6 to 148.62
Index ranges	-6 ≤ h ≤ 6, -11 ≤ k ≤ 7, -23 ≤ l ≤ 22	-18 ≤ h ≤ 18, -14 ≤ k ≤ 14, -25 ≤ l ≤ 24
Reflections collected	5339	56816
Independent reflections	1799 [R_{int} = 0.0395, R_{sigma} = 0.0387]	7283 [R_{int} = 0.0460, R_{sigma} = 0.0256]
Data/restraints/parameters	1799/0/111	7283/0/445
Goodness-of-fit on F^2	1.030	1.039
Final R indexes [I>=2σ (I)]	R_1 = 0.0290, wR_2 = 0.0774	R_1 = 0.0316, wR_2 = 0.0752
Final R indexes [all data]	R_1 = 0.0318, wR_2 = 0.0788	R_1 = 0.0352, wR_2 = 0.0771
Largest diff. peak/hole / e Å^{-3}	0.39/-0.20	1.81/-1.75

Identification code	**Complex 5b**	**Complex 5f**
Empirical formula	$C_{44}H_{42}Cl_2N_2O_2P_2PtS$	$C_{18}H_{19}AuN_4O_2S$
Formula weight	990.83	552.41
Temperature/K	100.0(2)	100.00(10)
Crystal system	monoclinic	monoclinic
Space group	$P2_1/c$	$P2_1/c$
a/Å	12.81780(10)	12.94247(16)
b/Å	21.7252(2)	19.2338(2)
c/Å	14.81870(10)	7.50278(9)
α/°	90	90
β/°	103.0940(10)	104.5517(12)
γ/°	90	90
Volume/Å^3	4019.26(6)	1807.77(4)
Z	4	4
ρ_{calc}g/cm^3	1.6373	2.0295
μ/mm^{-1}	9.310	16.548
F(000)	1969.5	1051.9
Crystal size/mm^3	1.12 × 0.12 × 0.1	0.05 × 0.05 × 0.02
Radiation	Cu Kα (λ = 1.54184)	Cu Kα (λ = 1.54184)
2Θ range for data collection/°	7.08 to 148.46	8.42 to 144.68
Index ranges	-16 ≤ h ≤ 15, -26 ≤ k ≤ 26, -18 ≤ l ≤ 18	-15 ≤ h ≤ 15, -23 ≤ k ≤ 21, -9 ≤ l ≤ 9
Reflections collected	64158	48018
Independent reflections	8104 [R_{int} = 0.0451, R_{sigma} = 0.0244]	3476 [R_{int} = 0.0556, R_{sigma} = 0.0211]
Data/restraints/parameters	8104/0/490	3476/0/240
Goodness-of-fit on F^2	1.025	1.063
Final R indexes [I>=2σ (I)]	R_1 = 0.0190, wR_2 = 0.0425	R_1 = 0.0304, wR_2 = 0.0790
Final R indexes [all data]	R_1 = 0.0209, wR_2 = 0.0432	R_1 = 0.0344, wR_2 = 0.0846
Largest diff. peak/hole / e Å^{-3}	0.60/-0.61	3.08/-1.73

Identification code	**Complex 5g**	**Complex 5h**
Empirical formula	$C_{25}H_{26}ClN_2O_2PPdS$	$C_{25}H_{26}ClN_2O_2PPtS$
Formula weight	591.41	680.07
Temperature/K	100.00(10)	100.0(3)
Crystal system	triclinic	triclinic
Space group	P-1	P-1
a/Å	9.70784(19)	9.69560(14)
b/Å	10.9768(3)	11.01772(16)
c/Å	12.7313(3)	12.69262(16)
α/°	68.297(2)	68.3323(13)
β/°	85.0358(17)	85.0689(11)
γ/°	81.1443(18)	81.4341(12)
Volume/Å^3	1244.81(5)	1245.30(3)
Z	2	2
ρ_{calc}g/cm^3	1.5777	1.8135
μ/mm^{-1}	8.597	13.122
F(000)	603.7	658.8
Crystal size/mm^3	0.05 × 0.04 × 0.03	0.05 × 0.05 × 0.04
Radiation	Cu Kα (λ = 1.54184)	Cu Kα (λ = 1.54184)
2Θ range for data collection/°	7.48 to 144.26	7.5 to 144.72
Index ranges	-11 ≤ h ≤ 11, -13 ≤ k ≤ 13, -15 ≤ l ≤ 15	-11 ≤ h ≤ 11, -13 ≤ k ≤ 13, -15 ≤ l ≤ 14
Reflections collected	33325	35228
Independent reflections	4736 [R_{int} = 0.0675, R_{sigma} = 0.0332]	4735 [R_{int} = 0.0509, R_{sigma} = 0.0258]
Data/restraints/parameters	4736/0/300	4735/0/300
Goodness-of-fit on F^2	1.028	1.049
Final R indexes [I>=2σ (I)]	R_1 = 0.0335, wR_2 = 0.0908	R_1 = 0.0178, wR_2 = 0.0429
Final R indexes [all data]	R_1 = 0.0357, wR_2 = 0.0922	R_1 = 0.0188, wR_2 = 0.0432
Largest diff. peak/hole / e Å^{-3}	1.49/-1.40	0.58/-1.05

Identification code	**Complex 6a**
Empirical formula	$C_{17}H_{26}Cl_2N_2O_2RuS$
Formula weight	494.44
Temperature/K	100.00(10)
Crystal system	tetragonal
Space group	$P4_2/n$
a/Å	18.4260(2)
b/Å	18.4260(2)
c/Å	12.1310(2)
α/°	90
β/°	90
γ/°	90
Volume/Å^3	4118.69(10)
Z	8
ρ_{calc}g/cm^3	1.5947
μ/mm^{-1}	9.606
F(000)	2029.4
Crystal size/mm^3	0.1 × 0.025 × 0.02
Radiation	Cu Kα (λ = 1.54184)
2Θ range for data collection/°	6.78 to 145.04
Index ranges	-22 ≤ h ≤ 22, -22 ≤ k ≤ 21, -11 ≤ l ≤ 14
Reflections collected	26726
Independent reflections	4021 [R_{int} = 0.0446, R_{sigma} = 0.0272]
Data/restraints/parameters	4021/0/239
Goodness-of-fit on F^2	1.047
Final R indexes [I>=2σ (I)]	R_1 = 0.0261, wR_2 = 0.0578
Final R indexes [all data]	R_1 = 0.0303, wR_2 = 0.0594
Largest diff. peak/hole / e Å^{-3}	0.62/-0.58

Selected bond distances and angles

	2a	2b	2c	2f
P1 - Pt	2.255(8)	2.280(6)	2.236(9)	2.303(6)
P2 - Pt	2.240(7)	2.257(6)	-	2.244(6)
N3 - Pt	-	-	2.076(4)	-
S1 - Pt	2.348(8)	2.337(6)	2.283(1)	2.325(6)
N1 - Pt	2.092(3)	2.077(2)	2.088(3)	-
N2 - Pt	-	-	-	2.095(2)
C1 - S	1.789(3)	1.771(3)	1.772(4)	1.787(3)
C1 - N1	1.299(4)	1.341(3)	1.332(7)	1.255(3)
C1 - N2	1.325(4)	1.318(3)	1.335(5)	1.431(4)
P1 - Pt - P2	99.97(3)	100.25(2)	-	96.99(2)
P1 - Pt - N3	-	-	92.48(1)	-
S1 - Pt - N1	68.44(8)	69.34(6)	70.01(1)	-
S1 - Pt - N2	-	-	-	70.03(6)

Bond	Bond length (Å)					
	aL1	**aL2**	**2aL1**	**1aL1**	**1bL3**	**a_2L1**
Arene - Ru	1.671(2)	1.666(2)	1.723(2)	1.737(3)	1.727(3)	1.687(5)
Ru - P	-	-	2.300(6)	2.349(5)	2.331(7)	-
Ru - Cl	2.412(5)	2.415(5)	-	-	-	-
Ru - S1	2.421(5)	2.429(6)	2.389(5)	2.379(7)	2.393(8)	2.413(1)
Ru - S1a	-	-	-	-	-	2.404(8)
Ru - N1	-	-	-	2.099(2)	-	-
Ru - N2	2.131(2)	2.144(2)	2.113(2)	-	2.117(2)	2.126(4)
S1- C1	1.715(2)	1.712(2)	1.766(2)	1.767(2)	1.776(3)	1.829(4)
C1 - N1	1.337(2)	1.336(3)	1.278(3)	1.328(3)	1.284(4)	1.270(5)
C1 - N2	1.351(3)	1.348(3)	1.393(3)	1.337(4)	1.378(4)	1.371(4)

	2dL1		**2cL1**		
Cp* - Rh	1.834(3)	**Cp* - Ir**	1.870(8)		
Rh - S	2.398(6)	**Ir - P**	2.276(2)		
Rh - P	2.276(8)	**Ir - S1**	2.362(2)	**Ir - S1a**	2.380(2)
Rh - Cl	2.420(1)	**S1 - C1**	1.735(7)	**S1a - C1a**	1.760(8)
S1 - C1	1.755(3)	**C1 - N1**	1.352(9)	**C1a - N1a**	1.343(9)
C1 - N1	1.360(3)	**C1 - N2**	1.315(9)	**C1a - N2a**	1.322(9)
C1 - N2	1.313(3)				

	4a	4b	4b(a)
P2 - Pt	2.246(8)	2.248(2)	2.250(2)
P3 - Pt	2.297(1)	2.308(2)	2.301(2)
S1 - Pt	2.326(1)	2.314(2)	2.318(2)
N1 - Pt	2.088(3)	-	-
N2 - Pt	-	2.067(6)	2.051(5)
C1 - S	1.796(4)	1.797(7)	1.806(8)
C1 - N1	1.345(7)	1.250(1)	1.250(1)
C1 - N2	1.287(5)	1.434(9)	1.422(9)
P1 - Pt - P2	97.11(4)	97.10(6)	96.7(6)
S1 - Pt - N1	69.78(1)	-	-
S1 - Pt - N2	-	70.48(2)	69.83(2)

Bond	Bond length (Å)		Bond	
	5a	5b		5f
Pt – P1	2.307(8)	2.306(5)	Au -N3	2.081(4)
Pt – P2	2.255(9)	2.249(5)	Au – C20	2.018(5)
Pt - S1	2.331(9)	2.325(5)	Au – S1	2.290(1)
Pt - N1	2.073(4)	2.083(2)	Au – N1	2.105(4)
S1- C1	1.784(4)	1.738(2)	S1 – C1	1.773(4)
C1 - N1	1.390(5)	1.382(3)	C1 – N1	1.368(5)
C1 - N2	1.269(5)	1.276(3)	C1 – N2	1.305(5)

	5g	5h		DA-L2
M-P1	2.246(6)	2.227(6)	S1 - C1	1.952(2)
M – Cl	2.320(9)	2.326(8)	C1 - N1	1.382(3)
M – S1	2.287(7)	2.290(7)	C1 - N2	1.370(3)
M – N1	2.139(2)	2.142(2)	N1 - C2	1.381(3)
S1 – C1	1.727(3)	1.722(3)	C2 - O1	1.224(2)
C1 – N1	1.331(4)	1.344(4)	N2 - C5	1.396(3)
C1 – N2	1.352(3)	1.347(3)	C5 - O2	1.206(2)

Bond	6a
Arene - Ru	1.673(2)
Ru – Cl1	2.441(6)
Ru – Cl2	2.425(5)
Ru - S1	2.399(5)
S1- C1	1.685(2)
C1 - N1	1.357(3)
C1 - N2	1.360(3)

Appendix 2

A complete reaction scheme for Chapter 3